UC Davis
UC Davis Electronic Theses and Dissertations

Title

Biomarkers of Prediction, Development, Progression and Severity of Fragile X Syndrome and FMR1 Associated Disorders

Permalink

https://escholarship.org/uc/item/3854c23f

Author

Zafarullah, Marwa

Publication Date

2021

Peer reviewed|Thesis/dissertation

Biomarkers of Prediction, Development, Progression and Severity of Fragile X Syndrome and
FMR1 Associated Disorders

By

Marwa Zafarullah
DISSERTATION

Submitted in partial satisfaction of the requirements for the degree of

DOCTOR OF PHILOSOPHY

in

Integrative Genetics and Genomics (IGG)

in the

OFFICE OF GRADUATE STUDIES

of the

UNIVERSITY OF CALIFORNIA

DAVIS

Approved:

_____
Flora Tassone, Chair

_____
David J. Segal

_____
Paul J. Hagerman

Committee in Charge
2021

i

Dedication

I dedicate my dissertation work to,

My great parents, **Muhammad Zafarullah** and **Rubina Zafar**, who never stop giving of themselves in countless ways, and whose words of encouragement and push for tenacity always ring in my ears,

My beloved siblings **Hira Zafer**, **Abdur Rehman Zafar**, and **Urba** who never left my side ever and always being there for me to share, and love,

My dearest husband, **Md Fazlay Rabbey**, who always supported me and be a light of hope in the darkest times of this graduate school journey,

My adorable daughter **Fatima Rabbey** whom I can't think myself to pause loving for a second and whose beautiful smile energizes me forever,

My amazing **friends**, who always encourage, support, and love me,

My all **family** near or far the symbol of love and giving,

All the **people** in my life who touch my heart.

"It would not be possible without you all."

ACKNOWLEDGEMENTS

Abstract

The Fragile X-associated disorders are a group of genetic diseases resulting from the expansion of the CGG repeats in the 5' untranslated region (5' UTR) of the *FMR1* gene, located on the X chromosome. Individuals with an expansion of greater than 200 CGG repeats have the full mutation, which leads to silencing of the gene and lack of the encoded protein, FMRP, causing Fragile X syndrome (FXS), the most common inherited form of intellectual disability. Individual carriers of a premutation allele (55-200 CGG repeat) are at risk of developing Fragile X-associated tremor/ataxia syndrome (FXTAS), a late onset neurodegenerative condition, which affects both males and females. Currently, there is no approved therapy or reliable biomarkers to determine therapeutic efficacy in FXS and associated disorders, in particular of FXTAS.

The first part of my dissertation (Chapters 2, 3 and 4) investigates the development of a potential biomarker for early diagnosis and progression of FXTAS. The second part of my dissertation (Chapters 5 and 6), reports on the development of a protocol to derive epithelial cells from urine samples of FXS patients and on the molecular methods to study and diagnose FXTAS.

Chapter 1 is a detailed introduction to the genetics of FXS, its pathophysiology and on currently available molecular biomarkers. In Chapter 2, I report on an investigation of the alternative splicing landscape at the *FMR1* locus in conjunction with brain measures. I show that increased levels of specific *FMR1* mRNA isoforms, those that encode truncated proteins, are present in premutation carriers who developed symptoms of FXTAS, relative to non-carrier healthy controls, suggesting a potential role in the development of the disorder. Chapter 3 reports on the identification of biomarkers for early

diagnosis and progression of FXTAS. Interestingly, lipid metabolism and, specifically, the sub-pathways involved in mitochondrial bioenergetics as observed in other neurodegenerative disorders; were found to be significantly altered in FXTAS. Further, in Chapter 4, I demonstrate that differential expression levels of some of the previously-identified metabolites are linked with areas within the pons. In addition, we observed a significant correlation of these metabolic signatures with the FXTAS stage, strengthening the likelihood that they contribute to the progression and pathogenesis of FXTAS.

In the second part of my thesis, which begins with Chapter 5, I describe a cost-effective and straightforward method to derive epithelial cell lines from urine samples collected from participants with FXS and healthy controls (TD). These cell lines can be used as a new model to study the molecular mechanisms behind FXS, including the expression of surface markers, inter and the intra-tissue CGG mosaicism, *FMR1* mRNA and FMRP expression levels. Finally, in Chapter 6, I provide the protocols for FXTAS diagnostic tools, in both humans and mouse.

Table of Contents

Development of Biomarkers

Molecular biomarker in Fragile X Syndrome (FXS)

> **Authors:** Marwa Zafarullah, and Flora Tassone

> **Published:** Brain Sciences 9(5):96 (2019) [*Online Link*]

FMR1 locus isoforms: potential biomarker candidates in fragile X-associated tremor/ataxia syndrome (FXTAS)

> **Authors:** Marwa Zafarullah, Hiu-Tung Tang, Blythe Durbin-Johnson, Emily Fourie, David Hessl, Susan M. Rivera, and Flora Tassone

> **Published:** Scientific Reports 10.1 (2020): 1-10. [*Online Link*]

Metabolic profiling reveals dysregulated lipid metabolism and potential biomarkers associated with the development and progression of Fragile X-Associated Tremor/Ataxia Syndrome (FXTAS)

> **Authors:** Marwa Zafarullah Grzegorz Palczewski, David Hessl, Susan M. Rivera, and Flora Tassone

> **Published:** The FASEB Journal 34.12 (2020): 16676-16692. [*Online Link*]

Methods and Protocols related to Fragile X syndrome and associated disorders

Chapter 1

Molecular Biomarkers in Fragile X Syndrome

Marwa Zafarullah [1] and Flora Tassone [1,2, *]

[1] Department of Biochemistry and Molecular Medicine, University of California Davis, School of Medicine, Sacramento, 95817 CA, USA; mzafarullah@ucdavis.edu
[2] MIND Institute, University of California Davis Medical Center, Sacramento, 95817 CA, USA
* **Correspondence:** ftassone@ucdavis.edu; Tel.: +1-(916)-703-0463

Abstract

Fragile X syndrome (FXS) is the most common inherited form of intellectual disability (ID) and a known monogenic cause of autism spectrum disorder (ASD). It is a trinucleotide repeat disorder, in which more than 200 CGG repeats in the 5' untranslated region (UTR) of the fragile X mental retardation 1 (*FMR1*) gene causes methylation of the promoter with consequent silencing of the gene, ultimately leading to the loss of the encoded fragile X mental retardation 1 protein, FMRP. FMRP is an RNA binding protein that plays a primary role as a repressor of translation of various mRNAs, many of which are involved in the maintenance and development of neuronal synaptic function and plasticity. In addition to intellectual disability, patients with FXS face several behavioral challenges, including anxiety, hyperactivity, seizures, repetitive behavior, and problems with executive and language performance. Currently, there is no cure or approved medication for the treatment of the underlying causes of FXS, but in the past few years, our knowledge about the proteins and pathways that are dysregulated by the loss of

FMRP has increased, leading to clinical trials and to the path of developing molecular biomarkers for identifying potential targets for therapies. In this paper, we review candidate molecular biomarkers that have been identified in preclinical studies in the FXS mouse animal model and are now under validation for human applications or have already made their way to clinical trials.

Keywords: fragile X syndrome; molecular biomarkers; *FMR1*; FMRP; intellectual disability; *Fmr1* KO mouse; ASD.

1. Introduction

A biomarker is "a characteristic that is objectively measured and evaluated as an indicator of normal biological processes, pathogenic processes, or pharmacologic responses to a therapeutic intervention" [1]. Biomarkers can be found in blood, plasma, or other tissues and are generally viewed as a molecular signature able to identify individuals who are at high risk for a specific condition. They can also be detected before disease symptoms and therefore used to predict the occurrence of a condition or the nature and severity of disease outcomes in an individual. Importantly, they can be used to evaluate the efficacy of response to pharmacological intervention.

Fragile X syndrome (FXS) is the most prevalent inherited form of intellectual disability and the single leading monogenic known cause of autism, as 60% of those with a full mutation present with autism spectrum disorder (ASD) [2]. The clinical symptoms include anxiety, impairment in cognitive, executive and language performance, hyperactivity,

impulsivity, insomnia, seizures, and physical features such as hypotonia, flat feet, hyperextensible joints, and macroorchidism [3]. FXS is caused by the abnormal expansion, to greater than 200 units, of a naturally occurring CGG repeat in the 5' untranslated region (UTR) of the fragile X mental retardation 1 (*FMR1*) gene, located on the X chromosome. This expansion, termed a full mutation, results in hypermethylation and transcriptional silencing of the gene, leading to the loss or reduction of fragile X mental retardation 1 protein (FMRP) expression and to the diagnosis of fragile X syndrome [4–6]. Individuals carrying expansions of 55–200 CGG repeats are termed premutation carriers and are at risk of developing the late-onset neurodegenerative syndrome, fragile X-associated tremor/ataxia syndrome (FXTAS), the fragile X-associated primary ovarian insufficiency (FXPOI) [7] and the fragile X-associated neuropsychiatric disorders (FXAND) [8].

FMRP is an RNA-binding protein and a translational regulator, whose function affects synaptic plasticity, spine morphology, and several cellular signaling pathways. Reduced expression of FMRP leads to the abnormalities in neurodevelopmental processes and the disturbed neuronal communications observed in FXS [9]. Young adults and adolescents with FXS show neuroanatomical abnormalities [10], and the regions of the brain that are significantly impacted by the loss of FMRP are the hippocampus (a structure that plays a critical role in the learning and memory and the regulation of mood and cognition [11]), the cerebellum, and the basal forebrain (nucleus basalis) [12]. Several studies in the *Fmr1* knockout (KO) mouse model suggest that FMRP plays a critical role during specific periods of cortical development with regional brain volume changes occurring in adult mouse brain [13,14]. Brain volume changes have also been observed in children with

FXS, specifically in the temporal lobe, cerebellum, caudate nucleus, and amygdala regions of the brain [15,16].

FMRP function appears to be mostly inhibitory as it prevents the activity of various biochemical pathways in a "controlled" manner [17]. In a sense, reduced FMRP leads to exaggerated or reduced biochemical reactions that can adversely affect neural function. The past two decades of research have shown defects in the central excitatory glutamatergic and inhibitory GABAergic pathways and in several other neurotransmitter systems including serotonin and dopamine [18,19]. Thus, the development of molecular measures that reflect the impact of a drug on one or more of the FMRP-regulated pathways [**Figure 1**], including the activity or the expression level of proteins in the translational activation pathway and particularly of those regulated by FMRP, could potentially act as molecular biomarkers for FXS.

The *Fmr1* knockout (KO) mouse model [20], lacks a functional *FMR1* gene and therefore does not express FMRP. Many studies have shown that the *Fmr1* KO mouse presents with some phenotypes that resemble the human disorder, including biochemistry [21], electrophysiology [22], neuropathology [23], and spine morphology [24]. Although the observed patterns of brain activity, including audiogenic seizures, are similar to those in individuals affected by FXS [25], these mice poorly mimic human behavior. Indeed, the strains of the *Fmr1* KO mouse that are often used to test drugs for FXS do not show the cognitive problems seen in patients with FXS [26]. Nevertheless, a large body of literature on the *Fmr1* KO mouse has paved the way to preclinical studies which have shown to rescue several of the FXS phenotypes [27] and have ultimately led to clinical trials in patients with FXS.

Hope has been tempered by the lack of translating the positive results observed in the *Fmr1* KO mouse model into therapy in a clinical setting. Currently, non-pharmacological and behavioral treatments are symptomatic, and they can be coupled with pharmacological treatments of anxiety, aggression, and attention deficit hyperactivity disorder (ADHD).

To date, there is no cure for FXS, and the recent failures of multiple clinical trials have highlighted the need for the development and validation of new biomarkers to better measure the clinical outcome of these treatments [28,29]. Many studies aimed to a better understanding of the underlying molecular mechanisms and pathways involved in FXS have led to the development of specific biomarkers for defining targeted therapeutic strategies intended to reverse the intellectual and behavioral problems of patients with FXS. In this paper, we will review the proposed candidate molecular biomarkers [**Figure 2**] that have been identified in *Fmr1* KO mouse as an early sign of drug promise and in some cases, later moved to a clinical trial in patients with FXS.

2. *FMR1* Molecular Measures

FMR1-related measures, including CGG repeat number, percent of methylation, *FMR1* mRNA and FMRP expression levels have been correlated to neurocognitive and social–affective functioning assessments and mental health problems in individuals with FXS [30–38]. The magnitude of the observed correlations generally suggests that these molecular biomarkers are likely accounting only for a proportion of the phenotypic variability of this disorder.

Variation in CGG repeat size and methylation, termed size- and methylation-mosaicism, respectively, could be a useful biomarker of various types of risks that could affect subjects with FXS. Methylation mosaicism determines the variation in gene expression as a function of the fraction of *FMR1* alleles that are fully hypermethylated, and ultimately reflects the levels of expression of both *FMR1* mRNA and FMRP. In the context of the FMR1 gene, mosaicism refers narrowly to the presence of a full mutation allele(s) and a premutation allele (size mosaicism) or the presence of a full methylated allele(s) and unmethylated alleles (methylation mosaicism), throughout the CGG repeat size range.

Sex differences undoubtedly contribute to the severity of the FXS phenotype; indeed, intellectual and developmental disability is observed in 85% of males and only in 25% of females [27,39,40]. In females, who have two X chromosomes, the process of X inactivation, early during embryonic development, leads to methylation and therefore inactivity of one X chromosome in each cell. However, due to the presence of the chromosome carrying the normal allele, the impact of the *FMR1* mutation in females is reduced relative to males, who have only one X chromosome [41]. The relative proportion of the normal allele on the active and inactive X chromosomes, so-called activation ratio (AR), has been shown to contribute to differences in affectedness among females, making the AR a useful biomarker for determining the severity of the phenotype. It should be noted that since X inactivation is a random process, it could be different in different tissues, such as blood and brain [42–44].

3. Metabotropic Glutamate Receptors (mGluRs)

The "mGluR theory of FXS" states that the absence of FMRP leads to excessive metabotropic glutamate receptors (mGluRs, mGluR1 and mGluR5) activated long-term depression (LTD) and reduced responsiveness to signals in the hippocampus and other parts of the brain involved in memory and learning. Together, they contribute to the neurological and psychiatric symptoms of FXS [45–47]. Reduction of mGluR signaling has been demonstrated in mouse and fly models to reverse the fragile X phenotypes, providing substantial support to the involvement of the mGluR5 pathway in FXS [48]. For more than a decade, our understanding of the molecular pathophysiology of FXS has been substantially advanced by the corroboration of "mGluR theory of FXS" in a wide range of experiments with a number of different mGluR5 inhibitors tested in both the *Fmr1* KO mouse [49–53] and in the Drosophila models of FXS [54–62]. *Fmr1* mutant mouse with a 50% reduction in mGluR5 expression was generated to demonstrate that a range of FXS phenotypes could be corrected by downregulating signaling through group 1 mGluRs [45]. Those findings showed that the decrease in mGlu5 expression levels from early embryonic development effectively prevented the onset of a broad range of FXS phenotypes, including audiogenic seizures, increased basal protein synthesis, spine density, although no effect on macroorchidism was observed.

MPEP (2-methyl-6-phenylethynyl-pyridine) was the first mGluR5-antagonist tested in the *Fmr1* KO mouse, which demonstrated rescue of behavioral defects, including open field performance [63], the rescue of the spine/filopodia ratio in *Fmr1* KO neurons to the levels observed in wild-type neurons [64]. Further, MPEP treated *Fmr1* KO mouse showed improved behavior by significantly fewer errors, less perseveration, and

impulsivity when navigating mazes, in addition to reverse postsynaptic density-95 (PSD-95) protein deficits which, if confirmed, could be considered a molecular biomarker [65]. Finally, MPEP prevented an abnormal clustering of DHPG (group I mGluR agonist (S)-3,5-dihydroxyphenylglycine) responsive cells (responsible for activation of ionotropic receptors in mouse FXS neurospheres) and corrected morphological defects of differentiated cells [66].

Similarly, a study of chronic treatment of *Fmr1* KO mouse with the long-acting mGlu5 inhibitor 2-chloro-4-((2,5-dimethyl-1-(4-(trifluoromethoxy)phenyl)-1H-imidazol-4-yl)ethynyl) pyridine (CTEP), fully corrected numerous phenotypes including increased synaptic spine density, protein synthesis rate, aberrant synaptic plasticity, learning and memory deficits, increased body growth rate, and sensitivity to audiogenic seizures [reference here]. In addition, that study showed a reduction of both extracellular signal-regulated kinase (ERK) activity and mTOR phosphorylation levels in the *Fmr1* KO but not in wild-type (WT) animals, suggesting that they could represent potential biomarkers in FXS [53]. Those studies have shown that the long-term, uninterrupted mGluR5 inhibition is essential for a successful pharmacological intervention, as a single dose of the mGluR5 inhibitors was not sufficient to correct the mouse phenotypes [50,53]. One of the potential molecular mechanisms for mGluR5 dysfunction in FXS is the decreased association of mGluR5 with the Homer family of scaffolding proteins. Indeed, genetic deletion of H1 (an activity-inducible isoform of Homer1) restored regular mGluR5-long Homer association in the *Fmr1* KO and corrected much of the mGluR5 dysfunction as well as behavioral phenotypes, including anxiety and audiogenic seizures [67]. Further, the disruption of mGluR5-Homer resulted in phenotypes of FXS including reduced mGluR5 association

with the postsynaptic density, deficits in agonist-induced translational control, protein synthesis-independent LTD, neocortical hyperexcitability, audiogenic seizures, and altered behaviors, such as anxiety and sensorimotor gating [68].

The Drosophila genome encodes only a single mGluR (DmGluRA), compared to the eight separate receptors in mammals [69]. The simplicity of the Drosophila system, coupled with the evolutionary conservation of the activation pathways, has provided an excellent model to test the mGluR hypothesis. Treatment with lithium and MPEP restored normal courtship behavior, mushroom, body defects, and short-term memory, but not β-lobe crossing, suggesting that other morphological abnormalities are responsible for the memory defects [54,70].

Molecular analyses revealed an inverse relationship between dFMRP and DmGluRA, with the latter overexpressed in *dFmr1* null animals and dFMRP overexpressed in DmGluRA nulls [57]. The DmGluRA null also shows more striking defects in activity-dependent synaptic function, including high transmission amplitudes during high-frequency stimulation and abnormally strong hyper potentiation following high-frequency stimulation [57,58]. The successful unbiased screen for small molecules that can rescue the lethality of glutamate-treated larvae and adults *dFmr1* mutants, using the mGluR5 noncompetitive antagonist MPEP or LiCl has been reported to rescue naïve courtship behavior, immediate recall memory, and short-term memory of d*Fmr1* mutants [56,59]. The compelling results of those preclinical studies, showing evidence of benefits in rodent and Drosophila disease models, have prompted the application of mGlu5 inhibitors as potential target treatments in human clinical trials for FXS. Thus, clinical trials in FXS

patients have been conducted to explore the safety, tolerability, and efficacy of a number of different mGluR5 antagonists.

Fenobam [71], the first mGlur5 antagonist drug evaluated in a single-dose open-label study of 12 male and female adults with FXS (mean age 23.9 years), showed trends of improvement in a prepulse-inhibition deficit relative to controls who did not receive the drug [72]. Subsequently, in an exploratory study, the efficacy of mavoglurant (AFQ056) [73] was tested in a randomized double-blind crossover study of 30 FXS males. In that study, seven patients with a hypermethylated full mutation with no detectable *FMR1* mRNA expression, improved stereotypic behavior, hyperactivity, and inappropriate speech; while no improvement was found in 18 patients with partial promoter methylation [74]. Thus, it appears that those with fully methylated alleles responded best, whereas those who were mosaics with partial methylation had a variable response with a lack of overall efficacy in that group. Although methylation is often regarded as a biomarker, results to date do not explain why some of those without methylated alleles responded while others did not [74]. In addition, the reported behavioral effects of stereotypic behavior, hyperactivity, and inappropriate speech were not replicated with adolescent FXS males and females, and with adults, with either full or partial *FMR1* methylation in subsequent 12-week double-blind mavoglurant studies [75].

Similarly, an extensive proof-of-concept study was conducted with basimglurant, a potent and selective mGluR5-negative allosteric modulator (NAM) [76,77], and mavoglurant, in male and female adults with FXS. In spite of their promising results in preclinical studies [77–80] those studies ended because no improvements were observed in the clinical phenotype of patients enrolled in the clinical trials using those modulators

[29,81,82]. Recently, in a phase 2, 12-week double-blind clinical trial, basimglurant did not demonstrate improvement over placebo in a parallel-group study of 183 adults and adolescents (aged 14–50, mean 23.4 years) with FXS [83]. Later, the study reported the long-term safety and efficacy of mavoglurant in the two open-label extensions in adolescent ($n = 119$, aged 12–19 years) and adult ($n = 148$, aged 18–45 years). In both studies, mavoglurant was well tolerated, and moderate behavioral improvements were observed in FXS as compared to the placebo control group. Thus, the compelling preclinical evidence for the therapeutic potential of mGlu5 inhibitors in the mouse and the Drosophila disease models has not translated in the anticipated benefits and improvement of the phenotype in FXS patients [84].

4. γ-Aminobutyric Acid (GABA) Receptors.

GABA is the most prominent inhibitory neurotransmitter, acting through three receptors in the brain. $GABA_A$ receptors are ligand-regulated chloride channels that upon activation cause hyperpolarization in mature neurons; $GABA_B$ receptors are heterodimeric G protein-coupled receptors (GPCRs) which are mostly expressed presynaptically in the brain; and, $GABA_C$ is a CYS-loop ligand-gated ion channel receptor with a similar pentameric structure to $GABA_A$ but which is homomeric. FMRP directly binds several $GABA_A$ receptor (α1, α2, α3, δ, and γ2) mRNAs, resulting in reduced expression in the cortex and cerebellum of young *Fmr1* KO mice. Thus, the mRNA expression levels of those subunits could, in principle, be used as biomarkers; however, they have not been studied in clinical trials for FXS with any GABA agonists [85]. The

introduction of a yeast artificial chromosome (YAC) containing the "healthy" human *FMR1* genomic region into the *Fmr1* KO mouse rescued (increased) the expression of those specific $GABA_A$ receptors subunits [86]. A recent electrophysiological study supported the notion that the δ subunit of the $GABA_A$ receptors ($GABA_A$Rs) is compromised in the *Fmr1* KO mouse, reporting a 4-fold decrease in tonic inhibition [87].

The delay in switching from depolarizing to hyperpolarizing GABA has also been observed in the cortex of *Fmr1* KO mouse during development [88]. Moreover, the oxytocin-mediated, GABA excitation–inhibition shift that occurs in newborn rodents during delivery is absent from the hippocampal neurons of *Fmr1* KO mouse. As a result, the hippocampal neurons have elevated intracellular chloride levels, increased excitatory GABA, enhanced the glutamatergic activity, and elevated gamma oscillations [89].

In one study, the response of FXS neurons (differentiated *in vitro* from human embryonic stem cells lacking synaptic activity) has been investigated by pulse application of the neurotransmitter GABA [reference]. The results confirmed that human FXS neurons do not respond to GABA, as FMRP plays a role in the development of the GABAergic synapse during neurogenesis, and that might be one of the potential reasons for the observed default synaptic activity in FXS patients. [90]. Some GABA agonists have been used in the *Fmr1* KO mouse to rescue behavioral abnormalities. The primary neuron excitability deficits in the amygdala of the *Fmr1* KO mouse was restored by gaboxadol (THIP), a $GABA_A$ receptor agonist, which also improved some specific behavioral characteristics, including hyperactivity and auditory seizures [91]. The treatment of the *Fmr1* KO mouse with bumetanide (specific NKCC1 chloride importer antagonist) normalized electrophysiological abnormalities in the mutant offspring as well as reducing

hyperactivity and autistic behaviors [89]. Finally, arbaclofen, a $GABA_B$ agonist, improved protein synthesis, the abnormal auditory-evoked gamma oscillations, working memory and anxiety-related behavior in *Fmr1* KO mouse [92–94].

Thus, these findings from different studies in the FXS animal models confirmed that GABA receptors are suitable targets for target treatment in FXS [18,39,95–103]. Indeed, two phase 3 placebo-controlled trials were conducted (with subjects aged 12–50 and in subjects aged 5–11) to determine the safety and efficacy of arbaclofen for improving social behavior in FXS patients. Although, arbaclofen did not meet the primary outcome measures of improved social avoidance in FXS in either study [104], in a double-blind placebo-controlled crossover trial [105], improved social function and behavior were reported in FXS patients. Acamprosate, which activates $GABA_B$ and $GABA_A$ receptors, also improved several phenotypes, such as cortical upstate duration, behavioral improvement, anxiety, locomotor tests in *Fmr1* KO mouse, and reduced ERK1/2 activation in brain tissue [106]. Acamprosate has also been tested in an open-label 10-week trial of 12 young children aged 6–17 years with FXS. It was found to be safe and well-tolerated, and resulted in better social behavior and reduced hyperactivity [107]. Ganaxolone is a neurosteroid and a positive $GABA_A$ modulator that rescued several phenotypes in the *Fmr1* KO mouse, inclduing increased marble-burying assay, sensory and sensorimotor gating in the acoustic startle response, and prepulse inhibition [86]. Ganaxolone, tested in a recent randomized double-blind placebo-controlled crossover trial in children with FXS, aged 6–17 years, was found to be safe and to have beneficial effects in some patients, particularly for those with higher anxiety or lower cognitive abilities [108]. These preclinical and clinical studies strengthen the hypothesis that GABA

receptors are involved in the pathogenesis of FXS and as they are the major inhibitory receptors in the brain, they point to the therapeutic potential of the GABA receptor particularly for the behavioral and epileptic phenotypes associated with fragile X syndrome.

5. De Novo Protein Synthesis

Synaptic strength plays a crucial role in learning and memory and it is compromised in many neurodevelopmental disorders. One of the molecular mechanisms that regulate spine morphology, and therefore synaptic strength, is local de novo protein synthesis, which enables synapses to alter their function and structure autonomously [109]. FMRP, an RNA binding protein that acts as a translational repressor of many synaptic proteins, is crucial in regulating this process, and the partial or complete lack of FMRP in FXS leads to increased protein translation at the synapses. The metabotropic glutamate receptor subtype 5 (mGluR5) theory of FXS also indicates that the imbalance of mechanisms involved in synaptic shaping and protein translation are responsible for many of the symptoms observed in FXS patients [49]. The lack of FMRP also leads to a loss of translational control and to increased rates of cerebral protein synthesis (rCPS) in some regions of the brain, including the hippocampus, thalamus, and hypothalamus of the *Fmr1* KO mouse model of FXS [110].

Fibroblasts from FXS patients also showed significantly elevated rates of basal protein synthesis along with increased levels of the phosphorylated target of rapamycin (p-mTOR), phosphorylated extracellular signal-regulated kinase ½ (ERK1/2), and

phosphorylated p70 ribosomal S6 kinase 1 (p-S6K1) [111]. Similarly, a recent study reported that the level of protein synthesis is increased in fibroblast cell lines derived from individuals with FXS and from *Fmr1* KO mouse [reference]. However, this cellular phenotype (elevated protein synthesis) exhibits a broad variation with cells from some individuals with FXS and from the *Fmr1* KO mouse showing a basal *de novo* protein synthesis within the normal range. These findings indicate that the molecular mechanisms that control protein synthesis are the primary targets in FXS. However, altered protein synthesis may not be the cause of all symptoms observed in FXS and, therefore, those with normal levels of protein synthesis are not likely going to benefit from target treatments aimed to lower protein synthesis [112]. Thus, de novo protein synthesis could be a very useful biomarker to predict phenotypic subgroups, symptoms severity, and treatment response. Further, as the rates of protein synthesis were decreased in both control and patient fibroblasts upon treatment with small molecules that block S6K1 and phosphoinositide 3-kinase (PI3K) catalytic subunit p110β of fibroblast cells derived from FXS patients, the roles of these targets as a potential biomarker should be considered [111]. FXS subjects, under propofol sedation, showed a reduced rCPS in whole brain, cerebellum, and cortex compared to sedated controls. Similar results have been observed in most regions examined in sedated *Fmr1* KO mice as compared to the WT mouse, suggesting that changes in synaptic signaling can correct increased rCPS in FXS [113]. Chronic dietary lithium treatment also demonstrated efficacy in reversing the increased rCPS in the *Fmr1* KO mouse [114].

Some studies have shown that the mechanisms regulating the levels of protein synthesis can be restored by reducing the mGluR5 signaling genetically or with

pharmacological treatments [46,53,100,115–118]. Moreover, haploinsufficiency of mGluR5; or reduction of MMP9, of striatal-enriched tyrosine phosphatase (STEP) signaling, or of S6K signaling; can not only restore the levels of protein synthesis but also restore the synaptic and behavioral phenotypes in the FXS mouse model [50,119–126]. Recently, a study showed that treatment of the *Fmr1* KO mouse with a cell-permeable peptide able to modulate ADAM metallopeptidase domain 10 (ADAM10) activity and amyloid-β protein precursor (APP) processing, restored protein synthesis to the wild-type (WT) level [127].

These preclinical and clinical studies suggest that basal protein synthesis could be considered as a potential biomarker and a molecular hallmark for FXS; unfortunately, replicating this optimal translational scenario has not been fully successful in the treatment setting [27]. The extent to which excessive protein synthesis is associated with cognitive and behavioral impairments also remains unknown. More importantly, none of the human studies have shown an effect on the primary outcome measures which were mainly behavioral questionnaires in children, adolescents, or adults with FXS [74,104,105]. Finally, although FMRP modulates protein synthesis, there are other factors (environmental and genetic) that may contribute to the modulation of homeostasis of molecules involved in synaptic plasticity.

6. Phosphoinositide 3-kinase (PI3K)

Phosphoinositide 3-kinase (PI3K) is the signaling molecule involved in cell motility, survival, growth, and proliferation. PI3K class I catalytic subunits, p110α, p110β, p110γ,

and p110δ, are specifically dysregulated in FXS [128]. FMRP regulates the synthesis and synaptic localization of p110β, which is a crucial signaling molecule downstream of group 1 metabotropic glutamate receptor (gp1 mGluRs) and other membrane receptors. Lack of FMRP in the *Fmr1* KO mouse leads to excess mRNA translation and synaptic protein expression of p110β [123]. Treatment with a p110β-selective antagonist was effective in rescuing the excess protein synthesis in the *Fmr1* KO mouse synaptoneurosomes and in lymphoblastoid cells derived from FXS patients [123,129]. Further, prefrontal cortex (PFC) selective knockdown of p110β reversed deficits in higher cognition, normalized excessive PI3K activity, restored stimulus-induced protein synthesis, and corrected increased dendritic spine density in the *Fmr1* KO mouse [130,131]. Thus, PI3K activity in patient cells might be a biomarker and could be used to assess the efficacy of drug response in target treatment in FXS.

7. Mammalian Target of Rapamycin (mTOR) and Substrate p70 Ribosomal S6 Kinase (S6K1)

Mammalian target of rapamycin (mTOR) is a 289 kDa serine/threonine kinase protein that controls various energetic functions at both the cellular and organism level; and is an essential regulator of cell proliferation, autophagy, translation, and growth [references]. In neuronal cells, protein synthesis plays a fundamental role in the regulation of lasting alterations in synaptic strength or plasticity, and of long-term potentiation (LTP); processes that are important in learning and memory [132,133]. The components of the mTOR signaling cascade, which is involved in protein synthesis-dependent phase of

synaptic strengthening, are present in dendrites, suggesting a role for mTOR in local translation and synaptic plasticity. mTOR is activated in dendrites by stimulation of group I mGluRs and it is required for mGluR-LTD [134,135]. It has been reported that increased activity in these systems can lead to repetitive and perseverative behavior patterns [132].

The best-characterized function of mTOR is the regulation of translation. mTOR regulates two critical and core components of the translational initiation machinery, p70 ribosomal S6 kinase 1 and 2 (S6K1/2), and the eIF4E-binding proteins (4E-BPs), and it is also known to regulate the activity of phosphatases such as protein phosphatase 2A (PP2A) [referemce]. These phosphatases, in turn, regulate mTOR substrates, thereby generating mTOR-dependent feedback loops that control initiation rates [references]. Increased phosphorylation of (mTOR) substrate, p70 ribosomal subunit 6 kinase 1 (S6K1) along with the high expression of mTOR regulator, and the serine/threonine protein kinase (Akt) was also observed in lymphocytes and brain tissues derived from subjects with FXS [136].

The enhanced mTOR signaling observed in the hippocampus of the *Fmr1* KO mouse is associated with the increase eukaryotic initiation factor complex F4 (eIF4F) [137] and with the increased phosphorylation of the cap-binding protein eukaryotic initiation factor 4E (eIF4E) [136] to further support the increased protein synthesis observed in FXS. These findings, in both FXS mice and humans, are consistent with the idea that the loss of FMRP results in the dysregulation of mechanisms of translational initiation control rather than transcriptional regulation and provide the direct evidence that mTOR dysregulation may be useful for designing targeted treatments in FXS [136]. Therefore, targets and substrates in the mTOR signaling pathways can act as potential molecular

biomarkers. Since the molecular signaling effects resulting from FMRP loss are likely causal in the wide-range of the symptoms of FXS, including autism, identifying the effects of FMRP loss on molecular signaling pathways, like those governing translation, is key to advancing our ability to treat the disorder.

Finally, metformin, a type 2 diabetes medication that can improve obesity and excessive appetite, has emerged as a candidate drug for targeted treatment of FXS based on preclinical studies [reference]. These studies have shown rescue of a number of FXS phenotypes including memory deficits, social novelty, grooming, dendritic spine morphology, and electrophysiology in the CA1 of the hippocampus [138,139]. Metformin suppresses mRNA translation via inhibition of ERK and mTOR pathways, which are overactive in FXS, supporting their potential role as molecular biomarkers, and therefore, may contribute to normalizing signaling pathways in the CNS of FXS patients. In humans, metformin has been used in the clinical treatment of several individuals with FXS and showed benefits not only in lowering weight gain but also in improving language and behavior [138]. Thus, metformin shows promises for targeting several signaling pathways disrupted in FXS and possibly rescuing some of the clinical symptoms observed in individuals with FXS. Interestingly, an ongoing double-blind placebo-controlled trial of metformin in individuals with FXS will assess safety and benefit of metformin in the treatment of language deficits, behavioral problems, and obesity in individuals with FXS.

8. Extracellular-Regulated Kinase (ERK)

The ERK pathway is a chain of proteins in the cell that acts as a nodal point for cell signaling cascades. The absence of FMRP in *Fmr1* KO mouse results in rapid

dephosphorylation of ERK upon mGluR1/5 stimulation, suggesting that over-activation of phosphatases in synapses affects the synaptic translation, transcription, and synaptic receptor regulation in FXS [53,119,140,141]. Delayed early-phase phosphorylation of ERK is observed in both neurons and thymocytes of the *Fmr1* KO mouse. Likewise, the early-phase kinetics of ERK activation in lymphocytes from human peripheral blood is also delayed in individuals with FXS, as compared to controls [142]. The correction of the delayed ERK activation time, resulting in a faster activation, was observed after 2 months of treatment with lithium or with riluzole in a pilot open-label trial in FXS [143,144]. These findings, based on a small number of subjects, suggest that ERK activity is a potential biomarker for measuring the metabolic status of the disease in FXS.

Recently, the significant FMRP-dependent over-activation of ERK was observed in both FXS mouse and humans. ERK activity was normalized in FXS platelets [145], and correlated with clinical response to lovastatin, pointing to this inhibitor of ERK pathway signaling cascade as a promising treatment for FXS [146]. The findings by Pellerin et al. [145] suggest that the use of platelet ERK activity represents a new, potentially interesting biomarker for future clinical trials. It may also pave the way for other promising and very exciting discoveries that will eventually improve FXS patients' assessment in future clinical trials where either lovastatin or other ERK-targeting drugs is applied.

9. Matrix Metalloproteinase-9 (MMP-9)

FMRP deficit is associated with alterations in the expression of a number of proteins, including matrix metalloproteinase 9 (MMP-9). MMP-9 is an extracellular Zn^{2+}-dependent

endopeptidase that is expressed in neurons and locally translated and released at the dendrites in response to enhanced neuronal activity driven by glutamate. MMP-9 plays an essential role both in establishing synaptic connections during development and in restructuring synaptic networks in the adult brain [147]. MMP-9 mRNA is part of the FMRP complex and localizes in dendrites. Translation of MMP-9 is increased at synapses in *Fmr1* KO mice suggesting its contribution to the aberrant dendritic spine morphology observed in the *Fmr1* KO mice and in FXS patients [148,149]. The genetic disruption of MMP-9 in the *Fmr1* KO mouse rescued key aspects of *Fmr1* abnormalities, including abnormal mGluR5-dependent LTD and dendritic spine abnormalities [150], providing evidence that elevated MMP-9 is responsiblefor the development of at least some of the FXS-associated defects in the *Fmr1* KO mouse. Interestingly, a high level of MMP-9 has been observed in the auditory cortex of adult *Fmr1* KO mice, and the deletion of MMP-9 reversed habituation defects [151]. Decreased MMP-9 activity in the hippocampus of the *Fmr1* KO mouse, following treatment with the antibiotic, minocycline, promoted dendritic spine maturation, improvement in anxiety, and strategic exploratory behavior [152]. These findings prompted the assessment of minocycline as a targeted treatment in humans with FXS through open-label trials, which have demonstrated benefits, including improvements in language, attention, social communication, and anxiety [153,154]. More recently, a controlled double-blind crossover study of minocycline for FXS treatment provided evidence for the safety of minocycline, and showed benefits in global functioning in children with FXS [155]. In addition, as expected, the higher plasma activity of MMP-9 observed in FXS patients was lowered by minocycline in some patients [156], as minocycline is known to be a MMP-9 inhibitor [152]. On the other hand, no changes in

plasma MMP 9 activity were found after treatment with sertraline [157], a selective serotonin-reuptake inhibitor that selectively blocks the uptake of serotonin at the presynaptic membrane; the block results in increased synaptic (CNS)serotonin concentration and, therefore, to an intensified serotonergic neurotransmission. Interestingly, a reduction of MMP-9 levels was also reported in the *Fmr1* KO mouse following metformin treatment [139]. The results of the preclinical and clinical studies indicate that minocycline, through its mechanism of action as an MMP inhibitor, may be an additional potential effective avenue as FXS therapeutic treatment and MMP-9 activity, a potential biomarker in FXS.

10. Brain-Derived Neurotrophic Factor (BDNF)

Brain-derived neurotrophic factor is involved in the regulation of various processes of normal neural circuit function and development. Dysregulation in BDNF/TrkB signaling in the *Fmr1* KO mouse leads to altered brain development, including excessive sponginess, dendritic arborization [158], and impaired synaptic plasticity [159]. These neural alterations are promoted by activity-dependent variation in the sensitivity to BDNF-TrkB signaling, compensating postsynaptic activity [158].

The effects of reduced BDNF expression on learning and behavioral phenotypes, including fear conditioning, pain behaviors, and hyperactivity, were examined in the *Fmr1* KO mouse crossed with a mouse carrying a deletion of one copy of the *Bdnf* gene (*Bdnf+/−*) [160]. The authors reported age-dependent alterations in the expression of BDNF in the hippocampus, reduced locomotor hyperactivity, deficits in sensorimotor

learning, and startle responses typical of *Fmr*1 KO mice. In addition, altered BDNF signaling in FMRP-deficient neural progenitor cells (NPCs) suggested that perturbations of brain development in FXS occur at very early stages of development [161].

A single-nucleotide polymorphism (SNP) in the human BDNF gene, leading to a methionine (Met) substitution for valine (Val) at amino acid 66, interferes with the intercellular trafficking and the activity-dependent secretion of BDNF in cortical neurons [references]. One study found that the Val66Met BDNF polymorphism associates with epilepsy in a Finnish FXS male [162], a result that was was not confirmed in a group of 77 patients with FXS [157]. However, a significant association between the BDNF polymorphism and improvements of several clinical measures was observed in a double-blind randomized placebo-controlled clinical trial of sertraline in FXS, aimed to determine the efficacy of treatment in young children with FXS [157]. In addition, an open-label study showed a significant increase in BDNF level after treatment with the GABA$_A$ agonist acamprosate [107]. Although more studies are warranted, these findings point to BDNF genotype as a potential molecular biomarker in FXS.

11. Amyloid-β Protein Precursor and Amyloid-β (APP, Aβ)

FMRP protein binds to the coding region of the APP mRNA and results in increased translation of the encoded product, the amyloid precursor protein (APP), which plays a vital role in the developing brain during synapse formation, while β-amyloid (Aβ) accumulation, results in synaptic loss and impaired neurotransmission. APP is processed by β- and γ-secretases to produce amyloid-β (Aβ), which is the prominent peptide found in the case of Alzheimer's disease (AD).

A study by Westmark et al. (year) found a 1.7-fold increase APP expression in the *Fmr1* KO mouse versus WT using western blot analysis and showed that the genetic knockdown of one APP allele in the *Fmr1* KO mouse rescued the FXS phenotypes including anxiety, seizures, mGLuR-LTD, and the ratio of mature versus immature dendritic spines [163]. APP and Aβ were evaluated as blood-based biomarkers and in a prospective open-label trial of acamprosate in pediatric subjects with FXS-associated autism spectrum disorder and found that acamprosate treatment significantly reduced sAPP and sAPPα [164].

Although blood levels of APP metabolites may not correlate with brain levels, which is one of the limitations of these studies, altogether these findings support a role for dysregulated APP production and processing in FXS and indicate that the APP metabolites may be viable biomarkers for FXS treatment.

12. Additional Potential Biomarkers

12.1. Ion Channels (CaV)

Voltage-gated ion channels are involved in neural transmission and some recent studies showed their involvement of these ion channels in FXS pathology [165]; more specifically, with the voltage-gated calcium channel (VGCC) family, namely Cav2.1 and Cav2.2 [166]. Synaptic transmission depends critically on presynaptic calcium entry via voltage-gated calcium (CaV) channels. FMRP regulates the expression of neuronal N-type CaV channels (CaV2.2) [166] and dysregulated calcium homeostasis, in addition to the decreased expression of the pore-forming subunit of the Cav2.1 channel, the

Cacna1a gene, in *Fmr1*-KO cultured neurons [167]. Their findings indicate that FMRP plays a key role in calcium homeostasis during brain development; furthermore, the authors suggest that calcium homeostasis could be used as a cellular biomarker and for the identification of new drugs for target treatment in FXS.

12.2. Glycogen Synthase Kinase-3 (GSK-3)

Glycogen synthase kinase-3 (GSK-3) is a serine/threonine protein kinase that, when phosphorylated, regulates a variety of developmental processes, such as cell migration, cell morphology, neurogenesis, and gliogenesis via interaction with a variety of signaling pathways [168]. The lack of FMRP results in an abnormal increase in GSK-3β mRNA and protein levels in several regions of the brain [169] of the *Fmr1* KO mouse and in decreased hippocampal neurogenesis that likely contributes to the pathogenesis of FXS [170].

Several studies have demonstrated that lithium treatment rescued the FXS-associated impairments sustainable throughout the aging process in the Drosophila model of FXS [54,59]. In addition, GSK-3 inhibitors and lithium treatment provided the direct evidence of GSK-3 involvement in the pathology of FXS by reducing audiogenic seizure activity, improving performance on the open–field, elevated plus maze and passive avoidance tests [171], improved social defects [172], rescue of the hippocampus-dependent learning deficits [173], and improved cognitive deficits [174] in the *Fmr1* KO mouse. Additionally, the attenuation of reactive astrocytes, which has been observed in many brain regions of the *Fmr1* KO mouse with lithium treatment, provides further evidence of the involvement of GSK-3 in FXS [175]. These findings raise the possibility

that GSK-3 activity may represent a biochemical mediator biomarker of impaired cognitive function in FXS, and that modulator of its activity may have potential as therapeutic agents [176].

12.3. Striatal-Enriched Protein Tyrosine Phosphatase (STEP)

Striatal-enriched protein tyrosine phosphatase (STEP) is a brain-specific tyrosine phosphatase that plays a significant role in the development of the CNS by regulating dendritic proteins involved in synaptic plasticity [177,178]. STEP dysregulation is involved in the pathophysiology of several neuropsychiatric disorders [179], including FXS, likely by dephosphorylating both NMDARs and AMPARs [177]. While the enhanced activity of mGluRs in the absence of FMRP upregulates the translation of STEP [178,180,181] in the hippocampus of the *Fmr1* KO mouse, genetic reduction of STEP significantly diminishes some FXS-associated behaviors in *Fmr1* KO including seizures, and restores select social and nonsocial anxiety-related behaviors [181]. Benzopentathiepin 8-(trifluoromethyl)-1,2,3,4,5-benzopentathiepin-6-amine hydrochloride (known as TC-2153) is a newly discovered STEP inhibitor [182]. A recent study [183] reported that this STEP inhibitor reduces seizure incidence and hyperactivity, anxiety and improves sociability, electrophysiological deficits in acute brain slices and spine morphology in *Fmr1* KO mouse. These observations suggest that STEP's expression and activity could be useful for evaluating the clinical benefits of pharmacological therapeutic approaches in FXS targeting STEP.

12.4. Plasma Cytokines and Chemokines

Cytokines are the most important mediators of cell–cell communication in the human immune system. They perform a variety of functions like modulation of the central nervous system (CNS), brain functioning, and responses to infections or injury. Significant differences in plasma cytokine and chemokines levels were reported in patients with FXS including a high level of IL-1α, RANTES, and IP-10 [184]. It is currently unknown whether the changes in the cytokine and chemokines are determinants in the development of FXS, and whether they occur throughout the lifetime of FXS patients; therefore, their potential use as biomarkers needs more investigation.

12.5. Diacylglycerol Kinase Kappa (Dgkκ)

Diacylglycerol kinase kappa (Dgkκ) is a master regulator that controls two critical signaling pathways involved in protein synthesis. Lack of FMRP in the *Fmr1* KO mouse neurons results in the loss of Dgkκ expression along with mGluR1 receptor dependent DGK activity, leading to synaptic plasticity alterations, dendritic spine abnormalities, and behavior disorders. These findings support the involvement of Dgkκ deregulation in FXS pathology and suggest that overexpression of Dgkκ in neurons could rescue the dendritic spine defects of the *Fmr1* KO mouse. Thus, DGKκ expression levels could represent a biomarker and targeting DGKκ signaling might provide new therapeutic approaches for FXS [185].

12.6. MicroRNAs (miRNAs)

MicroRNAs (miRNAs) are known as a class of small noncoding RNA molecules (19–23 nucleotides) that regulate almost 30% of genes at the post-transcriptional level in eukaryotic organisms [186]. Several studies have provided evidence of miRNA involvement in the pathogenesis of FXS by identifying and isolating several r(CGG)-derived miRNAs, including miR-fmr1-27 and miR-fmr1-42 in the zebrafish FXS model [187,188]. Their brains exhibit long dendrites and disconnected synapses, similar to those found in the human FXS hippocampal–neocortical junction [189]. Further, microarray analyses of miRNAs associated with FMRP in the *Fmr1* KO mouse brain identified miR-125a, miR-125b, and miR-132; and disruption of the regulation of these miRNAs in -mediating protein translation resulted in early neural development and synaptic physiology [190,191]. Another microarray study [192] of the *Fmr1* KO mouse showed the interaction of miR-34b, miR-340, and miR-148a with the Met 3′ UTR of the *FMR1* gene, suggesting that alterations in the miRNA expression resulting from the absence of FMRP, could contribute to the molecular pathology of FXS. Enhanced expression of miR-510, located on chromosome X in the 27.3Xq region, flanking to a fragile X site, was reported in full mutation female carriers [193]. Thus, although more studies are necessary to confirm their utility, many pieces of evidence indicate that miRNAs could be attractive candidate biomarkers in FXS.

13. Conclusions

FXS is a challenging disorder in terms of drug development and clinical implementation. An extensive body of preclinical work, carried out in the FXS animal

models, has provided ways to improve behavior, language, and cognitive ability; but several factors (complex clinical phenotype, genetic variability, gender differences, use of multiple medications, and limitations in the outcome measures and of tools) might have contributed to a lack of translation from the preclinical to clinical outcomes. When looking at the design of the preclinical studies to date, some limitations can be identified. Most of the FXS research in mammalian model systems is limited to two disease models, the *Fmr1* KO mouse and *Fmr1* KO drosophila animal model, but the central issue in using these models is variability and small effect size of the phenotype particularly in the area of cognitive defects. Moreover, overlapping phenotypes in these animal models sometimes may lead to over-prediction of the therapeutic potential of novel drug treatments.

Research to date on FXS has provided us with several potential candidate biomarkers that can, in principle, be used to assess efficacy; molecular biomarkers are promising, simple, and minimally invasive diagnostic tools that can objectively measure the biologically relevant effects of targeted treatments on the underlying molecular defects observed in FXS. However, the current research on molecular biomarkers in FXS suffers from a number of limitations. FXS is a neurological disorder, but brain tissue is not easily accessible. Therefore, biomarkers must be developed in a tissue that can be obtained easily, such as PBMCs, platelets, and fibroblasts. No single, consistent molecular or modification state (i.e., phosphorylation or acetylation) has been reported to be differentially regulated in FXS patients versus controls consistently across multiple testing sites. Although many molecular biomarkers have been proposed in FXS [**Figure 2**], noneprovides sufficient sensitivity/specificity to follow disease responses in a clinical trial

setting. No clinical history for any marker is available, and lengthy expensive processing and time consumption are required to generate test substrates such as primary fibroblasts (and induced pluripotent stem cells).

In summary, there is an urgent need to establish novel and reliable biomarkers in FXS, particularly blood-based biomarkers, essential to the development of new treatments. They can provide measures of disease severity and can be used to develop personalized treatments. Interestingly, when monitored over time, they can be used to evaluate treatment outcomes and help to identify responders, and therefore those individuals that following treatment have shown real benefit with phenotype improvements.

14. References

1. Biomarkers and surrogate endpoints: Preferred definitions and conceptual framework. *Clin. Pharmacol. Ther.* 2001, *69*, 89–95.

2. Harris, S.; Goodlin-Jones, B.; Nowicki, S.; Bacalman, S.; Tassone, F.; Hagerman, R. Autism Profiles of Young Males with Fragile X Syndrome. *J. Dev. Behav. Pediatr.* 2005, *26*, 464.

3. Landowska, A.; Rzonca, S.; Bal, J.; Gos, M. [Fragile X syndrome and *FMR1*-dependent diseases - clinical presentation, epidemiology and molecular background]. *Dev. N.a. Med.* 2018, *22*, 14–21.

4. Verkerk, A.J.; Pieretti, M.; Sutcliffe, J.S.; Fu, Y.-H.; Kuhl, D.P.; Pizzuti, A.; Reiner, O.; Richards, S.; Victoria, M.F.; Zhang, F.; et al. Identification of a gene

(FMR-1) containing a CGG repeat coincident with a breakpoint cluster region exhibiting length variation in fragile X syndrome. *Cell* 1991, *65*, 905–914.

5. Oberlé, I.; Rousseau, F.; Heitz, D.; Kretz, C.; Devys, D.; Hanauer, A.; Boué, J.; Bertheas, M.; Mandel, J. Instability of a 550-base pair DNA segment and abnormal methylation in fragile X syndrome. *Science* 1991, *252*, 1097–1102.

6. Pieretti, M.; Zhang, F.; Fu, Y.-H.; Warren, S.T.; Oostra, B.A.; Caskey, C.; Nelson, D.L. Absence of expression of the FMR-1 gene in fragile X syndrome. *Cell* 1991, *66*, 817–822.

7. Tassone, F.; Hall, D.A. *FXTAS, FXPOI, and Other Premutation Disorders*; Springer Nature, 2016;.

8. Hagerman, R.J.; Protic, D.; Rajaratnam, A.; Salcedo-Arellano, M.J.; Aydin, E.Y.; Schneider, A. Fragile X-Associated Neuropsychiatric Disorders (FXAND). *Front. Psychol.* 2018, *9*, 564.

9. Santos, A.R.; Bagni, C.; Kanellopoulos, A.K. Learning and behavioral deficits associated with the absence of the fragile X mental retardation protein: what a fly and mouse model can teach us. *Learn. Mem.* 2014, *21*, 543–55.

10. Sandoval, G.M.; Shim, S.; Hong, D.S.; Garrett, A.S.; Quintin, E.-M.; Marzelli, M.J.; Patnaik, S.; Lightbody, A.A.; Reiss, A.L. Neuroanatomical abnormalities in fragile X syndrome during the adolescent and young adult years. *J. Psychiatr.* 2018, *107*, 138–144.

11. Bostrom, C.; Yau, S.-Y.; Majaess, N.; Vetrici, M.; Gil-Mohapel, J.; Christie, B.R.; Yau, S.S.Y. Hippocampal dysfunction and cognitive impairment in Fragile-X Syndrome. *Neurosci. Biobehav. Rev.* 2016, *68*, 563–574.

12.   Hoeft, F.; Carter, J.C.; Lightbody, A.A.; Hazlett, H.C.; Piven, J.; Reiss, A.L. Region-specific alterations in brain development in one- to three-year-old boys with fragile X syndrome. *Proc. Acad. Sci.* 2010, *107*, 9335–9339.

13.   Harlow, E.G.; Till, S.M.; Russell, T.A.; Wijetunge, L.S.; Kind, P.; Contractor, A. Critical period plasticity is disrupted in the barrel cortex of *Fmr1* knockout mice. *Neuron* 2010, *65*, 385–398.

14.   Lai, J.; Lerch, J.; Doering, L.; Foster, J.; Ellegood, J.; Lai, J. Regional brain volumes changes in adult male *FMR1*-KO mouse on the FVB strain. *Neuroscience* 2016, *318*, 12–21.

15.   Hazlett, H.C.; Poe, M.D.; Lightbody, A.A.; Styner, M.; MacFall, J.R.; Reiss, A.L.; Piven, J. Trajectories of Early Brain Volume Development in Fragile X Syndrome and Autism. *J. Am. Acad. Child Adolesc. Psychiatry* 2012, *51*, 921–933.

16.   Measurement of Cerebral and Cerebellar Volumes in Children with Fragile X Sundrome. Available online: https://paperpile.com/app/p/2405c439-1b64-0314-96b7-37ba0f0ea488 (accessed 12 January 2019).

17.   Sunamura, N.; Iwashita, S.; Enomoto, K.; Kadoshima, T.; Isono, F. Loss of the fragile X mental retardation protein causes aberrant differentiation in human neural progenitor cells. *Sci. Rep.* 2018, *8*, 11585.

18.   Yang, Y.-M.; Arsenault, J.; Bah, A.; Krzeminski, M.; Fekete, A.; Chao, O.Y.; Pacey, L.K.; Wang, A.; Forman-Kay, J.; Hampson, D.R.; et al. Identification of a molecular locus for normalizing dysregulated GABA release from interneurons in the Fragile X brain. *Mol. N.a.* 2018, 1.

19. Hanson, A.C.; Hagerman, R.J. Serotonin dysregulation in Fragile X Syndrome: implications for treatment. *Intractable Rare Dis.* 2014, *3*, 110–117.

20. The Dutch-Belgian Fragile X Consorthium; Bakker, C.E.; Verheij, C.; Willemsen, R.; van der Helm, R.; Oerlemans, F.; Vermey, M.; Bygrave, A.; Hoogeveen, A.; Oostra, B.A.; et al. *Fmr1* Knockout Mice: A Model to Study Fragile X Mental Retardation. *Cell* 1994, *78*, 22–23.

21. Dahlhaus, R. Of Men and Mice: Modeling the Fragile X Syndrome. *Front. Neurosci.* 2018, *11*, 41.

22. Rais, M.; Binder, D.K.; Razak, K.A.; Ethell, I.M. Sensory Processing Phenotypes in Fragile X Syndrome. *ASN Neuro* 2018, *10*, 1759091418801092.

23. Greco, C.M.; Berman, R.F.; Martin, R.M.; Tassone, F.; Schwartz, P.H.; Chang, A.; Trapp, B.D.; Iwahashi, C.; Brunberg, J.; Grigsby, J.; et al. Neuropathology of Fragile X-Associated Tremor/ataxia Syndrome (FXTAS). *Brain* 2006, *129*, 243–255.

24. Irwin, S.A.; Galvez, R.; Greenough, W.T. Dendritic Spine Structural Anomalies in Fragile-X Mental Retardation Syndrome. *Cereb. Cortex* 2000, *10*, 1038–1044.

25. Bernardet, M.; Crusio, W.E. *Fmr1* KO Mice as a Possible Model of Autistic Features. *Sci. N.a. J.* 2006, *6*, 1164–1176.

26. Wright, J. Questions for Elizabeth Berry-Kravis: Dodging mouse traps | Spectrum | Autism Research News. Available online: https://www.spectrumnews.org/opinion/q-and-a/questions-for-elizabeth-berry-kravis-dodging-mouse-traps/ (accessed on 9 January 2019).

27. Berry-Kravis, E.M.; Lindemann, L.; Jønch, A.E.; Apostol, G.; Bear, M. F.; Carpenter, R.L.; Crawley, J.N.; Curie, A.; Des Portes, V.; Hossain, F.; et al. Drug Development for Neurodevelopmental Disorders: Lessons Learned from Fragile X Syndrome. *Nat. Rev. Drug Discov.* 2018, *17*, 280–299.

28. Scharf, S.H.; Jaeschke, G.; Wettstein, J.G.; Lindemann, L. Metabotropic glutamate receptor 5 as drug target for Fragile X syndrome. *Curr. Opin. Pharmacol.* 2015, *20*, 124–134.

29. Mullard, A. Fragile X drug development flounders. *Nat. Rev. Drug Discov.* 2016, *15*, 77.

30. De Caro, J.J.; Dominguez, C.; Sherman, S.L. Reproductive Health of Adolescent Girls Who Carry the *FMR1* Premutation: Expected Phenotype Based on Current Knowledge of Fragile X-Associated Primary Ovarian Insufficiency. *Ann. N. Y. Acad. Sci.* 2008, *1135*, 99–111.

31. Roberts, J.E.; Bailey, D.B.; Mankowski, J.; Ford, A.; Sideris, J.; Weisenfeld, L.A.; Heath, T.M.; Golden, R.N. Mood and anxiety disorders in females with the *FMR1* premutation. *Am. J. Med Genet. N.a. B: Neuropsychiatr. Genet.* 2009, *150*, 130–139.

32. Hamlin, A.; Liu, Y.; Nguyen, D.V.; Tassone, F.; Zhang, L.; Hagerman, R.J. Sleep apnea in fragile X premutation carriers with and without FXTAS. *Am. J. Med Genet. N.a. B: Neuropsychiatr. Genet.* 2011, *156*, 923–928.

33. Hamlin, A.A.; Sukharev, D.; Campos, L.; Mu, Y.; Tassone, F.; Hessl, D.; Nguyen, D.V.; Loesch, D.; Hagerman, R.J. Hypertension in *FMR1* Premutation

Males With and Without Fragile X-Associated Tremor/Ataxia Syndrome (FXTAS). *Am. J. Med Genet. N.a. A* 2012, *158*, 1304–1309.

34.   Bailey, D.B.; Raspa, M.; Bishop, E.; Mitra, D.; Martin, S.; Wheeler, A.; Sacco, P. Health and Economic Consequences of Fragile X Syndrome for Caregivers. *J. Dev. Behav. Pediatr.* 2012, *33*, 705–712.

35.   Ji, N.Y.; Findling, R.L. Pharmacotherapy for mental health problems in people with intellectual disability. *Curr. Opin.* 2016, *29*, 103–125.

36.   Lieb-Lundell, C.C.E. Three Faces of Fragile X. *Phys. Ther.* 2016, *96*, 1782–1790.

37.   Hoyos, L. R.; Thakur, M. Fragile X Premutation in Women: Recognizing the Health Challenges beyond Primary Ovarian Insufficiency. *J. Assist. Reprod. Genet.* 2017, *34*, 315–323.

38.   Napoli, E.; Schneider, A.; Hagerman, R.; Song, G.; Wong, S.; Tassone, F.; Giulivi, C. Impact of *FMR1* Premutation on Neurobehavior and Bioenergetics in Young Monozygotic Twins. *Front. Genet.* 2018, *9*, 9.

39.   Ligsay, A.; Hagerman, R.J. Review of targeted treatments in fragile X syndrome. *Intractable Rare Dis.* 2016, *5*, 158–167.

40.   Hagerman, P.J. The Fragile X Prevalence Paradox. *J. Med. Genet.* 2008, *45*, 498–499.

41.   Stembalska, A.; Łaczmańska, I.; Gil, J.; Pesz, K.A. Fragile X Syndrome in Females—A Familial Case Report and Review of the Literature. *Dev. Period. Med.* 2016, *20*, 99–104.

42.   Berry-Kravis, E.; Potanos, K.; Weinberg, D.; Zhou, L.; Goetz, C.G. Fragile X-Associated Tremor/ataxia Syndrome in Sisters Related to X-Inactivation. *Ann. Neurol.* 2005, *57*, 144–147.

43.   Van Esch, H. The Fragile X premutation: new insights and clinical consequences. *Eur. J. Med Genet.* 2006, *49*, 1–8.

44.   Seltzer, M.M.; Abbeduto, L.; Greenberg, J.S.; Almeida, D.; Hong, J.; Witt, W. Chapter 7 Biomarkers in the Study of Families of Children with Developmental Disabilities. *Families* 2009, *37*, 213–249.

45.   Bear, M.F.; Huber, K.M.; Warren, S.T. The mGluR theory of fragile X mental retardation. *N.a. Neurosci.* 2004, *27*, 370–377.

46.   Dölen, G.; Bear, M.F. Role for Metabotropic Glutamate Receptor 5 (mGluR5) in the Pathogenesis of Fragile X Syndrome. *J. Physiol.* 2008, *586*, 1503–1508.

47.   Kim, M.; Ceman, S. Fragile X Mental Retardation Protein: Past, Present and Future. *N.a. Pept. Sci.* 2012, *13*, 358–371.

48.   Darnell, J. C.; Klann, E. The Translation of Translational Control by FMRP: Therapeutic Targets for FXS. *Nat. Neurosci.* 2013, *16*, 1530–1536.

49.   Huber, K.M.; Gallagher, S.M.; Warren, S.T.; Bear, M.F. Altered Synaptic Plasticity in a Mouse Model of Fragile X Mental Retardation. *Proceed. Nat. Acad. Sci.* 2002, *99*, 7746–7750.

50.   Dölen, G.; Osterweil, E.; Rao, B.S.S.; Smith, G.B.; Auerbach, B.D.; Chattarji, S.; Bear, M.F. Correction of fragile X syndrome in mice. *Neuron* 2007, *56*, 955–962.

51. Krueger, D.D.; Bear, M.F. Toward Fulfilling the Promise of Molecular Medicine in Fragile X Syndrome. *Annu. Med.* 2011, *62*, 411–429.

52. Bhakar, A.L.; Dölen, G.; Bear, M.F. The Pathophysiology of Fragile X (and What It Teaches Us about Synapses). *Annu. Neurosci.* 2012, *35*, 417–443.

53. Michalon, A.; Sidorov, M.; Ballard, T.M.; Ozmen, L.; Spooren, W.; Wettstein, J.G.; Jaeschke, G.; Bear, M.F.; Lindemann, L. Chronic Pharmacological mGlu5 Inhibition Corrects Fragile X in Adult Mice. *Neuron* 2012, *74*, 49–56.

54. McBride, S.M.; Choi, C.H.; Wang, Y.; Liebelt, D.; Braunstein, E.; Ferreiro, D.; Sehgal, A.; Siwicki, K.K.; Dockendorff, T.C.; Nguyen, H.T.; et al. Pharmacological Rescue of Synaptic Plasticity, Courtship Behavior, and Mushroom Body Defects in a Drosophila Model of Fragile X Syndrome. *Neuron* 2005, *45*, 753–764.

55. Pan, L.; Broadie, K.S. Drosophila Fragile X Mental Retardation Protein and Metabotropic Glutamate Receptor A Convergently Regulate the Synaptic Ratio of Ionotropic Glutamate Receptor Subclasses. *J. Neurosci.* 2007, *27*, 12378–12389.

56. Chang, S.; Bray, S.M.; Li, Z.; Zarnescu, D.C.; He, C.; Jin, P.; Warren, S.T. Identification of small molecules rescuing fragile X syndrome phenotypes in Drosophila. *Nat. Methods* 2008, *4*, 256–263.

57. Pan, L.; Woodruff, E., 3rd; Liang, P.; Broadie, K. Mechanistic Relationships between Drosophila Fragile X Mental Retardation Protein and Metabotropic Glutamate Receptor A Signaling. *Mol. Cell. Neurosci.* 2008, *37*, 747–760.

58.   Repicky, S.; Broadie, K. Metabotropic Glutamate Receptor-Mediated Use-Dependent down-Regulation of Synaptic Excitability Involves the Fragile X Mental Retardation Protein. *J. Neurophysiol.* 2009, *101*, 672–687.

59.   Choi, C.H.; McBride, S.M.J.; Schoenfeld, B.P.; Liebelt, D.A.; Ferreiro, D.; Ferrick, N.J.; Hinchey, P.; Kollaros, M.; Rudominer, R.L.; Terlizzi, A.M.; et al. Age-dependent cognitive impairment in a Drosophila Fragile X model and its pharmacological rescue. *Biogerontology* 2009, *11*, 347–362.

60.   Kanellopoulos, A.K.; Semelidou, O.; Kotini, A.G.; Anezaki, M.; Skoulakis, E.M.C. Learning and Memory Deficits Consequent to Reduction of the Fragile X Mental Retardation Protein Result from Metabotropic Glutamate Receptor-Mediated Inhibition of cAMP Signaling in Drosophila. *J. Neurosci.* 2012, *32*, 13111–13124.

61.   Tessier, C.R.; Broadie, K. Molecular and Genetic Analysis of the Drosophila Model of Fragile X Syndrome. *Results Probl. Cell Differ.* 2012, *54*, 119–156.

62.   Drozd, M.; Bardoni, B.; Capovilla, M. Modeling Fragile X Syndrome in Drosophila. *Front. Neurosci.* 2018, *11*, 124.

63.   Yan, Q.; Rammal, M.; Tranfaglia, M.; Bauchwitz, R.; Bauchwitz, R. Suppression of two major Fragile X Syndrome mouse model phenotypes by the mGluR5 antagonist MPEP. *Neuropharmacology* 2005, *49*, 1053–1066.

64.   De Vrij, F.M.; Levenga, J.; Van Der Linde, H.C.; Koekkoek, S.K.; De Zeeuw, C.I.; Nelson, D.L.; Oostra, B.A.; Willemsen, R. Rescue of behavioral phenotype and neuronal protrusion morphology in *Fmr1* KO mice. *Neurobiol. Dis.* 2008, *31*, 127–132.

65.   Gandhi, R.M.; Kogan, C.S.; Messier, C.; Gandhi, R.M. 2-Methyl-6-(phenylethynyl) pyridine (MPEP) reverses maze learning and PSD-95 deficits in *Fmr1* knock-out mice. *Front. Cell. Neurosci.* 2014, *8*, 70.

66.   Achuta, V.S.; Grym, H.; Putkonen, N.; Louhivuori, V.; Kärkkäinen, V.; Koistinaho, J.; Roybon, L.; Castrén, M.L. Metabotropic Glutamate Receptor 5 Responses Dictate Differentiation of Neural Progenitors to NMDA-Responsive Cells in Fragile X Syndrome. *Dev. Neurobiol.* 2017, *77*, 438–453.

67.   Ronesi, J.A.; Collins, K.A.; Hays, S.A.; Tsai, N.-P.; Guo, W.; Birnbaum, S.G.; Hu, J.-H.; Worley, P.F.; Gibson, J.R.; Huber, K.M. Disrupted Homer scaffolds mediate abnormal mGluR5 function in a mouse model of fragile X syndrome. *Nat. Neurosci.* 2012, *15*, 431–440.

68.   Guo, W.; Molinaro, G.; Collins, K.A.; Hays, S.A.; Paylor, R.; Worley, P.F.; Szumlinski, K.K.; Huber, K.M. Selective Disruption of Metabotropic Glutamate Receptor 5-Homer Interactions Mimics Phenotypes of Fragile X Syndrome in Mice. *J. Neurosci.* 2016, *36*, 2131–2147.

69.   Bogdanik, L.; Mohrmann, R.; Ramaekers, A.; Bockaert, J.; Grau, Y.; Broadie, K.; Parmentier, M.-L. The Drosophila Metabotropic Glutamate Receptor DmGluRA Regulates Activity-Dependent Synaptic Facilitation and Fine Synaptic Morphology. *J. Neurosci.* 2004, *24*, 9105–9116.

70.   Michel, C.I.; Kraft, R.; Restifo, L.L. Defective Neuronal Development in the Mushroom Bodies of Drosophila Fragile X Mental Retardation 1 Mutants. *J. Neurosci.* 2004, *24*, 5798–5809.

71. Porter, R.H.P.; Jaeschke, G.; Spooren, W.; Ballard, T.M.; Büttelmann, B.; Kolczewski, S.; Peters, J.-U.; Prinssen, E.; Wichmann, J.; Vieira, E.; et al. Fenobam: A Clinically Validated Nonbenzodiazepine Anxiolytic Is a Potent, Selective, and Noncompetitive mGlu5 Receptor Antagonist with Inverse Agonist Activity. *J. Pharmacol. Exp. Ther.* 2005, *315*, 711–721.

72. Berry-Kravis, E.; Hessl, D.; Coffey, S.; Hervey, C.; Schneider, A.; Yuhas, J.; Hutchison, J.; Snape, M.; Tranfaglia, M.; Nguyen, D.V.; et al. A pilot open label, single dose trial of fenobam in adults with fragile X syndrome. *J. Med Genet.* 2009, *46*, 266–271.

73. Vranesic, I.; Ofner, S.; Flor, P.J.; Bilbe, G.; Bouhelal, R.; Enz, A.; Desrayaud, S.; McAllister, K.; Kuhn, R.; Gasparini, F. AFQ056/mavoglurant, a Novel Clinically Effective mGluR5 Antagonist: Identification, SAR and Pharmacological Characterization. *Bioorg. Med. Chem.* 2014, *22*, 5790–5803.

74. Jacquemont, S.; Curie, A.; Portes, V.D.; Torrioli, M.G.; Berry-Kravis, E.; Hagerman, R.J.; Ramos, F.J.; Cornish, K.; He, Y.; Paulding, C.; et al. Epigenetic Modification of the *FMR1* Gene in Fragile X Syndrome Is Associated with Differential Response to the mGluR5 Antagonist AFQ056. *Sci. Transl. Med.* 2011, *3*, 64ra1.

75. Berry-Kravis, E.; Hagerman, R.; Jacquemont, S.; Charles, P.; Visootsak, J.; Brinkman, M.; Rerat, K.; Koumaras, B.; Zhu, L.; Barth, G.M.; et al. Mavoglurant in fragile X syndrome: Results of two randomized, double-blind, placebo-controlled trials. *Sci. Transl. Med.* 2016, *8*, 321.

76. Jaeschke, G.; Kolczewski, S.; Spooren, W.; Vieira, E.; Bitter-Stoll, N.; Boissin, P.; Borroni, E.; Büttelmann, B.; Ceccarelli, S.; Clemann, N.; et al. Metabotropic Glutamate Receptor 5 Negative Allosteric Modulators: Discovery of 2-Chloro-4-[1-(4-fluorophenyl)-2,5-dimethyl-1H-imidazol-4-ylethynyl]pyridine (Basimglurant, RO4917523), a Promising Novel Medicine for Psychiatric Diseases. *J. Med. Chem.* 2015, *58*, 1358–1371.

77. Lindemann, L.; Porter, R.H.; Scharf, S.H.; Kuennecke, B.; Bruns, A.; Von Kienlin, M.; Harrison, A.C.; Paehler, A.; Funk, C.; Gloge, A.; et al. Pharmacology of Basimglurant (RO4917523, RG7090), a Unique Metabotropic Glutamate Receptor 5 Negative Allosteric Modulator in Clinical Development for Depression. *J. Pharmacol. Exp. Ther.* 2015, *353*, 213–233.

78. Gantois, I.; Pop, A.S.; De Esch, C.E.; Buijsen, R.A.; Pooters, T.; Gomez-Mancilla, B.; Gasparini, F.; Oostra, B.A.; D'Hooge, R.; Willemsen, R. Chronic administration of AFQ056/Mavoglurant restores social behaviour in *Fmr1* knockout mice. *Behav. Brain* 2013, *239*, 72–79.

79. Pop, A.S.; Levenga, J.; de Esch, C.E.F.; Buijsen, R.A.M.; Nieuwenhuizen, I.M.; Li, T.; Isaacs, A.; Gasparini, F.; Oostra, B.A.; Willemsen, R. Rescue of Dendritic Spine Phenotype in *Fmr1* KO Mice with the mGluR5 Antagonist AFQ056/Mavoglurant. *Psychopharmacology* 2014, *231*, 1227–1235.

80. Levenga, J.; Hayashi, S.; De Vrij, F.M.; Koekkoek, S.K.; Van Der Linde, H.C.; Nieuwenhuizen, I.; Song, C.; Buijsen, R.A.; Pop, A.S.; GomezMancilla, B.; et al. AFQ056, a new mGluR5 antagonist for treatment of fragile X syndrome. *Neurobiol. Dis.* 2011, *42*, 311–317.

81. Tranfaglia, M. Roche reports Fragile X clinical trial negative results. Available online: https://www.fraxa.org/roche-reports-clinical-trial-negative-results/ (accessed on 10 January 2019).

82. FRAXA Research Foundation. Novartis Discontinues Development of mavoglurant (AFQ056) for Fragile X Syndrome. Fragile X Research—FRAXA Research Foundation. Available online: https://www.fraxa.org/novartis-discontinues-development-mavoglurant-afq056-fragile-x-syndrome/ (accessed on 10 January 2019).

83. A Youssef, E.; Berry-Kravis, E.; Czech, C.; Hagerman, R.J.; Hessl, D.; Wong, C.Y.; Rabbia, M.; Deptula, D.; John, A.; Kinch, R.; et al. Effect of the mGluR5-NAM Basimglurant on Behavior in Adolescents and Adults with Fragile X Syndrome in a Randomized, Double-Blind, Placebo-Controlled Trial: FragXis Phase 2 Results. *Neuropsychopharmacol* 2017, *43*, 503–512.

84. Hagerman, R.; Jacquemont, S.; Berry-Kravis, E.; Des Portes, V.; Stanfield, A.; Koumaras, B.; Rosenkranz, G.; Murgia, A.; Wolf, C.; Apostol, G.; et al. Mavoglurant in Fragile X Syndrome: Results of Two Open-Label, Extension Trials in Adults and Adolescents. *Sci. Rep.* 2018, *8*, 16970.

85. D'Hulst, C.; Heulens, I.; Brouwer, J.R.; Willemsen, R.; De Geest, N.; Reeve, S.P.; De Deyn, P.P.; Hassan, B.A.; Kooy, R.F. Expression of the GABAergic system in animal models for fragile X syndrome and fragile X associated tremor/ataxia syndrome (FXTAS). *Brain Res.* 2009, *1253*, 176–183.

86. Braat, S.; D'Hulst, C.; Heulens, I.; De Rubeis, S.; Mientjes, E.; Nelson, D.L.; Willemsen, R.; Bagni, C.; Van Dam, D.; De Deyn, P.P.; et al. The GABAA receptor

is an FMRP target with therapeutic potential in fragile X syndrome. *Function of a membrane-embedded domain evolutionarily multiplied in the GPI lipid anchor pathway proteins PIG-B, PIG-M, PIG-U, PIG-W, PIG-V, and PIG-Z* 2015, *14*, 2985–2995.

87.   Zhang, N.; Peng, Z.; Tong, X.; Lindemeyer, A.K.; Cetina, Y.; Huang, C.S.; Olsen, R.W.; Otis, T.S.; Houser, C.R. Decreased Surface Expression of the δ Subunit of the GABAA Receptor Contributes to Reduced Tonic Inhibition in Dentate Granule Cells in a Mouse Model of Fragile X Syndrome. *Exp. Neurol.* 2017, *297*, 168–178.

88.   He, Q.; Nomura, T.; Xu, J.; Contractor, A. The Developmental Switch in GABA Polarity Is Delayed in Fragile X Mice. *J. Neurosci.* 2014, *34*, 446–450.

89.   Tyzio, R.; Nardou, R.; Ferrari, D.C.; Tsintsadze, T.; Shahrokhi, A.; Eftekhari, S.; Khalilov, I.; Tsintsadze, V.; Brouchoud, C.; Chazal, G.; et al. Oxytocin-Mediated GABA Inhibition During Delivery Attenuates Autism Pathogenesis in Rodent Offspring. *Science* 2014, *343*, 675–679.

90.   Telias, M.; Segal, M.; Ben-Yosef, D. Immature Responses to GABA in Fragile X Neurons Derived from Human Embryonic Stem Cells. *Front. Cell. Neurosci.* 2016, *10*, 167.

91.   Olmos-Serrano, J.L.; Corbin, J.G.; Burns, M.P. The GABAA Receptor Agonist THIP Ameliorates Specific Behavioral Deficits in the Mouse Model of Fragile X Syndrome. *Dev. Neurosci.* 2011, *33*, 395–403.

92.   Sinclair, D.; Featherstone, R.; Naschek, M.; Nam, J.; Du, A.; Wright, S.; Pance, K.; Melnychenko, O.; Weger, R.; Akuzawa, S.; et al. GABA-B Agonist

Baclofen Normalizes Auditory-Evoked Neural Oscillations and Behavioral Deficits in the *Fmr1* Knockout Mouse Model of Fragile X Syndrome. *Eneuro* 2017, *4*, ENEURO.0380–16.2017.

93.   Qin, M.; Huang, T.; Kader, M.; Krych, L.; Xia, Z.; Burlin, T.; Zeidler, Z.; Zhao, T.; Smith, C.B. R-Baclofen Reverses a Social Behavior Deficit and Elevated Protein Synthesis in a Mouse Model of Fragile X Syndrome. *Int. J. Neuropsychopharmacol.* 2015, *18*, 18.

94.   Henderson, C.; Wijetunge, L.; Kinoshita, M.N.; Shumway, M.; Hammond, R.S.; Postma, F.R.; Brynczka, C.; Rush, R.; Thomas, A.; Paylor, R.; et al. Reversal of Disease-Related Pathologies in the Fragile X Mouse Model by Selective Activation of GABAB Receptors with Arbaclofen. *Sci. Transl. Med.* 2012, *4*, 152.

95.   Kang, J.-Y.; Chadchankar, J.; Vien, T.N.; Mighdoll, M.I.; Hyde, T.M.; Mather, R.J.; Deeb, T.Z.; Pangalos, M.N.; Brandon, N.J.; Dunlop, J.; et al. Deficits in the activity of presynaptic γ-aminobutyric acid type B receptors contribute to altered neuronal excitability in fragile X syndrome. *J. Boil. Chem.* 2017, *292*, 6621–6632.

96.   Wang, L.; Wang, Y.; Zhou, S.; Yang, L.; Shi, Q.; Li, Y.; Zhang, K.; Yang, L.; Zhao, M.; Yang, Q.; et al. Imbalance between Glutamate and GABA in *Fmr1* Knockout Astrocytes Influences Neuronal Development. *Genes* 2016, *7*, 45.

97. Zhao, W.; Wang, J.; Song, S.; Li, F.; Yuan, F. Reduction of α1GABAA receptor mediated by tyrosine kinase C (PKC) phosphorylation in a mouse model of fragile X syndrome. *Int. J. Clin. Exp. Med.* 2015, *8*, 13219–13226.

98.   Fatemi, S.H.; Folsom, T.D. GABA receptor subunit distribution and FMRP–mGluR5 signaling abnormalities in the cerebellum of subjects with schizophrenia, mood disorders, and autism. *Schizophr. Res.* 2015, *167*, 42–56.

99.   Braat, S.; Kooy, R.F. Fragile X syndrome neurobiology translates into rational therapy. *Drug Discov. N.a.* 2014, *19*, 510–519.

100.   Lozano, R.; Hare, E.B.; Hagerman, R.J. Modulation of the GABAergic pathway for the treatment of fragile X syndrome. *Neuropsychiatr. Dis. Treat.* 2014, *10*, 1769–1779.

101.   Olmos-Serrano, J.L.; Paluszkiewicz, S.M.; Martin, B.S.; Kaufmann, W.E.; Corbin, J.G.; Huntsman, M.M. Defective GABAergic Neurotransmission and Pharmacological Rescue of Neuronal Hyperexcitability in the Amygdala in a Mouse Model of Fragile X Syndrome. *J. Neurosci.* 2010, *30*, 9929–9938.

102.   Curia, G.; Papouin, T.; Séguéla, P.; Avoli, M. Downregulation of Tonic GABAergic Inhibition in a Mouse Model of Fragile X Syndrome. *Cereb. Cortex* 2008, *19*, 1515–1520.

103.   Centonze, D.; Rossi, S.; Mercaldo, V.; Napoli, I.; Ciotti, M.T.; De Chiara, V.; Musella, A.; Prosperetti, C.; Calabresi, P.; Bernardi, G.; et al. Abnormal Striatal GABA Transmission in the Mouse Model for the Fragile X Syndrome. *Boil. N.a.* 2008, *63*, 963–973.

104.   Berry-Kravis, E.; Hagerman, R.; Visootsak, J.; Budimirovic, D.; Kaufmann, W.E.; Cherubini, M.; Zarevics, P.; Walton-Bowen, K.; Wang, P.; Bear, M.F.; et al. Arbaclofen in fragile X syndrome: results of phase 3 trials. *J. Neurodev. Disord.* 2017, *9*, 3.

105. Berry-Kravis, E.M.; Hessl, D.; Rathmell, B.; Zarevics, P.; Cherubini, M.; Walton-Bowen, K.; Mu, Y.; Nguyen, D.V.; Gonzalez-Heydrich, J.; Wang, P.P.; et al. Effects of STX209 (Arbaclofen) on Neurobehavioral Function in Children and Adults with Fragile X Syndrome: A Randomized, Controlled, Phase 2 Trial. *Sci. Transl. Med.* 2012, *4*, 152ra127.

106. Schaefer, T.L.; Davenport, M.H.; Grainger, L.M.; Robinson, C.K.; Earnheart, A.T.; Stegman, M.S.; Lang, A.L.; Ashworth, A.A.; Molinaro, G.; Huber, K.M.; et al. Acamprosate in a Mouse Model of Fragile X Syndrome: Modulation of Spontaneous Cortical Activity, ERK1/2 Activation, Locomotor Behavior, and Anxiety. *J. Neurodev. Disord.* 2017, *9*, 6.

107. Erickson, C.A.; Wink, L.K.; Ray, B.; Early, M.C.; Stiegelmeyer, E.; Mathieu-Frasier, L.; Patrick, V.; Lahiri, D.K.; McDougle, C.J. Impact of acamprosate on behavior and brain-derived neurotrophic factor: an open-label study in youth with fragile X syndrome. *Psychopharmacology* 2013, *228*, 75–84.

108. Ligsay, A.; Van Dijck, A.; Nguyen, D.V.; Lozano, R.; Chen, Y.; Bickel, E.S.; Hessl, D.; Schneider, A.; Angkustsiri, K.; Tassone, F.; et al. A randomized double-blind, placebo-controlled trial of ganaxolone in children and adolescents with fragile X syndrome. *J. Neurodev. Disord.* 2017, *9*, 26.

109. Jung, H.; Yoon, B.C.; Holt, C.E. Axonal mRNA Localization and Local Protein Synthesis in Nervous System Assembly, Maintenance and Repair. *Nat. Rev. Neurosci.* 2012, *13*, 308–324.

110.   Qin, M.; Kang, J.; Burlin, T.V.; Jiang, C.; Smith, C.B. Postadolescent Changes in Regional Cerebral Protein Synthesis: An In Vivo Study in the *Fmr1* Null Mouse. *J. Neurosci.* 2005, *25*, 5087–5095.

111.   Kumari, D.; Bhattacharya, A.; Nadel, J.; Moulton, K.; Zeak, N.M.; Glicksman, A.; Dobkin, C.; Brick, D.J.; Schwartz, P.H.; Smith, C.B.; et al. Identification of Fragile X Syndrome-Specific Molecular Markers in Human Fibroblasts: A Useful Model to Test the Efficacy of Therapeutic Drugs. *Hum. Mutat.* 2014, *35*, 1485–1494.

112.   Jacquemont, S.; Pacini, L.; E Jønch, A.; Cencelli, G.; Rozenberg, I.; He, Y.; D'Andrea, L.; Pedini, G.; Eldeeb, M.; Willemsen, R.; et al. Protein synthesis levels are increased in a subset of individuals with fragile X syndrome. *Hum. Mol. Genet.* 2018, *27*, 2039–2051.

113.   Qin, M.; Schmidt, K.C.; Zametkin, A.J.; Bishu, S.; Horowitz, L.M.; Burlin, T.V.; Xia, Z.; Huang, T.; Quezado, Z.M.; Smith, C.B. Altered Cerebral Protein Synthesis in Fragile X Syndrome: Studies in Human Subjects and Knockout Mice. *J. Cereb. Blood Flow Metab.* 2013, *33*, 499–507.

114.   Liu, Z.-H.; Huang, T.; Smith, C.B. Lithium Reverses Increased Rates of Cerebral Protein Synthesis in a Mouse Model of Fragile X Syndrome. *Neurobiol. Dis.* 2012, *45*, 1145.

115.   Gross, C.; Hoffmann, A.; Bassell, G.J.; Berry-Kravis, E.M. Therapeutic Strategies in Fragile X Syndrome: From Bench to Bedside and Back. *Neurotherapeutics* 2015, *12*, 584–608.

116.   Jacquemont, S.; Berry-Kravis, E.; Hagerman, R.; von Raison, F.; Gasparini, F.; Apostol, G.; Ufer, M.; Des Portes, V.; Gomez-Mancilla, B. The Challenges of Clinical Trials in Fragile X Syndrome. *Psychopharmacology* 2014, *231*, 1237–1250.

117.   Pop, A.S.; Gomez-Mancilla, B.; Neri, G.; Willemsen, R.; Gasparini, F. Fragile X Syndrome: A Preclinical Review on Metabotropic Glutamate Receptor 5 (mGluR5) Antagonists and Drug Development. *Psychopharmacology* 2014, *231*, 1217–1226.

118.   Osterweil, E.K.; Chuang, S.-C.; Chubykin, A.A.; Sidorov, M.; Bianchi, R.; Wong, R.K.S.; Bear, M.F. Lovastatin corrects excess protein synthesis and prevents epileptogenesis in a mouse model of fragile X syndrome. *Neuron* 2013, *77*, 243–250.

119.   Bhattacharya, A.; Kaphzan, H.; Alvarez-Dieppa, A.C.; Murphy, J.P.; Pierre, P.; Klann, E. Genetic Removal of p70 S6 Kinase 1 Corrects Molecular, Synaptic, and Behavioral Phenotypes in Fragile X Syndrome Mice. *Neuron* 2012, *76*, 325–337.

120.   Reversal of activity-mediated spine dynamics and learning impairment in a mouse model of Fragile X syndrome. Available online: https://www.ncbi.nlm.nih.gov/pubmed/24712992 (accessed on 11 January 2019).

121.   Dolan, B.M.; Duron, S.G.; Campbell, D.A.; Vollrath, B.; Rao, B.S.S.; Ko, H.-Y.; Lin, G.G.; Govindarajan, A.; Choi, S.-Y.; Tonegawa, S.; et al. Rescue of fragile X syndrome phenotypes in *Fmr1* KO mice by the small-molecule PAK inhibitor FRAX486. *Proc. Acad. Sci.* 2013, *110*, 5671–5676.

122.   Bhattacharya, A.; Mamcarz, M.; Mullins, C.; Choudhury, A.; Boyle, R.G.; Smith, D.G.; Walker, D.W.; Klann, E. Targeting Translation Control with p70 S6 Kinase 1 Inhibitors to Reverse Phenotypes in Fragile X Syndrome Mice. *Neuropsychopharmacology* 2016, *41*, 1991–2000.

123.   Gross, C.; Nakamoto, M.; Yao, X.; Chan, C.-B.; Yim, S.Y.; Ye, K.; Warren, S.T.; Bassell, G.J. Excess Phosphoinositide 3-Kinase Subunit Synthesis and Activity as a Novel Therapeutic Target in Fragile X Syndrome. *J. Neurosci.* 2010, *30*, 10624–10638.

124.   Hayashi, M.L.; Rao, B.S.S.; Seo, J.-S.; Choi, H.-S.; Dolan, B.M.; Choi, S.-Y.; Chattarji, S.; Tonegawa, S.; Rao, B.S.S. Inhibition of p21-activated kinase rescues symptoms of fragile X syndrome in mice. *Proc. Acad. Sci.* 2007, *104*, 11489–11494.

125.   Tian, M.; Zeng, Y.; Hu, Y.; Yuan, X.; Liu, S.; Li, J.; Lu, P.; Sun, Y.; Gao, L.; Fu, D.; et al. 7, 8-Dihydroxyflavone induces synapse expression of AMPA GluA1 and ameliorates cognitive and spine abnormalities in a mouse model of fragile X syndrome. *Neuropharmacology* 2015, *89*, 43–53.

126.   Sawicka, K.; Pyronneau, A.; Chao, M.; Bennett, M.V.L.; Zukin, R.S. Elevated ERK/p90 ribosomal S6 kinase activity underlies audiogenic seizure susceptibility in fragile X mice. *Proc. Acad. Sci.* 2016, *113*, E6290–E6297.

127.   Pasciuto, E.; Ahmed, T.; Wahle, T.; Gardoni, F.; D'Andrea, L.; Pacini, L.; Jacquemont, S.; Tassone, F.; Balschun, D.; Dotti, C.G.; et al. Dysregulated ADAM10-Mediated Processing of APP during a Critical Time Window Leads to Synaptic Deficits in Fragile X Syndrome. *Neuron* 2015, *87*, 382–398.

128. Gross, C.; Bassell, G.J. Neuron-specific regulation of class I PI3K catalytic subunits and their dysfunction in brain disorders. *Front. Neurosci.* 2014, *7*, 7.

129. Gross, C.; Bassell, G.J. Excess Protein Synthesis in FXS Patient Lymphoblastoid Cells Can Be Rescued with a p110β-Selective Inhibitor. *Mol. Med.* 2012, *18*, 336–345.

130. Gross, C.; Raj, N.; Molinaro, G.; Allen, A.G.; Whyte, A.J.; Gibson, J.R.; Huber, K.M.; Gourley, S.L.; Bassell, G.J. Selective role of the catalytic PI3K subunit p110β in impaired higher-order cognition in Fragile X syndrome. *Cell Rep.* 2015, *11*, 681–688.

131. Gross, C.; Chang, C.-W.; Kelly, S.M.; Bhattacharya, A.; McBride, S.M.; Danielson, S.W.; Jiang, M.Q.; Chan, C.B.; Ye, K.; Gibson, J.R.; et al. Increased expression of the PI3K enhancer PIKE mediates deficits in synaptic plasticity and behavior in Fragile X syndrome. *Cell Rep.* 2015, *11*, 727–736.

132. Klann, E.; Dever, T.E. Biochemical mechanisms for translational regulation in synaptic plasticity. *Nat. Rev. Neurosci.* 2004, *5*, 931–942.

133. Richter, J.D.; Sonenberg, N. Regulation of cap-dependent translation by eIF4E inhibitory proteins. *Nat. Cell Boil.* 2005, *433*, 477–480.

134. Brems, H.; Legius, E.; Bagni, C.; Borrie, S.C. Cognitive Dysfunctions in Intellectual Disabilities: The Contributions of the Ras-MAPK and PI3K-AKT-mTOR Pathways. *Annu. Genom. Hum. Genet.* 2017, *18*, 115–142.

135. Zhu, P.J.; Chen, C.-J.; Mays, J.; Stoica, L.; Costa-Mattioli, M. mTORC2, but not mTORC1, is required for hippocampal mGluR-LTD and associated behaviors. *Nat. Neurosci.* 2018, *21*, 799–802.

136. Hoeffer, C.A.; Sanchez, E.; Hagerman, R.J.; Mu, Y.; Nguyen, D.V.; Wong, H.; Whelan, A.M.; Zukin, R.S.; Klann, E.; Tassone, F. Altered mTOR signaling and enhanced CYFIP2 expression levels in subjects with Fragile X syndrome. *Genes, Brain* 2012, *11*, 332–341.

137. Sharma, A.; Hoeffer, C.A.; Takayasu, Y.; Miyawaki, T.; McBride, S.M.; Klann, E.; Zukin, R.S. Dysregulation of mTOR Signaling in Fragile X Syndrome. *J. Neurosci.* 2010, *30*, 694–702.

138. Monyak, R.E.; Emerson, D.; Schoenfeld, B.P.; Zheng, X.; Chambers, D.B.; Rosenfelt, C.; Langer, S.; Hinchey, P.; Choi, C.H.; McDonald, T.V.; et al. Insulin Signaling Misregulation Underlies Circadian and Cognitive Deficits in a Drosophila Fragile X Model. *Mol. Psychiatry* 2017, *22*, 1140–1148.

139. Gantois, I.; Khoutorsky, A.; Popic, J.; Aguilar-Valles, A.; Freemantle, E.; Cao, R.; Sharma, V.; Pooters, T.; Nagpal, A.; Skalecka, A.; et al. Metformin ameliorates core deficits in a mouse model of fragile X syndrome. *Nat. Med.* 2017, *23*, 674–677.

140. Kim, S.H.; Markham, J.A.; Weiler, I.J.; Greenough, W.T. Aberrant early-phase ERK inactivation impedes neuronal function in fragile X syndrome. *Proc. Acad. Sci.* 2008, *105*, 4429–4434.

141. Hou, L.; Antion, M.D.; Hu, D.; Spencer, C.M.; Paylor, R.; Klann, E. Dynamic Translational and Proteasomal Regulation of Fragile X Mental Retardation Protein Controls mGluR-Dependent Long-Term Depression. *Neuron* 2006, *51*, 441–454.

142. Weng, N.; Weiler, I.J.; Sumis, A.; Greenough, W.T.; Berry-Kravis, E.; Berry-Kravis, E. Early-phase ERK activation as a biomarker for metabolic status in

fragile X syndrome. *Am. J. Med Genet. N.a. B: Neuropsychiatr. Genet.* 2008, *147*, 1253–1257.

143. Berry-Kravis, E.; Sumis, A.; Hervey, C.; Nelson, M.; Porges, S.W.; Weng, N.; Weiler, I.J.; Greenough, W.T. Open-Label Treatment Trial of Lithium to Target the Underlying Defect in Fragile X Syndrome. *J. Dev. Behav. Pediatr.* 2008, *29*, 293–302.

144. Erickson, C.A.; Weng, N.; Weiler, I.J.; Greenough, W.T.; Stigler, K.A.; Wink, L.K.; McDougle, C.J. Open-label riluzole in fragile X syndrome. *Brain Res.* 2011, *1380*, 264–270.

145. Pellerin, D.; Çaku, A.; Fradet, M.; Bouvier, P.; Dubé, J.; Corbin, F. Lovastatin corrects ERK pathway hyperactivation in fragile X syndrome: potential of platelet's signaling cascades as new outcome measures in clinical trials. *Biomarkers* 2016, *21*, 1–12.

146. Zamzow, R. Drug duo delivers brain, behavioral benefits for fragile X syndrome | Spectrum | Autism Research News. Available online: https://www.spectrumnews.org/news/drug-duo-delivers-brain-behavioral-benefits-fragile-x-syndrome/ (accessed on 11 January 2019).

147. Reinhard, S.M.; Razak, K.; Ethell, I.M. A delicate balance: role of MMP-9 in brain development and pathophysiology of neurodevelopmental disorders. *Front. Cell. Neurosci.* 2015, *9*, 280.

148. Janusz, A.; Miłek, J.; Perycz, M.; Pacini, L.; Bagni, C.; Kaczmarek, L.; Dziembowska, M. The Fragile X Mental Retardation Protein Regulates Matrix Metalloproteinase 9 mRNA at Synapses. *J. Neurosci.* 2013, *33*, 18234–18241.

149.   Taylor, A.K.; Tassone, F.; Dyer, P.N.; Hersch, S.M.; Harris, J.B.; Greenough, W.T.; Hagerman, R.J. Tissue heterogeneity of the *FMR1* mutation in a high-functioning male with fragile X syndrome. *Am. J. Med Genet.* 1999, *84*, 233–239.

150.   Sidhu, H.; Dansie, L.E.; Hickmott, P.W.; Ethell, D.W.; Ethell, I.M. Genetic Removal of Matrix Metalloproteinase 9 Rescues the Symptoms of Fragile X Syndrome in a Mouse Model. *J. Neurosci.* 2014, *34*, 9867–9879.

151.   Lovelace, J.W.; Wen, T.H.; Reinhard, S.; Hsu, M.S.; Sidhu, H.; Ethell, I.M.; Binder, D.K.; Razak, K.A. Matrix metalloproteinase-9 deletion rescues auditory evoked potential habituation deficit in a mouse model of Fragile X Syndrome. *Neurobiol. Dis.* 2016, *89*, 126–135.

152.   Bilousova, T.V.; Dansie, L.; Ngo, M.; Aye, J.; Charles, J.R.; Ethell, D.W.; Ethell, I.M. Minocycline Promotes Dendritic Spine Maturation and Improves Behavioural Performance in the Fragile X Mouse Model. *J. Med. Genet.* 2009, *46*, 94–102.

153.   Utari, A.; Chonchaiya, W.; Rivera, S.M.; Schneider, A.; Hagerman, R.J.; Faradz, S.M.H.; Ethell, I.M.; Nguyen, D.V. Side Effects of Minocycline Treatment in Patients With Fragile X Syndrome and Exploration of Outcome Measures. *Am. J. Intellect. Dev. Disabil.* 2010, *115*, 433–443.

154.   Paribello, C.; Tao, L.; Folino, A.; Berry-Kravis, E.; Tranfaglia, M.; Ethell, I.M.; Ethell, D.W. Open-label add-on treatment trial of minocycline in fragile X syndrome. *BMC Neurol.* 2010, *10*, 91.

155.   Leigh, M.J.S.; Nguyen, D.V.; Mu, Y.; Winarni, T.I.; Schneider, A.; Chechi, T.; Polussa, J.; Doucet, P.; Tassone, F.; Rivera, S.M.; et al. A Randomized Double-Blind, Placebo-Controlled Trial of Minocycline in Children and Adolescents with Fragile X Syndrome. *J. Dev. Behav. Pediatr.* 2013, *34*, 147–155.

156.   Dziembowska, M.; Pretto, D.I.; Janusz, A.; Kaczmarek, L.; Leigh, M.J.; Gabriel, N.; Durbin-Johnson, B.; Hagerman, R.J.; Tassone, F. High MMP-9 activity levels in fragile X syndrome are lowered by minocycline. *Am. J. Med Genet. N.a. A* 2013, *161*, 1897–1903.

157.   AlOlaby, R.R.; Sweha, S.R.; Silva, M.; Durbin-Johnson, B.; Yrigollen, C.M.; Pretto, D.; Hagerman, R.J.; Tassone, F. Molecular biomarkers predictive of sertraline treatment response in young children with fragile X syndrome. *Brain Dev.* 2017, *39*, 483–492.

158.   Kim, S.W.; Cho, K.J. Activity-dependent alterations in the sensitivity to BDNF-TrkB signaling may promote excessive dendritic arborization and spinogenesis in fragile X syndrome in order to compensate for compromised postsynaptic activity. *Med Hypotheses* 2014, *83*, 429–435.

159.   Louhivuori, V.; Vicario, A.; Uutela, M.; Rantamäki, T.; Louhivuori, L.M.; Castrén, E.; Tongiorgi, E.; Åkerman, K.E.; Castrén, M.L. BDNF and TrkB in neuronal differentiation of *Fmr1*-knockout mouse. *Neurobiol. Dis.* 2011, *41*, 469–480.

160.   Uutela, M.; Lindholm, J.; Louhivuori, V.; Wei, H.; Louhivuori, L.M.; Pertovaara, A.; Akerman, K.; Castrén, E.; Castrén, M.L. Reduction of BDNF

expression in*Fmr1*knockout mice worsens cognitive deficits but improves hyperactivity and sensorimotor deficits. *Genes, Brain* 2012, *11*, 513–523.

161.   Castrén, M. L.; Castrén, E. BDNF in Fragile X Syndrome. *Neuropharmacology* 2014, *76*, 729–736.

162.   Louhivuori, V.; Arvio, M.; Soronen, P.; Oksanen, V.; Paunio, T.; Castrén, M.L. The Val66Met polymorphism in the BDNF gene is associated with epilepsy in fragile X syndrome. *Epilepsy Research* 2009, *85*, 114–117.

163.   Westmark, C.J.; Westmark, P.R.; O'Riordan, K.J.; Ray, B.C.; Hervey, C.M.; Salamat, M. S.; Abozeid, S.H.; Stein, K.M.; Stodola, L. A.; Tranfaglia, M.; et al. Reversal of Fragile X Phenotypes by Manipulation of AβPP/Aβ Levels in *Fmr1*KO Mice. *PLoS ONE* 2011, *6*, e26549.

164.   Erickson, C.A.; Ray, B.; Maloney, B.; Wink, L.K.; Bowers, K.; Schaefer, T.L.; McDougle, C.J.; Sokol, D.K.; Lahiri, D.K. Impact of Acamprosate on Plasma Amyloid-β Precursor Protein in Youth: A Pilot Analysis in Fragile X Syndrome-Associated and Idiopathic Autism Spectrum Disorder Suggests a Pharmacodynamic Protein Marker. *J. Psychiatr.* 2014, *59*, 220–228.

165.   Lee, H.Y.; Jan, L.Y. Fragile X syndrome: mechanistic insights and therapeutic avenues regarding the role of potassium channels. *Curr. Opin. Neurobiol.* 2012, *22*, 887–894.

166.   Ferron, L.; Nieto-Rostro, M.; Cassidy, J.S.; Dolphin, A.C. Fragile X mental retardation protein controls synaptic vesicle exocytosis by modulating N-type calcium channel density. *Nat. Commun.* 2014, *5*, 3628.

167.   Castagnola, S.; Delhaye, S.; Folci, A.; Paquet, A.; Brau, F.; Duprat, F.; Jarjat, M.; Grossi, M.; Béal, M.; Martin, S.; et al. New Insights Into the Role of Cav2 Protein Family in Calcium Flux Deregulation in *Fmr1*-KO Neurons. *Front. Mol. Neurosci.* 2018, *11*, 11.

168.   Castaño, Z.; Gordon-Weeks, P.R.; Kypta, R.M.; Gordon-Weeks, P.R.; Gordon-Weeks, P.R. The neuron-specific isoform of glycogen synthase kinase-3β is required for axon growth. *J. Neurochem.* 2010, *113*, 117–130.

169.   Min, W.W.; Yuskaitis, C.J.; Yan, Q.; Sikorski, C.; Chen, S.; Jope, R.S.; Bauchwitz, R.P. Elevated Glycogen Synthase Kinase-3 Activity in Fragile X Mice: Key Metabolic Regulator with Evidence for Treatment Potential. *Neuropharmacology* 2009, *56*, 463–472.

170.   Portis, S.; Giunta, B.; Obregon, D.; Tan, J. The role of glycogen synthase kinase-3 signaling in neurodevelopment and fragile X syndrome. *Int. J. Physiol. Pathophysiol. Pharmacol.* 2012, *4*, 140–148.

171.   Yuskaitis, C.J.; Mines, M.A.; King, M.K.; Sweatt, J.D.; Miller, C.A.; Jope, R.S. Lithium ameliorates altered glycogen synthase kinase-3 and behavior in a mouse model of Fragile X syndrome. *Biochem. Pharmacol.* 2010, *79*, 632–646.

172.   Mines, M.A.; Yuskaitis, C.J.; King, M.K.; Beurel, E.; Jope, R.S. GSK3 Influences Social Preference and Anxiety-Related Behaviors during Social Interaction in a Mouse Model of Fragile X Syndrome and Autism. *PLOS ONE* 2010, *5*, e9706.

173.   Guo, W.; Murthy, A.C.; Zhang, L.; Johnson, E.B.; Schaller, E.G.; Allan, A.M.; Zhao, X. Inhibition of GSK3β improves hippocampus-dependent learning and

rescues neurogenesis in a mouse model of fragile X syndrome. *Hum. Mol. Genet.* 2011, *21*, 681–691.

174.   Franklin, A.V.; King, M.K.; Palomo, V.; Martinez, A.; McMahon, L.L.; Jope, R.S. Glycogen Synthase Kinase-3 Inhibitors Reverse Deficits in Long-Term Potentiation and Cognition in Fragile X Mice. *Biol. Psychiatry* 2014, *75*, 198–206.

175.   Yuskaitis, C.J.; Beurel, E.; Jope, R.S. Evidence of Reactive Astrocytes but Not Peripheral Immune System Activation in a Mouse Model of Fragile X Syndrome. *Biochim. Biophys. Acta.* 2010, *1802*, 1006–1012.

176.   Mines, M.A.; Jope, R.S.; Mines, M.M. Glycogen Synthase Kinase-3: A Promising Therapeutic Target for Fragile X Syndrome. *Front. Neurosci.* 2011, *4*, 35.

177.   Goebel-Goody, S.M.; Lombroso, P.J. Taking STEPs Forward to Understand Fragile X Syndrome. *Results Probl. Cell Differ.* 2012, *54*, 223–241.

178.   Goebel-Goody, S.M.; Baum, M.; Paspalas, C.D.; Fernandez, S.M.; Carty, N.C.; Kurup, P.; Lombroso, P.J. Therapeutic Implications for Striatal-Enriched Protein Tyrosine Phosphatase (STEP) in Neuropsychiatric Disorders. *Pharmacol. Rev.* 2012, *64*, 65–87.

179.   Johnson, M.A.; Lombroso, P.J. A Common STEP in the Synaptic Pathology of Diverse Neuropsychiatric Disorders. *Yale J. Boil. Med.* 2012, *85*, 481–490.

180.   Darnell, J.C.; Van Driesche, S.J.; Zhang, C.; Hung, K.Y.S.; Mele, A.; Fraser, C.E.; Stone, E.F.; Chen, C.; Fak, J.J.; Chi, S.W.; et al. FMRP stalls ribosomal translocation on mRNAs linked to synaptic function and autism. *Cell* 2011, *146*, 247–261.

181.   Royston, S.; Tagliatela, S.M.; Naegele, J.R.; Lombroso, P.J.; Tagliatela, S.; Goebel-Goody, S.M.; Wilson-Wallis, E.D.; Goebel-Goody, S.M.; Wilson-Wallis, E.D.; Goebel-Goody, S.M.; et al. Genetic manipulation of STEP reverses behavioral abnormalities in a fragile X syndrome mouse model. *Genes, Brain* 2012, *11*, 586–600.

182.   Xu, J.; Chatterjee, M.; Baguley, T.D.; Brouillette, J.; Kurup, P.; Ghosh, D.; Kanyo, J.; Zhang, Y.; Seyb, K.; Ononenyi, C.; et al. Inhibitor of the Tyrosine Phosphatase STEP Reverses Cognitive Deficits in a Mouse Model of Alzheimer's Disease. *PLoS Biol.* 2014, *12*, e1001923.

183.   Chatterjee, M.; Kurup, P.K.; Lundbye, C.J.; Hugger Toft, A.K.; Kwon, J.; Benedict, J.; Kamceva, M.; Banke, T.G.; Lombroso, P.J. STEP Inhibition Reverses Behavioral, Electrophysiologic, and Synaptic Abnormalities in *Fmr1* KO Mice. *Neuropharmacology* 2018, *128*, 43–53.

184.   Ashwood, P.; Nguyen, D.V.; Hessl, D.; Hagerman, R.J.; Tassone, F. Plasma Cytokine Profiles in Fragile X Subjects: Is There a Role for Cytokines in the Pathogenesis? *Brain Behav. Immun.* 2010, *24*, 898–902.

185.   Tabet, R.; Moutin, E.; Becker, J.A.J.; Heintz, D.; Fouillen, L.; Flatter, E.; Krężel, W.; Alunni, V.; Koebel, P.; Dembélé, D.; et al. Fragile X Mental Retardation Protein (FMRP) Controls Diacylglycerol Kinase Activity. *Neurons. Proc. Natl. Acad. Sci. USA.* 2016, *113*, E3619–E3628.

186.   Lin, S.-L. microRNAs and Fragile X Syndrome. *Adv. Exp. Med. Biol.* 2015, *888*, 107–121.

187.   Lin, S.-L.; Chang, S.-J.; Ying, S.-Y. First in vivo evidence of microRNA-induced fragile X mental retardation syndrome. *Mol. N.a.* 2006, *11*, 616–617.

188.   Chang, S.-J.E.; Chang-Lin, S.; Chang, D.C.; Chang, C.P.; Lin, S.-L.; Ying, S.-Y. Repeat-Associated MicroRNAs Trigger Fragile X Mental Retardation-Like Syndrome in Zebrafish~!2008-10-29~!2008-11-12~!2008-11-26~!. *Open Neuropsychopharmacol. J.* 2008, *1*, 6–18.

189.   Lin, S.-L.; Ying, S.-Y. Role of Repeat-Associated MicroRNA (ramRNA) in Fragile X Syndrome (FXS). In *Current Perspectives in microRNAs (miRNA)*; Springer: Dordrecht, The Netherlands; 2008; pp. 245–266.

190.   Muddashetty, R.S.; Nalavadi, V.C.; Gross, C.; Yao, X.; Xing, L.; Laur, O.; Warren, S.T.; Bassell, G.J. Reversible Inhibition of PSD-95 mRNA Translation by miR-125a, FMRP Phosphorylation, and mGluR Signaling. *Mol. Cell* 2011, *42*, 673–688.

191.   Edbauer, D.; Neilson, J.R.; Foster, K.A.; Wang, C.-F.; Seeburg, D.P.; Batterton, M.N.; Tada, T.; Dolan, B.M.; Sharp, P.A.; Sheng, M. Regulation of synaptic structure and function by FMRP-associated microRNAs miR-125b and miR-132. *Neuron* 2010, *65*, 373–384.

192.   Liu, T.; Wan, R.-P.; Tang, L.-J.; Liu, S.-J.; Li, H.-J.; Zhao, Q.-H.; Liao, W.-P.; Sun, X.-F.; Yi, Y.-H.; Long, Y.-S. A MicroRNA Profile in *Fmr1* Knockout Mice Reveals MicroRNA Expression Alterations with Possible Roles in Fragile X Syndrome. *Mol. Neurobiol.* 2015, *51*, 1053–1063.

193.	Fazeli, Z.; Ghaderian, S.M.H.; Najmabadi, H.; Omrani, M.D. High expression of miR-510 was associated with CGG expansion located at upstream of *FMR1* into full mutation. *J. Cell. Biochem.* 2018, *120*, 1916–1923.

14. Figures
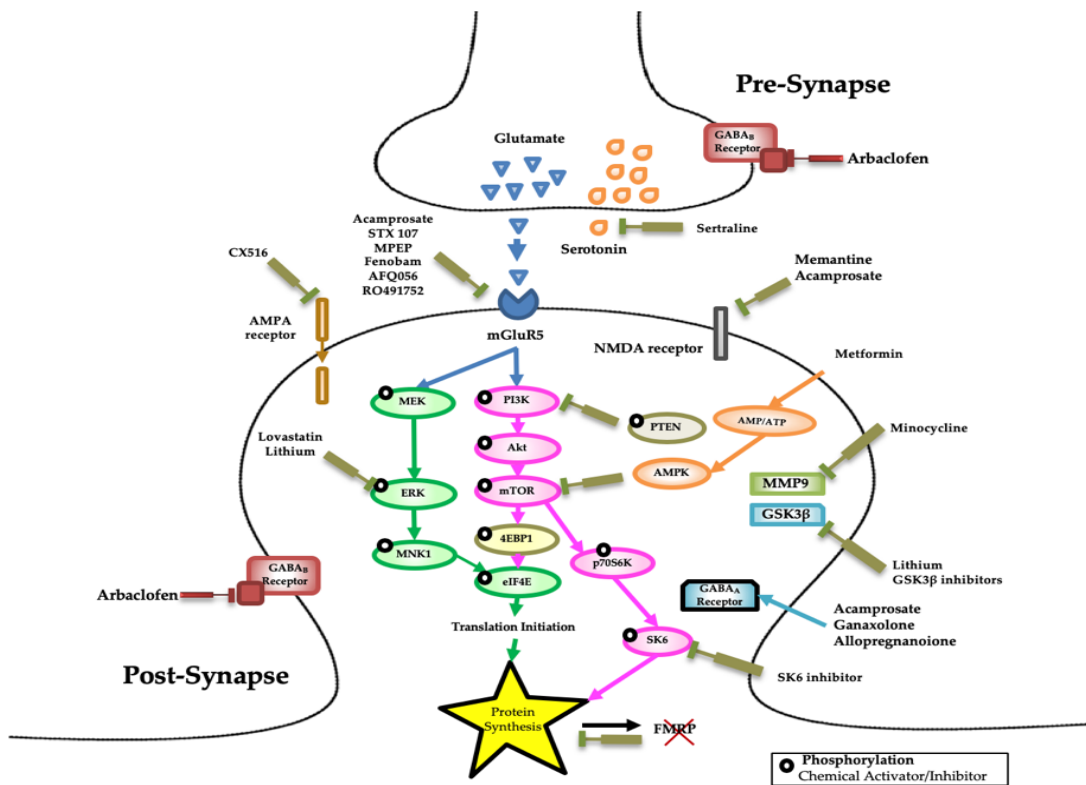
Figure 1. Potential therapeutic targets for fragile X syndrome (FXS). Diagram of the mechanisms implicated in FXS leading to altered synaptic plasticity. The figure also shows the molecular pathways targeted or understudy, for the reversal of cognitive and behavioral impairments in FXS patients. Several types of drugs,

modulators, and compounds (inhibitor, agonist, and antagonist) can interfere with different pathways disturbed in FXS and have been used in a number of pharmacological treatments some of which are currently under investigation and are indicated in the figure.
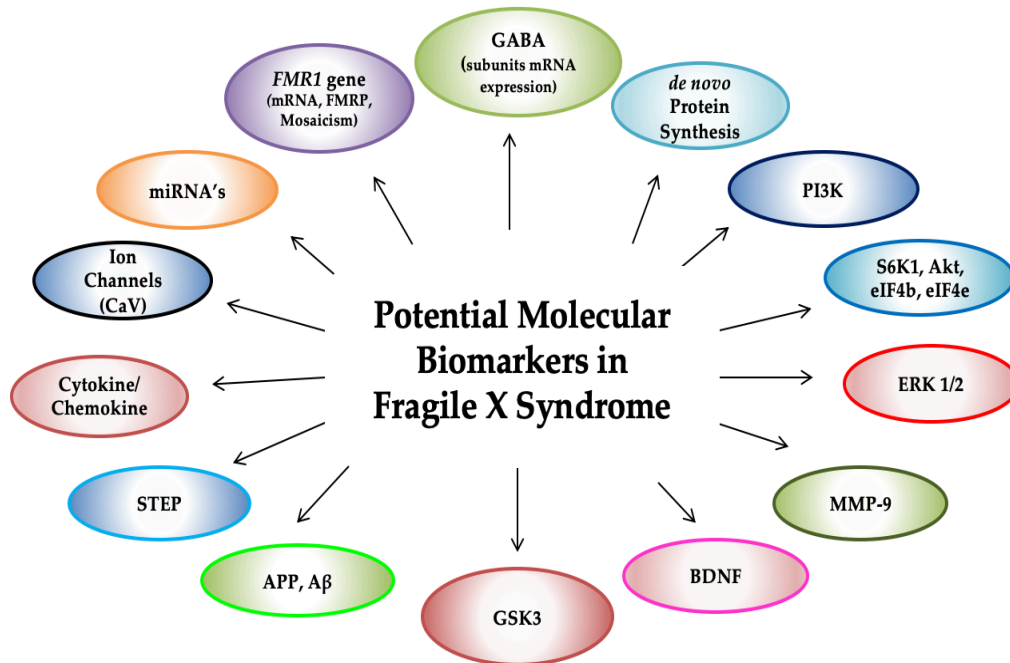
Figure

2. Candidate molecular biomarkers for FXS include a number of targets and substrates of several signaling pathways, in addition to fragile X mental retardation 1 (*FMR1*) molecular measures and metabolites, of which expression levels or activity have been found dysregulated in FXS animal models and in human FXS tissues. *Fmr1* mRNA and fragile X mental retardation 1 protein (FMRP) expression, de novo protein synthesis, γ-aminobutyric acid (GABA) receptors (GABA$_A$ and GABA$_B$), phosphoinositide 3-kinase (PI3K), extracellular-regulated kinase (ERK), matrix metalloproteinase-9 (MMP-9), brain-derived neurotrophic factor (BDNF), mammalian target of rapamycin (mTOR), p70

ribosomal S6 kinase (S6K1), ion channels (KNa, BKCa, CaV, Kv, HCN1), bone morphogenetic protein receptor Type 2 (BMPR2), Diacylglycerol Kinase Kappa (Dgкκ), endocannabinoid system (eCS), amyloid-β protein precursor (APP), microRNA's (miRNA's), striatal-enriched protein tyrosine phosphatase (STEP), glycogen synthase kinase-3 (GSK-3) cytokine and chemokine profiles, metabotropic glutamate receptor (mGluRs).

Chapter 2

FMR1 locus Isoforms: potential biomarker candidates in Fragile X-Associated Tremor/Ataxia Syndrome (FXTAS)

Marwa Zafarullah [1], Hiu-Tung Tang[1], Blythe Durbin-Johnson[2], Emily Fourie [3,4] David Hessl[5,6], Susan M. Rivera[3,4,5,] and Flora Tassone [1, 5*]

[1] Department of Biochemistry and Molecular Medicine, University of California Davis, School of Medicine, Sacramento, 95817 CA, USA.
[2] Division of Biostatistics, University of California Davis, School of Medicine, Davis, CA, USA.
[3] Center for Mind and Brain, University of California Davis, Davis, CA, USA.
[4] Department of Psychology, University of California, Davis, Davis, CA, USA.
[5] MIND Institute, University of California Davis Medical Center, Sacramento, 95817 CA, USA.
[6] Department of Psychiatry and Behavioral Sciences, University of California Davis Medical Center, Sacramento, 95817 CA, USA.
*   **Correspondence:** ftassone@ucdavis.edu; Tel.: +1-(916)-703-0463

Abstract

Fragile X Associated Tremor/Ataxia Syndrome (FXTAS) is a late adult-onset neurodegenerative disorder that affects movement and cognition in male and female carriers of a premutation allele of 55-200 CGG repeats in the Fragile X mental retardation (*FMR1)* gene. It is currently unknown if and when an individual carrier of a premutation allele will develop FXTAS, as clinical assessment fails to identify carriers at risk before significant neurological symptoms are evident. The primary objective of this study was to investigate the alternative splicing landscape at the *FMR1* locus in conjunction with brain measures in male individuals with a premutation allele enrolled in a very first longitudinal study, compared to age-matched healthy male controls, with the purpose of identifying biomarkers for early diagnosis, disease prediction and, a progression of FXTAS.

Our findings indicate that increased expression of *FMR1* mRNA isoforms, including *Iso4/4b*, *Iso10/10b*, as well as of the *ASFMR1 mRNAs Iso131bp*, are present in premutation carriers as compared to non-carrier healthy controls. More specifically, we observed a higher expression of *Iso4/4b and Iso10/10b,* which encode for truncated proteins*,* only in those premutation carriers who developed symptoms of FXTAS over time as compared to non-carrier healthy controls, suggesting a potential role in the development of the disorder. In addition, we found a significant association of these molecular changes with various measurements of brain morphology, including the Middle Cerebellar Peduncle (MCP), Superior Cerebellar Peduncle (SCP), Pons, and midbrain, indicating their potential contribution to the pathogenesis of FXTAS. Interestingly, the high expression levels of *Iso4/4b* observed both at visit 1 and visit 2 and found to be associated with a decrease in mean MCP width only in those individuals who developed FXTAS over time, suggests their role as potential biomarkers for early diagnosis of FXTAS.

Keywords: Fragile X-associated tremor/ataxia syndrome; molecular biomarkers; isoforms; alternative splicing; brain measures.

1. Introduction

The fragile X mental retardation (*FMR1*) gene consists of 17 exons spanning approximately 38 kb of genomic DNA. A trinucleotide repeat expansion, greater than 200 CGG, with consequent methylation of the 5'UTR (untranslated region) of *FMR1* gene, leads to Fragile X Syndrome (FXS), the most common form of intellectual disability and known monogenic cause of Autism Spectrum Disorder [1]. Expansions between 55-200

CGG repeats (known as premutation carriers) confer the risk of developing Fragile X-associated tremor/ataxia syndrome (FXTAS), a late-onset neurodegenerative disorder characterized by intention tremor, gait ataxia, autonomic dysfunction, and Parkinsonism [2]. In addition, females premutation carriers are at risk of developing Fragile X-associated primary ovarian insufficiency (FXPOI) that affects ovary function in women leading to early menopause and irregular elevation of follicle-stimulating hormone (FSH) [3]. The prevalence of the premutation allele among the general population is 1:110-200 females and 1:430 males with an estimated 40-75% of males and 8-16% of females developing FXTAS [4,5].

At the molecular level, FXTAS is characterized by an increased level of *FMR1* mRNA containing expanded CGG repeats [6]. The proposed molecular mechanisms of FXTAS pathogenesis include the sequestration of CGG binding proteins by the elevated levels of *FMR1* mRNA leading to RNA toxicity, the production of toxic FMRPolyG protein due to RAN translation and the chronic activation of DNA damage response [reviewed in [7].

Extensive alternative splicing of the *FMR1* gene has been observed [8–16]. Alternative splicing (AS) is a regulated process occurring during gene expression that increases protein diversity and represents a powerful evolutionary resource. It regulates the protein localization, enzymatic properties, stability, interaction with ligands and membranes [17] and is common in the nervous system playing a major role in neurogenesis, brain development [18,19] and cell survival [20]. It is increasingly recognized that disruption of the splicing process, which is regulated by different splicing factors, can contribute to a number of neurological disorders [19,21,22] including autism spectrum disorder (ASD) [23], Parkinson's disease [24], dementia [25], spinal muscular

atrophy (SMA) [26], Prader-Willi syndrome (PWS) [27], schizophrenia [28], myotonic dystrophy [29], amyotrophic lateral sclerosis [30,31] Alzheimer's disease [32].

In the *FMR1* gene, altered splicing has been observed in premutation carriers where increased levels of the *FMR1* isoforms have been detected [15,16]. Of the many *FMR1* mRNA isoforms that were demonstrated to exist in both humans and mice [11,14–16], *Iso10/10b* showed the highest levels of expression in premutation samples which, together with the *Iso4/4b* [**Figure 1**], result in truncated proteins that lack the function of the nuclear export signal (NES) and RGG box [15]. Of the 49 different *FMR1* isoforms identified, 30 appeared to be expressed only in premutation carriers compared to controls [16]. Additionally, two novel isoforms *IsoPB1.50* and *IsoPB1.21* retain a portion of the intronic sequence between exons 9 and 10, causing a frameshift, which leads to a premature stop codon and consequently encodes for truncated proteins. A differential increase of specific *FMR1* mRNA isoforms has been observed in premutation carriers, suggesting their potential functional relevance in the pathology of FXTAS due to RNA toxicity [15,16].

Comprehensive analysis of the transcriptional landscape of the human *FMR1* gene revealed the presence of long non-coding RNAs (*FMR 4* [33], *FMR 5* and *FMR6*) [34]. Importantly, a unique antisense transcript at the *FMR1* locus (*ASFMR1*), that similarly to the *FMR1* gene, is upregulated in premutations and not expressed in full mutations has been identified. Thus, the bidirectional expression of the *FMR1* and the *ASFMR1* genes has been suggested to potentially contribute to the clinical phenotype of FXTAS [35]. Interestingly, the *ASFMR1* also exhibits a premutation specific alternative splicing, the *Iso131bp* [**Figure 1**]*, which is mainly expressed in premutation carriers compared to

controls, providing a molecular abnormality potentially associated with FXTAS [15,36–38]. However, no studies have been conducted to determine whether altered expression *FMR1* and *ASFMR1 isoforms* are biomarkers of incipient FXTAS, particularly in relation to neurological and neuroanatomical changes.

In this study, we evaluated male premutation carriers enrolled in a longitudinal study at the UC Davis MIND Institute who have been followed for at least two longitudinal time points, and for whom neuroimaging, neuropsychological, and molecular measurements, as well as medical and neurological examinations, were collected. We have recently reported that the middle cerebellar peduncle (MCP) width decreased in a subgroup of these individuals who developed symptoms of FXTAS at subsequent visits (converters) compared to those who did not (non-converters) and compared to normal age-matched controls. Further, we reported reduced midbrain and pons cross-sectional areas in patients with FXTAS compared to both premutation carriers without FXTAS and controls [39]. These regions play an important role within the cortico-cerebellar pathway, which is necessary for the learning and coordination of various movements [40]. Measurements of these areas have been shown previously to successfully differentiate subcortical movement disorders, such as Parkinson's disease [41], which presents with tremor similar to that seen in FXTAS.

In the current study, we sought to determine whether the expression levels of alternative splicing isoforms at the *FMR1* locus were significantly different both in premutation carriers who did and did not develop symptoms of FXTAS over time compared to non-carrier healthy controls. In addition, we also investigated whether the changes in molecular measures were associated with changes in brain measures.

2. Materials and Methods

2.1 Study Participants

As part of two continuing longitudinal studies, male participants over the age of 40 years were recruited from the Sacramento, CA area, and throughout the United States and Canada. The study was carried out in accordance with the Institutional Review Board (IRB) at the University of California, Davis with written informed consent obtained from all participants in accordance with the Declaration of Helsinki. All experimental protocols carried out in this study were approved by institutional Review Board at the University of California, Davis. Participants were fluent in English, with no history of any serious medical or neurological conditions, including a history of alcoholism or drug abuse. FXTAS stage scoring was based on the clinical descriptions as previously described [42].

Three groups were included in this study: converters, non-converters, and healthy controls. They were matched by age and the length of the interval between visit 1 (V1) and visit 2 (V2); the converters and non-converters groups were also matched by CGG repeat number and they were selected on the basis of the brain measures availability. After two brain scans, on the basis of neurological assessment, FXTAS stage, and CGG repeat length, 15 participants were classified as "*Converters*" as they developed clear FXTAS symptomology between visits (FXTAS stage score was 0–1 at visit 1 and ≥2 at visit 2; 15 were defined as "*Non-converters*" because they continued to show no signs of FXTAS at V2 (FXTAS stage score was 0–1 at both V1 and V2) and 15 non-carrier healthy controls (FXTAS stage score was 0 at both V1 and V2).

2.2 CGG Repeat Length

Genomic DNA (gDNA) was isolated from 5 mL of peripheral blood leukocytes using the Gentra Puregene Blood Kit (Qiagen). CGG repeat allele size and methylation status were assessed using a combination of Southern Blot analysis and PCR amplification. For Southern blot analysis, 5–10 µg of isolated genomic DNA was digested with EcoRI and NruI, run on an agarose gel, transferred on a nylon membrane and hybridized with the *FMR1*-specific dig-labeled StB12.3 as detailed in [43]. PCR analysis was performed using *FMR1* specific primers (AmplideX PCR/CE, Asuragen, Inc.); amplicons were visualized by capillary electrophoresis, as previously reported an analyzed using Gene Mapper software [44].

2.3 mRNA Expression Levels

Total RNA was isolated from 2.5 ml of peripheral blood collected in PAXgene Blood RNA tubes using the PAXgene Blood RNA Kit (Qiagen, Valencia, CA, United States) and quantified using Agilent 2100 Bioanalyzer system. RNA isolation was performed in a clean and RNA designated area. cDNA was synthesized as previously described [45]. *FMR1* transcript levels measured by performing reverse transcription followed by real-time PCRs (qRT-PCR). qRT-PCR was performed using both Assays-On-Demand from Applied Biosystems (Applied Biosystems, Foster City, CA, United States) and custom-designed TaqMan primers and probe assays,[45]. Probe and primer assays designed to quantify *FMR1* transcripts for the isoform *IsoPB1.21 and IsoPB1.50*, isoform *Iso4/4b* and isoform *Iso10/10b* were as previously reported [16]. Custom designed primers and probe

were also designed to quantify the *ASFMR1* gene and *ASFMR1 131bp* splice isoform [35].

2.4 Brain Measures

The following methods including MRI acquisition and MRPI analysis were originally described in our previous report [39]. High resolution structural magnetic resonance imaging (MRIs) acquisition was obtained on a 3T Siemens Trio scanner using a 32-channel head coil and a T1-weighted 3D MPRAGE sequence with the following parameters: TR=2170ms, TE=4.86ms, flip angle=7º, FoV=256mm^2, 192 slices, 1mm slice thickness. The scans were first aligned along the anterior-posterior commissure line using acpcdetect (http://www.nitrc.org/projects/art) [46] or manually using DTI Studio (www.mristudio.org) [47]. Then MRI bias field correction was performed using N4 (http://stnava.github.io/ANTs/) [48].

A series of independent raters (two per measure) who were blinded to the participant age, group, and time point, quantitatively assessed all MR images for four measurements of brain morphology: MCP and superior cerebellar peduncle (SCP) widths as well as pons and midbrain cross-sectional areas based on methods previously described [49,50] and detailed below.

The pons and midbrain areas were assessed on the mid-sagittal slice, where horizontal lines were drawn through the superior and inferior pontine notches. The midbrain was measured as the area above the superior pontine line – midbrain tegmentum, while the pons was the area between the two horizontal lines of the superior and inferior notches. The width of both left and right MCPs were measured on parasagittal

slices. The linear distance of the MCP was delineated by the peripeduncular cerebrospinal fluid spaces of pontocerebellar cisterns, where the pons was still 'intact' and the cerebellum was fully formed (white matter connecting the cerebellar tonsil was present). Finally, the widths of both the left and right SCPs were measured on oblique coronal slices, at the midpoint of the SCP, when it first became separated from the inferior colliculi. The linear distance between the medial and lateral SCP borders was measured. For both MCP and SCP widths, a mean score was calculated by averaging the left and right measurements for each participant. The interrater reliability coefficients were excellent, greater than 0.98, for each of the four measurements. The mean score of the raters was used for further analysis.

2.5 Statistical Analysis

Statistical Analyses were conducted blind to treatment groups using R, version 3.6.0. Age and CGG repeat numbers were compared between groups using ANOVA F-tests, followed by pairwise comparisons in the event of a significant F test. The association between mRNA expression and CGG repeat length in each group, adjusted for age, was analyzed using linear models with CGG repeat length, group, the interaction between CGG repeat length and group, and age as covariates. mRNA expression was compared between groups, adjusting for age, using linear models with group and age as covariates. The change between timepoint 1 and time point 2 in mRNA expression was compared between groups, adjusting for age and visit interval, using linear models with the group, age, and visit interval as covariates. The association between each brain measure and each molecular measure was analyzed at each time point within each

group, adjusting for age, using linear models with molecular measure, group, the group–molecular measure interaction, and age as covariates. The association between changes in brain measures and changes in molecular measures, within each group, adjusting for age and visit interval, was analyzed using linear models including change in molecular measure, group, the group–molecular measure change interaction, age, and visit interval as covariates. mRNA and protein expression values were log-transformed prior to analysis in order to more closely satisfy model assumptions; brain measures were analyzed on their original scale. Due to the exploratory nature of this study, no adjustment for multiple testing was conducted [51,52]. The tables of all analyses conducted are reported in the supplemental materials.

3. Results

3.1 Demographics

Numbers of participants (N) for each group, age and CGG repeat number are as reported in [**Table 1**]. Participants ages did not differ significantly between the three groups. CGG repeat numbers were significantly lower in healthy controls than in all other groups, as expected (P < 0.001 in both comparisons) and were not significantly different between converters and non-converters (P = 0.445).

3.2 *FMR1* mRNA isoforms expression analysis

We measured the expression of *FMR1* mRNA, *FMR1* isoforms *Iso10/10b, Iso4/4b*, *IsoPB1.21, ASFMR1,* and *ASFMR1 Iso131* at V1, V2 and between the visits [**Supplementary Material Table S2a, S2b and S2c**]. As expected, the expression of

FMR1 mRNA was significantly higher in both converters and non-converters as compared to non-carrier healthy controls both at V1 [(P < 0.001] and V2 [P < 0.001] but no significant differences were observed between the two premutation groups [**Figure 2a.**]. *FMR1* expression levels were associated with CGG repeat length, with greater expression levels being associated with longer CGG repeat length, in both converters and non-converters compared to non-carrier healthy controls [P<0.001 for both comparisons; **Figure 2b.**].

The expression levels of Iso*10/ Iso10b,* CGG dependent [**Figure 3d**] were significantly higher in converters at V1 [P=0.0225] and V2 [P=0.0468] respectively, as compared to non-carrier healthy controls. Importantly, these markers were not significantly different in non-converters as compared to non-carrier healthy controls at either V1 [P=0.401] or V2 [P=0.592] [**Figure 3a**]. For *Iso4/4b* we observed significantly higher expression in converters as compared to non-carrier healthy controls at V1 [P=0.0323] but no difference was found at V2 [P=0.247] and with the CGG repeat number [**Figure 3e**]. The expression of these isoforms was not significantly different in non-converters as compared to non-carrier healthy controls both at V1 [P=0.542] and V2 [P=0.684] [**Figure 3b**]. The expression levels of additional transcripts encoding for truncated proteins, *IsoPB1.21 and IsoPB1.50* were not significantly different among groups both at V1 or V2.

Significantly increased expression levels of *ASFMR1 Iso131* bp, CGG dependent (P= 0.012 for the non-converter group and p=0.05 for the converter group; **Figure 3f)** were observed in the premutation groups, both converters, and non-converters, as compared to non-carrier healthy controls both at V1 [P <0.001] and V2 [P <0.001] with no difference in levels between the two premutation groups [**Figure 3c**].

However, when comparing the changes in the gene expression levels between V1 and V2 we found a significant greater change in the expression of *ASFMR1 Iso131 bp* in converters [P =0.006; **Figure 4**] as compared to non-carrier healthy controls while no significant difference was observed between non-converters and non-carrier healthy controls [P =0.102; **Figure 4**].Finally, when comparing the expression levels at V1 and V2 among the groups, no significant differences were detected for any of the *FMR1* splicing isoforms or the *ASFMR1* gene.

3.3 Brain measures v/s Molecular measures

We compared brain measures, including MCP and SCP width, midbrain, and pons cross-sectional area with the molecular measures at V1, V2 and between the visits [**Supplementary Material Table S3a, S3b and S3c**]. Changes in the measures of brain morphology were associated with the expression of some *FMR1* isoforms. Specifically, we found that the higher level of expression of the *Iso4/4b* mRNAs was associated with smaller MCP width in converters both at V1 [P=0.028, beta= -0.421; **Figure 5a.** and V2 [P=0.048, beta= -0.5311; **Figure 5b.**] but not in the non-converters at both V1[P=0.611, beta= -0.064; **Figure 5a.**] or V2 [P=0.333, beta= -0.392; **Figure 5b.**] and not in the healthy controls [P=0.53, V1; beta=0.085; p=0.365, beta= -0.376]. Further, the expression of the *ASFMR1* isoform (131 bp) also increased significantly with a decrease in changes in the pons [P=0.047, beta= -0.012] only in the converter group between V1 and V2.

Finally, we found a positive correlation, between the change in brain measures, including the mean SCP [P=0.017, beta=0.726] and midbrain area [P=0.031, beta=0.316] with increased expression of the *FMR1* mRNA, between the two visits only in the

converter group. We also found that the expression of *Iso10/10b* increased significantly with an increase with changes in the midbrain area [P=0.045, beta= 0.076].

4. Discussion

Alternative Splicing (AS) is a common process in the central nervous system and crucial for the differentiation and physiology of cells, particularly neurons. It is estimated that AS occurs in about 95% of human genes [53], contributing greatly to the regulation of mRNA levels and to proteomic diversity. Different studies have reported that AS events take place at the *FMR1* locus and have an impact on the expression and function of FMRP [10–12,14,54–57] We recently reported on the characterization of the *FMR1* isoforms and showed differential expression and distribution as a function of the CGG repeat number in premutation carriers. Differently from the 24 predicted *FMR1* mRNA variants, we also reported on the existence, of at least 49 different ones in several human tissues, 30 of which detected only in premutation carriers [15,16]. Thus, an altered alternative splicing phenomenon is present in premutation carriers.

In this study, we aimed to identify molecular biomarkers, specifically the expression levels of some alternatively spliced isoforms at the *FMR1* locus, for risk prediction, early diagnosis, and progression of developing FXTAS. Increased and CGG dependent expression levels of *FMR1* mRNA were observed in premutation groups (including both converters and non-converters) as compared to non-carrier healthy controls confirming many previous reports on this well-established altered molecular phenotype in premutation carriers. In addition to *FMR1 mRNA,* we also observed elevated expression

of various alternative splicing isoforms as a function of CGG repeat suggesting their potential contribution to the RNA toxicity in premutation carriers.

Taking advantage of the longitudinal study design, we investigated the expressional profile for these specific isoforms among our three groups and observed the higher expression of isoform *Iso10/10b* in converters as compared to non-carrier healthy controls at both visits. Importantly, the non-converter group did not show the differential expression for this isoform. This suggests that these isoforms, that encode for truncated proteins might be relevant in the pathogenesis of FXTAS and, pending replication and further confirmation, may eventually play a role in early testing and screening of premutation allele carriers at greater risk of developing the disorder.

Previous investigations on the *FMR1* transcriptional landscape reported the highest expression of isoform *Iso10/10b* in premutation carriers with and without FXTAS [15,16]. However, this study shows a higher expression of these isoforms in individuals, the converter group, who develop FXTAS over time. Similarly, we observed higher expression of the isoforms *Iso4/4b,* which encode for truncated proteins and are therefore missing the nuclear export signal and C-terminal RGG box, in the converter group, but not in the non-converter group, as compared to healthy controls, also suggesting the potential role of truncated proteins in the pathogenesis of FXTAS, which needs to be further investigated.

The midbrain, pons, and superior cerebellar peduncles (SCP) atrophy is the characteristic pathologic finding in patients with a number of neurodegenerative disorders including progressive supranuclear palsy (PSP) [58,59], Parkinson disease (PD), Multiple System Atrophy (MSA) [49,60] and Alzheimer disease [61]. These studies have proposed

a number of midbrain metrics as potential biomarkers for differentiation of the patients with different neurodegenerative conditions. Shelton et al. [39] suggested that the decreased MCP width observed in the premutation carriers who developed FXTAS over time (converters) could be a biomarker for early identification of incipient FXTAS. Of relevance, this study found a significant association of increased expression of Iso*4/4b* with decreased MCP width and of the expression of *ASFMR1* isoform (131 bp) with decreased changes in pons, only in the converter group, which supports their potential role as biomarkers and support evidence of their potential contribution to the pathogenesis of the disorder. Interestingly, in the current study we found a positive association of *FMR1* mRNA with mean SCP and midbrain and of isoform *Iso10/10b* with the midbrain, suggesting that some of the molecular measures may be linked with the changes in the brain structures. However, further studies are warranted to confirm these findings.

Generally, the mRNAs containing premature termination codons (PTCs) are degraded by the nonsense-mediated mRNA decay (NMD) system. However, this is not always the case as sometimes the mRNAs escape from the nonsense-mediated mRNA decay and results in truncated proteins [62,63]. Truncated proteins can form aggregates and can act in a dominant-negative manner. The accumulation of these abnormal truncated proteins leads to the gradual loss of function and structure of neurons including the death of neurons. These aggregations have been found to be associated with various neurodegenerative diseases such as Alzheimer's, Huntington's and Parkinson's diseases, ASD, and amyotrophic lateral sclerosis. Additionally, a truncated form of *DISC1* aggregates has been associated with major depression and schizophrenia [64]. Thus, it

is possible that the translation of these isoforms might contribute to the pathogenesis of the *FMR1* associated disorders. However, the exact mechanism and functional role are still unknown.

The previous report suggested that the antisense *FMR1* (*ASFMR1*) gene and the premutation specific *ASFMR1 Iso131* bp may contribute to the pathogenesis of FXTAS [35]. Although the expression of this splice isoform in premutation carriers was reported to be higher compared to controls, no difference in the expression levels was observed between non-FXTAS and FXTAS premutation carrier groups in previous studies [36,37]. The study presented here confirms the previous findings of a higher expression of this splice isoform in premutation carriers; however, and importantly, the observed significant change of expression levels between V1 and V2 only in the converter group but not in the non-converter or control groups, suggest its potential role in the progression of FXTAS. These findings suggest the presence of an altered bidirectional transcription alternative splicing in premutation carriers and their potential role in the development and progression of FXTAS.

Finally, further studies are required to investigate the function of this specific isoform. The longitudinal follows up of these individuals may help our understanding of the potential role of such isoforms in FXTAS.

5. Conclusions

In conclusion, this is a first study that suggest an elevated expression of some of the *FMR1* and *ASFMR1* mRNA splicing isoforms is present in premutation carriers who develop FXTAS compared to those who remain symptom free and to controls, providing

support for these measures as potential biomarkers for early identification and monitoring of disease progression. In addition, the association of these molecular measures with brain measures provide us better insight regarding disease pathogenesis. However, due to limitation of the small sample size further studies with larger sample size are required to test the initial findings and elucidate and confirm the role of the potential identified biomarkers.

6. Availability of Additional Data

All statistical data generated during the study is available at the end of this chapter as "Supplementary Data".

7. References

1. Hagerman RJ, Berry-Kravis E, Hazlett HC, Bailey DB Jr, Moine H, Kooy RF, et al. Fragile X syndrome. Nat Rev Dis Primers. 2017;3:17065.

2. Hall DA, Berry-Kravis E. Fragile X syndrome and fragile X-associated tremor ataxia syndrome. Handb Clin Neurol. 2018;147:377–91.

3. Fink DA, Nelson LM, Pyeritz R, Johnson J, Sherman SL, Cohen Y, et al. Fragile X Associated Primary Ovarian Insufficiency (FXPOI): Case Report and Literature Review. Front Genet. 2018;9:529.

4. Jacquemont S. Penetrance of the Fragile X–Associated Tremor/Ataxia Syndrome in a Premutation Carrier Population . JAMA. 2004. p. 460. Available from: http://dx.doi.org/10.1001/jama.291.4.460

5. Tassone F, Iong K, Tong T-H, Lo J, Gane LW, Berry-Kravis E, et al. FMR1 CGG allele size and prevalence ascertained through newborn screening in the United States . Genome Medicine. 2012. p. 100. Available from: http://dx.doi.org/10.1186/gm401

6. Tassone F, Hagerman RJ, Taylor AK, Gane LW, Godfrey TE, Hagerman PJ. Elevated Levels of FMR1 mRNA in Carrier Males: A New Mechanism of Involvement in the Fragile-X Syndrome . The American Journal of Human Genetics. 2000. p. 6–15. Available from: http://dx.doi.org/10.1086/302720

7. Hagerman RJ, Hagerman P. Fragile X-associated tremor/ataxia syndrome — features, mechanisms and management . Nature Reviews Neurology. 2016. p. 403–12. Available from: http://dx.doi.org/10.1038/nrneurol.2016.82

8. Ashley C, Wilkinson K, Reines D, Warren S. FMR1 protein: conserved RNP family domains and selective RNA binding . Science. 1993. p. 563–6. Available from: http://dx.doi.org/10.1126/science.7692601

9. Verheij C, Bakker CE, de Graaff E, Keulemans J, Willemsen R, Annemieke J M, et al. Characterization and localization of the FMR-1 gene product associated with fragile X syndrome . Nature. 1993. p. 722–4. Available from: http://dx.doi.org/10.1038/363722a0

10. Verkerk AJMH, Annemieke J M, de Graaff E, De Boulle K, Eichler EE, Konecki DS, et al. Alternative splicing in the fragile X gene FMR1 . Human Molecular Genetics. 1993. p. 399–404. Available from: http://dx.doi.org/10.1093/hmg/2.4.399

11. Huang T, Li L-Y, Shen Y, Qin X-B, Pang Z-L, Wu G-Y. Alternative splicing of the FMR1 gene in human fetal brain neurons . American Journal of Medical Genetics. 1996. p. 252–5. Available from: 3.0.co;2-w">http://dx.doi.org/10.1002/(sici)1096-8628(19960809)64:2<252::aid-ajmg3>3.0.co;2-w

12. Sittler A, Devys D, Weber C, -L. Mandel J. Alternative Splicing of Exon 14 Determines Nuclear or Cytoplasmic Localisation of FMR1 Protein Isoforms . Human Molecular Genetics. 1996. p. 95–102. Available from: http://dx.doi.org/10.1093/hmg/5.1.95

13. Xie W, Dolzhanskaya N, LaFauci G, Dobkin C, Denman RB. Tissue and developmental regulation of fragile X mental retardation 1 exon 12 and 15 isoforms. Neurobiol Dis. 2009;35:52–62.

14. Brackett DM, Qing F, Amieux PS, Sellers DL, Horner PJ, Morris DR. FMR1 transcript isoforms: association with polyribosomes; regional and developmental expression in mouse brain. PLoS One. 2013;8:e58296.

15. Pretto DI, Eid JS, Yrigollen CM, Tang H-T, Loomis EW, Raske C, et al. Differential increases of specificFMR1mRNA isoforms in premutation carriers . Journal of Medical Genetics. 2015. p. 42–52. Available from: http://dx.doi.org/10.1136/jmedgenet-2014-102593

16. Tseng E, Tang H-T, AlOlaby RR, Hickey L, Tassone F. Altered expression of the FMR1 splicing variants landscape in premutation carriers . Biochimica et Biophysica Acta (BBA) - Gene Regulatory Mechanisms. 2017. p. 1117–26. Available from: http://dx.doi.org/10.1016/j.bbagrm.2017.08.007

17. Kelemen O, Convertini P, Zhang Z, Wen Y, Shen M, Falaleeva M, et al. Function of alternative splicing. Gene. 2013;514:1–30.

18. Su C-H, Dhananjaya D, Tarn W-Y. Alternative Splicing in Neurogenesis and Brain Development . Frontiers in Molecular Biosciences. 2018. Available from: http://dx.doi.org/10.3389/fmolb.2018.00012

19. Raj B, Blencowe BJ. Alternative Splicing in the Mammalian Nervous System: Recent Insights into Mechanisms and Functional Roles. Neuron. 2015;87:14–27.

20. Paronetto MP, Passacantilli I, Sette C. Alternative splicing and cell survival: from tissue homeostasis to disease. Cell Death Differ. 2016;23:1919–29.

21. Feng D, Xie J. Aberrant splicing in neurological diseases . Wiley Interdisciplinary Reviews: RNA. 2013. p. 631–49. Available from: http://dx.doi.org/10.1002/wrna.1184

22. Cieply B, Carstens RP. Functional roles of alternative splicing factors in human disease . Wiley Interdisciplinary Reviews: RNA. 2015. p. 311–26. Available from: http://dx.doi.org/10.1002/wrna.1276

23. Quesnel-Vallières M, Dargaei Z, Irimia M, Gonatopoulos-Pournatzis T, Ip JY, Wu M, et al. Misregulation of an Activity-Dependent Splicing Network as a Common Mechanism Underlying Autism Spectrum Disorders. Mol Cell. 2016;64:1023–34.

24. Cognata VL, La Cognata V, D'Agata V, Cavalcanti F, Cavallaro S. Splicing: is there an alternative contribution to Parkinson's disease? . neurogenetics. 2015. p. 245–63. Available from: http://dx.doi.org/10.1007/s10048-015-0449-x

25. Hutton M, Lendon CL, Rizzu P, Baker M, Froelich S, Houlden H, et al. Association of missense and 5′-splice-site mutations in tau with the inherited dementia FTDP-17 . Nature. 1998. p. 702–5. Available from: http://dx.doi.org/10.1038/31508

26. Kashima T, Rao N, Manley JL. An intronic element contributes to splicing repression in spinal muscular atrophy . Proceedings of the National Academy of Sciences. 2007. p. 3426–31. Available from: http://dx.doi.org/10.1073/pnas.0700343104

27. Cassidy SB, Schwartz S, Miller JL, Driscoll DJ. Prader-Willi syndrome . Genetics in Medicine. 2012. p. 10–26. Available from: http://dx.doi.org/10.1038/gim.0b013e31822bead0

28. Stefansson H, Rujescu D, Cichon S, Pietiläinen OPH, Ingason A, Steinberg S, et al. Large recurrent microdeletions associated with schizophrenia. Nature. 2008;455:232–6.

29. Jiang H, Mankodi A, Swanson MS, Moxley RT, Thornton CA. Myotonic dystrophy type 1 is associated with nuclear foci of mutant RNA, sequestration of muscleblind proteins and deregulated alternative splicing in neurons . Human Molecular Genetics. 2004. p. 3079–88. Available from: http://dx.doi.org/10.1093/hmg/ddh327

30. Sreedharan J, Blair IP, Tripathi VB, Hu X, Vance C, Rogelj B, et al. TDP-43 Mutations in Familial and Sporadic Amyotrophic Lateral Sclerosis . Science. 2008. p. 1668–72. Available from: http://dx.doi.org/10.1126/science.1154584

31. Yan J, Deng H-. X, Siddique N, Fecto F, Chen W, Yang Y, et al. Frameshift and novel mutations in FUS in familial amyotrophic lateral sclerosis and ALS/dementia . Neurology. 2010. p. 807–14. Available from: http://dx.doi.org/10.1212/wnl.0b013e3181f07e0c

32. Koch L. Altered splicing in Alzheimer transcriptomes . Nature Reviews Genetics. 2018. p. 738–9. Available from: http://dx.doi.org/10.1038/s41576-018-0064-4

33. Khalil AM, Faghihi MA, Modarresi F, Brothers SP, Wahlestedt C. A novel RNA transcript with antiapoptotic function is silenced in fragile X syndrome. PLoS One. 2008;3:e1486.

34. Pastori C, Peschansky VJ, Barbouth D, Mehta A, Silva JP, Wahlestedt C. Comprehensive analysis of the transcriptional landscape of the human FMR1 gene reveals two new long noncoding RNAs differentially expressed in Fragile X syndrome and Fragile X-associated tremor/ataxia syndrome. Hum Genet. 2014;133:59–67.

35. Ladd PD, Smith LE, Rabaia NA, Moore JM, Georges SA, Scott Hansen R, et al. An antisense transcript spanning the CGG repeat region of FMR1 is upregulated in premutation carriers but silenced in full mutation individuals . Human Molecular Genetics. 2007. p. 3174–87. Available from: http://dx.doi.org/10.1093/hmg/ddm293

36. Olaby RRA, Al Olaby RR, Tang H-T, Durbin-Johnson B, Schneider A, Hessl D, et al. Assessment of Molecular Measures in Non-FXTAS Male Premutation Carriers . Frontiers in Genetics. 2018. Available from: http://dx.doi.org/10.3389/fgene.2018.00302

37. Vittal P, Pandya S, Sharp K, Berry-Kravis E, Zhou L, Ouyang B, et al. ASFMR1splice variant . Neurology Genetics. 2018. p. e246. Available from: http://dx.doi.org/10.1212/nxg.0000000000000246

38. Loesch DZ, Godler DE, Evans A, Bui QM, Gehling F, Kotschet KE, et al. Evidence for the toxicity of bidirectional transcripts and mitochondrial dysfunction in blood associated with small CGG expansions in the FMR1 gene in patients with parkinsonism. Genet Med. 2011;13:392–9.

39. Shelton AL, Wang JY, Fourie E, Tassone F, Chen A, Frizzi L, et al. Middle Cerebellar Peduncle Width—A Novel MRI Biomarker for FXTAS? . Frontiers in Neuroscience. 2018. Available from: http://dx.doi.org/10.3389/fnins.2018.00379

40. Ramnani N. The primate cortico-cerebellar system: anatomy and function. Nat Rev Neurosci. 2006;7:511–22.

41. Emamzadeh FN, Surguchov A. Parkinson's Disease: Biomarkers, Treatment, and Risk Factors . Frontiers in Neuroscience. 2018. Available from: http://dx.doi.org/10.3389/fnins.2018.00612

42. Bacalman S, Farzin F, Bourgeois JA, Cogswell J, Goodlin-Jones BL, Gane LW, et al. Psychiatric phenotype of the fragile X-associated tremor/ataxia syndrome (FXTAS) in males: newly described fronto-subcortical dementia. J Clin Psychiatry. 2006;67:87–94.

43. Tassone F, Pan R, Amiri K, Taylor AK, Hagerman PJ. A Rapid Polymerase Chain Reaction-Based Screening Method for Identification of All Expanded Alleles of the Fragile

X (FMR1) Gene in Newborn and High-Risk Populations . The Journal of Molecular Diagnostics. 2008. p. 43–9. Available from: http://dx.doi.org/10.2353/jmoldx.2008.070073

44. Filipovic-Sadic S, Sah S, Chen L, Krosting J, Sekinger E, Zhang W, et al. A novel FMR1 PCR method for the routine detection of low abundance expanded alleles and full mutations in fragile X syndrome. Clin Chem. 2010;56:399–408.

45. Tassone F, Hagerman RJ, Chamberlain WD, Hagerman PJ. Transcription of the FMR1 gene in individuals with fragile X syndrome . American Journal of Medical Genetics. 2000. p. 195–203. Available from: 3.0.co;2-r">http://dx.doi.org/10.1002/1096-8628(200023)97:3<195::aid-ajmg1037>3.0.co;2-r

46. Ardekani BA, Bachman AH. Model-based automatic detection of the anterior and posterior commissures on MRI scans . NeuroImage. 2009. p. 677–82. Available from: http://dx.doi.org/10.1016/j.neuroimage.2009.02.030

47. Mori S, Crain BJ, Chacko VP, Van Zijl PCM. Three-dimensional tracking of axonal projections in the brain by magnetic resonance imaging . Annals of Neurology. 1999. p. 265–9. Available from: 3.0.co;2-3">http://dx.doi.org/10.1002/1531-8249(199902)45:2<265::aid-ana21>3.0.co;2-3

48. Tustison NJ, Avants BB, Cook PA, Zheng Y, Egan A, Yushkevich PA, et al. N4ITK: Improved N3 Bias Correction . IEEE Transactions on Medical Imaging. 2010. p. 1310–20. Available from: http://dx.doi.org/10.1109/tmi.2010.2046908

49. Quattrone A, Nicoletti G, Messina D, Fera F, Condino F, Pugliese P, et al. MR Imaging Index for Differentiation of Progressive Supranuclear Palsy from Parkinson Disease and

the Parkinson Variant of Multiple System Atrophy . Radiology. 2008. p. 214–21. Available from: http://dx.doi.org/10.1148/radiol.2453061703

50. Nicoletti G, Fera F, Condino F, Auteri W, Gallo O, Pugliese P, et al. MR Imaging of Middle Cerebellar Peduncle Width: Differentiation of Multiple System Atrophy from Parkinson Disease . Radiology. 2006. p. 825–30. Available from: http://dx.doi.org/10.1148/radiol.2393050459

51. Althouse AD. Adjust for Multiple Comparisons? It's Not That Simple . The Annals of Thoracic Surgery. 2016. p. 1644–5. Available from: http://dx.doi.org/10.1016/j.athoracsur.2015.11.024

52. Hurlbert SH, Levine RA, Utts J. Coup de Grâce for a Tough Old Bull: "Statistically Significant" Expires . The American Statistician. 2019. p. 352–7. Available from: http://dx.doi.org/10.1080/00031305.2018.1543616

53. Pan Q, Shai O, Lee LJ, Frey BJ, Blencowe BJ. Deep surveying of alternative splicing complexity in the human transcriptome by high-throughput sequencing . Nature Genetics. 2008. p. 1413–5. Available from: http://dx.doi.org/10.1038/ng.259

54. Ashley CT, Sutcliffe JS, Kunst CB, Leiner HA, Eichler EE, Nelson DL, et al. Human and murine FMR-1: alternative splicing and translational initiation downstream of the CGG–repeat . Nature Genetics. 1993. p. 244–51. Available from: http://dx.doi.org/10.1038/ng0793-244

55. Ding J, Huang T, Li L, Fan Y, Shen Y. [Alternative splicing of the FMR1 gene in human fetal tissues]. Zhongguo Yi Xue Ke Xue Yuan Xue Bao. 1997;19:241–6.

56. Banerjee P, Schoenfeld BP, Bell AJ, Choi CH, Bradley MP, Hinchey P, et al. Short-and Long-Term Memory Are Modulated by Multiple Isoforms of the Fragile X Mental Retardation Protein . Journal of Neuroscience. 2010. p. 6782–92. Available from: http://dx.doi.org/10.1523/jneurosci.6369-09.2010

57. Fu X, Zheng D, Liao J, Li Q, Lin Y, Zhang D, et al. Alternatively spliced products lacking exon 12 dominate the expression of fragile X mental retardation 1 gene in human tissues . Molecular Medicine Reports. 2015. p. 1957–62. Available from: http://dx.doi.org/10.3892/mmr.2015.3574

58. Saeed U, Compagnone J, Aviv RI, Strafella AP, Black SE, Lang AE, et al. Imaging biomarkers in Parkinson's disease and Parkinsonian syndromes: current and emerging concepts . Translational Neurodegeneration. 2017. Available from: http://dx.doi.org/10.1186/s40035-017-0076-6

59. Mangesius S, Hussl A, Krismer F, Mahlknecht P, Reiter E, Tagwercher S, et al. MR planimetry in neurodegenerative parkinsonism yields high diagnostic accuracy for PSP. Parkinsonism Relat Disord. 2018;46:47–55.

60. Whitwell JL, Höglinger GU, Antonini A, Bordelon Y, Boxer AL, Colosimo C, et al. Radiological biomarkers for diagnosis in PSP: Where are we and where do we need to be? Mov Disord. 2017;32:955–71.

61. Lee JH, Ryan J, Andreescu C, Aizenstein H, Lim HK. Brainstem morphological changes in Alzheimer's disease . NeuroReport. 2015. p. 411–5. Available from: http://dx.doi.org/10.1097/wnr.0000000000000362

62. Fernandes R, Nogueira G, da Costa PJ, Pinto F, Romão L. Nonsense-Mediated mRNA Decay in Development, Stress and Cancer . The mRNA Metabolism in Human Disease. 2019. p. 41–83. Available from: http://dx.doi.org/10.1007/978-3-030-19966-1_3

63. Jaffrey SR, Wilkinson MF. Nonsense-mediated RNA decay in the brain: emerging modulator of neural development and disease . Nature Reviews Neuroscience. 2018. p. 715–28. Available from: http://dx.doi.org/10.1038/s41583-018-0079-z

64. Korth C. Aggregated proteins in schizophrenia and other chronic mental diseases . Prion. 2012. p. 134–41. Available from: http://dx.doi.org/10.4161/pri.18989

8. Tables

Table 1: Participants Baseline Characteristics by Group

		Healthy Control	Converters	Non-Converters	All Participants	P-Value (F-Test)
Age	**N**	15	15	15	45	0.936
	Mean (SD)	60.1 (6.7)	61 (6.7)	60.7 (6.4)	60.6 (6.4)	
	Median (Range)	60(49–69)	61 (52–72)	62 (47–70)	61 (47–72)	
CGG	**N**	15	15	15	45	<0.001
	Mean (SD)	28.5 (4.1)	90.1 (22.4)	81.9 (22.1)	66.9 (32.9)	
	Median (Range)	30(20–32)	84(60–141)	78 (56–135)	75 (20–141)	

9. Figures
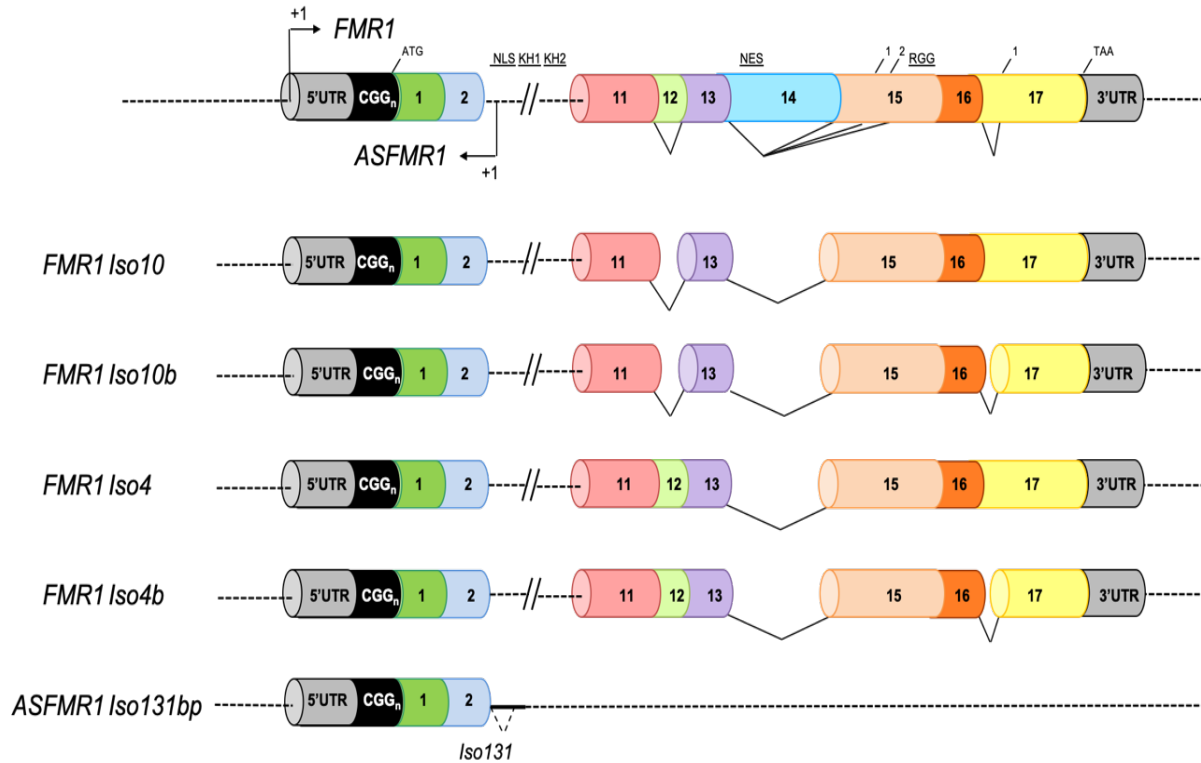
Figure 1: Schematic overview of the *FMR1* and *ASFMR1* isoforms.

Diagram representing the *FMR1* locus (top), 4 *FMR1* isoforms (*Iso10, Iso10b, Iso4 and Iso4b)* and the *ASFMR1 Iso131bp*. Exons are represented in different colors and the alternative splice sites are depicted for exon 12, 14,15 and 17. *FMR1* isoforms *Iso10,* and Iso10b both miss exon 12 and 14 but differ for the splicing acceptor site in exon 17. Likewise, the *FMR1 Iso4,* and *Iso4b* both miss exon 14 but differ for the splicing acceptor site in exon 17.
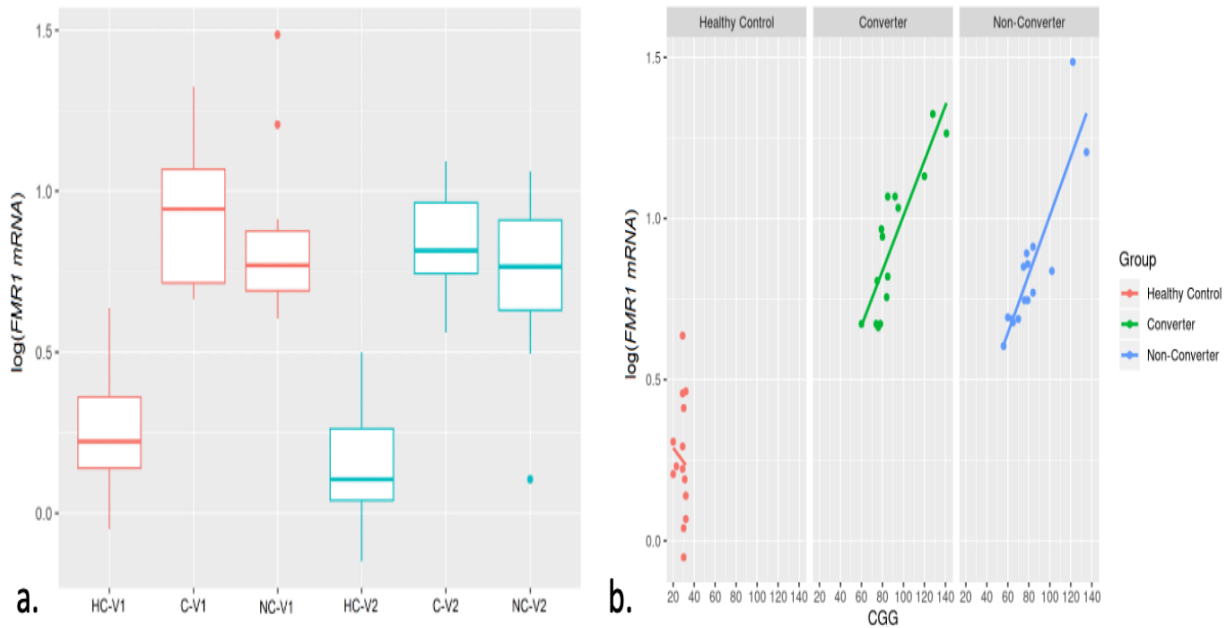
Figure 2: _FMR1_ mRNA expression among groups and by CGG repeat length.

a.) Box plots showing increased expression levels of _FMR1_ mRNA in both premutation groups (converters and non-converters) compared to non-carrier healthy controls at V1 [P < 0.001] and V2 [P < 0.001] but no significant differences were observed between the two premutation groups. The heavy line in each box represents the median, the lower and upper box edges represent the 25th and 75th percentiles, respectively, and the lower and upper whiskers represent the smallest and largest observations, respectively. b.) Scatter plots showing _FMR1_ mRNA expression as function of CGG repeat number at V1 in the three groups.
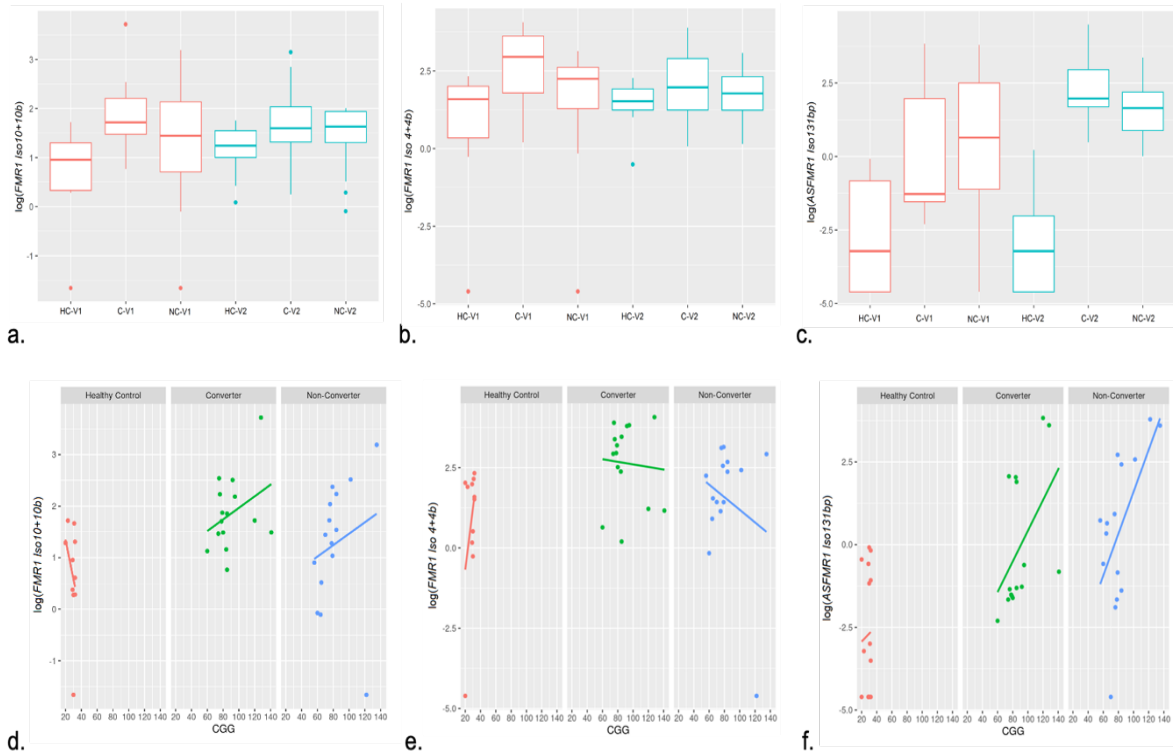
Figure 3: Isoform's mRNA expression levels among three groups and as function of the CGG repeat number. a.) Box plots showing increased levels of *FMR1 Iso10/10b* mRNA at both V1 and V2 (P=0.0225 and P=0.0468 respectively) only in the converter group but not in the non-converter group (P=0.401 at V1 and P=0.592 at V2) compared to non-carrier healthy controls. b.) Box plots showing increased levels of *FMR1 Iso4/4b mRNA* at V1 (P=0.0323) but not at V2 (P=0.247) in the converter group compared to non-carrier healthy controls. No differences were observed in the non-converter group at both visits (P=0.542 at V1 and P=0.684 at V2). c.) Box plots showing increased levels of *ASFMR1 Iso131bp mRNA* at both V1 (P <0.001) and V2 (P <0.001) in both the premutation groups compared to non-carrier healthy controls but not statistically significant differences between the two premutation groups. The heavy line in each box represents the median,

the lower and upper box edges represent the 25th and 75th percentiles, respectively, and the lower and upper whiskers represent the smallest and largest observations, respectively. Scatter plots showing d.) *FMR1* e.) of *FMR1 Iso4/4b* and f.) of *ASFMR1 Iso131bp* mRNA expression levels as function of the CGG repeat number at V1 in the three groups.
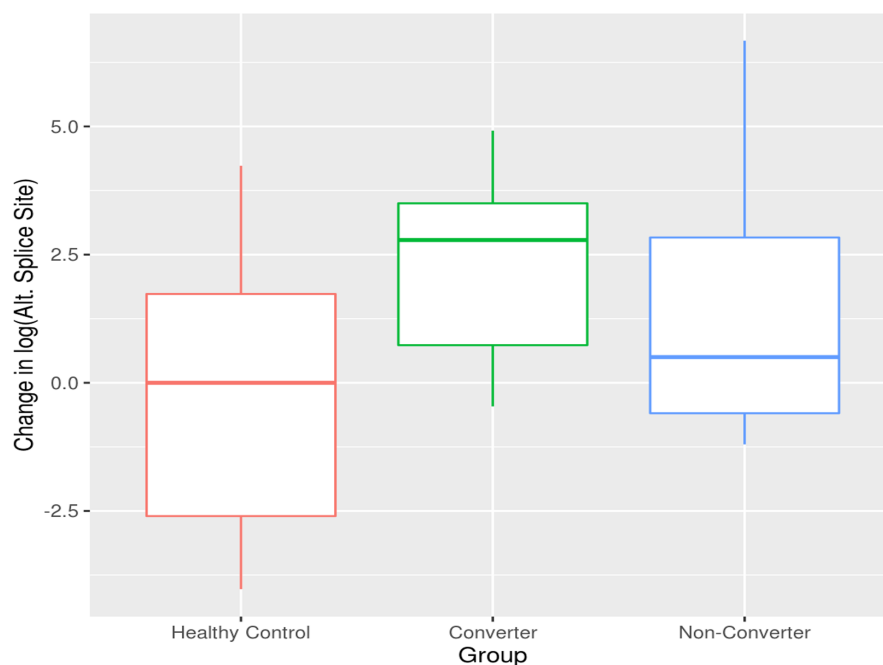
Figure 4: Changes in *ASFMR1 Iso131bp* expression levels between visits. Boxplots showing higher changes between V1 and V2 in the expression level of the *ASFMR1 Iso131bp* in the converter group as compared to non-carrier healthy controls while no significant change in non-converter versus control was observed. The heavy line in each box represents the median, the lower and upper box edges represent the 25th and 75th

percentiles, respectively, and the lower and upper whiskers represent the smallest and largest observations, respectively.

a.

b.
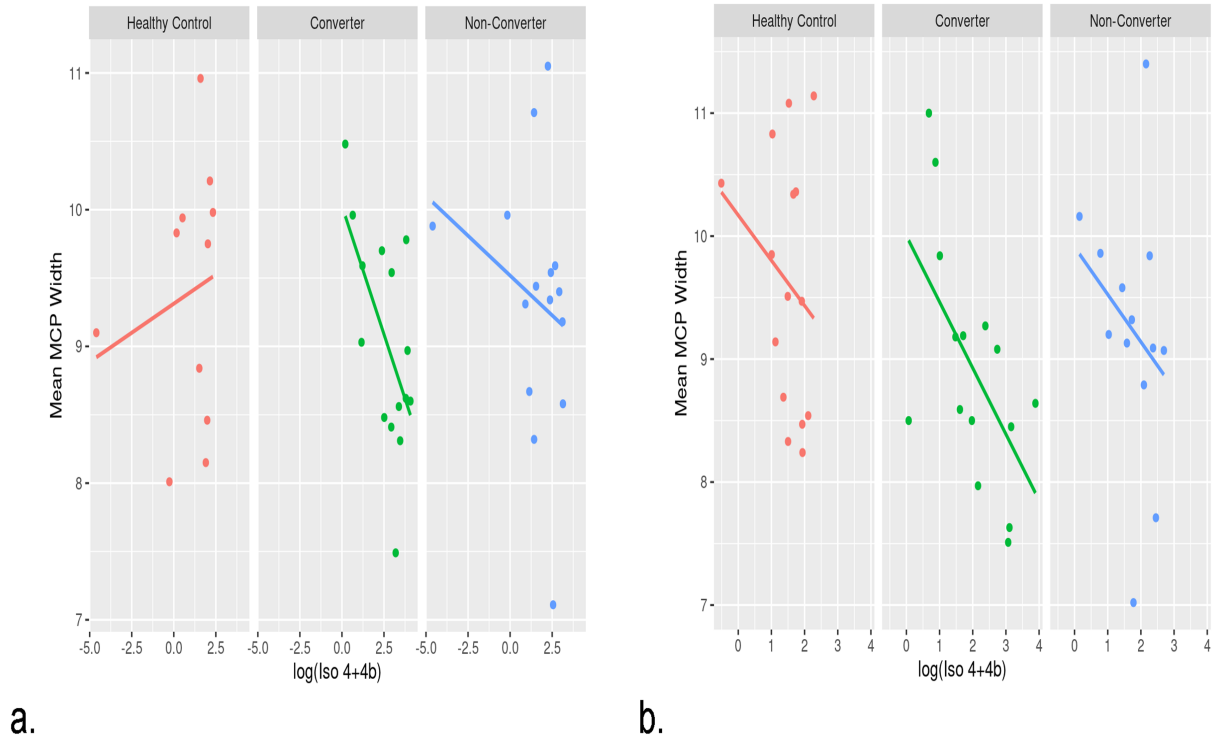
Figure 5: Molecular and brain measure correlations. Scatter plots demonstrating an inverse correlation between the mean MCP width and Iso4/4b in both V1 and V2 but only in the converter group while no significant correlation was observed in the non-converter group.

10. Supplementary Materials

Table S1: <u>Marker Expression by CGG Repeat Length, Baseline Visit</u>

	Healthy Control		Converter		Non-Converter	
	Fold Change (95% CI)	**P-Value**	**Fold Change (95% CI)**	**P-Value**	**Fold Change (95% CI)**	**P-Value**
FMR1	0.996(0.977, 1.014)	0.641	**1.008(1.004, 1.011)**	**<0.001**	**1.008(1.005, 1.012)**	**<0.001**
ASFMR1	1.028(0.905, 1.167)	0.667	1 (0.976, 1.026)	0.971	1.01 (0.985, 1.037)	0.414
Alt. Splice Site	1.024(0.792, 1.324)	0.852	1.051(0.999, 1.105)	0.053	**1.069(1.016, 1.126)**	**0.012**
Intron 9.5	0.93 (0.783, 1.104)	0.394	1.011(0.979, 1.045)	0.486	**0.955(0.921, 0.991)**	**0.015**
Iso 4+4b	1.205(0.947, 1.534)	0.125	0.998(0.954, 1.045)	0.946	0.983(0.938, 1.03)	0.47
Iso 10+10b	0.92 (0.802, 1.056)	0.23	1.015 0.989, 1.042)	0.244	1.016(0.989, 1.043)	0.247

[a] Adjusted for age

[b] Fold change is (multiplicative) change in expression for each unit increase in CGG repeat length.

Table S2a: <u>Comparison of Marker Expression Between Groups, Baseline Visit</u>

	Healthy Control - Converter		Healthy Control - Non-Converter		Converter - Non-Converter	
	Fold Change (95% CI)	**P-Value**	**Fold Change (95% CI)**	**P-Value**	**Fold Change (95% CI)**	**P-Value**
FMR1	**0.503 (0.425, 0.595)**	**<0.001**	**0.548 (0.463, 0.648)**	**<0.001**	1.089 (0.921, 1.288)	0.438
ASFMR1	0.486 (0.21, 1.126)	0.105	0.476 (0.206, 1.102)	0.092	0.98 (0.423, 2.267)	0.998

	0.065 (0.01, 0.423)	0.003	0.04 (0.006, 0.264)	<0.001	0.624 (0.096, 4.069)	0.815
Alt. Splice Site	**0.065 (0.01, 0.423)**	**0.003**	**0.04 (0.006, 0.264)**	**<0.001**	0.624 (0.096, 4.069)	0.815
Intron 9.5	0.391 (0.107, 1.425)	0.192	0.792 (0.214, 2.934)	0.901	2.024 (0.604, 6.783)	0.339
Iso 4+4b	**0.161 (0.029, 0.877)**	**0.032**	0.477 (0.087, 2.607)	0.542	2.967 (0.625, 14.095)	0.217
Iso 10+10b	**0.327 (0.123, 0.872)**	**0.023**	0.591 (0.222, 1.578)	0.401	1.807 (0.734, 4.445)	0.257

a Adjusted for age

Table S2b: <u>Comparison of Marker Expression Between Groups, Visit 2</u>

	Healthy Control - Converter		Healthy Control - Non-Converter		Converter - Non-Converter	
	Fold Change (95% CI)	**P-Value**	**Fold Change (95% CI)**	**P-Value**	**Fold Change (95% CI)**	**P-Value**
FMR1	**0.498 (0.421, 0.589)**	**<0.001**	**0.552 (0.467, 0.653)**	**<0.001**	1.108 (0.937, 1.311)	0.308
ASFMR1	0.614 (0.343, 1.098)	0.116	0.872 (0.488, 1.558)	0.834	1.419 (0.794, 2.537)	0.318
Alt. Splice Site	**0.005 (0.001, 0.015)**	**<0.001**	**0.01 (0.003, 0.031)**	**<0.001**	2.076 (0.641, 6.729)	0.297
Intron 9.5	0.508 (0.18, 1.432)	0.262	1.223 (0.434, 3.443)	0.884	2.407 (0.854, 6.781)	0.111
Iso 4+4b	0.591 (0.269, 1.298)	0.247	0.764 (0.348, 1.675)	0.684	1.291 (0.588, 2.834)	0.71
Iso 10+10b	**0.563 (0.319, 0.993)**	**0.047**	0.795 (0.451, 1.402)	0.592	1.412 (0.801, 2.491)	0.311

a Adjusted for age

Table S2c: <u>Comparison of Change in Marker Expression Between Groups</u>

	Healthy Control - Converter		Healthy Control - Non-Converter		Converter - Non-Converter	
	Fold Change (95% CI)	P-Value	Fold Change (95% CI)	P-Value	Fold Change (95% CI)	P-Value
Change in FMR1	0.99 (0.809, 1.211)	0.991	1.011 (0.818, 1.248)	0.992	1.021 (0.829, 1.258)	0.967
Change in ASFMR1	1.222 (0.479, 3.115)	0.862	1.485 (0.557, 3.957)	0.592	1.216 (0.463, 3.195)	0.876
Change in Alt. Splice Site	0.067 (0.009, 0.496)	0.006	0.164 (0.02, 1.327)	0.102	2.436 (0.311, 19.098)	0.549
Change in Intron 9.5	1.402 (0.571, 3.439)	0.631	1.974 (0.8, 4.87)	0.171	1.408 (0.593, 3.347)	0.602
Change in Iso 4+4b	4.141 (0.763, 22.49)	0.114	1.813 (0.336, 9.764)	0.667	0.438 (0.088, 2.185)	0.429
Change in Iso 10+10b	1.771 (0.687, 4.567)	0.314	1.647 (0.641, 4.226)	0.408	0.929 (0.378, 2.286)	0.979

[a] Adjusted for age and visit interval

Table S3a: <u>Brain Measures by Molecular Measures by Group, Baseline Visit</u>

Brain Measure	Molecular Measure	Healthy Control		Converter		Non-Converter	
		Regression Slope (95% CI)	P-Value	Regression Slope (95% CI)	P-Value	Regression Slope (95% CI)	P-Value
Mean MCP Width	FMR1	0.47 (-2.246, 3.186)	0.728	-1.31 (-3.76, 1.14)	0.286	-0.736 (-3.041, 1.568)	0.522
Mean MCP Width	ASFMR1	0.057 (-0.608, 0.721)	0.864	0.089 (-0.427, 0.604)	0.73	-0.168 (-0.654, 0.318)	0.489

97

Mean MCP Width	Alt. Splice Site	-0.128 (-0.395, 0.139)	0.337	0.133 (-0.107, 0.372)	0.27	0.117 (-0.101, 0.335)	0.285
Mean MCP Width	Intron 9.5	0.244 (-0.388, 0.876)	0.438	-0.325 (-1.01, 0.36)	0.342	-0.037 (-0.313, 0.239)	0.787
Mean MCP Width	Iso 4+4b	0.085 (-0.188, 0.359)	0.53	-0.421 (-0.794, -0.048)	0.028	-0.064 (-0.316, 0.188)	0.611
Mean MCP Width	Iso 10+10b	0.188 (-0.399, 0.774)	0.52	-0.603 (-1.283, 0.077)	0.08	-0.155 (-0.546, 0.235)	0.424
Mean SCP	FMR1	0.724 (-1.94, 3.388)	0.585	0.414 (-1.988, 2.817)	0.729	-1.693 (-3.953, 0.567)	0.138
Mean SCP	ASFMR1	0.038 (-0.618, 0.695)	0.907	0.281 (-0.229, 0.79)	0.272	0.076 (-0.404, 0.557)	0.75
Mean SCP	Alt. Splice Site	-0.033 (-0.304, 0.239)	0.81	0.097 (-0.147, 0.341)	0.425	-0.078 (-0.3, 0.144)	0.482
Mean SCP	Intron 9.5	0.133 (-0.471, 0.737)	0.657	0.485 (-0.17, 1.141)	0.141	-0.079 (-0.343, 0.185)	0.545
Mean SCP	Iso 4+4b	-0.053 (-0.338, 0.232)	0.707	0.1 (-0.29, 0.489)	0.606	0.125 (-0.138, 0.388)	0.342
Mean SCP	Iso 10+10b	0 (-0.599, 0.599)	0.999	0.43 (-0.264, 1.124)	0.217	-0.021 (-0.419, 0.378)	0.916
Midbrain	FMR1	9.447 (-65.863, 84.757)	0.801	-3.247 (-71.18, 64.686)	0.923	8.275 (-55.627, 72.178)	0.795
Midbrain	ASFMR1	-0.092 (-18.078, 17.895)	0.992	0.928 (-13.032, 14.888)	0.894	6.62 (-6.542, 19.781)	0.315
Midbrain	Alt. Splice Site	-0.574 (-8.019, 6.871)	0.877	2.294 (-4.397, 8.985)	0.492	2.179 (-3.912, 8.27)	0.473
Midbrain	Intron 9.5	-7.799 (-24.685, 9.088)	0.354	11.406 (-6.899, 29.711)	0.214	-4.691 (-12.066, 2.685)	0.205
Midbrain	Iso 4+4b	5.423 (-2.215, 13.061)	0.158	-2.703 (-13.129, 7.723)	0.602	-7.402 (-14.451, -0.354)	0.04

Region	Feature						
Midbrain	Iso 10+10b	-5.142 (-22.019, 11.736)	0.54	2.449 (-17.106, 22.004)	0.801	-9.35 (-20.575, 1.875)	0.1
Pons	FMR1	72.835 (-127.952, 273.621)	0.467	12.262 (-168.855, 193.38)	0.892	-79.858 (-250.231, 90.514)	0.349
Pons	ASFMR1	1.625 (-47.616, 50.866)	0.947	-11.225 (-49.444, 26.994)	0.556	3.517 (-32.516, 39.549)	0.844
Pons	Alt. Splice Site	-17.625 (-36.256, 1.007)	0.063	17.771 (1.027, 34.515)	0.038	0.331 (-14.912, 15.573)	0.965
Pons	Intron 9.5	9.255 (-39.126, 57.635)	0.7	19.327 (-33.117, 71.771)	0.459	-1.33 (-22.46, 19.801)	0.899
Pons	Iso 4+4b	14.559 (-5.231, 34.349)	0.144	-26.244 (-53.256, 0.768)	0.056	-18.735 (-36.998, -0.473)	0.045
Pons	Iso 10+10b	22.673 (-18.952, 64.298)	0.276	-11.832 (-60.06, 36.397)	0.621	-42.029 (-69.713, -14.345)	0.004
Pons/Midbrain Ratio	FMR1	0.161 (-1.727, 2.048)	0.864	0.783 (-0.919, 2.486)	0.358	-0.742 (-2.343, 0.86)	0.355
Pons/Midbrain Ratio	ASFMR1	0.099 (-0.362, 0.56)	0.666	-0.061 (-0.419, 0.296)	0.73	-0.162 (-0.499, 0.176)	0.338
Pons/Midbrain Ratio	Alt. Splice Site	-0.061 (-0.245, 0.124)	0.51	0.124 (-0.041, 0.29)	0.137	-0.071 (-0.222, 0.08)	0.349
Pons/Midbrain Ratio	Intron 9.5	0.161 (-0.291, 0.613)	0.474	-0.184 (-0.674, 0.306)	0.449	0.108 (-0.089, 0.306)	0.273
Pons/Midbrain Ratio	Iso 4+4b	-0.028 (-0.239, 0.184)	0.792	0.102 (-0.187, 0.391)	0.48	0.071 (-0.124, 0.267)	0.463
Pons/Midbrain Ratio	Iso 10+10b	0.198 (-0.25, 0.646)	0.376	0.033 (-0.486, 0.552)	0.898	-0.035 (-0.333, 0.263)	0.815
MCP/SCP Ratio	FMR1	-0.115 (-1.08, 0.85)	0.811	-0.451 (-1.321, 0.419)	0.301	0.392 (-0.426, 1.211)	0.338
MCP/SCP Ratio	ASFMR1	0.017 (-0.218, 0.253)	0.884	-0.088 (-0.271, 0.094)	0.334	-0.069 (-0.241, 0.103)	0.422

Brain Measure	Molecular Measure	Regression Slope (95% CI)	P-Value	Regression Slope (95% CI)	P-Value	Regression Slope (95% CI)	P-Value
MCP/SCP Ratio	Alt. Splice Site	-0.016 (-0.112, 0.081)	0.743	0 (-0.086, 0.087)	0.991	0.056 (-0.023, 0.136)	0.157
MCP/SCP Ratio	Intron 9.5	-0.014 (-0.22, 0.192)	0.887	-0.256 (-0.48, -0.033)	0.026	0.027 (-0.063, 0.117)	0.549
MCP/SCP Ratio	Iso 4+4b	0.036 (-0.059, 0.131)	0.452	-0.123 (-0.253, 0.007)	0.062	-0.059 (-0.147, 0.029)	0.179
MCP/SCP Ratio	Iso 10+10b	0.021 (-0.179, 0.221)	0.832	-0.287 (-0.518, -0.056)	0.017	-0.028 (-0.161, 0.105)	0.671

[a] Adjusted for age

[b] Regression slope is (additive) change in brain measure for each unit increase in the molecular measure.

Table S3b: Brain Measures by Molecular Measures by Group, Visit 2

		Healthy Control		Converter		Non-Converter	
Brain Measure	Molecular Measure	Regression Slope (95% CI)	P-Value	Regression Slope (95% CI)	P-Value	Regression Slope (95% CI)	P-Value
Mean MCP Width	FMR1	-2.308 (-5.407, 0.791)	0.14	0.998 (-2.708, 4.705)	0.588	1.432 (-0.988, 3.852)	0.238
Mean MCP Width	ASFMR1	-0.525 (-1.319, 0.269)	0.188	0.269 (-0.851, 1.389)	0.629	-0.089 (-0.983, 0.805)	0.842
Mean MCP Width	Alt. Splice Site	-0.334 (-0.645, -0.024)	0.036	-0.09 (-0.56, 0.381)	0.701	0.135 (-0.456, 0.726)	0.646
Mean MCP Width	Intron 9.5	-0.157 (-1.281, 0.967)	0.779	-0.486 (-1.354, 0.382)	0.264	-0.11 (-0.44, 0.22)	0.504

Mean MCP Width	Iso 4+4b	-0.376 (-1.206, 0.454)	0.365	-0.531 (-1.057, -0.004)	0.048	-0.392 (-1.201, 0.417)	0.333
Mean MCP Width	Iso 10+10b	-0.639 (-1.766, 0.489)	0.258	-0.249 (-1.034, 0.536)	0.524	-0.369 (-1.478, 0.741)	0.505
Mean SCP	FMR1	-0.207 (-3.342, 2.929)	0.894	2.065 (-1.684, 5.815)	0.271	1.748 (-0.701, 4.196)	0.156
Mean SCP	ASFMR1	0.236 (-0.569, 1.04)	0.556	0.102 (-1.032, 1.237)	0.856	-0.411 (-1.317, 0.494)	0.363
Mean SCP	Alt. Splice Site	-0.101 (-0.418, 0.217)	0.524	0.163 (-0.318, 0.644)	0.496	-0.489 (-1.093, 0.115)	0.109
Mean SCP	Intron 9.5	-0.135 (-1.271, 1.001)	0.811	0.155 (-0.722, 1.032)	0.722	0.165 (-0.168, 0.498)	0.321
Mean SCP	Iso 4+4b	-0.226 (-1.117, 0.665)	0.611	0.107 (-0.458, 0.672)	0.703	0.3 (-0.569, 1.168)	0.489
Mean SCP	Iso 10+10b	-0.229 (-1.386, 0.929)	0.691	0.142 (-0.664, 0.948)	0.723	-0.092 (-1.232, 1.047)	0.87
Midbrain	FMR1	-26.217 (-98.386, 45.953)	0.466	16.332 (-69.98, 102.644)	0.703	5.285 (-51.071, 61.641)	0.85
Midbrain	ASFMR1	16.94 (-0.283, 34.163)	0.054	3.749 (-20.54, 28.039)	0.756	4.422 (-14.972, 23.816)	0.647
Midbrain	Alt. Splice Site	6.395 (-0.459, 13.249)	0.067	4.181 (-6.204, 14.567)	0.42	-8.218 (-21.25, 4.814)	0.209
Midbrain	Intron 9.5	16.682 (-8.383, 41.747)	0.186	0.353 (-19.003, 19.708)	0.971	-0.979 (-8.33, 6.372)	0.789

Region	Target						
Midbrain	Iso 4+4b	13.59 (-5.232, 32.412)	0.152	-9.092 (-21.027, 2.843)	0.131	-6.987 (-25.338, 11.365)	0.445
Midbrain	Iso 10+10b	20.607 (-3.39, 44.605)	0.09	-1.854 (-18.565, 14.856)	0.823	-19.663 (-43.278, 3.951)	0.1
Pons	FMR1	-110.666 (-311.115, 89.784)	0.27	192.282 (-47.45, 432.013)	0.113	4.014 (-152.515, 160.543)	0.959
Pons	ASFMR1	8.536 (-43.814, 60.885)	0.743	5.031 (-68.796, 78.857)	0.891	-19.317 (-78.265, 39.631)	0.511
Pons	Alt. Splice Site	8.62 (-12.261, 29.5)	0.408	7.993 (-23.648, 39.635)	0.612	-19.648 (-59.352, 20.056)	0.322
Pons	Intron 9.5	-21.238 (-93.754, 51.278)	0.556	-33.847 (-89.845, 22.151)	0.228	3.558 (-17.711, 24.827)	0.736
Pons	Iso 4+4b	20.493 (-34.755, 75.741)	0.457	-31.064 (-66.096, 3.969)	0.081	18.354 (-35.513, 72.221)	0.494
Pons	Iso 10+10b	2.335 (-69.486, 74.155)	0.948	-17.942 (-67.954, 32.069)	0.472	-57.827 (-128.503, 12.849)	0.106
Pons/Midbrain Ratio	FMR1	0.082 (-1.189, 1.354)	0.896	0.717 (-0.804, 2.237)	0.346	-0.269 (-1.262, 0.724)	0.586
Pons/Midbrain Ratio	ASFMR1	-0.3 (-0.602, 0.001)	0.051	-0.067 (-0.492, 0.358)	0.752	-0.191 (-0.531, 0.148)	0.26
Pons/Midbrain Ratio	Alt. Splice Site	-0.078 (-0.206, 0.05)	0.224	-0.069 (-0.263, 0.125)	0.477	0.027 (-0.216, 0.27)	0.824
Pons/Midbrain Ratio	Intron 9.5	-0.433 (-0.848, -0.019)	0.041	-0.246 (-0.566, 0.074)	0.128	0.054 (-0.067, 0.176)	0.372

Brain Measure	Molecular Measure	Healthy Control Regression Slope (95% CI)	P-Value	Converter Regression Slope (95% CI)	P-Value	Non-Converter Regression Slope (95% CI)	P-Value
Pons/Midbrain Ratio	Iso 4+4b	-0.094 (-0.435, 0.248)	0.582	-0.011 (-0.228, 0.206)	0.918	0.277 (-0.056, 0.61)	0.101
Pons/Midbrain Ratio	Iso 10+10b	-0.316 (-0.76, 0.128)	0.158	-0.101 (-0.411, 0.208)	0.51	0.061 (-0.376, 0.498)	0.78
MCP/SCP Ratio	FMR1	-0.499 (-1.647, 0.648)	0.383	-0.456 (-1.828, 0.916)	0.505	-0.355 (-1.25, 0.541)	0.427
MCP/SCP Ratio	ASFMR1	-0.176 (-0.462, 0.109)	0.218	0.022 (-0.38, 0.425)	0.911	0.126 (-0.195, 0.447)	0.431
MCP/SCP Ratio	Alt. Splice Site	-0.021 (-0.134, 0.092)	0.712	-0.065 (-0.236, 0.107)	0.449	0.194 (-0.021, 0.409)	0.075
MCP/SCP Ratio	Intron 9.5	0.015 (-0.378, 0.407)	0.94	-0.188 (-0.491, 0.115)	0.217	-0.092 (-0.207, 0.023)	0.114
MCP/SCP Ratio	Iso 4+4b	-0.034 (-0.342, 0.274)	0.823	-0.145 (-0.34, 0.051)	0.142	-0.175 (-0.475, 0.125)	0.244
MCP/SCP Ratio	Iso 10+10b	-0.088 (-0.501, 0.324)	0.667	-0.121 (-0.409, 0.166)	0.398	0.004 (-0.402, 0.41)	0.985

[a] Adjusted for age
[b] Regression slope is (additive) change in brain measure for each unit increase in the molecular measure.

Table S3c: Changes in Brain Measures by Changes in Molecular Measures by Group

		Healthy Control		Converter		Non-Converter	
Brain Measure	**Molecular Measure**	**Regression Slope (95% CI)**	**P-Value**	**Regression Slope (95% CI)**	**P-Value**	**Regression Slope (95% CI)**	**P-Val**

Change in Mean MCP Width	Change in log(FMR1)	0.05 (-0.116, 0.217)	0.543	-0.028 (-0.272, 0.216)	0.815	0.038 (-0.12, 0.196)	0.629
Change in Mean MCP Width	Change in log(ASFMR1)	0.007 (-0.032, 0.047)	0.704	0.021 (-0.013, 0.055)	0.224	-0.029 (-0.061, 0.003)	0.075
Change in Mean MCP Width	Change in log(Alt. Splice Site)	0.002 (-0.014, 0.017)	0.827	-0.006 (-0.03, 0.017)	0.588	0.007 (-0.011, 0.025)	0.407
Change in Mean MCP Width	Change in log(Intron 9.5)	0.035 (-0.01, 0.081)	0.125	0.008 (-0.062, 0.079)	0.809	-0.026 (-0.084, 0.033)	0.375
Change in Mean MCP Width	Change in log(Iso 4+4b)	-0.003 (-0.028, 0.021)	0.786	-0.013 (-0.049, 0.023)	0.456	-0.003 (-0.024, 0.017)	0.736
Change in Mean MCP Width	Change in log(Iso 10+10b)	0.034 (-0.014, 0.081)	0.156	-0.009 (-0.068, 0.05)	0.754	-0.016 (-0.055, 0.022)	0.395
Change in Mean SCP	Change in log(FMR1)	0.211 (-0.189, 0.612)	0.292	0.726 (0.14, 1.313)	0.017	0.327 (-0.053, 0.708)	0.09
Change in Mean SCP	Change in log(ASFMR1)	-0.042 (-0.154, 0.069)	0.448	0.067 (-0.029, 0.164)	0.164	-0.03 (-0.12, 0.061)	0.51
Change in Mean SCP	Change in log(Alt. Splice Site)	0.007 (-0.032, 0.046)	0.728	-0.014 (-0.075, 0.046)	0.633	-0.053 (-0.1, -0.007)	0.025
Change in Mean SCP	Change in log(Intron 9.5)	0.048 (-0.082, 0.178)	0.456	0.085 (-0.115, 0.285)	0.39	-0.116 (-0.283, 0.051)	0.166
Change in Mean SCP	Change in log(Iso 4+4b)	0.017 (-0.052, 0.087)	0.611	0.007 (-0.096, 0.11)	0.89	-0.011 (-0.07, 0.048)	0.705
Change in Mean SCP	Change in log(Iso 10+10b)	0.055 (-0.082, 0.192)	0.417	0.091 (-0.078, 0.261)	0.28	-0.04 (-0.151, 0.07)	0.463
Change in Midbrain	Change in log(FMR1)	-0.069 (-0.264, 0.126)	0.48	0.316 (0.03, 0.601)	0.031	0.097 (-0.089, 0.282)	0.296
Change in Midbrain	Change in log(ASFMR1)	-0.015 (-0.067, 0.037)	0.557	0.03 (-0.015, 0.075)	0.183	0.004 (-0.038, 0.046)	0.841

Change in Midbrain	Change in log(Alt. Splice Site)	0 (-0.019, 0.019)	0.989	-0.018 (-0.048, 0.011)	0.223	0.006 (-0.017, 0.028)	0.62
Change in Midbrain	Change in log(Intron 9.5)	-0.018 (-0.075, 0.039)	0.515	0.073 (-0.014, 0.161)	0.098	0.03 (-0.043, 0.103)	0.407
Change in Midbrain	Change in log(Iso 4+4b)	-0.021 (-0.051, 0.01)	0.182	0.001 (-0.044, 0.046)	0.965	-0.007 (-0.033, 0.019)	0.592
Change in Midbrain	Change in log(Iso 10+10b)	-0.016 (-0.076, 0.043)	0.58	0.076 (0.002, 0.149)	0.045	-0.008 (-0.057, 0.04)	0.727
Change in Pons	Change in log(FMR1)	0.033 (-0.052, 0.117)	0.44	0.083 (-0.041, 0.207)	0.182	-0.039 (-0.12, 0.041)	0.327
Change in Pons	Change in log(ASFMR1)	-0.003 (-0.025, 0.019)	0.785	0.005 (-0.015, 0.024)	0.629	-0.004 (-0.022, 0.014)	0.663
Change in Pons	Change in log(Alt. Splice Site)	-0.003 (-0.011, 0.004)	0.385	-0.012 (-0.024, 0)	0.047	0.002 (-0.007, 0.011)	0.633
Change in Pons	Change in log(Intron 9.5)	0.003 (-0.023, 0.029)	0.807	-0.011 (-0.051, 0.029)	0.58	0.006 (-0.027, 0.039)	0.701
Change in Pons	Change in log(Iso 4+4b)	0.004 (-0.009, 0.017)	0.541	0.001 (-0.019, 0.02)	0.934	0.008 (-0.003, 0.019)	0.152
Change in Pons	Change in log(Iso 10+10b)	0.006 (-0.02, 0.033)	0.626	0.006 (-0.027, 0.038)	0.735	0.013 (-0.008, 0.035)	0.211
Change in Pons/Midbrain Ratio	Change in log(FMR1)	0.174 (-0.179, 0.528)	0.323	-0.151 (-0.669, 0.366)	0.556	-0.118 (-0.454, 0.218)	0.479
Change in Pons/Midbrain Ratio	Change in log(ASFMR1)	0.006 (-0.085, 0.097)	0.897	-0.02 (-0.099, 0.058)	0.607	-0.014 (-0.087, 0.06)	0.706
Change in Pons/Midbrain Ratio	Change in log(Alt. Splice Site)	-0.006 (-0.039, 0.027)	0.734	0.009 (-0.042, 0.06)	0.724	-0.009 (-0.049, 0.03)	0.629
Change in Pons/Midbrain Ratio	Change in log(Intron 9.5)	0.033 (-0.071, 0.138)	0.519	-0.075 (-0.236, 0.087)	0.351	-0.007 (-0.141, 0.128)	0.922
Change in Pons/Midbrain Ratio	Change in log(Iso 4+4b)	0.017 (-0.037, 0.07)	0.522	0.051 (-0.028, 0.131)	0.195	0.024 (-0.021, 0.07)	0.278

Change in Pons/Midbrain Ratio	Change in log(Iso 10+10b)	0.047 (-0.063, 0.158)	0.391	0.047 (-0.091, 0.184)	0.493	0.033 (-0.057, 0.123)	0.46
Change in MCP/SCP Ratio	Change in log(FMR1)	-0.253 (-0.689, 0.184)	0.248	-0.774 (-1.413, -0.135)	0.019	-0.288 (-0.703, 0.127)	0.168
Change in MCP/SCP Ratio	Change in log(ASFMR1)	0.076 (-0.045, 0.197)	0.213	-0.046 (-0.15, 0.058)	0.376	-0.001 (-0.099, 0.097)	0.985
Change in MCP/SCP Ratio	Change in log(Alt. Splice Site)	0.004 (-0.038, 0.046)	0.849	0.006 (-0.059, 0.071)	0.861	0.06 (0.01, 0.109)	0.02
Change in MCP/SCP Ratio	Change in log(Intron 9.5)	-0.022 (-0.166, 0.122)	0.76	-0.087 (-0.309, 0.135)	0.431	0.095 (-0.09, 0.281)	0.302
Change in MCP/SCP Ratio	Change in log(Iso 4+4b)	-0.02 (-0.095, 0.056)	0.6	-0.024 (-0.135, 0.088)	0.669	0.01 (-0.054, 0.073)	0.758
Change in MCP/SCP Ratio	Change in log(Iso 10+10b)	-0.046 (-0.195, 0.103)	0.533	-0.113 (-0.298, 0.071)	0.219	0.03 (-0.091, 0.15)	0.621

[a] Adjusted for age and visit interval
[b] Regression slope is (additive) change in change in brain measure for each unit increase in the change in the molecular measure.

Chapter 3

Metabolic profiling reveals dysregulated lipid metabolism and potential biomarkers associated with the development and progression of Fragile X-Associated Tremor/Ataxia Syndrome (FXTAS)

Marwa Zafarullah [1], Grzegorz Palczewski, David Hessl[5,6], Susan M. Rivera[3,4,5,] and Flora Tassone [1,5*]

[7] Department of Biochemistry and Molecular Medicine, University of California Davis, School of Medicine, Sacramento, 95817 CA, USA.
[8] Metabolon, Morrisville, NC, USA
[9] Center for Mind and Brain, University of California Davis, Davis, CA, USA.
[10] Department of Psychology, University of California, Davis, Davis, CA, USA.
[11] MIND Institute, University of California Davis Medical Center, Sacramento, 95817 CA, USA.
[12] Department of Psychiatry and Behavioral Sciences, University of California Davis Medical Center, Sacramento, 95817 CA, USA.
* **Correspondence:** ftassone@ucdavis.edu; Tel.: +1-(916)-703-0463

Abstract

Fragile X-associated Tremor/Ataxia Syndrome (FXTAS) is a neurodegenerative disorder associated with the *FMR1* premutation. It is currently unknown when, and if, individual premutation carriers will develop FXTAS. Thus, with the aim of identifying biomarkers for early diagnosis, development, and progression of FXTAS, we performed global metabolomic profiling of premutation carriers (PM) who, as part of an ongoing longitudinal study, emerged into two distinct categories: those who developed symptoms of FXTAS (converters, CON) at subsequent visits and those who did not (non-converters, NCON) and we compared to age-matched healthy controls (HC). We assessed CGG repeat allele size by Southern Blot and PCR analysis. Metabolomic profile was obtained

by ultra-performance liquid chromatography, accurate mass spectrometer, and an Orbitrap mass analyzer. In this study we found 47 metabolites were significantly dysregulated between HC and the premutation groups (PM). Importantly, we identified 24 metabolites that showed significant changes in expression in the CON as compared to the NCON both at V1 and V2, and 70 metabolites in CON as compared to NCON but only at V2. These findings suggest the potential role of the identified metabolites as biomarkers for early diagnosis and for FXTAS disease progression, respectively. Interestingly, the majority of the identified metabolites were lipids, followed by amino acids. To our knowledge, this the first report of longitudinal metabolic profiling and identification of unique biomarkers of FXTAS. The lipid metabolism and specifically the sub pathways involved in mitochondrial bioenergetics, as observed in other neurodegenerative disorders, are significantly altered in FXTAS.

Keywords: Fragile X-associated tremor/ataxia syndrome, molecular biomarkers, *FMR1,* metabolomic, fatty acids.

1.   Introduction

Today, neurodegenerative diseases represent one of the significant causes of death in an industrialized economy. The prevalence of age-dependent disorders has escalated in the past few years due to an increase in the elderly population (1). The development of unique targeted therapeutics for rare age-dependent neurodegenerative disorders faces many challenges, including the lack of biomarkers for early diagnosis and progression, complicated underlying molecular mechanisms, heterogeneous

phenotypes, limited historical data, and difficulty of assessing efficacy in clinical trials for which small patient populations limit enrollment. Thus, it is of importance to identify biomarkers, which can provide fast, objective evidence for changes of underlying disease pathophysiology, which may, in turn, be used for clinical benefit.

Fragile X-associated Tremor/Ataxia Syndrome (FXTAS) is a late-onset neurodegenerative disorder that affects some carriers of the fragile X mental retardation 1 (*FMR1*) premutation after the age of fifty. It is characterized by intention tremor, cerebellar ataxia, white matter/ global brain atrophy, autonomic dysfunction, and progressive Parkinsonism. Neuropathologically, FXTAS is distinguished by the presence of ubiquitin-positive intranuclear inclusions throughout the brain in astrocytes, neurons, and Purkinje cells (2). FXTAS is caused by the expanded CGG repeats (55–200 CGG) in the 5′UTR of the *FMR1* gene. In normal healthy individuals, the number of CGG repeats lies between 5-54 while individuals carrying alleles with a CGG repeat expansion greater than 200 develop fragile X syndrome (FXS), the most common form of intellectual disability and known monogenic cause of autism spectrum disorder (ASD) (3). The prevalence of the premutation allele among the general population is 1:110-200 females and 1:430 males with an estimated 40-75% of males and 8-16% of females developing FXTAS (4, 5). Currently, there is no effective treatment for FXTAS. As only a proportion of premutation carriers develop the disorder, clinical assessment fails to identify those carriers before significant neurological symptoms are evident. Thus, a deep understanding of the molecular basis of FXTAS pathogenesis requires the development of biomarkers for early identification and progression of the disorder. Importantly, the identification of reliable biomarkers will also lead to the development of medications,

which could prevent, reverse, or slow down the neurodegenerative progression of the disorder.

Metabolomics, the study of metabolites, is an emerging tool that focuses on the investigation of global metabolic changes within a given sample, followed by deep data mining and bioinformatic analysis (6). Metabolic profiling reflects not only the dynamic response to genetic modification, but also physiological, pathophysiological, and developmental stimuli. Now, advancement in metabolomic profiling technology and processing have made it possible to analyze several hundred metabolites efficiently and precisely to obtain a snapshot of the physiological state of an organism (7), and to identify biomarkers for disease development and progression (8). Although metabolic variations have been identified in various other neurodegenerative disorders and multiple metabolites with altered level have been suggested as strong candidates for the early diagnosis of diseases like Alzheimer's (AD) (9), Huntington's (HD) (10, 11) and Parkinson's Disease (PD) (12, 13) extensive studies focused on metabolic changes, and importantly at different time points, have not been carried out in the case of FXTAS.

In the recent past, Giulivi and colleagues have evaluated the plasma metabolic profile of human premutation carriers with FXTAS in comparison to non-carrier healthy controls. Their work highlighted a panel of four core serum metabolites (phenethylamine (PEA), oleamide, aconitate, and isocitrate) for sensitive and specific diagnosis of the premutation carriers with and without FXTAS, and oleamide/isocitrate as a biomarker of FXTAS (14). Later, based on the previously observed plasma metabolic profiles, they reported that FXTAS premutation carriers exhibited mitochondrial dysfunction, markers of neurodegeneration, and pro-inflammatory damage (15). Further, they also reported on

the increased mitochondrial oxidative stress in primary fibroblasts from premutation carriers, compared with age and sex-matched controls (16). In another study, the presence of the Warburg effect that involve the alteration of the glycolysis and oxidative phosphorylation has been reported in the peripheral blood mononuclear cells (PBMCs)'s derived from the controls, premutation allele carriers with and without FXTAS (17). A recent study took advantage of the FXTAS murine model and investigated the metabolic changes associated with FXTAS in the cerebellum. They showed that significant metabolic changes occur in sphingolipid and purine metabolism in the cerebella of FXTAS mice and *Schlank (Cers5), Sk2 (Sphk1)* and, *Ras (Impdh1)* are genetic modifiers of CGG toxicity in *Drosophila* (18). Later, Napoli *et al.* evaluated the effect of allopregnanolone on lymphocytic bioenergetics and plasma pharmaco metabolomics in a 12-week open-label intervention study with six male individuals with FXTAS. They observed a significant impact of allopregnanolone treatment on oxidative stress, GABA metabolism, and some mitochondria-related outcomes, and suggested allopregnanolone as a potential therapeutic for the cognitive and GABA metabolism improvement in FXTAS patients (19).

However, no study evaluating the metabolic alterations in premutation carriers who develop symptoms of FXTAS over time has been reported to date. Here, we present our findings on global metabolic profiling derived from male participants enrolled in an ongoing longitudinal study carried out at the UC Davis MIND Institute. The participants have been followed for at least two longitudinal time points (Visit 1, V1 and Visit 2, V2) during which neuroimaging, neuropsychological, molecular measurements as well as medical and neurological examinations were collected. A fraction of the premutation participants, all symptom-free at the time of enrollment, developed symptoms which

warranted a diagnosis of FXTAS during the course of the study, defined here as converters (CON.) The remaining premutation participants who did not develop symptoms that warranted a diagnosis of FXTAS are defined here as non-converters (NCON). In the current work, we show that significant metabolic changes occurred in CON as compared to the NCON and HC. More specifically, we report on the identification of both metabolic biomarkers of FXTAS development that changed only in the converter group at both V1 and V2 and of metabolic biomarkers of FXTAS progression were only altered at V2 in CON as compared to the non-converter premutation carriers. The majority of these identified metabolites are lipids, including the free fatty acids, acylcarnitine's, sphingolipids, diacylglycerol, endocannabinoid, phospholipids followed by amino acid, nucleotide, xenobiotics, carbohydrate, energy, and peptides classes.

2.   Materials and Methods

2.1   Study Participants

As part of a continuing longitudinal study, male participant premutation carriers, over the age of 40 years, and participant non-carrier age-matched controls were recruited as detailed in (20). All male participants were white in the race with 3, 1, 0 Hispanic, and Latino in HC, CON, and NCON. The studies and all protocols were carried out in accordance with the Institutional Review Board at the University of California, Davis. All participants gave written informed consent before participating in the study in line with the Declaration of Helsinki. FXTAS stage scoring was based on the clinical descriptions as previously described (21). As explained by (22), there are three categories used in the diagnosis of FXTAS termed as "definite", "probable" and "possible". "Definite" indicates

the presence of one major radiological sign plus one major clinical symptom. "Probable" shows the presence of either one major radiology sign plus one minor clinical symptom or two major clinical symptoms. "Possible" indicates the presence of one minor radiology sign plus one major clinical symptom. In addition, the diagnosis of FXTAS can also be clarified by the stage of the disease, which provides information on the impact of the disease on activities of daily living. Six FXTAS stages have been described and they include stage 0-normal function; stage 1-subtle or questionable signs such as subtle tremor or mild balance problems, with no interference in activities of daily living (ADLs); stage 2- minor but clear tremor and/or balance problems with minor interference with ADLs; stage 3-moderate tremor and/or balance problems and occasional falls with significant interference in ADLs; stage 4-severe tremor and /or balance problems (uses cane or walker); stage 5-the use of a wheelchair on the daily basis; stage 6-bedridden.

Three age-matched groups were included in this study: CON, NCON, and healthy controls. After two brain scans and on the basis of neurological assessment, FXTAS stage, and CGG repeat length, 10 participants were classified as "*CON"* as they developed clear FXTAS symptomology between visits (FXTAS stage score was 0–1 at visit 1 (V1) and ≥2 at visit 2 (V2); 10 were defined as "*NCON"* because they continued to show no signs of FXTAS at V2 (FXTAS stage score was 0–1 at both V1 and V2) and 10 HC (normal *FMR1* alleles/non-carriers).

2.2 CGG Repeat Length

Genomic DNA (gDNA) was isolated from 5 mL of peripheral blood leukocytes using the Gentra Puregene Blood Kit (Qiagen). CGG repeat allele size and methylation

status were assessed by using the combination of Southern Blot and PCR analysis. Details of the protocols are as previously reported (23, 24).

2.3   Sample preparation and metabolite profiling

Plasma metabolite profiling was determined by a non-targeted platform that allows the relative quantitative analysis of a large number of molecules (25). Samples were stored at -80 °C until processing and then prepared using the automated MicroLab STAR® (Hamilton Company, Reno, NV, USA). Several recovery standards were added prior to the first step in the extraction process for QC purposes. To remove protein, dissociate small molecules bound to protein or trapped in the precipitated protein matrix, and to recover chemically diverse metabolites, proteins were precipitated with methanol under vigorous shaking for 2 min (Glen Mills GenoGrinder 2000) followed by centrifugation. The resulting extract was divided into five fractions: two for analysis by two separate reverse phases (RP)/UPLC-MS/MS methods with positive ion mode electrospray ionization (ESI), one for analysis by RP/UPLC-MS/MS with negative ion mode ESI, one for analysis by HILIC/UPLC-MS/MS with negative ion mode ESI, and one sample were reserved for backup. Samples were placed briefly on a TurboVap® (Zymark) to remove the organic solvent. The sample extracts were stored overnight under nitrogen before preparation for analysis.

2.3.1   Ultrahigh Performance Liquid Chromatography-Tandem Mass Spectroscopy (UPLC-MS/MS)

All methods utilized a Waters ACQUITY ultra-performance liquid chromatography (UPLC) and a Thermo Scientific Q-Exactive high resolution/accurate mass spectrometer interfaced with a heated electrospray ionization (HESI-II) source and Orbitrap mass analyzer operated at 35,000 mass resolution. The sample extract was dried then reconstituted in solvents compatible with each of the four methods. Each reconstitution solvent contained a series of standards at fixed concentrations to ensure injection and chromatographic consistency. One aliquot was analyzed using acidic positive ion conditions, chromatographically optimized for more hydrophilic compounds. In this method, the extract was gradient eluted from a C18 column (Waters UPLC BEH C18-2.1x100 mm, 1.7 μm) using water and methanol, containing 0.05% perfluoropentanoic acid (PFPA) and 0.1% formic acid (FA). Another aliquot was also analyzed using acidic positive ion conditions; however, it was chromatographically optimized for more hydrophobic compounds. In this method, the extract was gradient eluted from the same aforementioned C18 column using methanol, acetonitrile, water, 0.05% PFPA, and 0.01% FA and was operated at an overall higher organic content. Another aliquot was analyzed using basic negative ion optimized conditions using a separate dedicated C18 column. The basic extracts were gradient eluted from the column using methanol and water, however with 6.5mM Ammonium Bicarbonate at pH 8. The fourth aliquot was analyzed via negative ionization following elution from a HILIC column (Waters UPLC BEH Amide 2.1x150 mm, 1.7 μm) using a gradient consisting of water and acetonitrile with 10mM Ammonium Formate, pH 10.8. The MS analysis alternated between MS and data-dependent MS^{n} scans using dynamic exclusion. The scan range varied slightly between methods but covered 70-1000 m/z.

2.3.2 Quality Assurance (QA) and Quality Control (QC)

Several types of controls were analyzed in concert with the experimental samples: a pooled matrix sample generated by taking a small volume of each experimental sample (or alternatively, use of a pool of well-characterized human plasma) served as a technical replicate throughout the data set; extracted water samples served as process blanks; and a cocktail of QC standards that were carefully chosen not to interfere with the measurement of endogenous compounds was spiked into every analyzed sample, allowed instrument performance monitoring and aided chromatographic alignment. Instrument variability was determined by calculating the median relative standard deviation (RSD) for the standards that were added to each sample prior to injection into the mass spectrometers. Overall process variability was determined by calculating the median RSD for all endogenous metabolites (i.e., non-instrument standards) present in 100% of the pooled matrix samples. Experimental samples were randomized across the platform run with QC samples spaced evenly among the injections.

2.3.3 Biochemical Identification

The informatics system consisted of four major components, the Laboratory Information Management System (LIMS), the data extraction and peak-identification software, data processing tools for QC and compound identification, and a collection of information interpretation and visualization tools for use by data analysts. The hardware and software foundations for these informatics components were the LAN backbone, and a database server running Oracle 10.2.0.1 Enterprise Edition.

LIMS: The purpose of the Metabolon LIMS system was to enable fully auditable laboratory automation through a secure, easy to use, and highly specialized system. The scope of the Metabolon LIMS system encompasses sample accessioning, sample preparation and instrumental analysis and reporting, and advanced data analysis. All of the subsequent software systems are grounded in the LIMS data structures. It has been modified to leverage and interface with the in-house information extraction and data visualization systems, as well as third party instrumentation and data analysis software.

Data Extraction and Compound Identification: Raw data was extracted, peak-identified and QC processed using Metabolon's hardware and software. These systems are built on a web-service platform utilizing Microsoft's NET technologies, which run on high-performance application servers and fiber-channel storage arrays in clusters to provide active failover and load-balancing. Compounds were identified by comparison to library entries of purified standards or recurrent unknown entities. Metabolon maintains a library based on authenticated standards that contain the retention time/index (RI), mass to charge ratio (*m/z*), and chromatographic data (including MS/MS spectral data) on all molecules present in the library. Furthermore, biochemical identifications are based on three criteria: retention index within a narrow RI window of the proposed identification, accurate mass match to the library +/- 10 ppm, and the MS/MS forward and reverse scores between the experimental data and authentic standards. The MS/MS scores are based on a comparison of the ions present in the experimental spectrum to the ions present in the library spectrum. While there may be similarities between these molecules based on one of these factors, the use of all three data points can be utilized to distinguish and differentiate biochemicals. More than 3300 commercially available purified standard

117

compounds have been acquired and registered into LIMS for analysis on all platforms for the determination of their analytical characteristics. Additional mass spectral entries have been created for structurally unnamed biochemicals, which have been identified by virtue of their recurrent nature (both chromatographic and mass spectral). These compounds have the potential to be identified by the future acquisition of a matching purified standard or by classical structural analysis.

Curation: A variety of curation procedures were carried out to ensure that a high-quality data set was made available for statistical analysis and data interpretation. The QC and curation processes were designed to ensure accurate and consistent identification of true chemical entities and to remove those representing system artifacts, misassignments, and background noise. Metabolon data analysts use proprietary visualization and interpretation software to confirm the consistency of peak identification among the various samples. Library matches for each compound were checked for each sample and corrected if necessary.

Metabolite Quantification and Data Normalization: Peaks were quantified using area-under-the-curve. For studies spanning multiple days, a data normalization step was performed to correct variation resulting from instrument inter-day tuning differences. Essentially, each compound was corrected in run-day blocks by registering the medians to equal one (1.00) and normalizing each data point proportionately. For studies that did not require more than one day of analysis, no normalization is necessary, other than for purposes of data visualization. In certain instances, biochemical data may have been normalized to an additional factor (e.g., cell counts, total protein was determined by

Bradford assay, osmolality, etc.) to account for differences in metabolite levels due to differences in the amount of material present in each sample.

2.4   Statistical Analysis

Statistical analysis of log-transformed data was conducted using "ArrayStudio" and for non-standard analysis "R" (http://cran.r-project.org/), which is a freely available, open-source software package and a commercial software package JMP (http://www.jmp.com) were used. ANOVA contrasts and Welch's two-sample t-test were used to identify biochemicals that differed significantly between experimental groups. Differences were considered significant at $p < 0.05$, with groups with altered levels identified using critical p-values calculated after correction for multiple comparisons. Analysis by two-way ANOVA with repeated measures performed to identify biochemicals exhibiting significant interaction and main effects for experimental parameters of Disease and Time. Multiple comparisons were accounted for by estimating the false discovery rate (FDR) using q values, a low ($q < 0.10$) is an indication of high confidence in a result (26).

3.   Results

3.1   Demographics

Male participants, included in each group were: premutation carriers who converted at V2 (CON; n=10), premutation carriers who did not convert at V2 (NCON; n=10) and healthy controls (HC; n=10). All participants were matched for age and CGG repeat length as reported in [**Table 1**]. Participant age, race, and ethnicity did not differ significantly between the three groups. CGG repeat numbers were significantly lower in

healthy controls than in other groups of CON and NCON as expected (P < 0.001 in both comparisons) and were not significantly different between the two premutation carrier groups (P = 0.76).

3.2 Differential metabolite levels between healthy control and premutation groups.

To identify metabolic biomarkers potentially associated with the development and progression of FXTAS, we compared the metabolic profile of HC to the premutation groups (PM) including CON and NCON. Within the 991 detected metabolites we identified 66 metabolites that showed statistically significant changes in level (P < 0.05) at V1, [**Supplementary Material S1 Table**] and 151 that showed significant alteration at V2 [**Supplementary Material S2 Table**] with 47 metabolites statistically different at V1 and V2 [**Fig 1a**] between HC and the PM groups. We also identified the proportion of each super pathway that is significantly altered in these 47 metabolites, and upon examination found that lipid was the most affected super pathway, followed by amino acids, xenobiotics, and others [**Fig 1b**].

Between the groups, CON vs. HC we found significant changes in 78 metabolites at V1, out of which, 70 showed increased levels while 8 showed decreased levels within the CON group. At V2, 169 metabolites were observed to be enriched (P < 0.05) within the CON group as compared to HC while 21 were less abundant. Further, in the comparison between NCON vs. HC, we identified 68 metabolites, of which 34 were more abundant and 34 less abundant at V1 within the NCON group, while 64 metabolites were more abundant and 7 less abundant at V2 [**Table 2**].

3.3   Identification of early metabolic biomarkers of FXTAS

From this untargeted metabolic profiling, we identified 24 metabolites that showed significant changes in expression ($P < 0.05$) in pairwise comparisons of an analysis of variance (ANOVA) model in the CON as compared to the NCON both at V1 and V2 suggesting their role as biomarkers for early diagnosis of FXTAS [**Fig 2a**]. More than half of the 24 altered metabolites were lipids, followed by amino acids, xenobiotics, peptide, carbohydrates, and nucleotides [**Fig 2b**].

In addition, we identified 70 metabolites that were significantly different ($P < 0.05$) in CON as compared to NCON only at V2, indicating their potential role as biomarkers for FXTAS disease progression [**Fig 3a**]. 72% of these identified metabolites were lipids, followed by xenobiotics (15%), amino acids (10%), energy, carbohydrates, and nucleotides (1% each) [**Fig 3b**].

3.4   Lipid metabolism is altered in individuals who develop FXTAS over time.

The high-throughput unbiased global metabolic profiling of HC, NCON, and CON showed that a significant number of metabolites were altered in several lipid pathways, including lipid catabolism, sphingolipids, and phospholipid metabolism [**Supplementary Material S3 Table**].

We identified 64 metabolites associated with lipid metabolism, of which 45 belonged to the subcategory of free fatty acids (FFA) and acylcarnitines. Of these 45 metabolites, 43 had increased, while 2 had decreased levels in the CON group as compared to the NCON group at V2 [**Fig 4a**]. Among the lipids, we observed the elevated level of all identified diacylglycerides, as well as nearly all monoacylglycerides, in CON

as compared to NCON at both V1 and V2 [**Fig 4b**]. This accumulation of serum monoacylglycerol (MAG) and diacylglycerol (DAG) species likely reflects increased liberation of FFA from circulating lipid stores. The elevated circulating acylcarnitine's, often indicative intercellular changes (27), suggests that the FFA is being utilized for beta-oxidation. Further evidence for changes in lipid metabolism is also apparent in the elevated levels of the ketone body β-hydroxybutyric acid (BHBA) and acetylcarnitine, reflective of changes in acetyl-CoA levels (28), at visit 2 within CON as compared to NCON. In total, these differences between CON and NCON may suggest a greater reliance on lipid oxidation for energy generation and a potential inability to process increased lipids.

The sphingolipid metabolic pathway has been observed to modulate CGG repeat toxicity and to be significantly perturbed in the cerebellum of the FXTAS murine model (18), but there is no study to date investigating the sphingolipid alterations in carriers who develop FXATS. We found the level of sphingoid bases, including sphingosine, the substrate of ceramide synthase [$p = 0.0181$; $q = 0.1462$; **Fig 4c**] and sphinganine [$p = 0.0182$; $q = 0.1462$; **Fig 4d**] are elevated in CON as compared to NCON only at V2. Interestingly, ceramides, the product of sphingoid base acylation, [**Fig 4e**] were all also found increased in CON as compared to NCON both at V1 and V2. The elevation of these sphingoid bases along with circulating ceramides, like those observed here in the converter groups, have been implicated in neurodegeneration, potentially by activating apoptotic pathways of neuronal cells. In addition, we observed the low level of 3 observed Hexosylceramides (HCER) and Lactosylceramides (LCER) in converters former at V2 while later both at V1 and V2 [**Fig 4f**].

Abnormal phospholipid metabolism and specifically choline-containing phospholipids are an indicator of neural membrane breakdown, and their increased levels have been found in the postmortem brain of AD patients (29). We identified two metabolites associated with phospholipids that were statistically significant between groups: choline and choline phosphate. The level of Choline was found elevated in CON as compared to NCON only at Visit 2 [p = 0.0119; q = 0.1288; **Fig 4g**], while the level of choline phosphate was significantly decreased in CON both at V1 [p = 0.0291, q = 0.3591; **Fig 4h**] and V2 [p = 0.0231; q= 0.1684; **Fig 4h**]. The increased levels of choline suggest that neural functional could be compromised and the decreased levels of the choline phosphate suggest an impaired neuron reception in individuals who developed the FXTAS over time.

The endocannabinoid system alterations have been found as a contributing factor to the development of AD's disease (AD), Huntington's disease (HD) and (PD) (30). We found three metabolites associated with endocannabinoid system including oleoyl ethanolamide [p = 0.0208; q = 0.1593], palmitoyl ethanolamide [p = 0.042; q = 0.1115] and linoleoyl ethanolamide [p = 0.0304; q = 0.1846], elevated in CON as compared to NCON only at V2 [**Fig 4i**]. All of the identified endocannabinoids are playing a biological role in chronic pain and inflammation.

3.5   Altered Amino acid profiling observed in converter group

In addition to lipids, several metabolites in the amino acid pathway were also significantly altered in the development (changed in CON as compared to NCON at both V1 and V2) as well as in the progression of FXTAS (changed in CON as compared to

NCON only at V2) [**Fig 5a**]. Notably, differences were observed in methionine, lysine, and branched-chain amino acid metabolism.

Within the total 14 identified metabolites associated with amino acids we found 2 metabolites including S-adenosylhomocysteine (SAH) [p = 0.0061; q =0.1218; **Fig 5b**] and lanthionine [p =0.0103; q = 0.1288; **Fig 5c**] associated with methionine, cysteine, SAM, and taurine metabolism increased only in CON as compared to NCON at V2. While three biomarkers of FXTAS development i.e., 6-oxopiperidine-2-carboxylate, N2-acetyl N6-methyllysine, and N2-acetyl N6 N6-dimethyllysine found associated with lysine metabolism with 6-oxopiperidine-2-carboxylate increased, and later two decreased in CON as compared to NCON both at V1 and V2 [**Fig 5d**]. Two metabolites i.e., hydantoin-5-propionate and trans-urocanate associated with Histidine Metabolism found only in CON of which level of hydantoin-5-propionate increased in CON as compared to NCON both at V1 [p = 0.0014; q =0.1458; **Fig 5e**] and V2 [p = 0.0108; q =0.1288; **Fig 5e**]. In contrast, the level of trans-urocanate found decreased in CON only at V2 [p = 0.0168; q =0.1422; **Fig 5f**].

From leucine, isoleucine, and valine metabolism, we identify two metabolites tiglylcarnitine (C5:1-DC) and isovalerylglycine, of which former found increased in CON as compared to NCON both at V1 [p = 0.0356; q =0.3724; **Fig 5g**] and V2 [p = 0.0202; q =0.1572; **Fig 5g**], while later found decreased only in CON as compared to NCON only at V2 [p = 0.0191; q =0.1503; **Fig 5h**]. The kynurenine pathway (KP) is the primary route of tryptophan degradation in mammalian cells and has been demonstrated to be involved in aging and many neurodegenerative disorders, including AD, PD, HD, and amyotrophic lateral sclerosis. Besides, it has been implicated in the pathogenesis of schizophrenia

and bipolar disorder (31–33). We found 8-methoxykynurenate associated with Tryptophan metabolism with an increased level in CON as compared to NCON both at V1 [p = 0.0140; q =0.2741; Fig 5i] and V2 [p = 0.0249; q =0.1692; **Fig 5i**].

3.6 Nucleotide, Carbohydrate, Energy and Peptide Pathways are dysregulated in individuals who develop symptoms of FXTAS over time.

The number of metabolites associated with other pathways, including nucleotide, carbohydrates, energy, and peptide is found dysregulated in the CON either at V2 or both at V1 and V2. As biomarker of disease development, we identified the N6-methyladenosine associated with purine metabolism with increased level in CON as compared to NCON both at V1 [p = 0.0093; q =0.2441; **Fig 6a**] and V2 [p = 0.0114; q =0.1288; **Fig 6a**]. While 5,6-dihydrouracil as a biomarker of progression and linked with pyrimidine metabolism found an increase in CON as compared to NCON only at V2 [p = 0.0445; q =0.2235; **Fig 6b**]. Interestingly, we observed the low level of lactate in CON at V1 [p = 0.0426; q =0.4019; **Fig 6c**] as compared to NCON, that significantly increased at V2 [p = 0.0397; q =0.2158; **Fig 6c**]. While on the other side, the level of Fumarate was found elevated only in CON as compared to NCON at V2 [p = 0.0083; q =0.1223; **Fig 6d**].

3.7 The metabolism of Xenobiotics is perturbed in FXTAS Converters.

The xenobiotics alterations have been found in the cerebellum of the murine model of FXTAS (18) here we identified 11 metabolites from Xenobiotic pathway of which mannonate found to be increased in CON both at V1 [p = 0.0175; q =0.3028; **Fig 7a**] and V2 [p = 0.0088; q =0.1244; **Fig 7a**], while 3-bromo-5-chloro-2,6-dihydroxybenzoic acid [p

= 0.0019; q =0.0841; **Fig 7b**], and dibutyl sulfosuccinate [p = 0.0119; q =0.1288; **Fig 7c**] found increased at only V2. Interestingly we observed the significantly decreased level of remaining 8 xenobiotic metabolites at V2 in CON as compared to NCON [**Fig 7d**].

4. Discussion

The present study identified several potential plasma metabolomic biomarkers for the early diagnosis and progression of FXTAS. Importantly, the study revealed the potential dysregulation of lipid metabolism in FXTAS as well as differences in the metabolism of numerous amino acids, nucleotides, xenobiotics, and carbohydrates. These findings both validate and expand upon an earlier, more limited study of plasma metabolic profiling of patients with a definitive diagnosis of FXTAS (14, 15) and in the cerebellum of the murine model(18), suggesting the involvement of pathways previously identified but now expanded [**S3 Table**] as well as the involvement and alterations of several other pathways. To our knowledge, this is the first report of the longitudinal metabolic profiling and on the identification of unique biomarkers that might in the future be used for early diagnosis, development, and the progression of FXTAS [**Fig 2a and 3a**].

Lipids regulate several cellular processes, including inflammation, cell proliferation, division, differentiation, aging and death (34) and their metabolism has been found to be altered in various neurodegenerative disorders including the AD and other dementia, Parkinson's disease, multiple sclerosis, Huntington disease, schizophrenia and bipolar disorders (35–37). A distinguished subclass of lipids, the FFA, is primarily utilized for energy production by the mitochondrial fatty acid β-oxidation (FAO) cycle, which

begins with the conjugation of an FFA with coenzyme A (CoA) and subsequently carnitine (38). Carnitines are found to accumulate to a lower extent in the brain as compared to peripheral tissues (39) and in the brain, these acylcarnitines can function in synthesizing lipids, modulating genes and proteins, increasing antioxidant activity, improving mitochondrial function, altering and stabilizing membrane composition and enhancing cholinergic neurotransmission (40). We observed an increased level of FFA and all identified acylcarnitines in CON, as compared to the NCON, suggesting abnormalities in mitochondrial energy substrate utilization and potentially fatty acid processing in individuals who developed FXTAS over time.

Altered DAGs metabolism is a common feature of the neurodegenerative diseases that ultimately result in cognitive deficits. Increased levels of sphingolipids, and DAG have been found in the plasma and brains of patients with AD (41) and PD (42). With regard to the mechanism, decreases in phosphocholine levels in PD suggest that the observed augmented degradation may contribute to increases in the pool size of free DAG (43). Interestingly, in our current study, we found increased levels of all DAG and decrease the level of choline phosphate only in CON as compared to the NCON both as V1 and V2 suggesting their potential involvement in the neurodegeneration of FXTAS.

Sphingolipids have been considered an important potential lipid messenger and have been involved in various neurodegenerative disorders such as PD, AD, and HD (44–47). Ceramides play a vital role in numerous fundamental cellular processes, including growth, differentiation, cell cycle arrest, senescence, survival, and apoptosis (48). An increased level of ceramide has been reported in brains with AD and the other neurodegenerative disorders suggesting their role in the atypical death of neuronal cells

(49). In this study, we identified altered levels of metabolites in the sphingolipid metabolic pathway, in particular, the levels of sphingosine, sphinganine, and ceramides being significantly higher in participants who developed FXTAS over time [**Fig 4c, 4d and 4e**] suggesting an aberration in neural health and development. In addition, in the CON group we observed low levels of the hexosylceramides (HCER) [**Fig 4f**], that has been pointed as a promising candidate marker of disease progression in multiple sclerosiss (50), and of lactosylceramides (LCER) [**Fig 4f**] which has been implicated in both neuroinflammatory diseases and in mitochondrial dysfunction, which are common features of FXTAS (51, 52).

The endocannabinoid system, which involves cannabinoid receptors type 1 (CB1R) and type 2 (CB2R), endogenous cannabinoids, and the enzymes that catabolize these compounds, have been shown to contribute to the development of neurodegenerative disorders including the including AD, HD and PD (30). These endocannabinoids, particularly palmitoylethanolamide, have been observed to have a biological function related to chronic pain and inflammation. Neuropsychiatric issues are common among premutation allele carriers, often exacerbated by chronic pain and fatigue, fibromyalgia, autoimmune disorders, and sleep problems (53). In this study we identified high levels of several endocannabinoids [**Fig 4i**] in CON as compared to NCON, potentially indicating their role in inflammation and chronic pain process commonly seen in patients with FXTAS.

Phospholipids are found in high concentrations in the myelin sheaths of neurons, influencing the conformation and function of membrane-bound receptors and ion channels. Abnormal phospholipid metabolism and specifically Choline containing

phospholipids are indicators of neural membrane breakdown and their increased levels have been observed in the postmortem brain of AD patients (29). In this study, we observed a significant increase in the level of choline [**Fig 4g**] in CON as compared to NCON at V2 which suggests their potential role in the increased *chronic* widespread musculoskeletal *pain* and inflammation associated with patients with FXTAS.

Amino acids (AA) play several integral roles in the central nervous system, where they act as neurotransmitters, regulators of metabolism, and neuromodulators (54). A number of studies with amino acid profiling have found differences between the level of amino acids in patients with various types of diseases and in healthy control groups for example in patients with AD (55–57) and PD (58, 59) and elderly patients (60). These studies indicated the potential application of measuring amino acid levels as a diagnostic tool for AD, PD, and biomarkers of aging. Here, we found that amino acid metabolism is significantly altered in the individuals who developed FXTAS over time as compared to the premutation allele carriers who did not show any symptoms of FXTAS suggesting a potential involvement in the early identification and progression of FXTAS.

Mitochondrial dysfunction is one of the important characteristics of the aging process and is associated with various Krebs' intermediates and a Warburg-like shift in energy substrate utilization. The brain is particularly vulnerable to oxidative stress and damage, because of its low antioxidant defenses, increased oxygen consumption, and high content of polyunsaturated fats (61). Mitochondrial alterations are also associated with various other neurodegenerative disorders and the bile acid metabolites are reported as the potential biomarker for the PD (62). Napoli and the colleagues reported variation in the energy metabolism of freshly isolated PBMCs from premutation allele carriers as

compared to age-matched healthy controls by finding the low oxidative phosphorylation and increased glycolysis (16, 17). In addition, a previous analysis of plasma metabolites, we reported an increased level of lactate in premutation carriers as compared to controls suggesting a lower Krebs cycle activity in mitochondria. In addition, an increased level of fumarate which may inhibit alpha-ketoglutarate-dependent prolyl-hydroxylases was previously reported (14). These findings along with a higher production of the reactive oxygen species as well as impaired redox regulated mitochondrial disulfide relay system and the mtDNA deletions in both the PBMCs and the fibroblast derived from the premutation allele carriers suggest the increased level of the oxidative nitrate damage (16, 17) . The resultant nitrate damage could be responsible for the mitochondrial dysfunction and neurons remodeling. Interestingly, in this study, we found a unique trend in which lactate was low in CON as compared to NCON at V1 but became significantly increased at V2 [**Fig 6c**]. This significant increment supports our previous findings and the mitochondrial dysfunction observed in individuals who develop the FXTAS (15). The increase in lactate in premutation carriers as compared to controls and more interestingly among the CON as compared to the NCON group suggests its potential role as an important biomarker to evaluate in clinical settings. In addition, we also found the increased level of fumarate [**Fig 6d**] in the converters as compared to non-converters suggesting its role in the observed mitochondrial functional impairment in FXTAS. Direct evidence for changes in inflammatory or redox balance is also apparent here, namely with increased levels of lanthionine, 5-oxoproline, cysteinglycine-oxidized, and cysteine glycine disulfide at V2 within the CON group as compared to NCON. These changes possibly reflect increased oxidative stress as a consequence of conversion from carrier

to symptomatic state. In addition, targeting of these metabolites could recover the mitochondrial function as shown by the Song and colleagues in fibroblast derived from carriers of a premutation allele (16).

A strong relationship between environmental factors and neurodegenerative disorders (63) suggests an important role of early life in the health and development of an individual. Specifically, it has been shown that environmental xenobiotics were extremely toxic causing mitochondrial dysfunction in dopaminergic neurons leading to PD phenotypes (64). In addition, a dietary intervention has been suggested to increase xenobiotic metabolism that could reduce oxidative stress and neuroendocrine disease in developing countries (65). We found a decreased level of the majority of identified xenobiotics in the CON as compared to the NCON that may suggest increasing oxidative stress and the role of xenobiotic dysregulation in FXTAS.

Nervonic acid, a long-chain unsaturated fatty acid, enriched in sphingomyelin enhances brain functions and prevents demyelination. In this study, nervonate levels were significantly elevated in the CON group at V2 [**Supplementary Material S1 Fig**] which suggests an altered myelin formation in neural cells. This would support myelin loss, which would support one of the pathologic features of FXTAS (66) and motor and sensory demyelinating polyneuropathy in the lower extremities of patients with FXTAS detected by nerve conduction studies (67).

5.   Conclusion

To date, there have been no identified molecular biomarkers of FXTAS, which has delayed treatment, diagnosis, and prognosis of patients. In this study, by using a unique

approach of high-throughput unbiased metabolic profiling of premutation carriers including longitudinal analysis, we identified a unique set of potential metabolomic biomarkers of early development and progression of FXTAS. In addition, we also observed a significant dysregulation in lipid metabolism, more specifically the sub pathways involved in mitochondrial bioenergetics. These identified metabolites could be of a great value not only for the early identification but also for the development of effective therapeutics of this devasting neurodegenerative disorder. However, due to the limitation of the small sample size, potential medication and diet effect further studies with larger sample size and more robust medication and diet history are required to test the initial findings and elucidate and confirm the role of the potential identified biomarkers. Finally, in addition, recent studies, in a wide range of neurological diseases have provide compelling evidence that both lifestyle and nutritional factors contribute to risk or protection for a wide range of neurological diseases. Thus, in future metabolomic studies it will be is important to include dietary patterns.

6. Availability of Additional Data

All statistical data generated during the study is available at the end of this chapter as "Supplementary Data".

7.   References

1.   Heemels, M.-T. (2016) Neurodegenerative diseases. *Nature* **539**, 179–179

2. Hagerman, R. J. and Hagerman, P. (2016) Fragile X-associated tremor/ataxia syndrome — features, mechanisms and management. *Nature Reviews Neurology* **12**, 403–412

3. Hagerman, R. J., Berry-Kravis, E., Hazlett, H. C., Bailey, D. B., Jr, Moine, H., Kooy, R. F., Tassone, F., Gantois, I., Sonenberg, N., Mandel, J. L., and Hagerman, P. J. (2017) Fragile X syndrome. *Nat Rev Dis Primers* **3**, 17065

4. Jacquemont, S. (2004) Penetrance of the Fragile X–Associated Tremor/Ataxia Syndrome in a Premutation Carrier Population. *JAMA* **291**, 460

5. Tassone, F., Iong, K., Tong, T.-H., Lo, J., Gane, L. W., Berry-Kravis, E., Nguyen, D., Mu, L. Y., Laffin, J., Bailey, D. B., and Hagerman, R. J. (2012) FMR1 CGG allele size and prevalence ascertained through newborn screening in the United States. *Genome Medicine* **4**, 100

6. Jové, M., Portero-Otín, M., Naudí, A., Ferrer, I., and Pamplona, R. (2014) Metabolomics of Human Brain Aging and Age-Related Neurodegenerative Diseases. *Journal of Neuropathology & Experimental Neurology* **73**, 640–657

7. Gu, Q., Spinelli, J. J., Dummer, T. B. J., McDonald, T. E., Moore, S. C., and Murphy, R. A. (2018) Metabolic profiling of adherence to diet, physical activity and body size recommendations for cancer prevention. *Sci. Rep.* **8**, 16293

8. Peng, B., Li, H., and Peng, X.-X. (2015) Functional metabolomics: from biomarker discovery to metabolome reprogramming. *Protein & Cell* **6**, 628–637

9. Lin, C., Huang, C., Huang, K., Lin, K., Yen, T., and Kuo, H. (2019) A metabolomic approach to identifying biomarkers in blood of Alzheimer's disease. *Annals of Clinical and Translational Neurology* **6**, 537–545

10. Graham, S. F., Kumar, P., Bahado-Singh, R. O., Robinson, A., Mann, D., and Green, B. D. (2016) Novel Metabolite Biomarkers of Huntington's Disease As Detected by High-Resolution Mass Spectrometry. *Journal of Proteome Research* **15**, 1592–1601

11. Skene, D. J., Middleton, B., Fraser, C. K., Pennings, J. L. A., Kuchel, T. R., Rudiger, S. R., Simon Bawden, C., and Jennifer Morton, A. (2017) Metabolic profiling of presymptomatic Huntington's disease sheep reveals novel biomarkers. *Scientific Reports* **7**

12. Havelund, J., Heegaard, N., Færgeman, N., and Gramsbergen, J. (2017) Biomarker Research in Parkinson's Disease Using Metabolite Profiling. *Metabolites* **7**, 42

13. Shao, Y. and Le, W. (2019) Recent advances and perspectives of metabolomics-based investigations in Parkinson's disease. *Molecular Neurodegeneration* **14**

14. Giulivi, C., Napoli, E., Tassone, F., Halmai, J., and Hagerman, R. (2016) Plasma Biomarkers for Monitoring Brain Pathophysiology in FMR1 Premutation Carriers. *Frontiers in Molecular Neuroscience* **9**

15. Giulivi, C., Napoli, E., Tassone, F., Halmai, J., and Hagerman, R. (2016) Plasma metabolic profile delineates roles for neurodegeneration, pro-inflammatory damage and mitochondrial dysfunction in the FMR1 premutation. *Biochemical Journal* **473**, 3871–3888

16. Song, G., Napoli, E., Wong, S., Hagerman, R., Liu, S., Tassone, F., and Giulivi, C. (2016) Altered redox mitochondrial biology in the neurodegenerative disorder fragile X-tremor/ataxia syndrome: use of antioxidants in precision medicine. *Mol. Med.* **22**, 548–559

17. Napoli, E., Song, G., Schneider, A., Hagerman, R., Al Azaim Eldeeb, M. A., Azarang, A., Tassone, F., and Giulivi, C. (2016) Warburg effect linked to cognitive-executive deficits in FMR1 premutation. *The FASEB Journal* **30**, 3334–3351

18. Kong, H. E., Lim, J., Zhang, F., Huang, L., Gu, Y., Nelson, D. L., Allen, E. G., and Jin, P. (2019) Metabolic pathways modulate the neuronal toxicity associated with fragile X-associated tremor/ataxia syndrome. *Human Molecular Genetics* **28**, 980–991

19. Napoli, E., Schneider, A., Wang, J. Y., Trivedi, A., Carrillo, N. R., Tassone, F., Rogawski, M., Hagerman, R. J., and Giulivi, C. (2019) Allopregnanolone Treatment Improves Plasma Metabolomic Profile Associated with GABA Metabolism in Fragile X-Associated Tremor/Ataxia Syndrome: a Pilot Study. *Mol. Neurobiol.* **56**, 3702–3713

20. Shelton, A. L., Wang, J. Y., Fourie, E., Tassone, F., Chen, A., Frizzi, L., Hagerman, R. J., Ferrer, E., Hessl, D., and Rivera, S. M. (2018) Middle Cerebellar Peduncle Width—A Novel MRI Biomarker for FXTAS? *Frontiers in Neuroscience* **12**

21. Bacalman, S., Farzin, F., Bourgeois, J. A., Cogswell, J., Goodlin-Jones, B. L., Gane, L. W., Grigsby, J., Leehey, M. A., Tassone, F., and Hagerman, R. J. (2006) Psychiatric phenotype of the fragile X-associated tremor/ataxia syndrome (FXTAS) in males: newly described fronto-subcortical dementia. *J. Clin. Psychiatry* **67**, 87–94

22. Zafarullah, M. and Tassone, F. (2019) Fragile X-Associated Tremor/Ataxia Syndrome (FXTAS). *Fragile-X Syndrome* 173–189

23. Tassone, F., Pan, R., Amiri, K., Taylor, A. K., and Hagerman, P. J. (2008) A Rapid Polymerase Chain Reaction-Based Screening Method for Identification of All

Expanded Alleles of the Fragile X (FMR1) Gene in Newborn and High-Risk Populations. *The Journal of Molecular Diagnostics* **10**, 43–49

24. Filipovic-Sadic, S., Sah, S., Chen, L., Krosting, J., Sekinger, E., Zhang, W., Hagerman, P. J., Stenzel, T. T., Hadd, A. G., Latham, G. J., and Tassone, F. (2010) A novel FMR1 PCR method for the routine detection of low abundance expanded alleles and full mutations in fragile X syndrome. *Clin. Chem.* **56**, 399–408

25. Evans, A. M., DeHaven, C. D., Barrett, T., Mitchell, M., and Milgram, E. (2009) Integrated, Nontargeted Ultrahigh Performance Liquid Chromatography/Electrospray Ionization Tandem Mass Spectrometry Platform for the Identification and Relative Quantification of the Small-Molecule Complement of Biological Systems. *Analytical Chemistry* **81**, 6656–6667

26. Storey, J. D. and Tibshirani, R. (2003) Statistical significance for genomewide studies. *Proceedings of the National Academy of Sciences* **100**, 9440–9445

27. Makrecka-Kuka, M., Sevostjanovs, E., Vilks, K., Volska, K., Antone, U., Kuka, J., Makarova, E., Pugovics, O., Dambrova, M., and Liepinsh, E. (2017) Plasma acylcarnitine concentrations reflect the acylcarnitine profile in cardiac tissues. *Scientific Reports* **7**

28. Schroeder, M. A., Atherton, H. J., Dodd, M. S., Lee, P., Cochlin, L. E., Radda, G. K., Clarke, K., and Tyler, D. J. (2012) The Cycling of Acetyl-Coenzyme A Through Acetylcarnitine Buffers Cardiac Substrate Supply. *Circulation: Cardiovascular Imaging* **5**, 201–209

29. Klein, J. (2000) Membrane breakdown in acute and chronic neurodegeneration: focus on choline-containing phospholipids. *Journal of Neural Transmission* **107**, 1027–1063

30. Basavarajappa, B. S., Shivakumar, M., Joshi, V., and Subbanna, S. (2017) Endocannabinoid system in neurodegenerative disorders. *J. Neurochem.* **142**, 624–648

31. Maddison, D. C. and Giorgini, F. (2015) The kynurenine pathway and neurodegenerative disease. *Seminars in Cell & Developmental Biology* **40**, 134–141

32. Majláth, Z., Toldi, J., and Vécsei, L. (2015) The Role of the Kynurenine Pathway in Neurodegenerative Diseases. *Targeting the Broadly Pathogenic Kynurenine Pathway* 193–204

33. Tan, L., Yu, J.-T., and Tan, L. (2012) The kynurenine pathway in neurodegenerative diseases: mechanistic and therapeutic considerations. *J. Neurol. Sci.* **323**, 1–8

34. Boojar, M. M. A., Boojar, M. M. A., and Golmohammad, S. (2018) Ceramide pathway: A novel approach to cancer chemotherapy. *Egyptian Journal of Basic and Applied Sciences* **5**, 237–244

35. Xu, Q. and Huang, Y. (2006) Lipid metabolism in Alzheimer's and Parkinson's disease. *Future Lipidology* **1**, 441–453

36. Yadav, R. S. and Tiwari, N. K. (2014) Lipid Integration in Neurodegeneration: An Overview of Alzheimer's Disease. *Molecular Neurobiology* **50**, 168–176

37. Shamim, A., Mahmood, T., Ahsan, F., Kumar, A., and Bagga, P. (2018) Lipids: An insight into the neurodegenerative disorders. *Clinical Nutrition Experimental* **20**, 1–19

38. Schulz, H. (2004) Fatty Acid Oxidation. *Encyclopedia of Biological Chemistry* 90–94

39. Nacz, K. (2004) Carnitine: transport and physiological functions in the brain. *Molecular Aspects of Medicine* **25**, 551–567

40. Jones, L. L., McDonald, D. A., and Borum, P. R. (2010) Acylcarnitines: role in brain. *Prog. Lipid Res.* **49**, 61–75

41. (2014) Critical Assessment of the Status of Biomarkers for Alzheimer's disease. *Journal of Parkinson's disease and Alzheimer's disease* **1**

42. Cheng, D., Jenner, A. M., Shui, G., Cheong, W. F., Mitchell, T. W., Nealon, J. R., Kim, W. S., McCann, H., Wenk, M. R., Halliday, G. M., and Garner, B. (2011) Lipid Pathway Alterations in Parkinson's Disease Primary Visual Cortex. *PLoS ONE* **6**, e17299

43. Wood, P. L., Tippireddy, S., Feriante, J., and Woltjer, R. L. (2018) Augmented frontal cortex diacylglycerol levels in Parkinson's disease and Lewy Body Disease. *PLoS One* **13**, e0191815

44. Mielke, M. M. and Lyketsos, C. G. (2010) Alterations of the Sphingolipid Pathway in Alzheimer's Disease: New Biomarkers and Treatment Targets? *NeuroMolecular Medicine* **12**, 331–340

45. Piccinini, M., Scandroglio, F., Prioni, S., Buccinnà, B., Loberto, N., Aureli, M., Chigorno, V., Lupino, E., DeMarco, G., Lomartire, A., Rinaudo, M. T., Sonnino, S., and Prinetti, A. (2010) Deregulated Sphingolipid Metabolism and Membrane Organization in Neurodegenerative Disorders. *Molecular Neurobiology* **41**, 314–340

46. Wang, G., Silva, J., Dasgupta, S., and Bieberich, E. (2008) Long-chain ceramide is elevated in presenilin 1 (PS1M146V) mouse brain and induces apoptosis in PS1 astrocytes. *Glia* **56**, 449–456

47. Cutler, R. G., Kelly, J., Storie, K., Pedersen, W. A., Tammara, A., Hatanpaa, K., Troncoso, J. C., and Mattson, M. P. (2004) Involvement of oxidative stress-induced abnormalities in ceramide and cholesterol metabolism in brain aging and Alzheimer's disease. *Proceedings of the National Academy of Sciences* **101**, 2070–2075

48. Mullen, T. D. and Obeid, L. M. (2012) Ceramide and Apoptosis: Exploring the Enigmatic Connections between Sphingolipid Metabolism and Programmed Cell Death. *Anti-Cancer Agents in Medicinal Chemistry* **12**, 340–363

49. Filippov, V., Song, M. A., Zhang, K., Vinters, H. V., Tung, S., Kirsch, W. M., Yang, J., and Duerksen-Hughes, P. J. (2012) Increased Ceramide in Brains with Alzheimer's and Other Neurodegenerative Diseases. *Journal of Alzheimer's Disease* **29**, 537–547

50. Checa, A., Khademi, M., Sar, D. G., Haeggström, J. Z., Lundberg, J. O., Piehl, F., Olsson, T., and Wheelock, C. E. (2015) Hexosylceramides as intrathecal markers of worsening disability in multiple sclerosis. *Multiple Sclerosis Journal* **21**, 1271–1279

51. Pannu, R. (2004) A Novel Role of Lactosylceramide in the Regulation of Lipopolysaccharide/Interferon- -Mediated Inducible Nitric Oxide Synthase Gene Expression: Implications for Neuroinflammatory Diseases. *Journal of Neuroscience* **24**, 5942–5954

52. Novgorodov, S. A., Riley, C. L., Yu, J., Keffler, J. A., Clarke, C. J., Van Laer, A. O., Baicu, C. F., Zile, M. R., and Gudz, T. I. (2016) Lactosylceramide contributes to mitochondrial dysfunction in diabetes. *Journal of Lipid Research* **57**, 546–562

53. Hagerman, R. J., Protic, D., Rajaratnam, A., Salcedo-Arellano, M. J., Aydin, E. Y., and Schneider, A. (2018) Fragile X-Associated Neuropsychiatric Disorders (FXAND). *Front. Psychiatry* **9**, 564

54. Socha, E., Koba, M., and Kośliński, P. (2019) Amino acid profiling as a method of discovering biomarkers for diagnosis of neurodegenerative diseases. *Amino Acids* **51**, 367–371

55. Van Assche, R., Temmerman, L., Dias, D. A., Boughton, B., Boonen, K., Braeckman, B. P., Schoofs, L., and Roessner, U. (2015) Metabolic profiling of a transgenic Caenorhabditis elegans Alzheimer model. *Metabolomics* **11**, 477–486

56. Corso, G., Cristofano, A., Sapere, N., la Marca, G., Angiolillo, A., Vitale, M., Fratangelo, R., Lombardi, T., Porcile, C., Intrieri, M., and Di Costanzo, A. (2017) Serum Amino Acid Profiles in Normal Subjects and in Patients with or at Risk of Alzheimer Dementia. *Dement. Geriatr. Cogn. Dis. Extra* **7**, 143–159

57. Gong, Y., Liu, Y., Zhou, L., Di, X., Li, W., Li, Q., and Bi, K. (2015) A UHPLC–TOF/MS method based metabonomic study of total ginsenosides effects on Alzheimer disease mouse model. *Journal of Pharmaceutical and Biomedical Analysis* **115**, 174–182

58. Blesa, J., Trigo-Damas, I., Quiroga-Varela, A., and Jackson-Lewis, V. R. (2015) Oxidative stress and Parkinson's disease. *Frontiers in Neuroanatomy* **9**

59. Figura, M., Kuśmierska, K., Bucior, E., Szlufik, S., Koziorowski, D., Jamrozik, Z., and Janik, P. (2018) Serum amino acid profile in patients with Parkinson's disease. *PLoS One* **13**, e0191670

60. Adachi, Y., Ono, N., Imaizumi, A., Muramatsu, T., Andou, T., Shimodaira, Y., Nagao, K., Kageyama, Y., Mori, M., Noguchi, Y., Hashizume, N., and Nukada, H. (2018) Plasma Amino Acid Profile in Severely Frail Elderly Patients in Japan. *International Journal of Gerontology* **12**, 290–293

61. Cenini, G., Lloret, A., and Cascella, R. (2020) Oxidative Stress and Mitochondrial Damage in Neurodegenerative Diseases: From Molecular Mechanisms to Targeted Therapies. *Oxidative Medicine and Cellular Longevity* **2020**, 1–2

62. Zhao, H., Wang, C., Zhao, N., Li, W., Yang, Z., Liu, X., Le, W., and Zhang, X. (2018) Potential biomarkers of Parkinson's disease revealed by plasma metabolic profiling. *Journal of Chromatography B* **1081-1082**, 101–108

63. Lahiri, D. K. and Maloney, B. (2010) The "LEARn" (Latent Early-life Associated Regulation) model integrates environmental risk factors and the developmental basis of Alzheimer's disease, and proposes remedial steps. *Experimental Gerontology* **45**, 291–296

64. Ekstrand, M. I., Terzioglu, M., Galter, D., Zhu, S., Hofstetter, C., Lindqvist, E., Thams, S., Bergstrand, A., Hansson, F. S., Trifunovic, A., Hoffer, B., Cullheim, S., Mohammed, A. H., Olson, L., and Larsson, N.-G. (2007) Progressive parkinsonism in mice with respiratory-chain-deficient dopamine neurons. *Proceedings of the National Academy of Sciences* **104**, 1325–1330

65. (2014) Increased Risk for Obesity and Diabetes with Neurodegeneration in Developing Countries. *Journal of Molecular and Genetic Medicine* **s1**

66. Greco, C. M., Tassone, F., Garcia-Arocena, D., Tartaglia, N., Coffey, S. M., Vartanian, T. K., Brunberg, J. A., Hagerman, P. J., and Hagerman, R. J. (2008) Clinical and Neuropathologic Findings in a Woman With the FMR1 Premutation and Multiple Sclerosis. *Archives of Neurology* **65**

67. Eker, A., Fahrioglu, U., and Serakinci, N. (2016) Late Onset Tremor and Ataxia Syndrome: FXTAS and its Ignored Peripheral Nervous System Findings in Diagnostic Criteria. *Noro Psikiyatri Arsivi* **53**, 92–93

8. Tables

Table 1: Demographic information on age and CGG repeats in three male participant groups: HC, CON and NCON.

		Healthy Controls (HC)	Converters (CON)	Non-Converters (NCON)	All Patients	P-Value (F-Test)
Age	**N**	10	10	10	30	0.936
	Mean (SD)	65.60 (3.239)	63.50 (6.786)	63.20 (4.849)	64.10 (5.101)	
	Median (Range)	64.50 (62--70)	63.50 (53--75)	64.00 (52-69)	64.00 (62-75)	
CGG	**N**	10	10	10	30	<0.001
	Mean (SD)	28.90 (4.095)	93.30 (22.91)	75.70 (18.73)	65.97 (32.26)	
	Median (Range)	30 (20--32)	84.50 (74--141)	74 (56--122)	72 (20--141)	

Table 2: Differential metabolites expression among the HC and the premutation groups including both the CON and NCON at Visit 1 (V1), Visit 2 (V2) and both at Visit 1 (V1) and Visit 2 (V2).

Statistical Comparisons							
Welch's two Sample t-Test	**PM Groups vs HC**						
	CON-V1	**CON-V2**	**NCON-V1**	**NCON-V2**	**Total Visit 1**	**Total Visit 2**	**Total at V1 & V2**
Total biochemicals p ≤ 0.05	78	190	68	71	66	151	47
Biochemicals (⬆⬇)	70 | 8	169 | 21	34 | 34	64 | 7	51 | 15	140 | 11	39 | 8

9. Figures

a.

b.
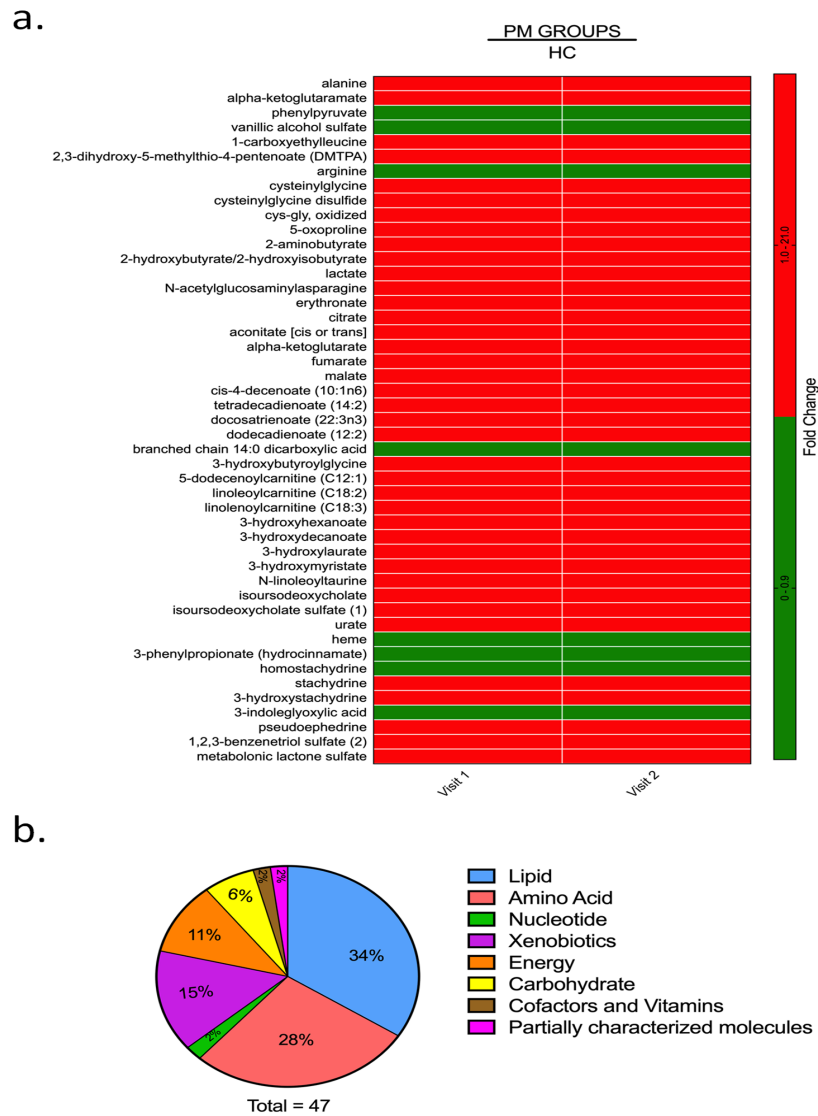
Fig 1: Differential metabolite expression levels among the HC and the PM groups.

a. Heatmap of the 47 most significantly altered metabolites ($P < 0.05$) in the PM group as compared to HC at both V1 and V2. Heatmap was generated using PRISM software; red indicates high, and green indicates low intensity of the metabolite. **b.** Representation of the super pathways of metabolism affected in these 47 significantly altered metabolites ($P < 0.05$).
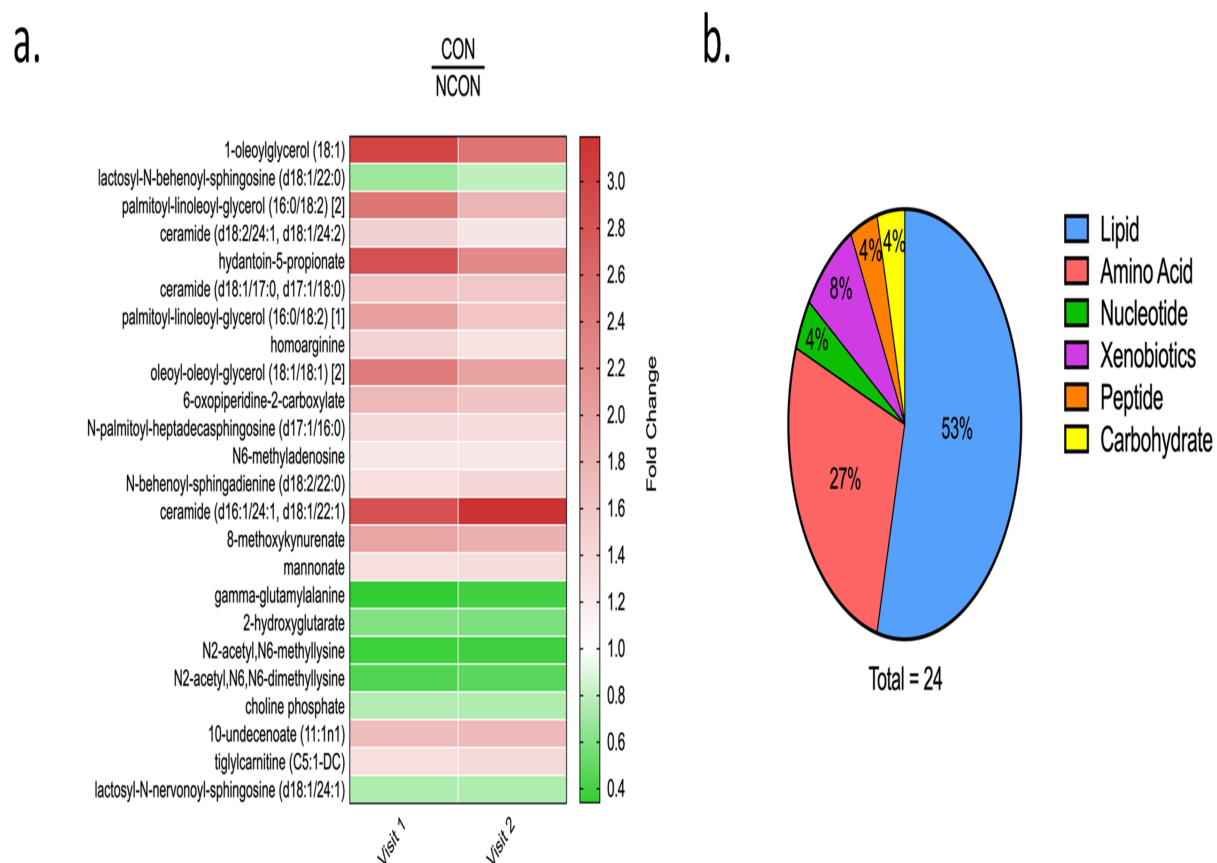
Fig 2: Identification of metabolic biomarkers for early diagnosis of FXTAS

a. Heatmap of the 24 most significantly altered metabolite expression levels ($P \leq 0.05$) in CON at V1 and V2 which distinguish the CON from the NCON. Heatmap was generated using PRISM software; red indicates high, and green indicates low intensity of the metabolite compared to the median (white). **b.** Representation of the super pathways of metabolism involved in these 24 significantly altered metabolites ($P \leq 0.05$).
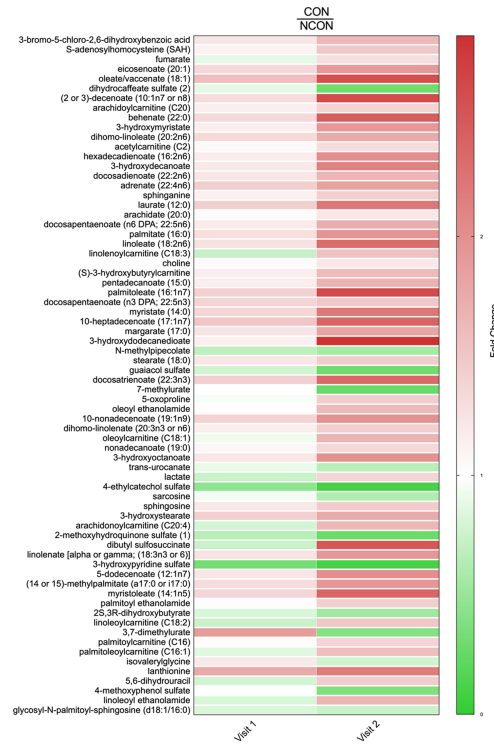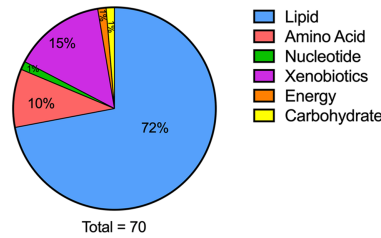
Fig 3: Metabolic profiling identified biomarkers of FXTAS disease progression.

a. Heatmap of the 70 most significantly altered metabolites ($P \leq 0.05$) in CON compared to NCON at V2 which represent biomarkers of FXTAS disease progression. Heatmap was generated using PRISM software; red indicates high and green indicates low intensity of the metabolite compare to the median (white). **b.** Representation of the super pathways of metabolism affected in these 70 significantly altered metabolites ($P \leq 0.05$).

146
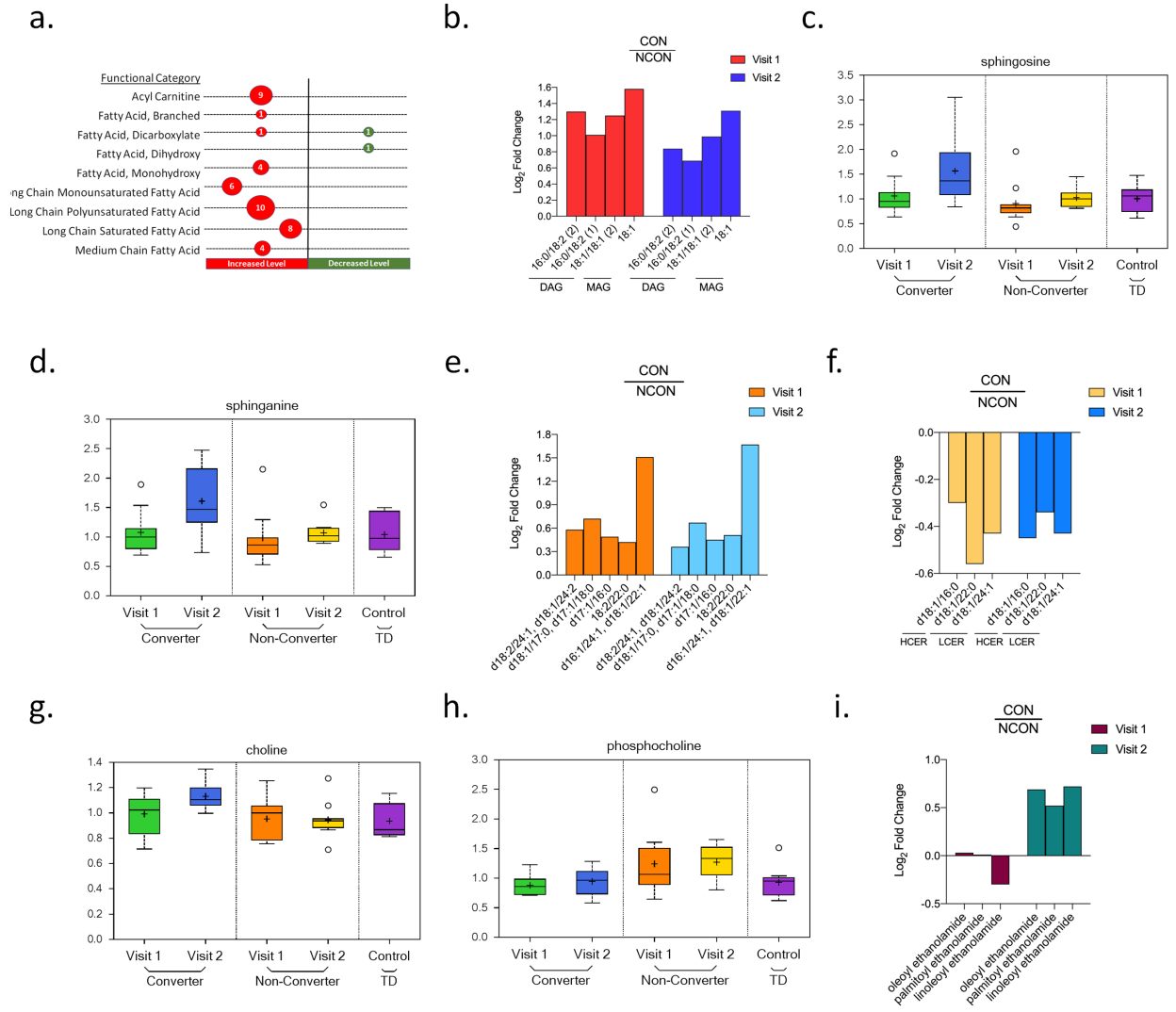
Fig 4: Lipid metabolism is dysregulated in individuals who develop FXTAS over time.

a. Number of differentially expressed metabolites by functional categories are shown; circle sizes are proportional to the number of metabolites; red indicates increased, and green indicates decrease level in CON as compared to NCON. **b.** Log$_2$ Fold Change representation of diacylglycerides (DAG) and monoacylglycerides (MAG) in CON as compared to NCON both at V1 and V2. **c.** Box plots showing increased levels of sphingosine in CON as compared to NCON at V2. The heavy line in each box represents

the median, the lower and upper box edges represent the 25th and 75th percentiles, respectively, and the lower and upper whiskers represent the smallest and largest observations, respectively. **d.** Box plots showing increased levels of sphingosine and sphinganine in CON as compared to NCON at V2. **e.** Log$_2$ Fold Change representation of ceramides in CON as compared to NCON at V1 and V2. **f.** Log$_2$ Fold Change representation of Hexocylceramides (HCER) and of Lactosylceramides (LCER) in CON as compared to NCON at V1 and V2. **g.** Box plots showing increased level of choline in CON as compared to NCON at V2. **h.** Box plots showing decreased levels of choline phosphate in CON as compared to NCON at V1 and V2. **i.** Log$_2$ Fold Change representation of endocannabinoids in CON as compared to NCON at V1 and V2.
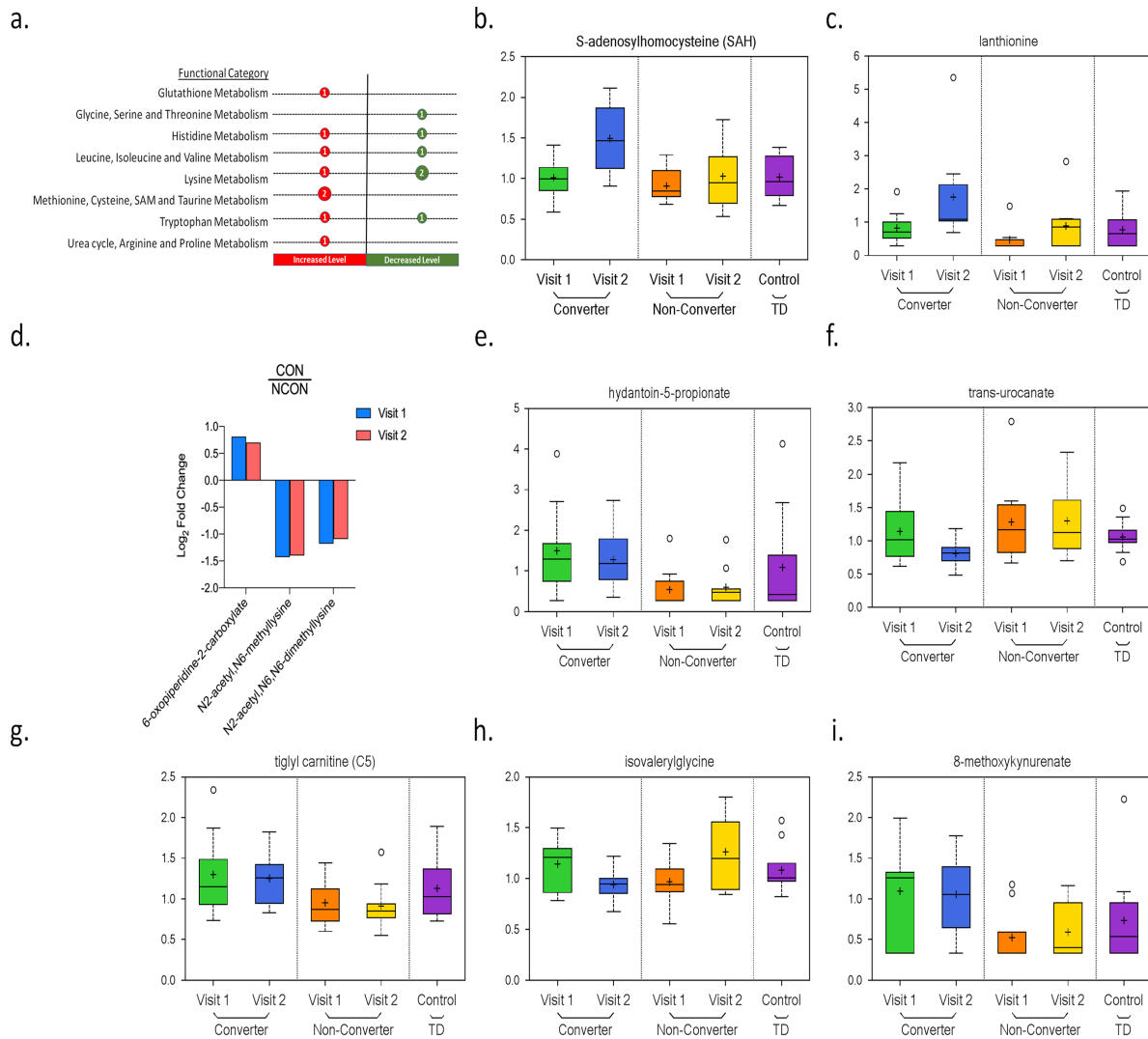
Fig 5: Altered amino-acid profiling observed in CON group.

a. Number of differentially expressed metabolites by functional categories are shown, circle sizes are proportional to the number of metabolites, red indicates increased, and green indicates decrease level in CON as compared to NCON. **b.** Box plots showing increased levels of S-adenosylhomocysteine in CON as compared to NCON at V2. For Box Plots the heavy line in each box represents the median, the lower and upper box

edges represent the 25th and 75th percentiles, respectively, and the lower and upper whiskers represent the smallest and largest observations, respectively. **c.** Box plots showing increased levels of lanthionine in CON as compared to NCON at V2. **d.** Log$_2$ Fold Change representation of metabolites associates with Lysine metabolism in CON as compared to NCON at V1 and V2. **e.** Box plots showing increased levels of hydantoin-5-propionate in CON as compared to NCON at V1 and V2. **f.** Box plots showing decreased levels of trans-urocanate in CON as compared to NCON at V2. **g.** Box plots showing increased level of tiglylcarnitine (C5:1-DC) in CON as compared to NCON at V1 and V2. **h.** Box plots showing decreased level of isovalerylglycine in CON as compared to NCON at V2. **i.** Box plots showing increased level of 8-methoxykynurenate in CON as compared to NCON at V1 and V2.
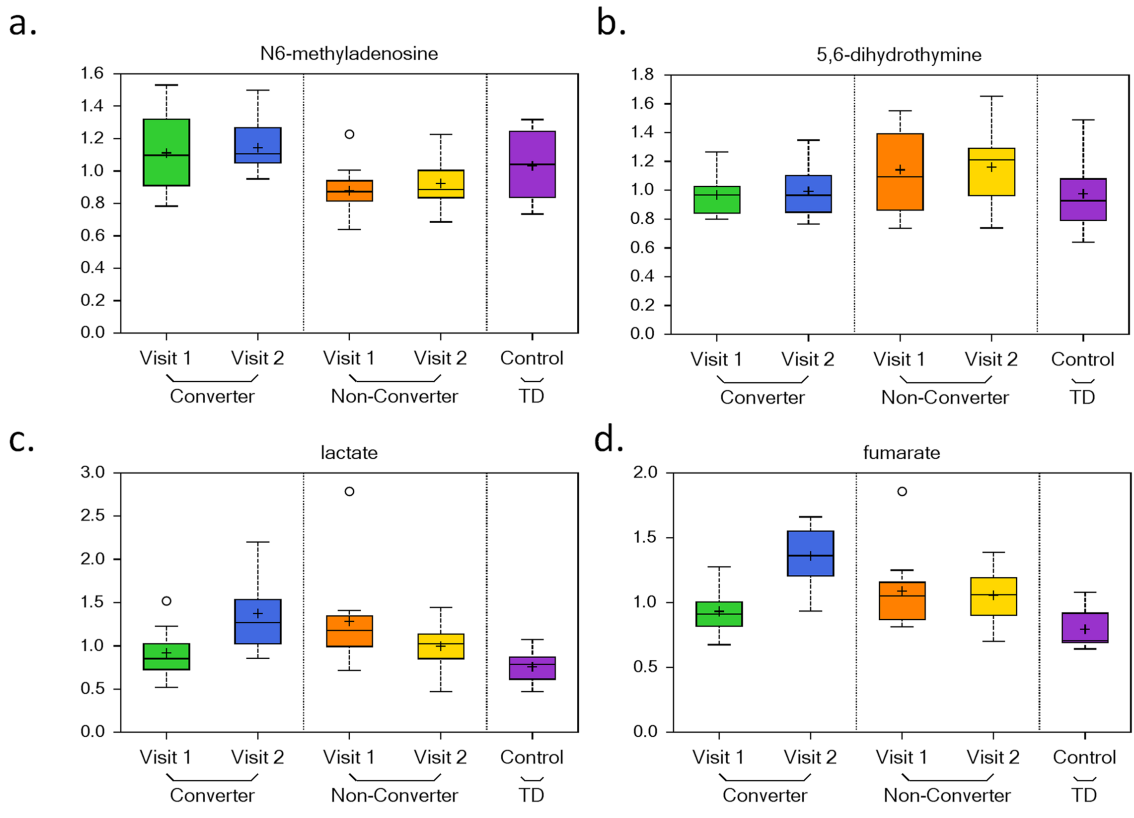
Fig 6: Nucleotide, carbohydrate, energy, and peptide pathways are dysregulated in individuals who develop symptoms of FXTAS over time.

a. Box plots showing a biomarker of early disease diagnosis N6-methyladenosine increased levels in CON as compared to NCON at V1 and V2. For Box Plots the heavy line in each box represents the median, the lower and upper box edges represent the 25th and 75th percentiles, respectively, and the lower and upper whiskers represent the smallest and largest observations, respectively. **b.** Box plots showing a biomarker of disease progression 5,6-dihydrouracil increased levels in CON as compared to NCON at V2. **c.** Box plots showing decreased levels of lactate CON as compared to NCON at V1 that significantly increased at V2. **d.** Box plots showing increased levels of fumarate in CON as compared to NCON at V2.
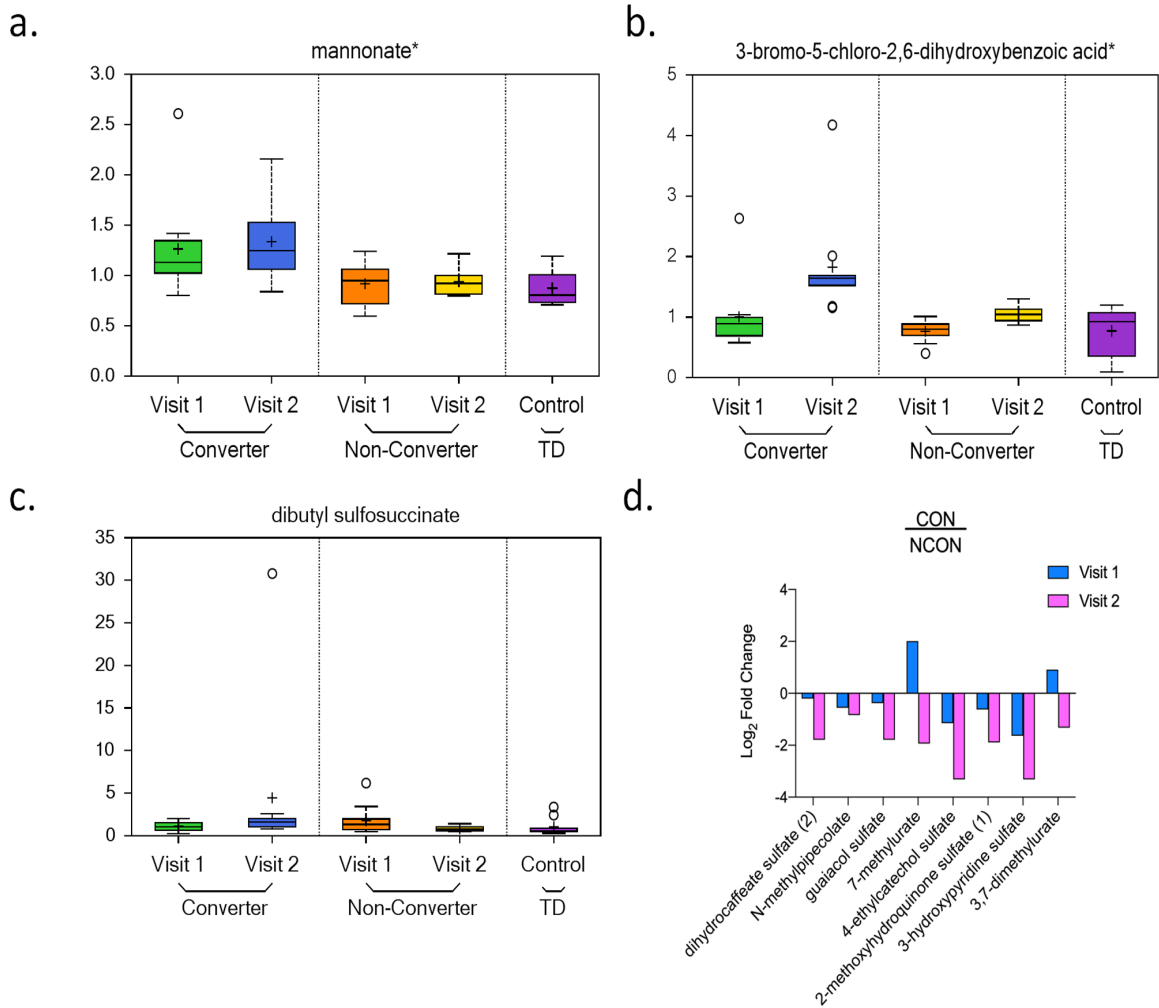
Fig 7: <u>Xenobiotics metabolism is perturbed in CON group</u>**.**

a. Box plots showing increased level of mannonate in CON as compared to NCON at V1 and V2. For Box Plots the heavy line in each box represents the median, the lower and upper box edges represent the 25th and 75th percentiles, respectively, and the lower and upper whiskers represent the smallest and largest observations, respectively. **b & c**. Box plots showing an increased level of 3-bromo-5-chloro-2,6-dihydroxybenzoic acid and dibutyl sulfosuccinate in CON as compared to NCON at V2. **d.** Log_2 Fold Change representation of remaining 8 xenobiotics that are decreasing in CON as compared to NCON at V2.

12. Supplementary Material

S1 Table: <u>List of 66 metabolites significantly altered between non-carrier healthy controls and the premutation groups including converters and non-converters at Visit 1 (V1).</u>

	Super Pathway	Sub Pathway	Biochemical Name	Expression Level	p-value	q-value
				Welch's *t*-Test Group Control		
1	Amino Acid	Alanine and Aspartate Metabolism	alanine	↑	0.0050	0.4154
2	Amino Acid	Glutamate Metabolism	alpha-ketoglutaramate*	↑	0.0250	0.5811
3	Amino Acid	Glutamate Metabolism	S-1-pyrroline-5-carboxylate	↓	0.0219	0.5778
4	Amino Acid	Phenylalanine Metabolism	phenylpyruvate	↓	0.0158	0.5130
5	Amino Acid	Tyrosine Metabolism	vanillic alcohol sulfate	↓	0.0423	0.6059
6	Amino Acid	Leucine, Isoleucine and Valine Metabolism	1-carboxyethylleucine	↑	0.0277	0.5811
7	Amino Acid	Leucine, Isoleucine and Valine Metabolism	N-acetylisoleucine	↑	0.0335	0.6059
8	Amino Acid	Methionine, Cysteine, SAM and Taurine Metabolism	2,3-dihydroxy-5-methylthio-4-pentenoate (DMTPA)*	↑	0.0420	0.6059
9	Amino Acid	Urea cycle; Arginine and Proline Metabolism	arginine	↓	0.0338	0.6059
10	Amino Acid	Glutathione Metabolism	cysteinylglycine	↑	0.0093	0.4495
11	Amino Acid	Glutathione Metabolism	cysteinylglycine disulfide*	↑	0.0083	0.4495
12	Amino Acid	Glutathione Metabolism	cys-gly, oxidized	↑	0.0279	0.5811
13	Amino Acid	Glutathione Metabolism	5-oxoproline	↑	0.0096	0.4495
14	Amino Acid	Glutathione Metabolism	2-aminobutyrate	↑	0.0112	0.4748
15	Amino Acid	Glutathione Metabolism	2-hydroxybutyrate/2-hydroxyisobutyrate	↑	0.0044	0.4154
16	Carbohydrate	Glycolysis, Gluconeogenesis, and Pyruvate Metabolism	lactate	↑	0.0087	0.4495
17	Carbohydrate	Aminosugar Metabolism	N-acetylglucosaminylasparagine	↑	0.0303	0.5964
18	Carbohydrate	Aminosugar Metabolism	erythronate*	↑	0.0266	0.5811
19	Energy	TCA Cycle	citrate	↑	0.0146	0.5130

20	Energy	TCA Cycle	aconitate [cis or trans]	↑	0.0020	0.2970
21	Energy	TCA Cycle	alpha-ketoglutarate	↑	0.0401	0.6059
22	Energy	TCA Cycle	fumarate	↑	0.0066	0.4280
23	Energy	TCA Cycle	malate	↑	0.0360	0.6059
24	Lipid	Medium Chain Fatty Acid	cis-4-decenoate (10:1n6)*	↑	0.0402	0.6059
25	Lipid	Long Chain Polyunsaturated Fatty Acid (n3 and n6)	tetradecadienoate (14:2)*	↑	0.0146	0.5130
26	Lipid	Long Chain Polyunsaturated Fatty Acid (n3 and n6)	docosatrienoate (22:3n3)	↑	0.0133	0.5093
27	Lipid	Fatty Acid, Dicarboxylate	dodecadienoate (12:2)*	↑	0.0205	0.5598
28	Lipid	Fatty Acid, Dicarboxylate	branched chain 14:0 dicarboxylic acid**	↓	0.0493	0.6191
29	Lipid	Fatty Acid Metabolism (Acyl Glycine)	3-hydroxybutyroylglycine**	↑	0.0471	0.6191
30	Lipid	Fatty Acid Metabolism (Acyl Carnitine, Monounsaturated)	5-dodecenoylcarnitine (C12:1)	↑	0.0045	0.4154
31	Lipid	Fatty Acid Metabolism (Acyl Carnitine, Polyunsaturated)	linoleoylcarnitine (C18:2)*	↑	0.0177	0.5356
32	Lipid	Fatty Acid Metabolism (Acyl Carnitine, Polyunsaturated)	linolenoylcarnitine (C18:3)*	↑	0.0282	0.5811
33	Lipid	Fatty Acid, Monohydroxy	3-hydroxyhexanoate	↑	0.0051	0.4154
34	Lipid	Fatty Acid, Monohydroxy	3-hydroxydecanoate	↑	0.0297	0.5964
35	Lipid	Fatty Acid, Monohydroxy	3-hydroxylaurate	↑	0.0280	0.5811
36	Lipid	Fatty Acid, Monohydroxy	3-hydroxymyristate	↑	0.0191	0.5419
37	Lipid	Fatty Acid, Dihydroxy	2S,3R-dihydroxybutyrate	↑	0.0171	0.5354
38	Lipid	Endocannabinoid	N-linoleoyltaurine*	↑	0.0431	0.6077
39	Lipid	Phosphatidylserine (PS)	1-stearoyl-2-oleoyl-GPS (18:0/18:1)	↓	0.0347	0.6059
40	Lipid	Monoacylglycerol	1-myristoylglycerol (14:0)	↓	0.0486	0.6191
41	Lipid	Ceramides	N-palmitoyl-sphingadienine (d18:2/16:0)*	↓	0.0279	0.5811
42	Lipid	Secondary Bile Acid Metabolism	isoursodeoxycholate	↑	0.0003	0.2661
43	Lipid	Secondary Bile Acid Metabolism	isoursodeoxycholate sulfate (1)	↑	0.0010	0.2970
44	Lipid	Secondary Bile Acid Metabolism	glycoursodeoxycholate	↑	0.0411	0.6059
45	Lipid	Secondary Bile Acid Metabolism	glycocholenate sulfate*	↑	0.0372	0.6059
46	Nucleotide	Purine Metabolism, (Hypo)Xanthine/Inosine containing	urate	↑	0.0448	0.6191
47	Nucleotide	Pyrimidine Metabolism, Orotate containing	dihydroorotate	↑	0.0419	0.6059
48	Cofactors and Vitamins	Hemoglobin and Porphyrin Metabolism	heme	↓	0.0270	0.5811
49	Xenobiotics	Benzoate Metabolism	3-hydroxyhippurate	↑	0.0407	0.6059
50	Xenobiotics	Benzoate Metabolism	4-allylcatechol sulfate	↓	0.0347	0.6059
51	Xenobiotics	Benzoate Metabolism	4-acetylphenol sulfate	↓	0.0477	0.6191

	Super Pathway	Sub Pathway	Biochemical Name	Total	p-value	q-value
52	Xenobiotics	Benzoate Metabolism	3-(3-hydroxyphenyl)propionate	↑	0.0152	0.5130
53	Xenobiotics	Benzoate Metabolism	3-phenylpropionate (hydrocinnamate)	↓	0.0017	0.2970
54	Xenobiotics	Food Component/Plant	2-piperidinone	↑	0.0277	0.5811
55	Xenobiotics	Food Component/Plant	dihydrocaffeate sulfate (2)	↑	0.0192	0.5419
56	Xenobiotics	Food Component/Plant	cinnamoylglycine	↓	0.0084	0.4495
57	Xenobiotics	Food Component/Plant	homostachydrine*	↓	0.0059	0.4156
58	Xenobiotics	Food Component/Plant	stachydrine	↑	0.0054	0.4154
59	Xenobiotics	Food Component/Plant	3-hydroxystachydrine*	↑	0.0021	0.2970
60	Xenobiotics	Food Component/Plant	2-keto-3-deoxy-gluconate	↑	0.0376	0.6059
61	Xenobiotics	Food Component/Plant	3-indoleglyoxylic acid	↓	0.0121	0.4859
62	Xenobiotics	Drug - Respiratory	pseudoephedrine	↑	0.0348	0.6059
63	Xenobiotics	Chemical	perfluorooctanesulfonate (PFOS)	↑	0.0486	0.6191
64	Xenobiotics	Chemical	1,2,3-benzenetriol sulfate (2)	↑	0.0353	0.6059
65	Partially Characterized Molecules	Partially Characterized Molecules	metabolonic lactone sulfate	↑	0.0109	0.4748
66	Partially Characterized Molecules	Partially Characterized Molecules	branched-chain, straight-chain, or cyclopropyl 10:1 fatty acid (2)*	↑	0.0020	0.2970

S2 Table: List of 151 metabolites significantly altered between non-carrier healthy controls and the premutation groups including converters and non-converters at Visit 2 (V2).

				Welch's *t*-Test		
				Group Control		
	Super Pathway	Sub Pathway	Biochemical Name	Total Visit 2	p-value	q-value
1	Amino Acid	Alanine and Aspartate Metabolism	alanine	↑	0.0337	0.2151
2	Amino Acid	Alanine and Aspartate Metabolism	N-acetylalanine	↑	0.0295	0.1950
3	Amino Acid	Glutamate Metabolism	alpha-ketoglutaramate*	↑	0.0034	0.0864
4	Amino Acid	Glutamate Metabolism	4-hydroxyglutamate	↑	0.0493	0.2593
5	Amino Acid	Glutamate Metabolism	beta-citrylglutamate	↑	0.0044	0.0922
6	Amino Acid	Lysine Metabolism	N,N,N-trimethyl-5-aminovalerate	↑	0.0274	0.1875

#	Super Pathway	Sub Pathway	Biochemical		Value 1	Value 2
7	Amino Acid	Phenylalanine Metabolism	phenylpyruvate	↓	0.0010	0.0514
8	Amino Acid	Tyrosine Metabolism	vanillic alcohol sulfate	↓	0.0122	0.1322
9	Amino Acid	Leucine, Isoleucine and Valine Metabolism	N-acetylleucine	↑	0.0237	0.1794
10	Amino Acid	Leucine, Isoleucine and Valine Metabolism	1-carboxyethylleucine	↑	0.0424	0.2381
11	Amino Acid	Leucine, Isoleucine and Valine Metabolism	3-methyl-2-oxovalerate	↑	0.0222	0.1710
12	Amino Acid	Leucine, Isoleucine and Valine Metabolism	3-hydroxy-2-ethylpropionate	↑	0.0491	0.2593
13	Amino Acid	Leucine, Isoleucine and Valine Metabolism	N-acetylvaline	↑	0.0082	0.1220
14	Amino Acid	Leucine, Isoleucine and Valine Metabolism	3-methyl-2-oxobutyrate	↑	0.0066	0.1041
15	Amino Acid	Methionine, Cysteine, SAM and Taurine Metabolism	2,3-dihydroxy-5-methylthio-4-pentenoate (DMTPA)*	↑	0.0098	0.1304
16	Amino Acid	Methionine, Cysteine, SAM and Taurine Metabolism	hypotaurine	↑	0.0008	0.0514
17	Amino Acid	Methionine, Cysteine, SAM and Taurine Metabolism	taurine	↑	0.0159	0.1512
18	Amino Acid	Methionine, Cysteine, SAM and Taurine Metabolism	N-acetyltaurine	↑	0.0141	0.1478
19	Amino Acid	Urea cycle; Arginine and Proline Metabolism	arginine	↓	0.0201	0.1611
20	Amino Acid	Urea cycle; Arginine and Proline Metabolism	homocitrulline	↑	0.0495	0.2593
21	Amino Acid	Urea cycle; Arginine and Proline Metabolism	N-methylproline	↑	0.0474	0.2548
22	Amino Acid	Guanidino and Acetamido Metabolism	4-guanidinobutanoate	↓	0.0408	0.2309
23	Amino Acid	Glutathione Metabolism	cysteinylglycine	↑	0.0150	0.1512
24	Amino Acid	Glutathione Metabolism	cysteinylglycine disulfide*	↑	0.0044	0.0922
25	Amino Acid	Glutathione Metabolism	cys-gly, oxidized	↑	0.0053	0.0954
26	Amino Acid	Glutathione Metabolism	5-oxoproline	↑	0.0009	0.0514
27	Amino Acid	Glutathione Metabolism	2-aminobutyrate	↑	0.0451	0.2498
28	Amino Acid	Glutathione Metabolism	2-hydroxybutyrate/2-hydroxyisobutyrate	↑	0.0018	0.0735
29	Carbohydrate	Glycolysis, Gluconeogenesis, and Pyruvate Metabolism	pyruvate	↑	0.0076	0.1145
30	Carbohydrate	Glycolysis, Gluconeogenesis, and Pyruvate Metabolism	lactate	↑	0.0012	0.0568
31	Carbohydrate	Aminosugar Metabolism	N-acetylneuraminate	↑	0.0023	0.0825
32	Carbohydrate	Aminosugar Metabolism	N-acetylglucosaminylasparagine	↑	0.0279	0.1876
33	Carbohydrate	Aminosugar Metabolism	erythronate*	↑	0.0404	0.2309
34	Energy	TCA Cycle	citrate	↑	0.0025	0.0828
35	Energy	TCA Cycle	aconitate [cis or trans]	↑	0.0001	0.0243
36	Energy	TCA Cycle	alpha-ketoglutarate	↑	0.0012	0.0565
37	Energy	TCA Cycle	fumarate	↑	0.0000	0.0147
38	Energy	TCA Cycle	malate	↑	0.0010	0.0514
39	Energy	Oxidative Phosphorylation	phosphate	↑	0.0389	0.2309
40	Lipid	Medium Chain Fatty Acid	cis-4-decenoate (10:1n6)*	↑	0.0208	0.1637

#						
41	Lipid	Medium Chain Fatty Acid	(2 or 3)-decenoate (10:1n7 or n8)	↑	0.0098	0.1304
42	Lipid	Medium Chain Fatty Acid	10-undecenoate (11:1n1)	↑	0.0292	0.1945
43	Lipid	Medium Chain Fatty Acid	5-dodecenoate (12:1n7)	↑	0.0029	0.0828
44	Lipid	Long Chain Saturated Fatty Acid	myristate (14:0)	↑	0.0323	0.2083
45	Lipid	Long Chain Saturated Fatty Acid	pentadecanoate (15:0)	↑	0.0182	0.1512
46	Lipid	Long Chain Saturated Fatty Acid	palmitate (16:0)	↑	0.0049	0.0933
47	Lipid	Long Chain Saturated Fatty Acid	margarate (17:0)	↑	0.0195	0.1578
48	Lipid	Long Chain Saturated Fatty Acid	stearate (18:0)	↑	0.0023	0.0825
49	Lipid	Long Chain Saturated Fatty Acid	nonadecanoate (19:0)	↑	0.0090	0.1289
50	Lipid	Long Chain Monounsaturated Fatty Acid	myristoleate (14:1n5)	↑	0.0151	0.1512
51	Lipid	Long Chain Monounsaturated Fatty Acid	palmitoleate (16:1n7)	↑	0.0111	0.1307
52	Lipid	Long Chain Monounsaturated Fatty Acid	10-heptadecenoate (17:1n7)	↑	0.0264	0.1853
53	Lipid	Long Chain Monounsaturated Fatty Acid	oleate/vaccenate (18:1)	↑	0.0063	0.1036
54	Lipid	Long Chain Monounsaturated Fatty Acid	10-nonadecenoate (19:1n9)	↑	0.0037	0.0864
55	Lipid	Long Chain Monounsaturated Fatty Acid	eicosenoate (20:1)	↑	0.0045	0.0922
56	Lipid	Long Chain Monounsaturated Fatty Acid	erucate (22:1n9)	↑	0.0146	0.1509
57	Lipid	Long Chain Polyunsaturated Fatty Acid (n3 and n6)	tetradecadienoate (14:2)*	↑	0.0005	0.0514
58	Lipid	Long Chain Polyunsaturated Fatty Acid (n3 and n6)	docosapentaenoate (n3 DPA; 22:5n3)	↑	0.0030	0.0828
59	Lipid	Long Chain Polyunsaturated Fatty Acid (n3 and n6)	docosahexaenoate (DHA; 22:6n3)	↑	0.0171	0.1512
60	Lipid	Long Chain Polyunsaturated Fatty Acid (n3 and n6)	docosatrienoate (22:3n3)	↑	0.0025	0.0828
61	Lipid	Long Chain Polyunsaturated Fatty Acid (n3 and n6)	hexadecadienoate (16:2n6)	↑	0.0226	0.1722
62	Lipid	Long Chain Polyunsaturated Fatty Acid (n3 and n6)	linoleate (18:2n6)	↑	0.0053	0.0954
63	Lipid	Long Chain Polyunsaturated Fatty Acid (n3 and n6)	linolenate [alpha or gamma; (18:3n3 or 6)]	↑	0.0048	0.0933
64	Lipid	Long Chain Polyunsaturated Fatty Acid (n3 and n6)	dihomo-linoleate (20:2n6)	↑	0.0008	0.0514
65	Lipid	Long Chain Polyunsaturated Fatty Acid (n3 and n6)	arachidonate (20:4n6)	↑	0.0092	0.1289
66	Lipid	Long Chain Polyunsaturated Fatty Acid (n3 and n6)	adrenate (22:4n6)	↑	0.0037	0.0864
67	Lipid	Long Chain Polyunsaturated Fatty Acid (n3 and n6)	docosapentaenoate (n6 DPA; 22:5n6)	↑	0.0117	0.1322
68	Lipid	Long Chain Polyunsaturated Fatty Acid (n3 and n6)	docosadienoate (22:2n6)	↑	0.0016	0.0713
69	Lipid	Long Chain Polyunsaturated Fatty Acid (n3 and n6)	mead acid (20:3n9)	↑	0.0055	0.0954
70	Lipid	Fatty Acid, Branched	(12 or 13)-methylmyristate (a15:0 or i15:0)	↑	0.0246	0.1812
71	Lipid	Fatty Acid, Branched	(14 or 15)-methylpalmitate (a17:0 or i17:0)	↑	0.0250	0.1820
72	Lipid	Fatty Acid, Dicarboxylate	3-hydroxydodecanedioate*	↑	0.0119	0.1322
73	Lipid	Fatty Acid, Dicarboxylate	dodecadienoate (12:2)*	↑	0.0032	0.0864
74	Lipid	Fatty Acid, Dicarboxylate	branched chain 14:0 dicarboxylic acid**	↓	0.0498	0.2593

75	Lipid	Fatty Acid Metabolism (Acyl Glycine)	N-palmitoylglycine		0.02 73	0.18 75
76	Lipid	Fatty Acid Metabolism (Acyl Glycine)	3-hydroxybutyroylglycine**	↑	0.01 00	0.13 06
77	Lipid	Fatty Acid Metabolism (Acyl Carnitine, Short Chain)	acetylcarnitine (C2)	↑	0.01 63	0.15 12
78	Lipid	Fatty Acid Metabolism (Acyl Carnitine, Medium Chain)	octanoylcarnitine (C8)	↑	0.04 70	0.25 48
79	Lipid	Fatty Acid Metabolism (Acyl Carnitine, Medium Chain)	decanoylcarnitine (C10)	↑	0.04 02	0.23 09
80	Lipid	Fatty Acid Metabolism (Acyl Carnitine, Medium Chain)	laurylcarnitine (C12)	↑	0.03 08	0.19 98
81	Lipid	Fatty Acid Metabolism (Acyl Carnitine, Long Chain Saturated)	myristoylcarnitine (C14)	↑	0.03 87	0.23 09
82	Lipid	Fatty Acid Metabolism (Acyl Carnitine, Long Chain Saturated)	palmitoylcarnitine (C16)	↑	0.01 80	0.15 12
83	Lipid	Fatty Acid Metabolism (Acyl Carnitine, Long Chain Saturated)	stearoylcarnitine (C18)	↑	0.03 94	0.23 09
84	Lipid	Fatty Acid Metabolism (Acyl Carnitine, Monounsaturated)	cis-4-decenoylcarnitine (C10:1)	↑	0.03 98	0.23 09
85	Lipid	Fatty Acid Metabolism (Acyl Carnitine, Monounsaturated)	5-dodecenoylcarnitine (C12:1)	↑	0.00 29	0.08 28
86	Lipid	Fatty Acid Metabolism (Acyl Carnitine, Monounsaturated)	myristoleoylcarnitine (C14:1)*	↑	0.01 61	0.15 12
87	Lipid	Fatty Acid Metabolism (Acyl Carnitine, Monounsaturated)	palmitoleoylcarnitine (C16:1)*	↑	0.00 46	0.09 29
88	Lipid	Fatty Acid Metabolism (Acyl Carnitine, Monounsaturated)	oleoylcarnitine (C18:1)	↑	0.01 08	0.13 07
89	Lipid	Fatty Acid Metabolism (Acyl Carnitine, Monounsaturated)	eicosenoylcarnitine (C20:1)*	↑	0.00 68	0.10 48
90	Lipid	Fatty Acid Metabolism (Acyl Carnitine, Polyunsaturated)	linoleoylcarnitine (C18:2)*	↑	0.02 47	0.18 12
91	Lipid	Fatty Acid Metabolism (Acyl Carnitine, Polyunsaturated)	linolenoylcarnitine (C18:3)*	↑	0.02 08	0.16 37
92	Lipid	Fatty Acid Metabolism (Acyl Carnitine, Polyunsaturated)	dihomo-linoleoylcarnitine (C20:2)*	↑	0.04 73	0.25 48
93	Lipid	Fatty Acid Metabolism (Acyl Carnitine, Polyunsaturated)	arachidonoylcarnitine (C20:4)	↑	0.03 02	0.19 80
94	Lipid	Fatty Acid Metabolism (Acyl Carnitine, Polyunsaturated)	adrenoylcarnitine (C22:4)*	↑	0.04 64	0.25 48
95	Lipid	Fatty Acid Metabolism (Acyl Carnitine, Hydroxy)	(R)-3-hydroxybutyrylcarnitine	↑	0.01 94	0.15 78
96	Lipid	Fatty Acid Metabolism (Acyl Carnitine, Hydroxy)	(S)-3-hydroxybutyrylcarnitine	↑	0.01 08	0.13 07
97	Lipid	Fatty Acid Metabolism (Acyl Carnitine, Hydroxy)	3-hydroxydecanoylcarnitine	↑	0.01 70	0.15 12
98	Lipid	Fatty Acid Metabolism (Acyl Carnitine, Hydroxy)	3-hydroxyoleoylcarnitine	↑	0.00 39	0.08 80
99	Lipid	Ketone Bodies	3-hydroxybutyrate (BHBA)	↑	0.01 11	0.13 07
100	Lipid	Fatty Acid, Monohydroxy	3-hydroxyhexanoate	↑	0.00 10	0.05 14
101	Lipid	Fatty Acid, Monohydroxy	3-hydroxyoctanoate	↑	0.01 05	0.13 07
102	Lipid	Fatty Acid, Monohydroxy	3-hydroxydecanoate	↑	0.00 06	0.05 14
103	Lipid	Fatty Acid, Monohydroxy	3-hydroxylaurate	↑	0.00 03	0.04 43
104	Lipid	Fatty Acid, Monohydroxy	3-hydroxymyristate	↑	0.00 03	0.04 43
105	Lipid	Fatty Acid, Monohydroxy	3-hydroxystearate	↑	0.00 58	0.09 98
106	Lipid	Fatty Acid, Monohydroxy	3-hydroxyoleate*	↑	0.03 39	0.21 51
107	Lipid	Fatty Acid, Monohydroxy	9-hydroxystearate	↑	0.02 45	0.18 12
108	Lipid	Fatty Acid, Monohydroxy	16-hydroxypalmitate	↑	0.04 07	0.23 09

109	Lipid	Endocannabinoid	N-oleoyltaurine	↑	0.0123	0.1322
110	Lipid	Endocannabinoid	N-palmitoyltaurine	↑	0.0054	0.0954
111	Lipid	Endocannabinoid	N-linoleoyltaurine*	↑	0.0357	0.2190
112	Lipid	Endocannabinoid	N-oleoylserine	↑	0.0278	0.1876
113	Lipid	Phospholipid Metabolism	phosphoethanolamine	↑	0.0252	0.1820
114	Lipid	Phospholipid Metabolism	glycerophosphoethanolamine	↑	0.0259	0.1835
115	Lipid	Phosphatidylcholine (PC)	1,2-dipalmitoyl-GPC (16:0/16:0)	↑	0.0177	0.1512
116	Lipid	Phosphatidylcholine (PC)	1-palmitoyl-2-stearoyl-GPC (16:0/18:0)	↑	0.0352	0.2176
117	Lipid	Lysophospholipid	1-arachidonoyl-GPC (20:4n6)*	↑	0.0347	0.2169
118	Lipid	Lysophospholipid	1-arachidonoyl-GPE (20:4n6)*	↑	0.0477	0.2548
119	Lipid	Lysoplasmalogen	1-(1-enyl-palmitoyl)-GPE (P-16:0)*	↑	0.0098	0.1304
120	Lipid	Lysoplasmalogen	1-(1-enyl-stearoyl)-GPE (P-18:0)*	↑	0.0183	0.1512
121	Lipid	Glycerolipid Metabolism	glycerol	↑	0.0008	0.0514
122	Lipid	Glycerolipid Metabolism	glycerol 3-phosphate	↑	0.0396	0.2309
123	Lipid	Monoacylglycerol	1-arachidonylglycerol (20:4)	↑	0.0019	0.0735
124	Lipid	Monoacylglycerol	2-arachidonoylglycerol (20:4)	↑	0.0180	0.1512
125	Lipid	Sphingolipid Synthesis	sphinganine-1-phosphate	↑	0.0063	0.1036
126	Lipid	Lactosylceramides (LCER)	lactosyl-N-behenoyl-sphingosine (d18:1/22:0)*	↑	0.0217	0.1687
127	Lipid	Dihydrosphingomyelins	behenoyl dihydrosphingomyelin (d18:0/22:0)*	↑	0.0111	0.1307
128	Lipid	Sphingosines	sphingosine 1-phosphate	↑	0.0348	0.2169
129	Lipid	Primary Bile Acid Metabolism	chenodeoxycholic acid sulfate (1)	↑	0.0175	0.1512
130	Lipid	Secondary Bile Acid Metabolism	isoursodeoxycholate	↑	0.0027	0.0828
131	Lipid	Secondary Bile Acid Metabolism	isoursodeoxycholate sulfate (1)	↑	0.0036	0.0864
132	Nucleotide	Purine Metabolism, (Hypo)Xanthine/Inosine containing	urate	↑	0.0390	0.2309
133	Cofactors and Vitamins	Nicotinate and Nicotinamide Metabolism	nicotinamide adenine dinucleotide (NAD+)	↑	0.0114	0.1313
134	Cofactors and Vitamins	Hemoglobin and Porphyrin Metabolism	heme	↓	0.0259	0.1835
135	Xenobiotics	Benzoate Metabolism	3-phenylpropionate (hydrocinnamate)	↓	0.0033	0.0864
136	Xenobiotics	Food Component/Plant	3-formylindole	↓	0.0131	0.1390
137	Xenobiotics	Food Component/Plant	homostachydrine*	↓	0.0065	0.1039
138	Xenobiotics	Food Component/Plant	mannonate*	↑	0.0091	0.1289
139	Xenobiotics	Food Component/Plant	stachydrine	↑	0.0005	0.0514
140	Xenobiotics	Food Component/Plant	3-hydroxystachydrine*	↑	0.0000	0.0147
141	Xenobiotics	Food Component/Plant	thymol sulfate	↓	0.0158	0.1512

159

	Super Pathway	Sub Pathway	Biochemical Name			
142	Xenobiotics	Food Component/Plant	3-indoleglyoxylic acid	↓	0.0172	0.1512
143	Xenobiotics	Drug - Metabolic	metformin	↑	0.0442	0.2465
144	Xenobiotics	Drug - Respiratory	pseudoephedrine	↑	0.0171	0.1512
145	Xenobiotics	Chemical	1,2,3-benzenetriol sulfate (2)	↑	0.0171	0.1512
146	Xenobiotics	Chemical	2-methoxyresorcinol sulfate	↑	0.0378	0.2304
147	Xenobiotics	Chemical	3,5-dichloro-2,6-dihydroxybenzoic acid	↑	0.0103	0.1307
148	Xenobiotics	Chemical	3-bromo-5-chloro-2,6-dihydroxybenzoic acid*	↑	0.0177	0.1512
149	Partially Characterized Molecules	Partially Characterized Molecules	glucuronide of C10H18O2 (1)*	↑	0.0272	0.1875
150	Partially Characterized Molecules	Partially Characterized Molecules	metabolonic lactone sulfate	↑	0.0154	0.1512
151	Partially Characterized Molecules	Partially Characterized Molecules	branched-chain, straight-chain, or cyclopropyl 12:1 fatty acid*	↑	0.0122	0.1322

S3 Table: <u>List of metabolites significantly altered in the lipid pathway only in converters as compared to non-converters.</u>

		Super Pathway	Sub Pathway	Biochemical Name	ANOVA Contrasts					
					Converter Non-Converter		Converter Non-Converter			
							Visit 1		Visit 2	
					Visit 1	Visit 2	p-value	q-value	p-value	q-value
1	1	Lipid	Ceramides	ceramide (d18:2/24:1, d18:1/24:2)*	↑	↑	0.0010	0.1306	0.0329	0.1916
	2	Lipid	Ceramides	ceramide (d18:1/17:0, d17:1/18:0)*	↑	↑	0.0021	0.1458	0.0044	0.1123
	3	Lipid	Ceramides	N-palmitoyl-heptadecasphingosine (d17:1/16:0)*	↑	↑	0.0079	0.2330	0.0129	0.1323
	4	Lipid	Ceramides	N-behenoyl-sphingadienine (d18:2/22:0)*	↑	↑	0.0105	0.2441	0.0026	0.0941
	5	Lipid	Ceramides	ceramide (d16:1/24:1, d18:1/22:1)*	↑	↑	0.0127	0.2538	0.0064	0.1218
	6	Lipid	Hexosylceramides (HCER)	glycosyl-N-palmitoyl-sphingosine (d18:1/16:0)		↓	0.1263	0.5604	0.0262	0.1723

	7	Lipid	Lactosylceramides (LCER)	lactosyl-N-behenoyl-sphingosine (d18:1/22:0)*	↓	↓	0.0008	0.1306	0.0310	0.1854
	8	Lipid	Lactosylceramides (LCER)	lactosyl-N-nervonoyl-sphingosine (d18:1/24:1)*	↓	↓	0.0459	0.4090	0.0475	0.2321
2	1	Lipid	Diacylglycerol	palmitoyl-linoleoyl-glycerol (16:0/18:2) [2]*	↑	↑	0.0009	0.1306	0.0229	0.1684
	2	Lipid	Diacylglycerol	palmitoyl-linoleoyl-glycerol (16:0/18:2) [1]*	↑	↑	0.0038	0.1617	0.0404	0.2158
	3	Lipid	Diacylglycerol	oleoyl-oleoyl-glycerol (18:1/18:1) [2]*	↑	↑	0.0055	0.1926	0.0249	0.1692
	4	Lipid	Monoacylglycerol	1-oleoylglycerol (18:1)	↑	↑	0.0005	0.1306	0.0031	0.0955
3	1	Lipid	Endocannabinoid	oleoyl ethanolamide		↑	0.9293	0.8948	0.0208	0.1593
	2	Lipid	Endocannabinoid	palmitoyl ethanolamide		↑	0.9183	0.8945	0.0042	0.1115
	3	Lipid	Endocannabinoid	linoleoyl ethanolamide		↑	0.3556	0.7069	0.0304	0.1846
4	1	Lipid	Fatty Acid Metabolism (Acyl Carnitine, Hydroxy)	(S)-3-hydroxybutyrylcarnitine		↑	0.5025	0.7715	0.0386	0.2138
	2	Lipid	Fatty Acid Metabolism (Acyl Carnitine, Long Chain Saturated)	arachidoylcarnitine (C20)*		↑	0.3473	0.7016	0.0299	0.1835
	3	Lipid	Fatty Acid Metabolism (Acyl Carnitine, Long Chain Saturated)	palmitoylcarnitine (C16)		↑	0.7977	0.8780	0.0085	0.1223
	4	Lipid	Fatty Acid Metabolism (Acyl Carnitine, Monounsaturated)	oleoylcarnitine (C18:1)		↑	0.5929	0.7978	0.0040	0.1115
	5	Lipid	Fatty Acid Metabolism (Acyl Carnitine, Monounsaturated)	palmitoleoylcarnitine (C16:1)*			0.4062	0.7306	0.0266	0.1732
	6	Lipid	Fatty Acid Metabolism (Acyl Carnitine, Polyunsaturated)	linolenoylcarnitine (C18:3)*		↑	0.0921	0.5219	0.0258	0.1720
	7	Lipid	Fatty Acid Metabolism (Acyl Carnitine, Polyunsaturated)	arachidonoylcarnitine (C20:4)		↑	0.3251	0.6952	0.0496	0.2384
	8	Lipid	Fatty Acid Metabolism	linoleoylcarnitine (C18:2)*		↑	0.0655	0.4623	0.0154	0.1422

161

		(Acyl Carnitine, Polyunsaturated)			⬆				
9	Lipid	Fatty Acid Metabolism (Acyl Carnitine, Short Chain)	acetylcarnitine (C2)		⬆	0.6976	0.8344	0.0470	0.2314
10	Lipid	Fatty Acid, Branched	(14 or 15)-methylpalmitate (a17:0 or i17:0)		⬆	0.1873	0.5942	0.0018	0.0821
11	Lipid	Fatty Acid, Dicarboxylate	2-hydroxyglutarate	⬇	⬇	0.0218	0.3200	0.0156	0.1422
12	Lipid	Fatty Acid, Dicarboxylate	3-hydroxydodecanedioate*		⬆	0.7154	0.8416	0.0049	0.1171
13	Lipid	Fatty Acid, Dihydroxy	2S,3R-dihydroxybutyrate		⬆	0.4085	0.7306	0.0231	0.1684
14	Lipid	Fatty Acid, Monohydroxy	3-hydroxymyristate		⬇	0.4690	0.7638	0.0014	0.0821
15	Lipid	Fatty Acid, Monohydroxy	3-hydroxydecanoate		⬆	0.4746	0.7643	0.0062	0.1218
16	Lipid	Fatty Acid, Monohydroxy	3-hydroxyoctanoate		⬆	0.5049	0.7720	0.0248	0.1692
17	Lipid	Fatty Acid, Monohydroxy	3-hydroxystearate		⬆	0.0943	0.5232	0.0082	0.1223
18	Lipid	Long Chain Monounsaturated Fatty Acid	eicosenoate (20:1)		⬆	0.2311	0.6245	0.0110	0.1288
19	Lipid	Long Chain Monounsaturated Fatty Acid	oleate/vaccenate (18:1)		⬆	0.1262	0.5604	0.0030	0.0955
20	Lipid	Long Chain Monounsaturated Fatty Acid	palmitoleate (16:1n7)		⬆	0.2216	0.6151	0.0016	0.0821
21	Lipid	Long Chain Monounsaturated Fatty Acid	10-heptadecenoate (17:1n7)		⬆	0.1002	0.5429	0.0011	0.0816
22	Lipid	Long Chain Monounsaturated Fatty Acid	10-nonadecenoate (19:1n9)		⬆	0.1706	0.5766	0.0067	0.1223
23	Lipid	Long Chain Monounsaturated Fatty Acid	myristoleate (14:1n5)		⬆	0.3256	0.6952	0.0081	0.1223
24	Lipid	Long Chain Polyunsaturated Fatty Acid (n3 and n6)	dihomo-linoleate (20:2n6)		⬆	0.1247	0.5604	0.0039	0.1115
25	Lipid	Long Chain Polyunsaturated Fatty Acid (n3 and n6)	hexadecadienoate (16:2n6)		⬆	0.5236	0.7817	0.0093	0.1260
26	Lipid	Long Chain Polyunsaturated Fatty Acid (n3 and n6)	docosadienoate (22:2n6)		⬆	0.2967	0.6820	0.0102	0.1288
27	Lipid	Long Chain Polyunsaturat	adrenate (22:4n6)		⬆	0.0508	0.4308	0.0016	0.0821

#		Sub Pathway	Biochemical						
			ed Fatty Acid (n3 and n6)						
28	Lipid	Long Chain Polyunsaturated Fatty Acid (n3 and n6)	docosapentaenoate (n6 DPA; 22:5n6)		↑	0.3896	0.7260	0.0082	0.1223
29	Lipid	Long Chain Polyunsaturated Fatty Acid (n3 and n6)	linoleate (18:2n6)		↑	0.3452	0.7016	0.0017	0.0821
30	Lipid	Long Chain Polyunsaturated Fatty Acid (n3 and n6)	docosapentaenoate (n3 DPA; 22:5n3)		↑	0.1036	0.5509	0.0395	0.2158
31	Lipid	Long Chain Polyunsaturated Fatty Acid (n3 and n6)	docosatrienoate (22:3n3)		↑	0.1930	0.5969	0.0026	0.0941
32	Lipid	Long Chain Polyunsaturated Fatty Acid (n3 and n6)	dihomo-linolenate (20:3n3 or n6)		↑	0.4124	0.7306	0.0423	0.2195
33	Lipid	Long Chain Polyunsaturated Fatty Acid (n3 and n6)	linolenate [alpha or gamma; (18:3n3 or 6)]		↑	0.4493	0.7512	0.0331	0.1916
34	Lipid	Long Chain Saturated Fatty Acid	behenate (22:0)*		↑	0.2313	0.6245	0.0009	0.0721
35	Lipid	Long Chain Saturated Fatty Acid	arachidate (20:0)		↑	0.5907	0.7978	0.0209	0.1593
36	Lipid	Long Chain Saturated Fatty Acid	palmitate (16:0)		↑	0.1808	0.5891	0.0006	0.0721
37	Lipid	Long Chain Saturated Fatty Acid	pentadecanoate (15:0)		↑	0.2303	0.6245	0.0001	0.0721
38	Lipid	Long Chain Saturated Fatty Acid	myristate (14:0)		↑	0.1258	0.5604	0.0003	0.0721
39	Lipid	Long Chain Saturated Fatty Acid	margarate (17:0)		↑	0.1822	0.5892	0.0005	0.0721
40	Lipid	Long Chain Saturated Fatty Acid	stearate (18:0)		↑	0.1838	0.5923	0.0099	0.1288
41	Lipid	Long Chain Saturated Fatty Acid	nonadecanoate (19:0)		↑	0.4895	0.7643	0.0142	0.1378
42	Lipid	Medium Chain Fatty Acid	10-undecenoate (11:1n1)	↑	↑	0.0327	0.3704	0.0286	0.1800
43	Lipid	Medium Chain Fatty Acid	(2 or 3)-decenoate (10:1n7 or n8)		↑	0.2805	0.6735	0.0004	0.0721
44	Lipid	Medium Chain Fatty Acid	laurate (12:0)		↑	0.1408	0.5633	0.0022	0.0904
45	Lipid	Medium Chain Fatty Acid	5-dodecenoate (12:1n7)		↑	0.4263	0.7340	0.0108	0.1288
5 1	Lipid	Phospholipid Metabolism	choline phosphate	↓	↓	0.0291	0.3591	0.0231	0.1684
2	Lipid	Phospholipid Metabolism	choline		↑	0.5482	0.7929	0.0119	0.1288

6	1	Lipid	Sphingolipid Synthesis	sphinganine				0.4391	0.7490	0.0182	0.1462
	2	Lipid	Sphingosines	sphingosine				0.2300	0.6245	0.0181	0.1462

S1 Fig: <u>Box plot showing an increased levels of Nervonate in converters as compared to non-converters at V2.</u> For all Box Plots the heavy line in each box represents the median, the lower and upper box edges represent the 25th and 75th percentiles, respectively, and the lower and upper whiskers represent the smallest and largest observations, respectively.
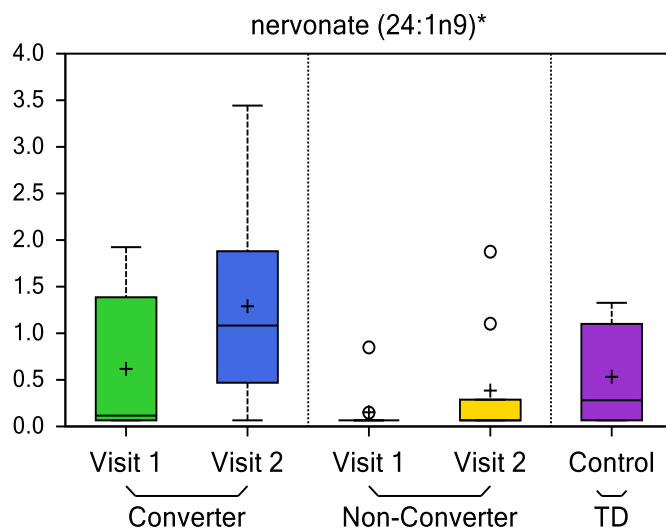
Chapter 4

Metabolomic Biomarkers are Associated with Area of the Pons in Fragile X Premutation Carriers at Risk for Developing FXTAS

Marwa Zafarullah[1], Blythe Durbin-Johnson[2], Emily S. Fourie[3, 4], David R. Hessl[5,6], Susan M. Rivera[3,4,5], and Flora Tassone [1, 5*]

[1]   Department of Biochemistry and Molecular Medicine, University of California Davis, School of Medicine, Sacramento, 95817 CA, USA.
[2]   Division of Biostatistics, University of California Davis, School of Medicine, Davis, CA, USA.
[3]   Center for Mind and Brain, University of California Davis, Davis, CA, USA.
[4]   Department of Psychology, University of California, Davis, Davis, CA, USA.
[5]   MIND Institute, University of California Davis Medical Center, Sacramento, 95817 CA, USA.
[6]   Department of Psychiatry and Behavioral Sciences, University of California Davis Medical Center, Sacramento, 95817 CA, USA.
*   **Correspondence:** ftassone@ucdavis.edu; Tel.: +1-(916)-703-0463

Abstract

Fragile X-associated tremor/ataxia syndrome (FXTAS) is a late adult-onset neurodegenerative disorder that affects movement and cognition in male and female carriers of a premutation allele (55–200 CGG repeats; PM) in the fragile X mental retardation (*FMR1*) gene. It is currently unknown how the observed brain changes are associated with metabolic signatures in individuals who develop the disorder over time.

The primary objective of this study was to investigate the correlation between longitudinal changes in the brain (area of the pons, midbrain, and MCP width) and the changes in the expression level of metabolic biomarkers of early diagnosis and progression of FXTAS in PM who, as part of an ongoing longitudinal study, emerged into two distinct categories. These included those who developed symptoms of FXTAS (converters, CON) at subsequent visits and those who did not meet the criteria of diagnosis (non-converters, NCON) and were compared to age-matched healthy controls (HC). We assessed CGG repeat allele size by Southern Blot and PCR analysis. Magnetic

Resonance Imaging (MRIs) acquisition was obtained on a 3T Siemens Trio scanner and metabolomic profile was obtained by ultra-performance liquid chromatography, accurate mass spectrometer, and an Orbitrap mass analyzer.

Our findings indicate that differential metabolite levels are linked with the area of the pons between healthy control and premutation groups. More specifically, we observed a significant association of ceramides and mannonate metabolites with a decreased area of the pons, both at visit 1 (V1) and visit 2 (V2) only in the CON as compared to the NCON group suggesting their potential role in the development of the disorder. In addition, we found a significant correlation of these metabolic signatures with the FXTAS stage at V2 indicating their contribution to the progression and pathogenesis of FXTAS. Interestingly, these metabolites as part of lipid and sphingolipid lipids pathways provide evidence of the role their dysregulation plays in the development of FXTAS and inform us as potential targets for personalized therapeutic development.

Keywords: Fragile X-associated tremor/ataxia syndrome; area of the pons; metabolic biomarkers; brain measures, lipids, premutation carriers.

1.   Introduction

Aging is a complex and evolutionarily conserved process that is found to be one of the main risk factors for a number of human neurodegenerative disorders (1). Aging and many aging-associated disorders share a range of molecular or cellular pathologies which can involve a dysregulated energy balance. Increasing evidence suggests that

metabolic alterations can strongly influence the development and the progression of various neurodegenerative disorders. Although the brain represents only 2% of the total body weight, it accounts for 20% of an individual's energy expenditure at rest (2). Thus, compromised energy metabolism and adverse changes are potentially contributing to increased vulnerability of the brain to develop neurodevelopmental and neurodegenerative processes (3).

Fragile X-associated Tremor/Ataxia Syndrome (FXTAS) is a late-onset neurodegenerative disorder, mostly affecting carriers of the fragile X mental retardation 1 (*FMR1*) gene mutation after the age of 50. Currently, there is no effective treatment for FXTAS, and the cognitive and/or motor symptoms progressively worsen over time, causing reduced quality of life, increased medical costs, and eventually, death. FXTAS is caused by the expanded CGG repeats (55–200 CGG) within the 5′UTR of the *FMR1* gene. In normal healthy individuals, the number of CGG repeats lies between 5-54 while individuals carrying alleles with a CGG repeat expansion greater than 200 develop fragile X syndrome (FXS), the most common form of intellectual disability and known monogenic cause of autism spectrum disorder (ASD) (4). The high prevalence of the premutation allele among the general population (1:110-200 females and 1:430 males) leads to an estimate of approximately 1.5 million individuals in the general US population being at risk for *FMR1* associated disorders, over their life spans. In addition, among the PM population, an estimated 40-75% of male and 8-16% of female PMs are at risk of developing FXTAS (5,6).

FXTAS core features include progressive intention tremor and cerebellar gait ataxia, autonomic dysfunction, and parkinsonism. Neuropathologically, it is characterized

by the presence of ubiquitin-positive intranuclear inclusions in neurons and astrocytes throughout the brain and in Purkinje cells (7). In addition to the clinical and neuropathological features, the radiological signs, including white matter hyperintensities (wmhs) in the middle cerebellar peduncles (the 'MCP sign') (8) also contribute to the diagnosis of FXTAS. Similarly, a significant prevalence of wmhs in the splenium of the corpus callosum (9,10), generalized brain atrophy, increased T2 signal in area of the pons and periventricular regions along with the subcortical gray matter damage with atrophy of the midbrain are part of the pathogenesis of FXTAS (5,11).

The brainstem is the central axis of the brain and both of its regions, the area of the pons and the midbrain play an important role in sensation and movement (12). The upper area of the pons and midbrain tegmentum are the main components of the ascending reticular activating system and associated with various other neurodegenerative disorders (13). Measurements of these areas have been shown previously to successfully differentiate subcortical movement disorders, such as Parkinson's disease (14), which presents with resting tremor that has also been observed in FXTAS. In addition, middle cerebellar peduncle (MCP) width showed a great sensitivity and specificity in differentiating multiple system atrophy from other disorders (15). We recently reported the MCP width as novel biomarker for FXTAS; decreased MCP width was observed in individuals who later developed symptoms of FXTAS as compared to premutation carriers who did not, and healthy controls. In addition, we also found reduced midbrain and area of the pons cross-sectional areas in patients with FXTAS compared to premutation carriers without FXTAS and controls (16). In a more recent study, we reported the association between these brain measures, including reduced MCP and

SCP width, midbrain, and area of the pons cross-sectional area with increased expression levels of the Iso10/10b, Iso4/4b *FMR1* mRNA isoforms of the *ASFMR1* 131bp mRNA isoform (17), suggesting their potential role in the pathogenesis of FXTAS.

Metabolic alterations and mitochondrial dysfunction have been extensively investigated in numerous age-related neurodegenerative disorders (18). However, the relationships between systemic abnormalities in metabolism and the pathogenesis of FXTAS are poorly understood. Previous metabolomic studies have investigated a panel of four core serum metabolites (phenethylamine (PEA), oleamide, aconitate, and isocitrate) for sensitive and specific diagnosis of the premutation carriers with and without FXTAS and found oleamide/isocitrate as a biomarker of FXTAS (19). Later, mitochondrial dysfunction, markers of neurodegeneration, and pro-inflammatory damage in premutation carriers were reported (20). Increased mitochondrial oxidative stress in primary fibroblasts derived from premutation carriers, compared with age and sex-matched controls has also been observed (21). Napoli and colleagues found the presence of the Warburg effect (which involves an increase in the rate of glucose uptake and preferential production of lactate, even in the presence of oxygen) in the peripheral blood mononuclear cells (PBMCs)'s derived from the controls, in premutation allele carriers with and without FXTAS (22). Later, Napoli et al. observed a significant impact of allopregnanolone treatment on oxidative stress, GABA metabolism, and mitochondria-related outcomes, and suggested allopregnanolone as a potential therapeutic for the cognitive and GABA metabolism improvement in FXTAS patients (23). In the premutation animal model's significant metabolic changes were found in the sphingolipid and purine metabolism in the cerebellum of premutation mice while the *Schlank (Cers5)*, *Sk2 (Sphk1)*

and *Ras (Impdh1)* genes were suggested as genetic modifiers of CGG toxicity in Drosophila (24). It is, however, unclear how global perturbations in metabolism may be related to severity of FXTAS pathology and the eventual expression of symptoms in individuals at risk for developing FXTAS. Our recent study identified metabolic biomarkers of FXTAS early diagnosis and disease progression by characterizing individuals who developed symptoms of FXTAS over time. Specifically, we found that lipid metabolism and specifically the sub pathways involved in mitochondrial bioenergetics, are significantly altered in FXTAS (25).

To date, no study evaluating the metabolic alterations in correlation with brain changes in premutation carriers who develop symptoms of FXTAS over time has been reported. In the current study, we evaluated male participants, carriers of the *FMR1* premutation allele, enrolled in an ongoing longitudinal study carried out at the UC Davis MIND Institute. The participants were followed for at least two longitudinal time points (Visit 1, V1 and Visit 2, V2) during which neuroimaging, neuropsychological, molecular measurements, as well as medical and neurological examinations were collected. A subset of the premutation participants, all symptom-free at the time of enrollment, developed symptoms that warranted a diagnosis of FXTAS by Visit 2. We define these individuals as converters (CON). The remaining premutation participants, who did not develop symptoms of FXTAS by Visit 2, we define as non-converters (NCON). In the current work, we investigated whether the expression levels of identified metabolic biomarkers were associated with changes in brain measures including the midbrain and pons cross-sectional area and MCP width, in the CON group compared to the NCON and HC groups. In addition, we also investigated the association of metabolite expression with

the progression of FXTAS. Understanding the metabolic variations along with brain changes in premutation carriers who developed FXTAS symptoms over time is likely to provide insights into novel disease-modifying treatments for this progressive neurodegenerative disorder.

2.   Materials and Methods

2.1   Study Participants

As part of a continuing longitudinal study at UC Davis MIND institute, male premutation carriers, > 45 years of age, and non-carrier age-matched controls were recruited from throughout the USA and Canada [as detailed in (16)]. All male participants were white in race; there were three Hispanic participants in the HC group, one in the CON group, and zero in NCON group. The studies and all protocols were carried out in accordance with the Institutional Review Board at the University of California, Davis. All participants gave written informed consent before participating in the study in line with the Declaration of Helsinki. FXTAS stage scoring was based on the clinical descriptions as previously described (26). Three categories were used in the diagnosis of FXTAS as explained in (27) and termed as "definite", "probable" and "possible". Three age-matched groups were included in this study: CON, NCON, and HC. Using the data from two brain scans, from neurological assessment, FXTAS stage, and CGG repeat length, 10 participants were classified as "CON" as they developed clear FXTAS symptomology between visits (FXTAS stage score was 0–1 at V1 and ≥2 at V2); 10 were defined as "NCON" because they continued to show no signs of FXTAS at V2 (FXTAS stage score was 0–1 at both V1 and V2) and 10 as HC (normal *FMR1* alleles/non-carriers).

2.2   CGG Repeat Length

Genomic DNA (gDNA) was isolated from 5 mL of peripheral blood leukocytes using the Gentra Puregene Blood Kit (Qiagen). CGG repeat allele size and methylation status were assessed by using the combination of Southern Blot and PCR analysis as previously reported (28,29).

2.3   Brain Measures

The following methods including MRI acquisition and MRPI analysis were originally described in our previous report (16). High resolution structural magnetic resonance imaging (MRIs) acquisition was obtained on a 3T Siemens Trio scanner using a 32-channel head coil and a T1-weighted 3D MPRAGE sequence with the following parameters: TR=2170ms, TE=4.86ms, flip angle=7º, FoV=256mm2, 192 slices, 1mm slice thickness. The scans were first aligned along the anterior-posterior commissure line using acpc detect (http://www.nitrc.org/projects/art) (30) or manually using DTI Studio (www.mristudio.org) (31). Then MRI bias field correction was performed using N4 (http://stnava.github.io/ANTs/) (32). A series of independent raters (two per measure) who were blinded to the participant age, group, and time point, quantitatively assessed all MR images for four measurements of brain morphology: MCP width as well pons and midbrain cross-sectional areas were based on methods previously described (33,34).

2.4   Sample preparation and metabolite profiling

Plasma metabolite profiling was determined by a non-targeted platform that allows the relative quantitative analysis of a large number of molecules (35). Samples were stored at -80 °C until processing and then prepared using the automated MicroLab STAR® (Hamilton Company, Reno, NV, USA). Several recovery standards were added prior to the first step in the extraction process for QC purposes. To remove protein, dissociate small molecules bound to protein or trapped in the precipitated protein matrix, and to recover chemically diverse metabolites, proteins were precipitated with methanol under vigorous shaking for 2 min (Glen Mills GenoGrinder 2000) followed by centrifugation. The resulting extract was divided into five fractions: two for analysis by two separate reverse phases (RP)/UPLC-MS/MS methods with positive ion mode electrospray ionization (ESI), one for analysis by RP/UPLC-MS/MS with negative ion mode ESI, one for analysis by HILIC/UPLC-MS/MS with negative ion mode ESI, and one sample were reserved for backup. Samples were placed briefly on a TurboVap® (Zymark) to remove the organic solvent. The sample extracts were stored overnight under nitrogen before preparation for further analysis as explained in (25).

2.5   Statistical Analysis

The association between brain measures and metabolites at a single visit was analyzed using linear regression models that included a brain measure as the area of the pons and a metabolite as the single covariate. The association between changes in brain measures and in metabolites between visits was analyzed using linear regression models that included change in a brain measure as the area of the pons and change in metabolite, baseline metabolite level, and baseline brain measure as covariates. Models fitted to visit

1 data included all subjects (control, NCON, and CON), and models fitted to visit 2 data included all premutation subjects (NCON and CON). Specifically, all the Visit 1 regression analyses included all subjects (n=30), and all the Visit 2 regression analyses included all premutation subjects (n=20). P-values were adjusted for multiple testing (within each analysis, across metabolites) using the Benjamini-Hochberg false discovery rate controlling method (36). Analyses were conducted using R version 4.0.2 (2020-06-22) (37).

3.   Results

3.1   Demographics

Three groups of male participants were included in this study: 1) premutation carriers who converted at V2 (CON; n=10), 2) premutation carriers who did not convert at V2 (NCON; n=10) and 3) healthy controls (HC; n=10). All participants in the CON and NCOV groups were matched for age and CGG repeat length as reported in [Table 1]. Participant race, age, and ethnicity did not differ significantly between the three groups. As expected, CGG repeat size was significantly lower in healthy controls than in the CON and NCON groups ($P < 0.001$ in both comparisons), but it was not significantly different between the two premutation carrier groups of CON and NCON ($P = 0.76$).

3.2   Differential metabolite levels linked with area of the pons area in healthy control and premutation groups.

We have recently reported 94 potential metabolic biomarkers for early diagnosis and progression of FXTAS that showed significant changes in expression ($P \leq 0.05$) in

the CON as compared to the NCON both at V1 and V2 or only at V2 (25). In this study, we investigated the correlation between these potential metabolic biomarkers and brain measures (midbrain, area of the pons, and MCP width) among healthy control (HC), and premutation carriers including converter and non-converter (CON and NCON) at V1. We found a significant association (P ≤ 0.05) of expression level of six metabolites with area of the pons among all three groups (HC, CON, and NCON) at V1 [Figure 1]. While no significant correlation of the midbrain and MCP width with the identified metabolites at baseline has been observed.

3.3 Expression levels of metabolic biomarkers associated with brain measures.

Within the two premutation groups, the levels of 11 metabolites showed a significant correlation (P ≤ 0.05) with decreased area of the pons at V1 while four showed a significant correlation at V2 only in the CON group but not in the NCON group. Interestingly, level of ceramide (d16:1/24:1, d18:1/22:1) correlated with area of the pons area both at V1 [Regression Slope -72.3 (-118.7, -25.9); P-value 0.0496; Figure 2a] and V2 [Regression Slope -56.7 (-88.3, -25.2); P-value 0.0597; Figure 2b]. Similarly, we also observed a significant correlation between mannonate and area of the area of the pons both at V1 [Regression Slope -97.3 (-162.3, -32.3); P-value 0.0496; Figure 2c] and V2 [Regression Slope -135 (-203.8, -67.2); P-value 0.0543; Figure 2d]. No significant correlations were observed between the midbrain area and MCP width and any metabolites both at V1 and V2 between CON and NCON premutation groups.

3.4 Metabolite expression levels correlate with FXTAS progression.

We evaluated the differential expression of the metabolic biomarkers with the progression of FXTAS and with the FXTAS stage in the CON and NCON participants at V2. We observed that 27 metabolites significantly correlated with change in FXTAS stage from V1 to V2 with the majority of these metabolites being lipids followed by xenobiotics, amino acids, and energy [Table 2]. Further we observed a significant correlation between the expression levels of several of these metabolites with the FXTAS stage [Figure 3A]. Interestingly, six of these metabolites including palmitate (16:0) [Figure 3A], palmitoylcarnitine (C16), palmitoleate (16:1n7), fumarate, lactosyl-N-behenoyl-sphingosine (d18:1/22:0), and ceramide (d16:1/24:1, d18:1/22:1) have been reported to be critically involved in the development of other neurodegenerative disorders. In addition, these metabolites are part of the lipid and fatty acid metabolism [Figure 3B] and sphingolipid metabolism [Figure 3C]. We previously shown that lipid metabolism was associated with the development and progression of FXTAS (changes of the FXTAS stage from V1 to V2) (25) and this association has also been reported in the premutation mouse model (24).

4.   Discussion

The present study results provide evidence that brain measures, specifically the area of the pons cross-sectional area, correlate with plasma levels of metabolites that are part of fatty acid and sphingolipid metabolism. These findings expand upon our previous study of plasma metabolic profiling of participants who developed symptoms of FXTAS over time (25), potentially representing biomarkers of early diagnosis and progression of

FXTAS and suggest that these factors play a role in the brain structure of individuals with FXTAS.

Magnetic resonance imaging (MRI) takes advantage of a strong magnetic field for non-invasively imaging of parts of the brain parts to identify regional tissue abnormalities and to obtain volumes of brain structures. The imaging profile provides an opportunity to not only visualize the neuroanatomical and functional signatures of various neurodegenerative disorders, but it can also identify disease-specific biomarkers of the underlying processes. Various imaging biomarkers have been reported in Parkinson's disease (PD) (38), Amyotrophic Lateral Sclerosis (ALS) (39), Alzheimer Disease (AD) (40), and Dementia (41) and recently by our team in FXTAS (16).

The brainstem (which includes midbrain, area of the pons, and the medulla oblongata) is a critical regulator of vital bodily functions (42) with midbrain and area of the pons primarily supporting cognition and mood while medulla oblongata regulates cardiovascular and respiratory functions (43). Interestingly, lesions and atrophy of these brainstem structures represent the hallmarks of various neurological disorders and recent findings have pointed to a much deeper involvement of the brainstem nuclei which could change our understanding of the cause, prevalence and early diagnosis of these devastating diseases. Altered volume of midbrain, area of the pons, and medulla oblongata have been reported in individuals with schizophrenia (SCZ), bipolar disorder (BD), multiple sclerosis (MS), dementia, mild cognitive impairment (MCI), and Parkinson's disease (PD) in comparison to healthy controls (HC) (44,45). Interestingly, reduction in area of the pons over time can significantly discriminate MSA from Progressive Supranuclear Palsy (PSP) (46). Moreover, the Fractional Anisotropy (FA) and Apparent

Diffusion Coefficient (ADC) values in the area of the pons can differentiate the middle cerebellar peduncles parkinsonian subtype (MSA-P) patients from PD with 100% specificity (47). Interestingly, the voxel-based morphometry (VBM) analysis has also identified neurodegenerative changes primarily in the midbrain and area of the pons of PSP patients as compared to controls (48). Finally, degeneration of the locus coeruleus (LC), a long and narrow nucleus in the area of the pons, correlates with cognitive dysfunction and potentiate pathology of AD (49).

In our earlier studies, we observed the variation in the MCP width, area of the pons and midbrain cross-sectional areas as well as their significant association with the molecular measures in individuals who developed symptoms of FXTAS over time as compared to non-symptomatic premutation carriers and healthy controls, suggesting their role in FXTAS pathogenesis and progression (16,17). These findings point toward the critical involvement of the area of the pons in neurodegenerative disorders, which could potentially provide information about the neuropathology of the disease and lead to early clinical diagnosis of these diseases.

Metabolomics is the omics platform that measures levels of metabolites in biological samples (50) uncovering potential biomarkers of aging and neurodegenerative diseases such as AD (51), Parkinson (52), Huntington (53), MS (54), and Amyotrophic Lateral Sclerosis (55) and FXTAS (25). A larger number of untargeted metabolomics-based studies have been reported using plasma/serum samples, due to its minimally invasive nature and relatively easy availability of blood samples. Unique metabolic signatures associated with altered energy homeostasis, Krebs cycle, changes in lipid membrane associated with abnormal CSF Aβ42 levels, altered mitochondrial function,

neurotransmitter and lipid biosynthesis are altered in plasma of patients with mild cognitive impairment and more pronounced in patients with AD (56–61). Majorly disturbed metabolic pathways observed in PD are also related to the metabolism of lipids, energy (TCA cycle, glycolysis, acylcarnitines), and fatty acids and tryptophan; with the latter presenting a high correlation with the progression of PD (62–68). The energy and phospholipid metabolism have also been found to be impaired in patients with HD that ultimately affects the function of neurons (53,69). Glucose metabolism is dysregulated in AD patients (70) and in area of the pons and cerebellum of MSA patients (71,72), while an association of fatty acid metabolism with the development of ALS was observed (73). Finally, in our recent study we reported on the identification of metabolic biomarkers of early diagnosis and progression of FXTAS and on their association with altered lipid metabolism including free fatty acids, acylcarnitine, sphingolipids, diacylglycerol, and phospholipids, in individuals who developed the symptoms of FXTAS over time (25).

In this study we observed an association of metabolic biomarkers, including ceramides and mannonate, in CON as compared to NCON [Figure 2] with brain measures, specifically with area of the pons area, suggesting the potential role of altered metabolomics in the pathogenesis of FXTAS. We also found their significant association with the FXTAS stage [Table 2] ultimately providing the insight into the FXTAS disease progression with the dysregulation of the metabolic pathways.

The Krebs cycle or the TCA cycle is an important pathway in the production of ATP through the oxidative phosphorylation of acetyl-CoA in the mitochondria. With the onset of the neurodegenerative processes in PD, the metabolism of TCA cycle has found to be dysregulated indicating an energy shortage and mitochondrial dysfunction in PD (74).

Similarly, the previous studies in FXTAS (19,20,22) reported on altered plasma and PBMCs levels (either increased or decreased) of several intermediates of the Krebs cycle in individuals with FXTAS as compared to controls. In accordance with these previous studies, we found a significance correlation of various Krebs cycle intermediates, including palmitate (16:0), palmitoleate (16:1n7), palmitoylcarnitine (C16) and fumarate [Figure 3b, bold] with the FXTAS stage [Figure 3a] supporting the observed mitochondrial dysfunction as a contributing factor in the pathogenesis of the FXTAS.

Sphingolipids include ceramides, sphingosine-1-phosphate, lactosyl-N-behenoyl-sphingosine and sphingomyelins which play an important role in neuronal functions as sphingolipids are critical to prevent the cell death, loss of synaptic plasticity, and neurodegeneration (75). High levels of ceramide have been detected in the CNS and in plasma of AD patients and of PD patients, indicating that ceramide metabolism could be associated with various stages of PD and AD progression and hippocampal atrophy (76–78) and suggested as a pharmacological target for the AD treatment (79). In a recent study, the sphingolipid metabolism and specifically the levels of sphingosine, sphingosine 1-phosphate, and sphingomyelin were found to be altered in the cerebellum of FXTAS mice (24). We have reported on increased ceramides levels in the CON as compared to NCON group (25) and, interestingly, in this study we observed a significant association with area of the pons both at V1 and V2 [Figure 2a, 2b]. Further, the sphingolipid metabolism intermediates lactosyl-N-behenoyl-sphingosine (d18:1/22:0) and ceramide (d16:1/24:1, d18:1/22:1) [Figure 3c, bold] both were significantly associated with FXTAS stage suggesting their role in the development of FXTAS and the pathway as the potential target for personalized therapeutic development.

5. Conclusion

In this study, we found a significant correlation of the metabolic biomarkers with the area of the pons in individuals who developed FXTAS over the time. We also report their significant association with the progression of the disorder and their role in context of dysregulated lipid and sphingolipid metabolism. These findings could be of a great value as the area of the pons provides distinct information about neuroanatomical and pathophysiological processes and its association with the FXTAS biomarkers can assist in identifying the premutation carriers at risk as well as assist in evaluating disease progression and therapeutic responses to targeted drug development. Further research is needed to replicate these findings in a larger well-characterized cohort to further explore the role of other brainstem structures in FXTAS and human health and disease.

6. Reference

2. Niccoli T, Partridge L. Ageing as a risk factor for disease. *Curr Biol* (2012) **22**:R741–52.

3. Schönfeld P, Reiser G. Why does brain metabolism not favor burning of fatty acids to provide energy? Reflections on disadvantages of the use of free fatty acids as fuel for brain. *J Cereb Blood Flow Metab* (2013) **33**:1493–1499.

4. Camandola S, Mattson MP. Brain metabolism in health, aging, and neurodegeneration. *EMBO J* (2017) **36**:1474–1492.

5. Hagerman RJ, Berry-Kravis E, Hazlett HC, Bailey DB Jr, Moine H, Kooy RF, Tassone F, Gantois I, Sonenberg N, Mandel JL, et al. Fragile X syndrome. *Nat Rev Dis Primers* (2017) **3**:17065.

6. Jacquemont S, Hagerman RJ, Leehey MA, Hall DA, Levine RA, Brunberg JA, Zhang L, Jardini T, Gane LW, Harris SW, et al. Penetrance of the fragile X-associated tremor/ataxia syndrome in a premutation carrier population. *JAMA* (2004) **291**:460–469.

7. Tassone F, long KP, Tong T-H, Lo J, Gane LW, Berry-Kravis E, Nguyen D, Mu LY, Laffin J, Bailey DB, et al. *FMR1* CGG allele size and prevalence ascertained through newborn screening in the United States. *Genome Med* (2012) **4**:100.

8. Hagerman RJ, Hagerman P. Fragile X-associated tremor/ataxia syndrome - features, mechanisms and management. *Nat Rev Neurol* (2016) **12**:403–412.

9. Rivera SM, Stebbins GT, Grigsby J. "Radiological Findings in FXTAS," in *The Fragile X-Associated Tremor Ataxia Syndrome (FXTAS)* (Springer, New York, NY), 55–66.

10. Apartis E, Blancher A, Meissner WG, Guyant-Maréchal L, Maltête D, De Broucker T, Legrand A-P, Bouzenada H, Thanh HT, Sallansonnet-Froment M, et al. FXTAS: new insights and the need for revised diagnostic criteria. *Neurology* (2012) **79**:1898–1907.

11. Kalus S, King J, Lui E, Gaillard F. Fragile X-associated tremor/ataxia syndrome: An under-recognised cause of tremor and ataxia. *J Clin Neurosci* (2016) **23**:162–164.

12. Scaglione C, Ginestroni A, Vella A, Dotti MT, Nave RD, Rizzo G, De Cristofaro MT, De Stefano N, Piacentini S, Martinelli P, et al. MRI and SPECT of midbrain and striatal degeneration in fragile X-associated tremor/ataxia syndrome. *J Neurol* (2008) **255**:144–146.

13. Grinberg LT, Rueb U, Heinsen H. Brainstem: neglected locus in neurodegenerative diseases. *Front Neurol* (2011) **2**:42.

14. Yang A, h. Xiao X, l. Wang Z. Evaluation of Normal Changes in Pons Metabolites due to Aging Using Turbo Spectroscopic Imaging. *AJNR Am J Neuroradiol* (2014) **35**:2099–2105.

15. Emamzadeh FN, Surguchov A. Parkinson's Disease: Biomarkers, Treatment, and Risk Factors. *Front Neurosci* (2018) **12**: doi:10.3389/fnins.2018.00612

16. Chelban V, Bocchetta M, Hassanein S, Haridy NA, Houlden H, Rohrer JD. An update on advances in magnetic resonance imaging of multiple system atrophy. *J Neurol* (2019) **266**:1036–1045.

17. Shelton AL, Wang JY, Fourie E, Tassone F, Chen A, Frizzi L, Hagerman RJ, Ferrer E, Hessl D, Rivera SM. Middle Cerebellar Peduncle Width-A Novel MRI Biomarker for FXTAS? *Front Neurosci* (2018) **12**:379.

18. Zafarullah M, Tang H-T, Durbin-Johnson B, Fourie E, Hessl D, Rivera SM, Tassone F. *FMR1* locus isoforms: potential biomarker candidates in fragile X-associated tremor/ataxia syndrome (FXTAS). *Sci Rep* (2020) **10**:11099.

19. Cenini G, Lloret A, Cascella R. Oxidative Stress in Neurodegenerative Diseases: From a Mitochondrial Point of View. *Oxid Med Cell Longev* (2019) **2019**:2105607.

20. Giulivi C, Napoli E, Tassone F, Halmai J, Hagerman R. Plasma Biomarkers for Monitoring Brain Pathophysiology in *FMR1* Premutation Carriers. *Front Mol Neurosci* (2016) **9**:71.

21. Giulivi C, Napoli E, Tassone F, Halmai J, Hagerman R. Plasma metabolic profile delineates roles for neurodegeneration, pro-inflammatory damage and mitochondrial dysfunction in the *FMR1* premutation. *Biochem J* (2016) **473**:3871–3888.

22. Song G, Napoli E, Wong S, Hagerman R, Liu S, Tassone F, Giulivi C. Altered redox mitochondrial biology in the neurodegenerative disorder fragile X-tremor/ataxia syndrome: use of antioxidants in precision medicine. *Mol Med* (2016) **22**:548–559.

23. Napoli E, Song G, Schneider A, Hagerman R, Eldeeb MAAA, Azarang A, Tassone F, Giulivi C. Warburg effect linked to cognitive-executive deficits in *FMR1* premutation. *FASEB J* (2016) **30**:3334–3351.

24. Napoli E, Schneider A, Wang JY, Trivedi A, Carrillo NR, Tassone F, Rogawski M, Hagerman RJ, Giulivi C. Allopregnanolone Treatment Improves Plasma Metabolomic Profile Associated with GABA Metabolism in Fragile X-Associated Tremor/Ataxia Syndrome: a Pilot Study. *Mol Neurobiol* (2019) **56**:3702–3713.

25. Kong HE, Lim J, Zhang F, Huang L, Gu Y, Nelson DL, Allen EG, Jin P. Metabolic pathways modulate the neuronal toxicity associated with fragile X-associated tremor/ataxia syndrome. *Hum Mol Genet* (2019) **28**:980–991.

26. Zafarullah M, Palczewski G, Rivera SM, Hessl DR, Tassone F. Metabolic profiling reveals dysregulated lipid metabolism and potential biomarkers associated with the development and progression of Fragile X-Associated Tremor/Ataxia Syndrome (FXTAS). *FASEB J* (2020) **34**:16676–16692.

27. Bacalman S, Farzin F, Bourgeois JA, Cogswell J, Goodlin-Jones BL, Gane LW, Grigsby J, Leehey MA, Tassone F, Hagerman RJ. Psychiatric phenotype of the fragile X-associated tremor/ataxia syndrome (FXTAS) in males: newly described fronto-subcortical dementia. *J Clin Psychiatry* (2006) **67**:87–94.

28. Zafarullah M, Tassone F. Fragile X-Associated Tremor/Ataxia Syndrome (FXTAS). *Methods Mol Biol* (2019) **1942**: doi:10.1007/978-1-4939-9080-1_15

29. Tassone F, Pan R, Amiri K, Taylor AK, Hagerman PJ. A rapid polymerase chain reaction-based screening method for identification of all expanded alleles of the fragile X (*FMR1*) gene in newborn and high-risk populations. *J Mol Diagn* (2008) **10**:43–49.

30. Filipovic-Sadic S, Sah S, Chen L, Krosting J, Sekinger E, Zhang W, Hagerman PJ, Stenzel TT, Hadd AG, Latham GJ, et al. A novel *FMR1* PCR method for the routine detection of low abundance expanded alleles and full mutations in fragile X syndrome. *Clin Chem* (2010) **56**:399–408.

31. Ardekani BA, Bachman AH. Model-based automatic detection of the anterior and posterior commissures on MRI scans. *Neuroimage* (2009) **46**: doi:10.1016/j.neuroimage.2009.02.030

32. Mori S, Crain BJ, Chacko VP, van Zijl PC. Three-dimensional tracking of axonal projections in the brain by magnetic resonance imaging. *Ann Neurol* (1999) **45**: doi:3.0.co;2-3">10.1002/1531-8249(199902)45:2<265::aid-ana21>3.0.co;2-3

33. Tustison NJ, Avants BB, Cook PA, Zheng Y, Egan A, Yushkevich PA, Gee JC. N4ITK: improved N3 bias correction. *IEEE Trans Med Imaging* (2010) **29**: doi:10.1109/TMI.2010.2046908

34. Quattrone A, Nicoletti G, Messina D, Fera F, Condino F, Pugliese P, Lanza P, Barone P, Morgante L, Zappia M, et al. MR imaging index for differentiation of progressive supranuclear palsy from Parkinson disease and the Parkinson variant of multiple system atrophy. *Radiology* (2008) **246**: doi:10.1148/radiol.2453061703

35. Nicoletti G, Fera F, Condino F, Auteri W, Gallo O, Pugliese P, Arabia G, Morgante L, Barone P, Zappia M, et al. MR imaging of middle cerebellar peduncle width: differentiation of multiple system atrophy from Parkinson disease. *Radiology* (2006) **239**: doi:10.1148/radiol.2393050459

36. Evans AM, DeHaven CD, Barrett T, Mitchell M, Milgram E. Integrated, nontargeted ultrahigh performance liquid chromatography/electrospray ionization tandem mass spectrometry platform for the identification and relative quantification of the small-molecule complement of biological systems. *Anal Chem* (2009) **81**:6656–6667.

37. Benjamini Y, Hochberg, Y. Controlling the false discovery rate: a practical and powerful approach to multiple testing. Journal of the Royal Statistical Society Series (1995) **57**:289-300

38. The R Project for Statistical Computing. Available at: https://www.r-project.org/ [Accessed April 6, 2021]

39. Saeed U, Compagnone J, Aviv RI, Strafella AP, Black SE, Lang AE, Masellis M. Imaging biomarkers in Parkinson's disease and Parkinsonian syndromes: current and emerging concepts. *Transl Neurodegener* (2017) **6**:8.

40. Mazón M, Vázquez Costa JF, Ten-Esteve A, Martí-Bonmatí L. Imaging Biomarkers for the Diagnosis and Prognosis of Neurodegenerative Diseases. The Example of Amyotrophic Lateral Sclerosis. *Front Neurosci* (2018) **12**:784.

41. Braun DJ, Van Eldik LJ. In vivo Brainstem Imaging in Alzheimer's Disease: Potential for Biomarker Development. *Front Aging Neurosci* (2018) **10**: doi:10.3389/fnagi.2018.00266

42. Kehoe EG, McNulty JP, Mullins PG, Bokde AL. Advances in MRI biomarkers for the diagnosis of Alzheimer's disease. *Biomark Med* (2014) **8**: doi:10.2217/bmm.14.42

43. Del Negro CA, Funk GD, Feldman JL. Breathing matters. *Nat Rev Neurosci* (2018) **19**: doi:10.1038/s41583-018-0003-6

44. Sara SJ. The locus coeruleus and noradrenergic modulation of cognition. *Nat Rev Neurosci* (2009) **10**:211–223.

45. Przedborski S. The two-century journey of Parkinson disease research. *Nat Rev Neurosci* (2017) **18**:251–259.

46. Elvsåshagen T, Bahrami S, van der Meer D, Agartz I, Alnæs D, Barch DM, Baur-Streubel R, Bertolino A, Beyer MK, Blasi G, et al. The genetic architecture of human brainstem structures and their involvement in common brain disorders. *Nat Commun* (2020) **11**:4016.

47. Reginold W, Lang AE, Marras C, Heyn C, Alharbi M, Mikulis DJ. Longitudinal quantitative MRI in multiple system atrophy and progressive supranuclear palsy. *Parkinsonism Relat Disord* (2014) **20**:222–225.

48. Ito M, Watanabe H, Kawai Y, Atsuta N, Tanaka F, Naganawa S, Fukatsu H, Sobue G. Usefulness of combined fractional anisotropy and apparent diffusion coefficient values for detection of involvement in multiple system atrophy. *J Neurol Neurosurg Psychiatry* (2007) **78**:722–728.

49. Boxer AL, Geschwind MD, Belfor N, Gorno-Tempini ML, Schauer GF, Miller BL, Weiner MW, Rosen HJ. Patterns of brain atrophy that differentiate corticobasal degeneration syndrome from progressive supranuclear palsy. *Arch Neurol* (2006) **63**:81–86.

50. Theofilas P, Ehrenberg AJ, Dunlop S, Di Lorenzo Alho AT, Nguy A, Leite REP, Rodriguez RD, Mejia MB, Suemoto CK, Ferretti-Rebustini REDL, et al. Locus coeruleus volume and cell population changes during Alzheimer's disease progression: A stereological study in human postmortem brains with potential implication for early-stage biomarker discovery. *Alzheimers Dement* (2017) **13**:236–246.

51. Bourgognon J-M, Steinert JR. The metabolome identity: basis for discovery of biomarkers in neurodegeneration. *Neural Regeneration Res* (2019) **14**:387–390.

52. Wilkins JM, Trushina E. Application of Metabolomics in Alzheimer's Disease. *Front Neurol* (2018) **8**: doi:10.3389/fneur.2017.00719

53. Shao Y, Le W. Recent advances and perspectives of metabolomics-based investigations in Parkinson's disease. *Mol Neurodegener* (2019) **14**:3.

54. Graham SF, Pan X, Yilmaz A, Macias S, Robinson A, Mann D, Green BD. Targeted biochemical profiling of brain from Huntington's disease patients reveals novel metabolic pathways of interest. *Biochim Biophys Acta Mol Basis Dis* (2018) **1864**: doi:10.1016/j.bbadis.2018.04.012

55. Stoessel D, Stellmann J-P, Willing A, Behrens B, Rosenkranz SC, Hodecker SC, Stürner KH, Reinhardt S, Fleischer S, Deuschle C, et al. Metabolomic Profiles for Primary Progressive Multiple Sclerosis Stratification and Disease Course Monitoring. *Front Hum Neurosci* (2018) **12**:226.

56. Kirk SE, Tracey TJ, Steyn FJ, Ngo ST. Biomarkers of Metabolism in Amyotrophic Lateral Sclerosis. *Front Neurol* (2019) **10**: doi:10.3389/fneur.2019.00191

57. Trushina E, Dutta T, Persson XM, Mielke MM, Petersen RC. Identification of altered metabolic pathways in plasma and CSF in mild cognitive impairment and Alzheimer's disease using metabolomics. *PLoS One* (2013) **8**: doi:10.1371/journal.pone.0063644

58. Kaddurah-Daouk R, Zhu H, Sharma S, Bogdanov M, Rozen SG, Matson W, Oki NO, Motsinger-Reif AA, Churchill E, Lei Z, et al. Alterations in metabolic pathways and networks in Alzheimer's disease. *Transl Psychiatry* (2013) **3**:e244.

59. Graham SF, Chevallier OP, Elliott CT, Hölscher C, Johnston J, McGuinness B, Kehoe PG, Passmore AP, Green BD. Untargeted metabolomic analysis of human plasma indicates differentially affected polyamine and L-arginine metabolism in mild cognitive impairment subjects converting to Alzheimer's disease. *PLoS One* (2015) **10**:e0119452.

60. Sonntag K-C, Ryu W-I, Amirault KM, Healy RA, Siegel AJ, McPhie DL, Forester B, Cohen BM. Late-onset Alzheimer's disease is associated with inherent changes in bioenergetics profiles. *Sci Rep* (2017) **7**:14038.

61. Mapstone M, Cheema AK, Fiandaca MS, Zhong X, Mhyre TR, MacArthur LH, Hall WJ, Fisher SG, Peterson DR, Haley JM, et al. Plasma phospholipids identify antecedent memory impairment in older adults. *Nat Med* (2014) **20**:415–418.

62. Toledo JB, Arnold M, Kastenmüller G, Chang R, Baillie RA, Han X, Thambisetty M, Tenenbaum JD, Suhre K, Thompson JW, et al. Metabolic network failures in Alzheimer's disease: A biochemical road map. *Alzheimers Dement* (2017) **13**:965–984.

63. Roede JR, Uppal K, Park Y, Lee K, Tran V, Walker D, Strobel FH, Rhodes SL, Ritz B, Jones DP. Serum metabolomics of slow vs. rapid motor progression Parkinson's disease: a pilot study. *PLoS One* (2013) **8**:e77629.

64. Trupp M, Jonsson P, Ohrfelt A, Zetterberg H, Obudulu O, Malm L, Wuolikainen A, Linder J, Moritz T, Blennow K, et al. Metabolite and peptide levels in plasma and CSF differentiating healthy controls from patients with newly diagnosed Parkinson's disease. *J Parkinsons Dis* (2014) **4**:549–560.

65. Lei S, Zavala-Flores L, Garcia-Garcia A, Nandakumar R, Huang Y, Madayiputhiya N, Stanton RC, Dodds ED, Powers R, Franco R. Alterations in energy/redox metabolism induced by mitochondrial and environmental toxins: a specific role for glucose-6-phosphate-dehydrogenase and the pentose phosphate pathway in paraquat toxicity. *ACS Chem Biol* (2014) **9**:2032–2048.

66. Schulte EC, Altmaier E, Berger HS, Do KT, Kastenmüller G, Wahl S, Adamski J, Peters A, Krumsiek J, Suhre K, et al. Alterations in Lipid and Inositol Metabolisms in Two Dopaminergic Disorders. *PLoS One* (2016) **11**:e0147129.

67. Saiki S, Hatano T, Fujimaki M, Ishikawa K-I, Mori A, Oji Y, Okuzumi A, Fukuhara T, Koinuma T, Imamichi Y, et al. Decreased long-chain acylcarnitines from insufficient β-oxidation as potential early diagnostic markers for Parkinson's disease. *Sci Rep* (2017) **7**:7328.

68. Havelund JF, Andersen AD, Binzer M, Blaabjerg M, Heegaard NHH, Stenager E, Faergeman NJ, Gramsbergen JB. Changes in kynurenine pathway metabolism in Parkinson patients with L-DOPA-induced dyskinesia. *J Neurochem* (2017) **142**:756–766.

69. Okuzumi A, Hatano T, Ueno S-I, Ogawa T, Saiki S, Mori A, Koinuma T, Oji Y, Ishikawa K-I, Fujimaki M, et al. Metabolomics-based identification of metabolic alterations in PARK2. *Ann Clin Transl Neurol* (2019) **6**:525–536.

70. Kumar KK, Goodwin CR, Uhouse MA, Bornhorst J, Schwerdtle T, Aschner M, McLean JA, Bowman AB. Untargeted metabolic profiling identifies interactions between Huntington's disease and neuronal manganese status. *Metallomics* (2015) **7**: doi:10.1039/c4mt00223g

71. An Y, Varma VR, Varma S, Casanova R, Dammer E, Pletnikova O, Chia CW, Egan JM, Ferrucci L, Troncoso J, et al. Evidence for brain glucose dysregulation in Alzheimer's disease. *Alzheimers Dement* (2018) **14**:318–329.

72. Juh R, Kim J, Moon D, Choe B, Suh T. Different metabolic patterns analysis of Parkinsonism on the 18F-FDG PET. *Eur J Radiol* (2004) **51**:223–233.

73. Eckert T, Barnes A, Dhawan V, Frucht S, Gordon MF, Feigin AS, Eidelberg D. FDG PET in the differential diagnosis of parkinsonian disorders. *Neuroimage* (2005) **26**: doi:10.1016/j.neuroimage.2005.03.012

74. Goutman SA, Boss J, Guo K, Alakwaa FM, Patterson A, Kim S, Savelieff MG, Hur J, Feldman EL. Untargeted metabolomics yields insight into ALS disease mechanisms. *J Neurol Neurosurg Psychiatry* (2020) **91**:1329–1338.

75. Graham SF, Rey NL, Yilmaz A, Kumar P, Madaj Z, Maddens M, Bahado-Singh RO, Becker K, Schulz E, Meyerdirk LK, et al. Biochemical Profiling of the Brain and Blood

Metabolome in a Mouse Model of Prodromal Parkinson's Disease Reveals Distinct Metabolic Profiles. *J Proteome Res* (2018) **17**: doi:10.1021/acs.jproteome.8b00224

76. Alessenko AV, Albi E. Exploring Sphingolipid Implications in Neurodegeneration. *Front Neurol* (2020) **11**:437.

77. Di Pardo A, Maglione V. Sphingolipid Metabolism: A New Therapeutic Opportunity for Brain Degenerative Disorders. *Front Neurosci* (2018) **12**:249.

78. Kim M, Nevado-Holgado A, Whiley L, Snowden SG, Soininen H, Kloszewska I, Mecocci P, Tsolaki M, Vellas B, Thambisetty M, et al. Association between Plasma Ceramides and Phosphatidylcholines and Hippocampal Brain Volume in Late Onset Alzheimer's Disease. *J Alzheimers Dis* (2017) **60**: doi:10.3233/JAD-160645

79. Mielke MM, Maetzler W, Haughey NJ, Bandaru VVR, Savica R, Deuschle C, Gasser T, Hauser A-K, Gräber-Sultan S, Schleicher E, et al. Plasma ceramide and glucosylceramide metabolism is altered in sporadic Parkinson's disease and associated with cognitive impairment: a pilot study. *PLoS One* (2013) **8**:e73094.

80. van Kruining D, Luo Q, van Echten-Deckert G, Mielke MM, Bowman A, Ellis S, Oliveira TG, Martinez-Martinez P. Sphingolipids as prognostic biomarkers of neurodegeneration, neuroinflammation, and psychiatric diseases and their emerging role in lipidomic investigation methods. *Adv Drug Deliv Rev* (2020) **159**:232–244.

7. Tables

Table 1: Demographic information on age and CGG repeats in three male participant groups: HC, CON and NCON.

		Healthy Controls (HC)	Converters (CON)	Non-Converters (NCON)	All Patients	P-Value (F-Test)
Age	**N**	10	10	10	30	0.936
	Mean (SD)	65.60 (3.239)	63.50 (6.786)	63.20 (4.849)	64.10 (5.101)	
	Median (Range)	64.50 (62-70)	63.50 (53-75)	64.00 (52-69)	64.00 (62-75)	
CGG	**N**	10	10	10	30	<0.001
	Mean (SD)	28.90 (4.095)	93.30 (22.91)	75.70 (18.73)	65.97 (32.26)	
	Median (Range)	30 (20-32)	84.50 (74-141)	74 (56-122)	72 (20-141)	

Table 2: Metabolite expression correlated with progression of FXTAS.

Sr #	Super Pathway	Metabolite	Regression Slope (95% CI)	Raw P-Value	Adjusted P-Value

1	Lipid	myristate (14:0)	0.805 (0.376, 1.233)	< 0.001	0.0541
2	Lipid	pentadecanoate (15:0)	1.4 (0.569, 2.241)	0.00239	0.0541
3	Lipid	1-oleoylglycerol (18:1)	1.02 (0.399, 1.639)	0.00284	0.0541
4	Lipid	margarate (17:0)	1.1 (0.429, 1.766)	0.00287	0.0541
5	Lipid	(14 or 15)-methylpalmitate (a17:0 or i17:0)	0.89 (0.347, 1.432)	0.00288	0.0541
6	Lipid	(2 or 3)-decenoate (10:1n7 or n8)	0.763 (0.273, 1.253)	0.00426	0.058
7	Lipid	palmitate (16:0)	0.86 (0.30, 1.42)	0.00469	0.058
8	Lipid	10-heptadecenoate (17:1n7)	0.515 (0.175, 0.855)	0.00516	0.058
9	Xenobiotics	mannonate*	1.87 (0.62, 3.12)	0.00566	0.058
10	Lipid	behenate (22:0)*	0.817 (0.258, 1.376)	0.0066	0.058
11	Amino Acid	trans-urocanate	-1.32 (-2.227, -0.404)	0.00716	0.058
12	Amino Acid	8-methoxykynurenate	1.36 (0.402, 2.313)	0.00796	0.058
13	Lipid	ceramide (d16:1/24:1, d18:1/22:1)*	0.795 (0.232, 1.359)	0.00828	0.058
14	Xenobiotics	7-methylurate	-0.633 (-1.085, -0.181)	0.00868	0.058
15	Xenobiotics	3-bromo-5-chloro-2,6-dihydroxybenzoic acid*	0.847 (0.228, 1.467)	0.01013	0.058
16	Lipid	10-undecenoate (11:1n1)	0.995 (0.265, 1.725)	0.01035	0.058
17	Lipid	ceramide (d18:1/17:0, d17:1/18:0)*	1.34 (0.35, 2.32)	0.01075	0.058
18	Lipid	myristoleate (14:1n5)	0.392 (0.100, 0.684)	0.01127	0.058
19	Lipid	palmitoylcarnitine (C16)	1.9 (0.469, 3.335)	0.01212	0.058
20	Lipid	lactosyl-N-behenoyl-sphingosine (d18:1/22:0)*	-2.56 (-4.487, -0.624)	0.01235	0.058
21	Lipid	5-dodecenoate (12:1n7)	0.618 (0.139, 1.097)	0.0143	0.0595
22	Lipid	palmitoleate (16:1n7)	0.323 (0.0722, 0.5745)	0.01451	0.0595
23	Lipid	N-behenoyl-sphingadienine (d18:2/22:0)*	1.69 (0.365, 3.010)	0.01525	0.0595
24	Lipid	arachidate (20:0)	3.32 (0.71, 5.93)	0.01554	0.0595

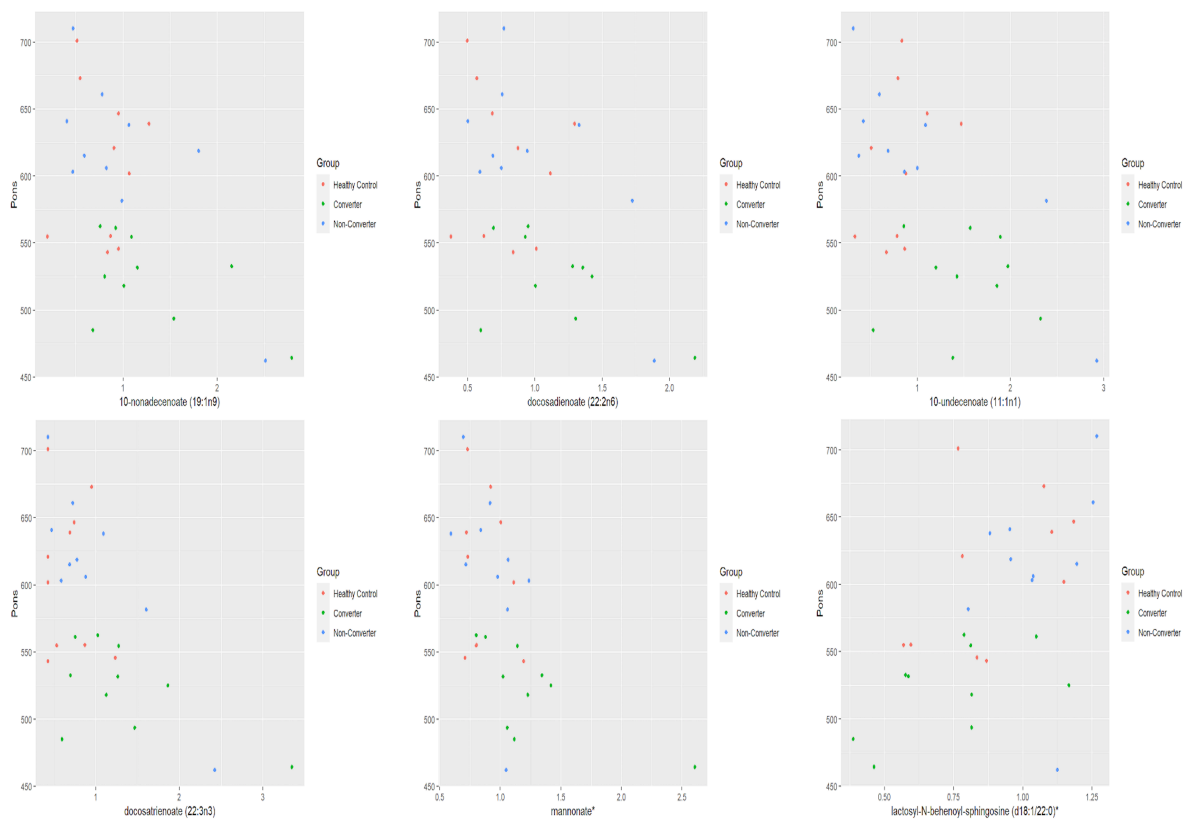| 25	Xenobiotics	3,7-dimethylurate	-0.652 (-1.167, -0.138)	0.01583	0.0595
26	Energy	fumarate	2.13 (0.435, 3.828)	0.01663	0.0598
27	Lipid	3-hydroxymyristate	0.701 (0.14, 1.26)	0.01719	0.0598

8. Figures

Figure 1: <u>Pons by metabolite expression among HC, CON and NCON.</u> Scatter plots showing correlation between pons and metabolite expression levels. The dots in red are representing the plotted values obtained for HC, green for CONV and blue for NCON. *The identity of these metabolites has not been officially confirmed based on the standard.
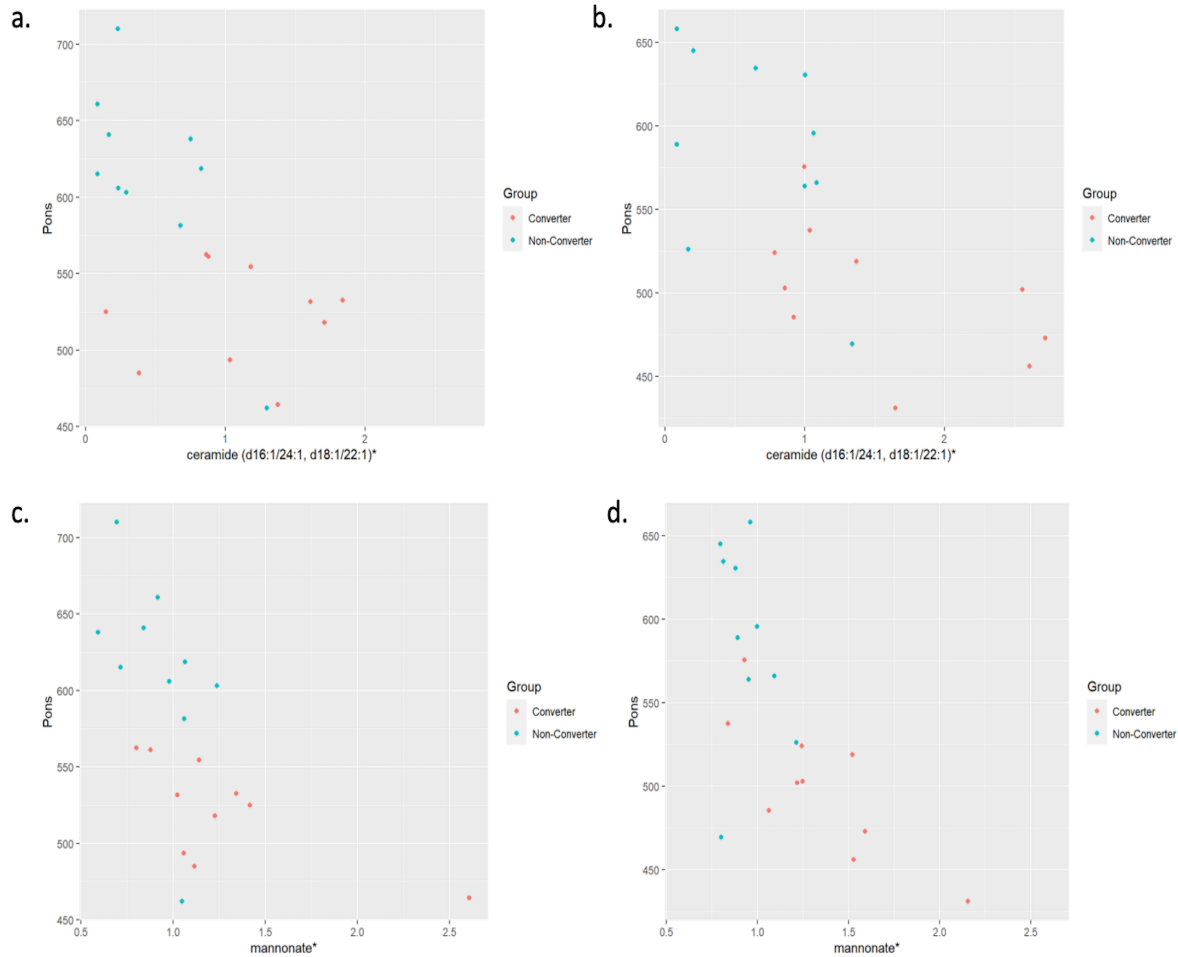
Figure 2: Distribution of metabolic biomarkers with pons between CON and NCON groups. **a.** Scatter plots showing correlation between pons and ceramide in CON and NCON at V1. The dots in red are representing the plotted values obtained for CON, and turquoise for NCON. **b.** Scatter plots showing correlation between pons and ceramide in CON and NCON at V2. **c.** Scatter plots showing correlation between pons and mannonate in CON and NCON at V1. **d.** Scatter plots showing correlation between pons and mannonate in CON and NCON at V2. *The identity of these metabolites has not been officially confirmed based on the standard.
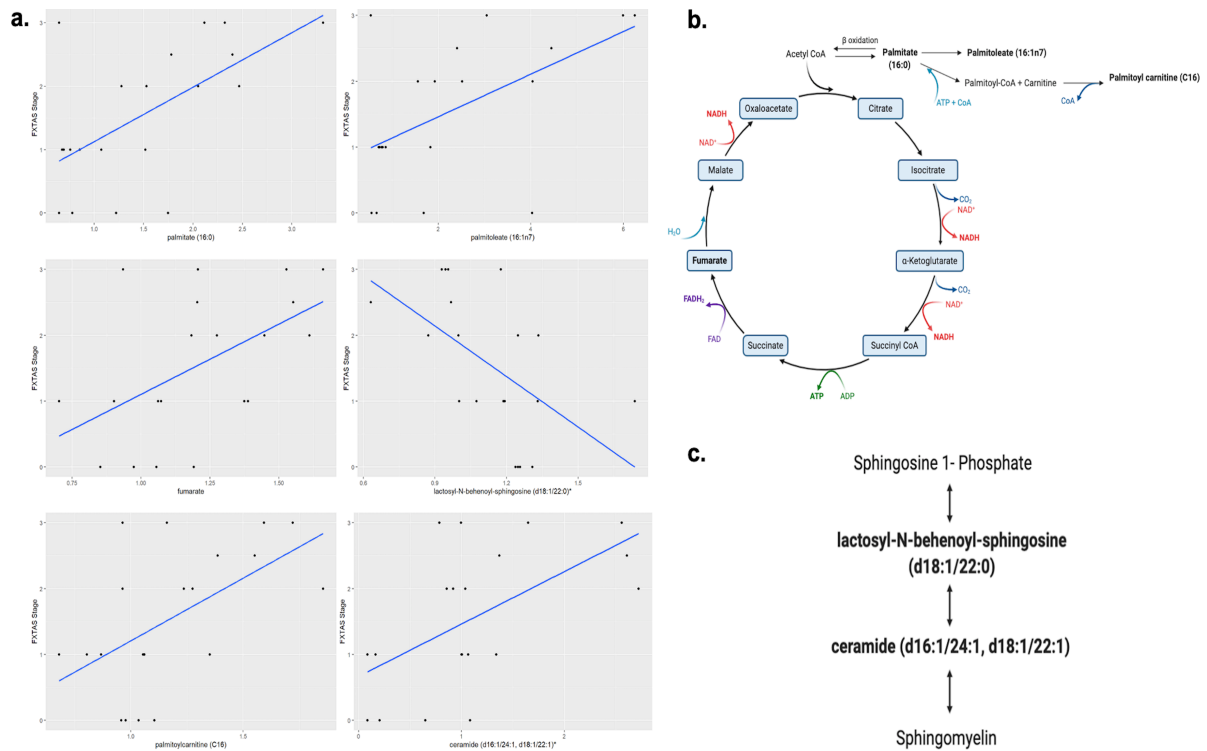
Figure 3: Fatty acid and sphingolipids metabolism associated with FXTAS development.

a. Six identified metabolites in FXTAS associated with other neurodegenerative disorder, here the comparison with the FXTAS stage is shown; data are presented as FXTAS stage (y axis) and associated metabolite (x axis) by using scatter plots. **b**. Disturbance of fatty acid and lipids metabolism pathway is shown. **c**. Sphingolipid metabolism pathway are shown. Bold metabolites, $p \leq 0.05$ linked with the development of FXTAS. *The identity of these metabolites has not been officially confirmed based on the standard.

Chapter 5

Urine-derived epithelial cell lines: a new tool to model Fragile X Syndrome (FXS)

Marwa Zafarullah [1], Mittal Jasoliya[1] and Flora Tassone [1, 2*]

[13] Affiliation 1; e-mail@e-mail.com Department of Biochemistry and Molecular Medicine, University of California Davis, School of Medicine, Sacramento, 95817 CA, USA; mzafarullah@ucdavis.edu; mjjasoliya@ucdavis.edu

[14] MIND Institute, University of California Davis Medical Center, Sacramento, 95817 CA, USA.

* **Correspondence:** ftassone@ucdavis.edu; Tel.: +1-(916)-703-0463

Abstract

Fragile X syndrome (FXS) is an X-linked neurodevelopmental condition associated with intellectual disability and behavioral problems due to the lack of the Fragile X mental retardation protein (FMRP), which plays a crucial role in synaptic plasticity and memory. A desirable *in vitro* cell model to study FXS would be one that can be generated by simple isolation and culture method from a collection of a non-invasive donor specimen. Currently, the various donor-specific cells can be isolated mainly from peripheral blood and skin biopsy. However, they are somewhat invasive methods for establishing cell lines from the primary subject material. In this study, we have characterized a cost-effective and straightforward method to derive epithelial cell lines from urine samples collected from participants with FXS and healthy controls (TD).

The urine-derived cells expressed epithelial cell surface markers via fluorescence-activated cell sorting (FACS). We observed inter, and the intra-tissue CGG mosaicism in

the PBMC's and the urine-derived cells from participants with FXS potentially related to the observed variations in the phenotypic and clinical presentation of FXS. We characterized these urine-derived epithelial cells for *FMR1* mRNA and FMRP expression and observed some expression in the lines derived from full mutation mosaic participants. Further, FMRP expression was localized in the cytoplasm of the urine-derived epithelial cells of healthy controls. Deficient FMRP expression was also observed in mosaic males, while as expected, no expression was observed in cells derived from participants with a hypermethylated full mutation.

Keywords: Fragile X syndrome, epithelial cells, *FMR1 mRNA,* FMRP, neurodevelopmental disorders, urine-derived cells.

1. Introduction

Neurodevelopmental disorders are conditions categorized by impairments of intelligence or social skills with an onset in the developmental period. Fragile X syndrome (FXS), the most common inherited cause of intellectual disability (ID) and the single leading monogenic currently known cause of Autism Spectrum Disorder (ASD) [1], is caused by an expansion of a CGG trinucleotide repeat, greater than 200, in the 5' untranslated region of the fragile X mental retardation1 (*FMR1*) gene. This leads to transcriptional silencing of the gene with consequent absence of the encoded product, the fragile X mental retardation protein (FMRP), which plays a crucial role in synaptic plasticity and memory. Males with FXS have mild to severe ID, and while 70% of the girls are less affected, they typically present with learning problems. Behavior problems

include anxiety, sensory hyperarousal, hyperactivity, social deficits, language deficit, and obesity.

Size and methylation mosaicism of the CGG repeats has been observed in many patients with FXS. Pretto and colleagues [2] suggested that in individuals with FXS, mosaicism (size or methylation) can result in low FMRP expression, which may be enough to impact their cognitive functions positively. Early studies reported that 38% of patients with FXS were mosaics, presenting with both premutation and full mutation alleles [3]. Further, a small screening study found 80% of mosaicism among the identified individuals with FXS, which suggests that mosaicism is quite common in FXS [4].

Due to the high prevalence of neurodevelopmental disorders, including FXS, desirable cells for investigation and cell therapy would be ones that can be generated by a simple isolation and culture method using a donor sample obtained in a non-invasive manner. To date, the collection of different donor-specific cells that can be isolated from peripheral blood, skin, and hair require invasive methods for sample isolation and incorporate complicated, costly reagents and time consuming for the culturing process. These cells also take a considerable time for their *in vitro* isolation and expansion. Previous studies have suggested that donor-derived urine cells offer a cost-effective and straightforward method of isolation of cell lines. Moreover, urine-derived primary cells are a source for generating induced pluripotent stem cells (iPSCs) and have been applied as modeling platform for various disorders including kidney disorders, muscular dystrophy, and paroxysmal kinesigenic dyskinesia [5–8]. Importantly, iPSCs derived from urine are shown to possess the differentiation potential into functional glutaminergic, dopaminergic, and motor neurons [8,9] whose impairment has been well documented in FXS.

This study reports for the first time, an optimized protocol for establishing FXS patient-primary cell models derived from urine samples. We determined the percentage of epithelial, hematopoietic, and erythroid cells in the established cell population using flow cytometry. Additionally, we show that FXS-derived epithelial cells had 0.1% residual FMRP compared to healthy-individual derived epithelial cells by two independent methods. Because the loss of FMRP is the primary cause of FXS, our data suggest that FXS patient's urine-derived epithelial cells are a viable option in understanding the disease's underlying molecular mechanisms potentially leading to therapeutic intervention.

Overall, FXS patient urine-derived epithelial cells can be a less invasive primary cell model for understanding the molecular mechanisms of FXS pathogenesis. It can also be used as personalized modeling of an individual's response to various drugs and identifying potentially effective therapy based on the individual's genetic makeup.

2. Materials and Methods

2.1 Study Participants

As part of ongoing metformin clinical trial at the UC Davis MIND Institute, urine samples were collected from 25 participants with FXS, including 24 males and one female, age (6-25 years) and seven healthy individuals (TD), including two males and five females, age (16-32 years). Participants of this study or their parents/legal guardians signed a written informed consent to provide urine samples for epithelial cell generation and further experimentation following a protocol following the Institutional Review Board at the University of California, Davis. (Metformin ICF 1.5 Version, Date: May 13, 2020). All

participants gave written informed consent before participating in the study in line with the Declaration of Helsinki of 1975 (https://www.wma.net/what-we-do/medical-ethics/declaration-of-helsinki/), revised in 2013.Nineteen epithelial cell lines derived from 12 male participants with FXS and from seven TD (two males and five females) were established [**Table 1**].

2.2 Collection of Urine

For the best results, participants were advised to drink a full glass of water about one hour before collecting, and urine samples were processed within 1-2 hours. Urine samples were collected into a sterile container after cleaning the urethral area with disinfectant wipes immediately before collection. To significantly reduce the opportunities for contaminants to enter the urine stream during the collection of the specimen, the first portion of the urine stream was discarded, and 30-50mL were then collected into a clean container. Urine samples were placed on ice or at 4°C immediately after collection to avoid a decreased yield due to prolonged processing time.

2.3 Primary Culture of Urine-Derived Epithelial Cells

Twelve well plates were coated with iMatrix (Reprocell, Beltsville, MD, United States) before processing the urine sample. For coating, 4.8 uL iMatrix-511 solution was added to 1 mL Dulbecco's phosphate-buffered saline (DPBS) (Thermo Fisher Scientific, Waltham, MA, United States) per well, followed by mixing and incubating at 37 °C for 3 hr. or at 4°C overnight. iMatrix solution was aspirated immediately before plating the cells, to avoid dryness of the coating solution. For processing, midstream urine was collected,

followed by transferring it into a sterile 50-ml centrifuge tube. Samples were centrifuged at 1000 rpm for 10min at room temperature. The supernatant was carefully aspirated, leaving only 1-2 ml into the tube above the cell pellet. Cell pellets were then washed once with 10 ml of washing buffer (500 ml DPBS supplemented with 50 mg ml^{-1} Primocin (Invitrogen, San Diego, CA, United States) and resuspended into 2 mL of primary media. Cells were plated into iMatrix coated well plates and incubated at 37°C for 24h. Primary media consisted of DMEM/F12 + GlutaMAX nutrient mix (1:1) (Thermo Fisher Scientific, Waltham, MA, United States), supplemented with 10% (vol/vol) human serum (Sigma-Aldrich, St Louis, MO, United States), 50 mg ml^{-1}of Primocin (Invitrogen, San Diego, CA, United States) and, the REGM SingleQuot kit supplements (Lonza, Basel, Switzerland) (do not use FBS to reduce background). The media was filter-sterilized using a 0.2 µm filter unit and then supplemented with 50 mL human serum. On day two, media was removed, and 1 ml of primary fresh medium was added to the plated cells. Cells were fed until small colonies of approximately 5-6 dense cells appeared, which took 2-3 weeks after plating and reaching 80–90% density after 24 days of plating.

2.4 Proliferation of Urine-Derived Epithelial Cells

Cells were harvested with TrypLE™ (Thermo Fisher Scientific, Waltham, MA, United States), counted using a hemocytometer, and viability was determined by trypan blue. They were resuspended into complete primary culture media and then plated into iMatrix coated six wells plate (or directly transfer into the coated T-25 flask, depending on cell density) and incubated at 37°C. Media was changed every other day until 70-80% confluency was reached (~1,000.000 cells), mostly after Day 6 of plating into T-25. After

harvesting the cells at passage 1 (P1), cells were split 1:4 into T-25 plates for further expansion and aliquoted 3:4 into 1ml of CryoStem™ Freezing Medium (Thermo Fisher Scientific, Waltham, MA, United States) in cryotubes and aliquots were stored in liquid nitrogen.

2.5 Fluorescence-Activated Cell Sorting (FACS)

Aliquots from cultured urine-derived cells from P1 were thawed in RPMI supplemented with 10% FBS and 1uM DNase I. Cells were washed with PBS, stained with RayBright LIVE 780 and washed with FACS buffer. Cells were blocked with FcR blocking buffer and surface stained with antibody CD45 (RayBright 488), CD235a (BV421), CD326 (PE). After staining, cells were washed with a FACS buffer, fixed and permeabilized with RayBio fixation and permeabilization buffer for 20min. Finally, cells were stained with Alexa Fluor 647 anti-Cytokeratin 14 in a permeabilization buffer for 30 min. After staining, the cells were analyzed using a fluorescence-activated cell sorter (RayBiotech, GA, USA).

2.6 CGG Repeat Allele Size and Methylation Status

Genomic DNA (gDNA) was isolated from $1x10^6$ derived epithelial cells and from 3 mL of peripheral blood using the Gentra Puregene Blood Kit (Qiagen, Valencia, CA, United States). CGG repeat allele size and methylation status were assessed using a combination of PCR and Southern Blot analysis on DNA isolated from peripheral blood and by PCR on DNA isolated from the epithelial cells. PCR was carried out using *FMR1*

specific primers (AmplideX PCR/CE, Asuragen, Inc.), and amplicons were visualized by capillary electrophoresis and analyzed as previously reported [10]. Southern blot was performed using the Stb12.3 *FMR1* specific chemiluminescent intronic probe, as detailed in [11].

2.7 mRNA Expression Levels

Total RNA was isolated from 1×10^6 urine-derived epithelial cells using Trizol (Thermo Fisher Scientific, Waltham, MA, United States) and quantified using the Agilent 2100 Bioanalyzer system. RNA isolation was performed in a clean and RNA designated area. cDNA was synthesized as previously described [12]. *FMR1* transcript levels and of the reference gene β-glucuronidase (*GUS*), were measured by qRT-PCR using either Assays-On-Demand from Applied Biosystems (Applied Biosystems, Foster City, CA, United States) or custom-designed TaqMan primers and probe assays as previously described [12].

2.8 Western Blot Analysis

Cells were lysed using lysis buffers (Cell Signaling Technology, Inc. Danvers, MA, United States) supplemented with a complete protease inhibitor cocktail (Roche Applied Science, Penzberg, Germany) and phenylmethylsulfonyl fluoride (Sigma-Aldrich Corp, St Louis, MO, United States). Lysates were centrifuged at 16,000 rpm for 15min at 4°C to remove cellular debris followed by protein quantification using Bradford assay (BioRad Laboratories, Inc. Hercules, CA, United States). Ten μg protein was loaded on a 4–12% Bis-Tris gels (BioRad Laboratories, Inc. Hercules, CA, United States) and run at 80V for

30min and 110V for 90 min. Resolved proteins were then transferred onto nitrocellulose membranes using the Trans-Blot Turbo transfer system (BioRad Laboratories, Inc. Hercules, CA, United States) at 25V, 1.0A for 30 minutes. Membranes were stained with Ponceau to test for transfer efficiency, blocked with 3% milk for 1hr at room temperature followed by incubation with 1:1000 diluted FMRP primary antibodies (MAB 2160, MiliporeSigma, Burlington, MA, United States) overnight at 4°C. Membranes were then washed in 1X-TBST and incubated with HRP linked secondary antibody diluted 1:10,000 (Catalog# 1706516, Biorad Laboratories, Inc. Hercules, CA, United States) for 1hr at room temperature. Bands were then visualized using Chemiluminescent substrate, Super Signal West Dura (Thermo Fisher Scientific, Waltham, MA, United States). Densitometry analysis of bands for relative protein quantification was performed using the Alpha Innotech Gel Imaging System (Cambridge Scientific, Watertown, MA).

2.9 Immunofluorescence Staining

Urine-derived epithelial cells were grown in primary media on 22×22 mm iMatrix coated glass coverslip for 24h at 37°C. Cells were fixed for 10 minutes at room temperature in DPBS containing 4% paraformaldehyde, washed in PBSt (DPBS containing 10% Tween 20), permeabilized in 0.1% Triton X-100 in DPBS at Room temperature for 10min and washed three times in PBSt for 5min each. Permeabilized cells were blocked with 5% goat serum for 1hour at room temperature, then incubated overnight at 4 °C with purified anti-FMRP antibody (5ug/mL) (BioLegend, San Diego, CA, United States) in diluted 5% goat serum and washed three times in PBSt for 5 min each. Cells were incubated in Alexa-488-coupled anti-mouse immunoglobulin antibody

(2ug/mL) (Thermo Fisher Scientific, Waltham, MA, United States) in 5% goat serum at room temperature for 1 hour and then washed three times in PBSt for 5 min each. Once washed, cells were incubated in DAPI (4',6-Diamidino-2-Phenylindole, Dihydrochloride) by (Thermo Fisher Scientific, Waltham, MA, United States) at room temperature for 5min. After washing with PBSt at room temperature and mounted in Vectashield mounting media (Vector Laboratories, Burlingame, CA, United States) cells were visualized using an Olympus FLUOVIEW FV1000 confocal microscope. Pictures of different samples were blindly taken using the same settings.

3. Results

3.1 Isolation and Expansion of Urine-Derived Epithelial Cells

A total of 32 urine samples were collected from 25 FXS and 7 TD individuals by following a protocol, as illustrated in [**Figure 1**], under a sterilized environment. No bacterial contamination was present in any of the cultured samples. The average number of live cells in these samples was 4-10, as measured by trypan blue staining. Living cells were attached to the coated plate and started expanding within 2-3 weeks, while the dead cells didn't attach and were removed from the culture media [**Figure 2a**]. Consistently with previous reports [13,14], we observed both types of urinary cell morphologies: type I, that showed a smooth-edged contour and, type II, that had a cobblestone-like cell morphology with random arrangements. Interestingly, we found that both types of colonies were present in the same specimen, although type II usually became more prevalent [**Figure 2b**]. Besides, we found that urine from females mainly consisted of squamous cells [**Figure 2c**]. After plating the cells in primary media, it took about 2-3

weeks for the colonies to appear [**Figure 2d**]. Once cells began growing, they expanded rapidly, becoming 70-80% confluent in 6-7 days [**Figure 2e**]. Once harvested at passage 1 (P1) and transferred (~0.2*10^6 cells) to a T-25 flask [**Figure 2f**], cells only took less than a week to reach 80% confluency 1x10^6 cells) [**Figure 2g**]. However, after four passages the number of cells in primary culture [**Figure 2h**] did not reach a cell density of more than 25% [**Figure 2i**].

3.2 Urine-Derived Cells Expressed Epithelial Cell surface markers

To validate that the newly generated urinary cell colonies were epithelial cells and distinguish them from other urinary cell types, we performed Fluorescence-Activated Cell Sorting (FASC) using a marker of human epithelial cells, white and red blood cells [**Figure 3**]. FACS revealed that Urine-derived Cells at P1 stained 48-76% positive for surface markers characteristic of epithelial cells, i.e., pan-cytokeratin (CK14, 15, 16, 19) and CD326. Besides, these cells stained 0.013-0.025% for the general hematopoietic cell marker CD45 and 0.07-0.1% for the CD235a, a marker for the human erythroid cells and their progenitors [**Supplementary Material Table S1**] indicating that the established cell lines were mostly constituted by epithelial cells and not by hematopoietic or erythroid progenitor cells.

3.3 Intra- and Inter-tissue mosaicism detected in PBMCs and Urine-Derived Epithelial Cells

CGG repeat size of the *FMR1* allele was determined in both PBMCs and urine-derived epithelial cell samples from participants (n=10). Interestingly, we observed no

difference in the CGG repeat pattern between PBMCs [**Figure 4a**] and the urine-derived epithelial cells [**Figure 4b**] from the same individual. However, we did observe significant differences between PBMCs [**Figure 4c and Figure 4e**] and urine-derived epithelial cells and the CGG allele distribution in other cases [**Figure 4d and Figure 4f**] suggesting the presence of inter-tissue mosaicism. In addition to inter-tissue differences between PBMC's and urine-derived epithelial cells, we also observed, in some cases, multiple CGG size alleles within the same tissues [**Figure 4a, 4c, and 4e**] representing intra-tissue mosaicism.

3.4 Urine-Derived Epithelial Cells express *FMR1* mRNA and FMRP protein

Expression of the *FMR1* mRNA and FMRP was measured in a subgroup of the established epithelial cells derived from participants with FXS and TD. The *FMR1mRNA* expression levels, normalized against the GUS gene, were, as expected, significantly higher ($P < 0.0001$) in TD (n=1) as compared to FXS participants (n=5) [**Figure 5a**]. FMRP expression was measured using Western Blot analysis. We observed a complete loss or significantly lower (<=0.1%) FMRP expression (n=9, $p < 0.0001$) in patients with FXS derived epithelial cells compared to TD (n=3). Interestingly, we observed a very small amount of FMRP expression by Western Blot analysis, in protein extracts derived from patients with a mosaicism, including Case 5, Case 7 and Case 9, but only after a long exposure time [**Figure 5b**]. We further confirmed FMRP expression and its localization in epithelial cells using *in-situ* immunofluorescence. Consistently with Western Blot analysis, high FMRP expression, localized in the cytoplasm of the epithelial cells derived from TD, was detected. In contrast, complete loss or low FMRP expression was observed in the

cells derived from FXS participants with a fully methylated full mutation (**Table 1**, Case 5, Case 6 and Case 8) [**Figure 5c**]. Although Case 8 present with 85% methylation, we did not detect any FMRP expression by immunofluorescence or Western blot analysis likely due to deficit in translational efficiency of the large unmethylated alleles (240-350 CGG repeats; see **Table 1**).

3.5 Factors affecting the establishment of Urine-Derived Epithelial Cells

In our experience, we observed that the health status of the donor affected the urine-derived cells attachment and growth *in vitro*, as the large debris in the urine samples decreases the growth of the healthy cells [**Figure 6a, 6b**]. To find if the plate coating material had an impact on the growth of the epithelial cells, we compared the widely used coating material Poly L-lysine with iMatrix. Interestingly, we also found that the plate coating material impacts the growth and morphology of epithelial cells as we observed healthy growth on iMatrix coated plates [**Figure 6c**] while cell morphology and health appeared to be compromised as we observed distorted mesh-like pattern when cells were grown on plated coated with Poly L-Lysine [**Figure 6d**]. To determine whether the urine sample could be stored for transportation before culturing the epithelial cells, we froze the portion of freshly donated urine for 24 hr at -20°C before isolating and culturing the cells by our standard procedure. Significantly, on Day 12, we didn't observe any cell growth from the urine samples stored for 24h at -20°C [**Figure 6e**] as compared with cells isolated from freshly collected urine samples [**Figure 6f**].

4. Discussion

Urine-derived epithelial cells present a unique cell source with proliferation ability and an advantageous *in vitro* model to study FXS. They could be used to investigate FXS disease mechanisms, identify new biomarkers, evaluate therapeutic approaches, generating iPSCs, and be used for drug screening. As urine can be collected by totally non-invasive procedures, this method can be used universally to any neurodevelopmental disease. Using this non-invasive approach, we have generated 19 epithelial cell lines, and we are continuing to create more lines to be used for future basic and translational studies in FXS. To the authors' knowledge, this paper is the first report on establishing epithelial cell lines from the urine of the participants with FXS and proposed as an *in vitro* model to investigate the mechanism of disease development.

One of our initial concerns was determining whether the urine-derived cells from individuals with FXS could expand *in vitro* as efficiently as other cell types. We observed that, in our hands, cell colonies arising within 2-3 weeks of isolation could be established as a stable cell population within just the following six days. The second biggest concern was to make sure that the established cell lines were constituted by epithelial cells. FACS analysis determined that the majority of cells harvested at P1 were indeed epithelial cells as defined by the presence of epithelial-specific surface markers, i.e., pan-cytokeratin (CK14, 15, 16, 19) and CD326. Moreover, we detected the expression of *FMR1* mRNA and FMRP in these cells, although, as expected, we observed low expression levels in the cells derived from participants with FXS compared to TD.

CGG size mosaicism is common in individuals with the *FMR1* full mutation [2,15–19]. Although, depending on the allele size and the methylation status, FMRP can be

212

produced, mosaic individuals usually present with developmental delay due to the low *FMR1* gene expression and the inefficient translation of the extended CGG repeat mRNA. In addition, mostly, DNA testing is performed on PBMC's which results may not accurately show the mutation pattern in other tissues such as the brain. Mosaicism in different tissues has been investigated and reported [2,17,20–22], with similarities across tissues in some cases and extreme differences in others. Thus, it is difficult to predict on an individual basis whether the *FMR1* mutation observed in blood will show the same or different pattern in other tissues. For this reason, we assessed the impact of CGG size mosaicism in the participants by comparing DNA isolated from both PBMCs and urine-derived cells. Consistent with other reports, we observed mosaicism in some cases, with a similar CGG allele size and distribution between the two different tissues, while different in others, underling the complexity of the CGG repeat instability. The observed intra-and inter-tissue mosaicism, as demonstrated by the presence of multiple size alleles and methylation status in PBMC's and across different tissues, could be associated with the variability in the wide spectrum of clinical involvement in FXS.

The difficulties presented in obtaining tissues from patients with neurodevelopmental disorders and lack of adequate preclinical models with high predictive and translational power pose limitations in the study of these disorders and in developing effective target treatments. As brain biopsies are impractical and risky, many studies develop methods to differentiate urine-derived cells into neural-lineage cells [23–25]. The human urinary cells represent a promising source of stem cells as they can also be converted into neural stem cells by using a non-integration-free method with small molecules, which is less time consuming than going through iPSCs [26]. As urine-derived stem cells have a similar

phenotype to mesenchymal stroma cells (MSC), they can be reprogrammed into iPSCs and converted into astrocytes, oligodendrocytes, and neurons. Thus, urine-derived cells represent an alternative source of cells for developing iPSCs, with the advantage of being collected by a noninvasive method [27]. They may play an essential role in identifying and developing safe and effective therapies for patients with neurodevelopmental conditions, such as FXS. Moreover, this unique epithelial cell modeling and their further differentiation into neural lineage cells will provide valuable information for predicting drug response and assessing environmental disease triggers. Furthermore, the development of epithelial cells provides a new platform in the field of FXS modeling and works in complementary ways; it is expected to benefit research and clinical applications in personalized medicine.

Because of the simplicity, safeness, the low-cost, and the noninvasive process described here, epithelial cell lines can be generated in a relatively short time from a significant proportion of patients with FXS or other neurodevelopmental disabilities, including Autism Spectrum Disorders. Importantly, the establishment of these cell lines, coupled with extensive phenotypic information, including a clinical history of FXS-related comorbidities will potentially result in a reasonable biobank of cell lines from phenotypically well-characterized individuals with FXS that can be used initially to identify potential molecular biomarkers predictors of drug efficacy, in pharmacology and toxicology tests and then should eventually evolve into a community resource for various advance studies on the pathology of FXS.

One limitation of this study is related to the few numbers of cells and to the amount of the debris and contaminants in the urine sample that significantly decrease the chances of epithelial cell line establishment. In addition, it is challenging to collect the first urine

and, in enough volume, (~40ml) from young patients with FXS to ensure the success of the procedure. Thus, optimization and standardization of the urine samples collection method is required to significantly improve the growth and proliferation of urine derived epithelial cells.

5. Conclusions

In summary, there are several advantages in using urine-derived epithelial cells as a tool for FXS modeling: a) specimens and cells can be easily harvested; b) epithelial cells do not require processing by enzyme digestion or culture on a layer of feeder cells to support cell growth; c) since invasive surgical biopsy procedures are not necessary to harvest cells from urine, potential complications such as urethral or bladder trauma and urinary tract infection and patient morbidity are avoided; d) epithelial cells are not exposed to ultraviolet (UV) rays (such as mostly skin fibroblasts or hair follicles do) and thus, they are less likely to contain potential genetic mutations and UV-induced DNA damage; e) as epithelial cells are autologous somatic cells, there are no ethical issues involved in their use for future preclinical and clinical studies.

6. Availability of Additional Data

All statistical data generated during the study is available at the end of this chapter as "Supplementary Data".

7. References

1. Harris, J.C. New classification for neurodevelopmental disorders in DSM-5. *Current Opinion in Psychiatry* 2014, *27*, 95–97.

2. Pretto, D.; Yrigollen, C.M.; Tang, H.-T.; Williamson, J.; Espinal, G.; Iwahashi, C.K.; Durbin-Johnson, B.; Hagerman, R.J.; Hagerman, P.J.; Tassone, F. Clinical and molecular implications of mosaicism in FMR1 full mutations. *Frontiers in Genetics* 2014, *5*.

3. Nolin, S.L.; Glicksman, A.; Ersalesi, N.; Dobkin, C.; Ted Brown, W.; Cao, R.; Blatt, E.; Sah, S.; Latham, G.J.; Hadd, A.G. Fragile X full mutation expansions are inhibited by one or more AGG interruptions in premutation carriers. *Genetics in Medicine* 2015, *17*, 358–364.

4. Chen, X.; Wang, J.; Xie, H.; Zhou, W.; Wu, Y.; Wang, J.; Qin, J.; Guo, J.; Gu, Q.; Zhang, X.; et al. Fragile X syndrome screening in Chinese children with unknown intellectual developmental disorder. *BMC Pediatr.* **2015**, *15*, 77.

5. Kim, E.Y.; Page, P.; Dellefave-Castillo, L.M.; McNally, E.M.; Wyatt, E.J. Direct reprogramming of urine-derived cells with inducible MyoD for modeling human muscle disease. *Skeletal Muscle* 2016, *6*.

6. Lazzeri, E.; Ronconi, E.; Angelotti, M.L.; Peired, A.; Mazzinghi, B.; Becherucci, F.; Conti, S.; Sansavini, G.; Sisti, A.; Ravaglia, F.; et al. Human Urine-Derived Renal Progenitors for Personalized Modeling of Genetic Kidney Disorders. *Journal of the American Society of Nephrology* 2015, *26*, 1961–1974.

7. Afzal, M.Z.; Strande, J.L. Generation of Induced Pluripotent Stem Cells from Muscular Dystrophy Patients: Efficient Integration-free Reprogramming of Urine Derived Cells. *Journal of Visualized Experiments* 2015.

8. Zhang, S.-Z.; Li, H.-F.; Ma, L.-X.; Qian, W.-J.; Wang, Z.-F.; Wu, Z.-Y. Urine-derived induced pluripotent stem cells as a modeling tool for paroxysmal kinesigenic dyskinesia. *Biology Open* 2015, *4*, 1744–1752.

9. Zhang, D.; Wei, G.; Li, P.; Zhou, X.; Zhang, Y. Urine-derived stem cells: A novel and versatile progenitor source for cell-based therapy and regenerative medicine. *Genes Dis* **2014**, *1*, 8–17.

10. Filipovic-Sadic, S.; Sah, S.; Chen, L.; Krosting, J.; Sekinger, E.; Zhang, W.; Hagerman, P.J.; Stenzel, T.T.; Hadd, A.G.; Latham, G.J.; et al. A novel FMR1 PCR method for the routine detection of low abundance expanded alleles and full mutations in fragile X syndrome. *Clin. Chem.* **2010**, *56*, 399–408.

11. Tassone, F.; Pan, R.; Amiri, K.; Taylor, A.K.; Hagerman, P.J. A Rapid Polymerase Chain Reaction-Based Screening Method for Identification of All Expanded Alleles of the Fragile X (FMR1) Gene in Newborn and High-Risk Populations. *The Journal of Molecular Diagnostics* 2008, *10*, 43–49.

12. Tassone, F.; Hagerman, R.J.; Chamberlain, W.D.; Hagerman, P.J. Transcription of the FMR1 gene in individuals with fragile X syndrome. *American Journal of Medical Genetics* 2000, *97*, 195–203.

13. Zhou, T.; Benda, C.; Dunzinger, S.; Huang, Y.; Ho, J.C.; Yang, J.; Wang, Y.; Zhang, Y.; Zhuang, Q.; Li, Y.; et al. Generation of human induced pluripotent stem cells from urine samples. *Nat. Protoc.* **2012**, *7*, 2080–2089.

14. Sauer, V.; Tchaikovskaya, T.; Wang, X.; Li, Y.; Zhang, W.; Tar, K.; Polgar, Z.; Ding, J.; Guha, C.; Fox, I.J.; et al. Human Urinary Epithelial Cells as a Source of Engraftable Hepatocyte-Like Cells Using Stem Cell Technology. *Cell Transplant.* **2016**, *25*, 2221–2243.

15. Loesch, D.Z.; Sherwell, S.; Kinsella, G.; Tassone, F.; Taylor, A.; Amor, D.; Sung, S.; Evans, A. Fragile X-associated tremor/ataxia phenotype in a male carrier of unmethylated full mutation in the FMR1 gene. *Clinical Genetics* 2012, *82*, 88–92.

16. Tassone, F.; Hagerman, R.J.; Loesch, D.Z.; Lachiewicz, A.; Taylor, A.K.; Hagerman, P.J. Fragile X males with unmethylated, full mutation trinucleotide repeat expansions have elevated levels ofFMR1 messenger RNA. *American Journal of Medical Genetics* 2000, *94*, 232–236.

17. Pretto, D.I.; Mendoza-Morales, G.; Lo, J.; Cao, R.; Hadd, A.; Latham, G.J.; Durbin-Johnson, B.; Hagerman, R.; Tassone, F. CGG allele size somatic mosaicism and methylation inFMR1premutation alleles. *Journal of Medical Genetics* 2014, *51*, 309–318.

18. Hadd, A.G.; Filipovic-Sadic, S.; Zhou, L.; Williams, A.; Latham, G.J.; Berry-Kravis, E.; Hall, D.A. A methylation PCR method determines FMR1 activation ratios and differentiates premutation allele mosaicism in carrier siblings. *Clinical Epigenetics* 2016, *8*.

19. Mailick, M.R.; Movaghar, A.; Hong, J.; Greenberg, J.S.; DaWalt, L.S.; Zhou, L.; Jackson, J.; Rathouz, P.J.; Baker, M.W.; Brilliant, M.; et al. Health Profiles of Mosaic Versus Non-mosaic FMR1 Premutation Carrier Mothers of Children With Fragile X Syndrome. *Frontiers in Genetics* 2018, *9*.

20. Tassone, F.; Longshore, J.; Zunich, J.; Steinbach, P.; Salat, U.; Taylor, A.K. Tissue-specific methylation differences in a fragile X premutation carrier. *Clinical Genetics* 1999, *55*, 346–352.

21. Genc, B. Methylation mosaicism of 5'-(CGG)n-3' repeats in fragile X, premutation and normal individuals. *Nucleic Acids Research* 2000, *28*, 2141–2152.

22. Bonarrigo, F.A.; Russo, S.; Vizziello, P.; Menni, F.; Cogliati, F.; Giorgini, V.; Monti, F.; Milani, D. Think About It. *Journal of Child Neurology* 2014, *29*, NP74–NP77.

23. Bharadwaj, S.; Liu, G.; Shi, Y.; Wu, R.; Yang, B.; He, T.; Fan, Y.; Lu, X.; Zhou, X.; Liu, H.; et al. Multipotential differentiation of human urine-derived stem cells: Potential for therapeutic applications in urology. *STEM CELLS* 2013, *31*, 1840–1856.

24. Zhang, S.-Z.; Ma, L.-X.; Qian, W.-J.; Li, H.-F.; Wang, Z.-F.; Wang, H.-X.; Wu, Z.-Y. Modeling Neurological Disease by Rapid Conversion of Human Urine Cells into Functional Neurons. *Stem Cells Int.* **2016**, *2016*, 2452985.

25. Wang, L.; Wang, L.; Huang, W.; Su, H.; Xue, Y.; Su, Z.; Liao, B.; Wang, H.; Bao, X.; Qin, D.; et al. Generation of integration-free neural progenitor cells from cells in human urine. *Nature Methods* 2013, *10*, 84–89.

26. Cheng, L.; Hu, W.; Qiu, B.; Zhao, J.; Yu, Y.; Guan, W.; Wang, M.; Yang, W.; Pei, G. Generation of neural progenitor cells by chemical cocktails and hypoxia. *Cell Research* 2014, *24*, 665–679.

27. Bento, G.; Shafigullina, A.K.; Rizvanov, A.A.; Sardão, V.A.; Macedo, M.P.; Oliveira, P.J. Urine-Derived Stem Cells: Applications in Regenerative and Predictive Medicine. *Cells* 2020, *9*, 573.

8. Tables

Table 1. Demographic, and molecular information for participants included in the study.

Participants	Age	Gender	Peripheral blood Mutation category	Peripheral blood CGG repeat number *	Peripheral blood % Methylation	Mutation category	Epithelial Cells CGG repeat number	Peripheral blood *FMR1* mRNA level (StErr)	Epithelial cells *FMR1* mRNA level
Case 1	14	M	Full mutation	>200		Full mutation	>200	0	0
Case 2	20	M	Full mutation	>200		Full mutation	>200	0	
Case 3	8	M	Full mutation	>200		Full mutation	>200	0	
Case 4	25	M	Full mutation	>200		Full mutation	>200	0	
Case 5	13	M	Full mutation	>200		Full mutation	>200	0.01 (0.002)	0
Case 6	20	M	Full mutation	>200		Full mutation	>200	0.009 (0.001)	0
Case 7	18	M	Full mutation, Meth mosaic	>200 (30-200) **	> 95%	Full mutation, Meth mosaic	>200** (30)	0.29 (0.03)	
Case 8	8	M	Full mutation, Meth mosaic	>200 (240-350) **	85%	Full mutation	>200***	0.47 (0.01)	0
Case 9	8	M	Full mutation	>200***		Full mutation	>200	0.16 (0.004)	0
Case 10	13	M	Full mutation	>200		Full mutation	>200	0	
Case 11	15	M	Full mutation, Size mosaic	>200 (103) **	96%	Full mutation, Size mosaic	>200 (103) **	0.15 (0.06)	
Case 12	17	M	Full mutation	>200		Full mutation	>200	0	

220

*CGG repeat number measured in peripheral blood.

** Numbers between parenthesis indicate the range of CGG repeat number of unmethylated alleles.

*** Very light smear of unmethylated alleles was detected by Southern Blot.
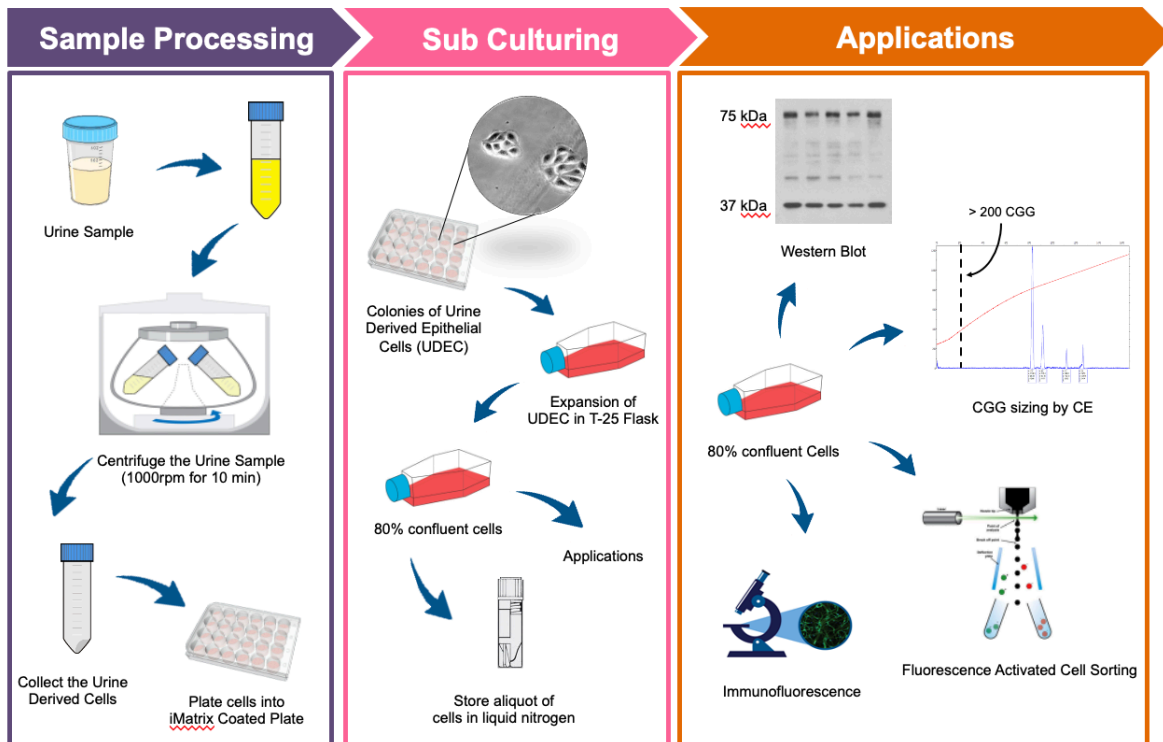
9. Figures

Figure 1: Schematic representation of the urine derived epithelial cell culture establishment protocol. For sample processing, a urine sample was collected, transferred into a sterile 50-ml centrifuge tube, and centrifuged at 1000rpm for 10min at room temperature. Collected urine derived cells were plated into iMatrix coated wells and incubated at 37°C for 24h. Cells were fed until small colonies of approximately 5-6 cells appeared, which on average took 2-3 weeks after plating, to reach 80–90% density. Cells

were harvested, aliquoted and stored in cryotubes in liquid nitrogen for different applications (Western Blots, CGG repeat sizing, Immunofluorescence and Fluorescence Activated Cell Sorting).
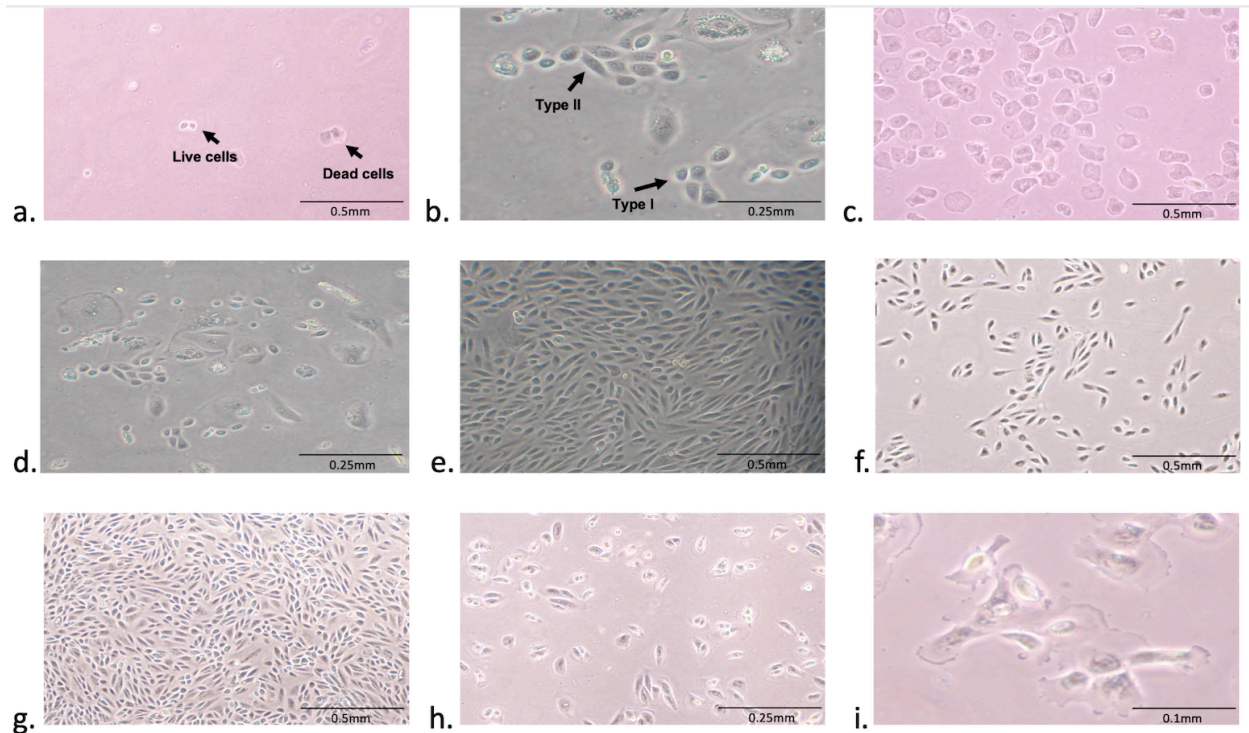
Figure 2: <u>Isolation and Expansion of Urine derived Epithelial Cells.</u> **a.** A representation of living and dead cells in urine samples. **b.** Urinary cell morphologies: Type I shows a smooth-edged contour and Type II, have cobble stone-like cell morphology with random arrangements. **c.** Squamous cells in the urine sample of female individuals. **d.** Epithelial cell colonies appear within 2-3 weeks after plating. **e.** 70-80% cell confluency **f.** Expansion of epithelial cells at P1 in T-2 flask. **g.** 80% cell confluency in a T-25 flask. **h** Number of cells decreased after 4 passages. **i.** Slow growth of epithelial cells at later passages. 10

X magnification was used for image a, c, e, f and g, while b, d and h has been captured at 20x magnification, the 40 X magnification was used for image i.
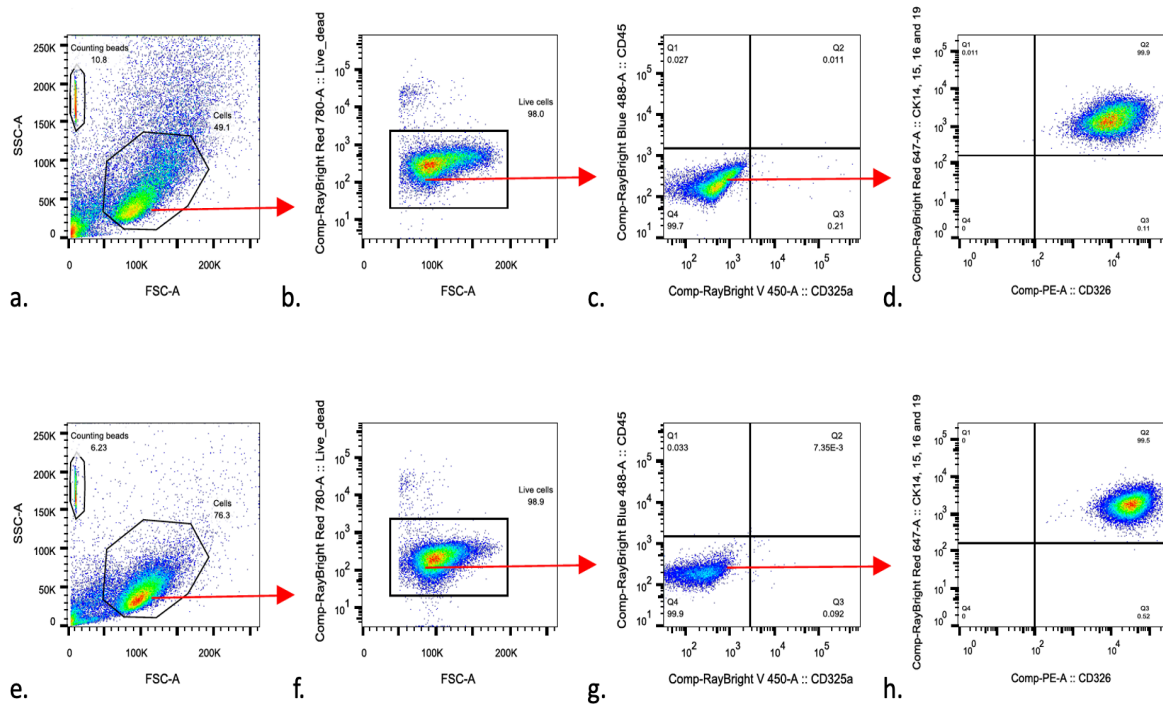

Figure 3: Urine Derived Cells Express Epithelial Cell surface markers.

Fluorescence-activated cell sorting analysis of urine derived epithelial cells at P1 from Case 1 (top panel, a, b, c and d) and Case 3 (bottom panel, e, f, g, h). Cells were stained with antibody against epithelial surface markers pan-cytokeratin (CK14, CK15, CK16, CK19) and CD326. In addition, cells were stained with antibody to the hematopoietic cell marker CD45 (RayBright 488) and to a marker for the human erythroid cells and their progenitors CD235a (BV421). From left to right the cells were separated from precipitation and debris by gating them for the further analyses (as shown by the red arrow). Only alive cells (b and f, corresponding to 98% and 98.8% of alive cells respectively) were included

in the analysis. The cells stained negative for both CD45 and CD325a (c and g) while stained strongly positive for the CD326, CK14, CK15, CK16, and CK19 (d and h).
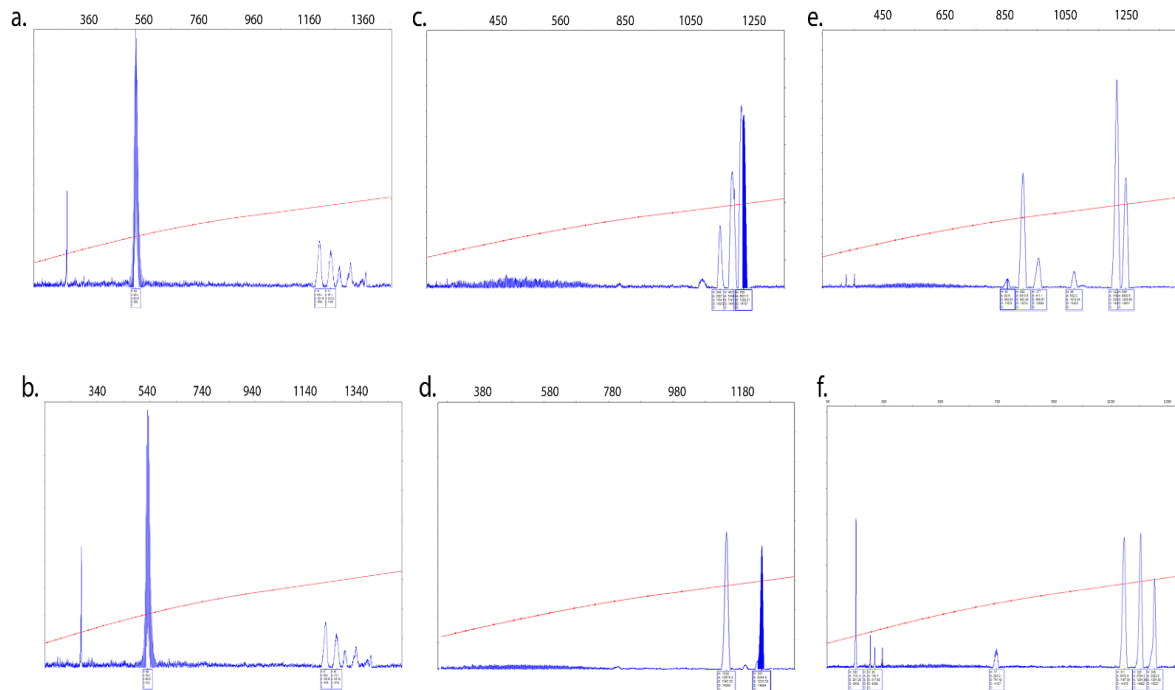

Figure 4: Size mosaicism occur between PBMCs and Urine Derived Epithelial Cells. Representative capillary electrophoregrams of three individuals with a full mutation are illustrated. Several similar peaks, each representing single distinct alleles, were observed with similarity between PBMCs (a) and epithelial cells (b) [Case 11]. Interestingly, a different CGG profile between PBMCs (c, e) and epithelial cells (d, f) [Case 7 and Case 2 respectively] and within the two tissues was observed in two other case indicating the presence of both inter and intra-tissue mosaicisms. The X axis marks the size of the alleles in base pairs. The Y-axis marks the fluorescence intensity of each allele. The

numbers inside the boxes indicate H: Height, A: Area, S: Size, D: Data point. Only the S

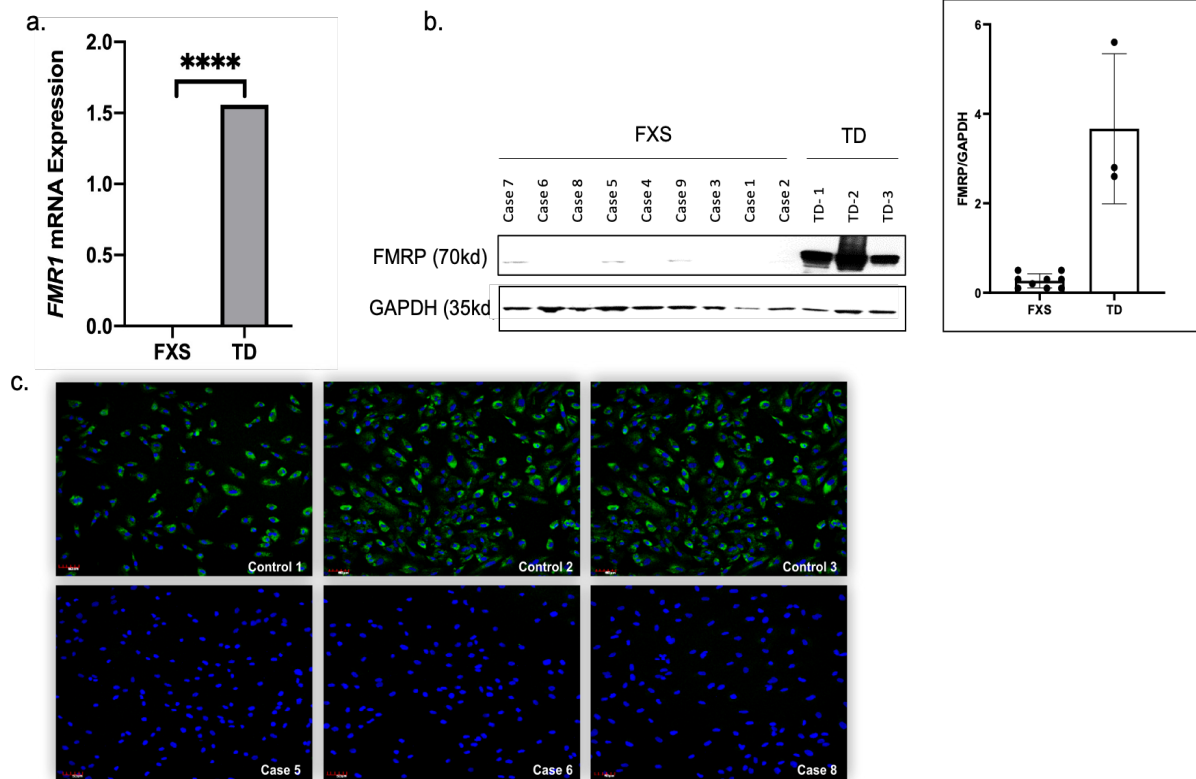number (base pairs) is used to calculate the CGG repeat number

Figure 5: <u>Urine Derived Epithelial Cells expressed *FMR1* mRNA and FMRP protein.</u> **a.**

Bar plot showing the significantly higher expression (p< 0.0001) of *FMR1* mRNA in TD

(n=1) as compared to FXS patients (n=5). **b.** Western blot protein expression patterns

showing complete loss or significantly lower (<=0.1%) FMRP expression (n=9, p <

0.0001) in FXS patient derived epithelial cells compared to TD (n=3). Data also show ratio

of FMRP protein/GAPDH. **c.** Confocal images and *in-situ* immunofluorescence showing

high expression of FMRP protein (green) localized to cytoplasm of the epithelial cells derived from normal individuals (Top panel; n=3), while complete loss or low FMRP expression has been observed in the cells derived from FXS patients (Bottom panel; n=3).
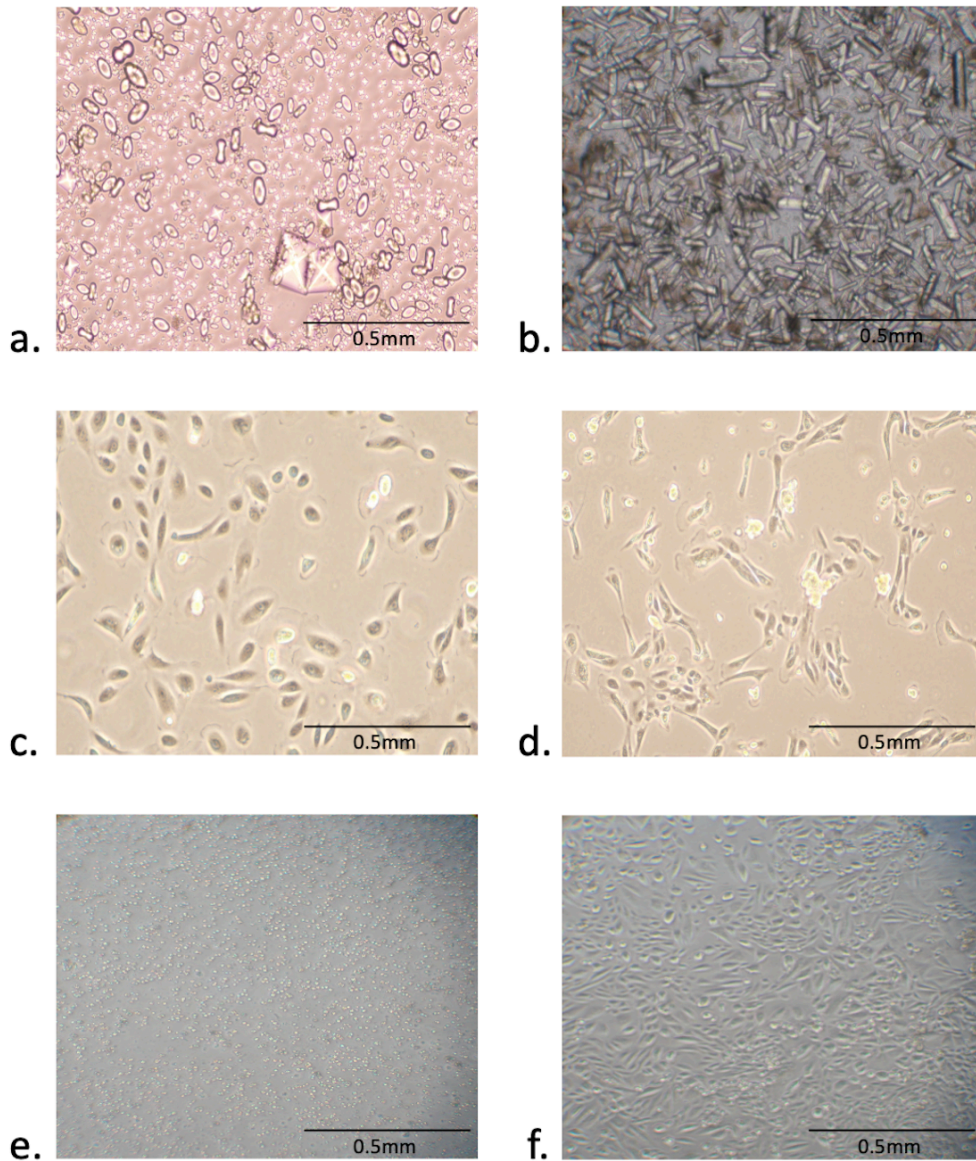

Figure 6: <u>Factors affected Urine Derived Epithelial Cells</u> **a. & b.** Representation of high debris in the urine samples of FXS patients. **c. & d.** Plate coating material impacts the

growth and morphology of epithelial cells. Normal growth on iMatrix coated plates (c.) v/s distorted mesh like growth pattern of cells on Poly L-lysine (d). **e. & f.** Urine storage conditions affect the growth of the derived epithelial cells. No cells growth observed from the urine samples stored for 24h at -20°C before isolating cells (e) as compared to freshly collected and processed urine sample (f).

10. Supplementary Materials

	Table S1: FACS analysis of Urine Derived Cells.										
	Cells | Freq.	Counting bea	Cells/Single	Cells/Single	Cells/Single	Cells/Single	Cells/Single	Cells/Single	Cells/Single	Cells/Single	Cells/Single (
P1_168-18 (I	49.1 %	10.8 %	98.0 %	0.013 %	5.19E-3 %	0.10 %	47.5 %	5.19E-3 %	47.4 %	0.054 %	0 %
P1_179-18 (I	76.3 %	6.23 %	98.9 %	0.025 %	5.53E-3 %	0.069 %	75.1 %	0 %	74.7 %	0.39 %	0 %
Note: 50000 counting beads were added to each sample.											
	Ttoal cells plus b	Live cells%	live epithelia	otal leukocyte	Total RBC						
68-18 (IC)_0C	462963	98.0 %	219444	60	463						
79-18 (IC)_0C	802568	98.9 %	599518	201	554						

Chapter 6

Fragile X-Associated Tremor/Ataxia Syndrome (FXTAS)

Marwa Zafarullah[1] and Flora Tassone [1,2]*

[1] Department of Biochemistry and Molecular Medicine, University of California Davis School of   Medicine, Davis, CA, USA
[2] MIND Institute, University of California Davis Medical Center, Sacramento, CA, USA
* **Correspondence:** ftassone@ucdavis.edu; Tel.: +1-(916)-703-0463

Abstract

Individuals carrying a *FMR1* expansion between 55 and 200 CGG repeats, are at risk of developing the Fragile X-associated tremor/ataxia syndrome (FXTAS), a late onset neurodegenerative disorder characterized by cerebellar gait ataxia, intentional tremor, neuropathy, parkinsonism, cognitive decline, and psychological disorders, such as anxiety and depression. In addition, brain atrophy, white matter disease and hyperintensities of the middle cerebellar peduncles, can also be present. The neuropathological distinct feature of FXTAS is represented by the presence of eosinophilic intranuclear inclusion in neurons and astrocytes throughout the brain and in other tissues. In this chapter, protocols for available diagnostic tools in both humans and mouse, the clinical features and the basic molecular mechanisms leading to FXTAS, and the animal models proposed to study this disorder.

Keywords: Tremor, Ataxia, FXTAS, *FMR1*, FMRP, qRT-PCR, TP- PCR

1. Introduction

The human *FMR1* gene spans approximately 38kb of genomic DNA, consists of 17 exons [1] and it undergoes alternative splicing involving multiple exons [2]. The length of the trinucleotide CGG repeats in the promoter defines different allele categories [3]. Those harboring between 55 and 200 CGG repeats, are named premutations which are unstable upon transmission and have the propensity to expand into a full mutation allele in following generations [4,5]. Premutation alleles have a prevalence among the general population of ~1 in 110–260 females and ~1 in 400–850 males; however, the prevalence can vary depending on ethnicity [6], being the highest in Colombia and Israel [7,8].

Many studies in recent years have reported that premutation carriers are at increased risk for a number of medical problems which include but are not limited to hypertension [9], central pain sensitivity syndrome, sleep problems, restless legs syndrome (RLS) [10], migraine [11] and gait issues [12]. In addition, the presence of a premutation can also cause developmental problems such as ASD and ADHD particularly in young boys [13-15], cognitive [16] and psychiatric features, including anxiety [17,18] and depression [19] in both children and adults.

Carriers of a premutation allele are at the risk of developing both Fragile X-associated tremor/ataxia syndrome (FXTAS) and Fragile X –associated primary ovarian insufficiency (FXPOI). About 40% of male carriers over the age of 50 develop FXTAS. The penetrance is age related, such that 75% of men ≥80 years of age are affected [20]. Approximately 8% of female carriers develop FXTAS [21]. In addition, approximately 20 % of female carriers of a premutation allele, develop Fragile X-associated primary

ovarian insufficiency, a loss of normal ovary function before the age of 40, compared 1% women in the general population [22,23].

The main clinical features of fragile X-associated tremor/ataxia syndrome (FXTAS) include the presence of gait ataxia and intentional tremor [24]. Observed imaging abnormalities comprise global brain atrophy and cerebellar white matter changes, including involvement of the middle cerebellar peduncles (MCP) [25,26].

Male premutation carriers over age 50 with and without FXTAS have increased rates of anxiety, hostility, apathy, irritability, agitation, obsessive compulsiveness, and depression [27], while female carriers, with and without FXTAS, show a high rate of depressive symptoms as compared to normal individuals [28]. Importantly, female premutation carriers, particularly those with core features of FXTAS, present with thyroid dysfunction (17% in the non-FXTAS group and 50% in the FXTAS group) [29].

Individuals with a premutation allele have up to eight-fold elevation of *FMR1* mRNA expression levels, which positively correlate with the (CGG)n repeat length. Interestingly, although *FMR1* transcript levels increase with increased CGG repeats, the levels of FMRP gradually decreases with increasing (CGG)n length due to decreased translational efficiency of long expanded CGG alleles [30, 31]. Thus, differently from fragile X syndrome (FXS), which is caused by the lack of FMRP, FXTAS and the premutation disorders arise through a distinct and different molecular mechanism involving the presence of elevated levels of *FMR1* expanded CGG-repeat transcripts, leading to RNA toxicity.

Various models have been proposed to explain the disease mechanisms for FXTAS. The first proposed model was the RNA gain-of-function model or sequestration

model based on the proposed myotonic dystrophy [32]. This model postulates that the excessive expanded CGG containing mRNA, binds several CGG binding proteins which sequestration affects their normal cellular functions [24]. Among these proteins, Sam68 is an RNA-binding protein involved in alternative splicing regulation that co-localize with CGG aggregates [33] and DGCR8 which with Drosha forms a protein complex involved in the biogenesis of miRNA. As result reduced levels of many miRNAs but increased levels of their precursors have been detected in brain tissues derived from individuals with FXTAS [34].

Repeat-associated non-AUG (RAN) translation is an alternative proposed mechanism for explaining the pathogenesis of FXTAS [35], which posits that the translation of the *FMR1* mRNA occurs upstream of the expanded repeat generating three different homopolypeptides. However, among the three, the polyarginine (FMRpolyG) is produced more efficiently and results in a toxic homopolypeptide that can affect cellular functions and consequently plays a role in FXTAS [36,37].

The third proposed mechanism is based on DNA damage response model leading to the formation of secondary R-loop structures. The transcription of highly GC-rich region, such as the 5' UTR region of *FMR1* gene, promotes the formation of R-loops in which the nascent RNA forms a stable RNA: DNA hybrid with the template DNA strand. Recent study shows that R-loops formed over CGG repeats may be susceptible to an increased frequent formation and greater structural complexity, CGG-repeat length dependent [38]. The above-mentioned models are not mutually exclusive and likely they all contribute to the development of FXTAS but, how exactly they are leading and, what is their relative contribution to the pathogenesis of this disorder, remain unknown.

1.1   Clinical features and methods for the diagnosis of FXTAS

For the diagnostic criteria of FXTAS [**Table 1**], tremor and ataxia are considered the main clinical features for a definite diagnosis of FXTAS. At the molecular level the presence of an expanded allele from the gray through the premutation range is required for the diagnosis of FXTAS [39].

Three categories, termed as "definite", "probable" and "possible" are used in the diagnosis of FXTAS. "Definite" indicates the presence of one major radiological sign plus one major clinical symptom. "Probable" indicates the presence of either one major radiology sign plus one minor clinical symptom or two major clinical symptoms. "Possible" indicates the presence of one minor radiology sign plus one major clinical symptom [**Table 1**]. In addition, the diagnosis of FXTAS can also be clarified by the stage of disease, which provide information of the impact of disease on activities of daily living. Six FXTAS stages have been described and they include; stage 0: normal function; stage 1: subtle or questionable signs such as subtle tremor or mild balance problems, with no interference in ADLs; stage 2: minor but clear, tremor and/or balance problems with minor interference with ADLs; stage 3: moderate tremor and/or balance problems and occasional falls with significant interference in ADLs; stage 4: severe tremor and /or balance problems (uses cane or walker); stage 6: bedridden.

1.2. Molecular features and methods for the diagnosis of FXTAS

The molecular diagnosis of the FXTAS is based on the CGG repeat allele size length and specifically on the presence of premutation allele. Recently, the CGG range was extended throughout the intermediate allele range [40] as it has been shown that the

individuals carrying the gray zone expansion can be affected by FXTAS [41, 42]. Although the molecular diagnosis of fragile X syndrome and associated disorders is accomplished by the combination of polymerase chain reaction (PCR) and Southern blot analyses [**Figure 1**], the size of the CGG repeat length and the molecular diagnosis of FXTAS is generally carried out by the PCR approach which reliably can estimate their exact CGG repeat number from normal to premutation range.

The conventional flanking or repeat-spanning PCR techniques use two locus-specific primers to amplify across the *FMR1* CGG repeats; however, these approaches do not allow amplification of large premutation alleles, and they do not provide information on the presence and distribution of the AGG interruptions. These old PCR methods, that used slab-gel electrophoresis for the detection of the CGG containing amplicons, have been replaced by the more robust fluorescent PCRs and by capillary electrophoresis, for better allelic resolution and for a more accurate CGG- repeat sizing. Indeed, a number of different PCR-based methods have been proposed over the years to overcome the failure of the amplification of large *FMR1* alleles due to their high CG content and to the tendency to form undenaturable secondary structures.

One important issue in common to all the earlier assays is that they are not always able to resolve the apparent homozygosity in females, meaning that they cannot distinguish between the presence of two identical *FMR1* alleles within the normal range versus one normal allele and one, unamplified, full mutation allele. This obstacle was overcome using the CGG/CCG primer [43] and by the development of a newer and more robust PCR-based approach, the triplet-primed PCR (TP-PCR) assay [44], which

currently represents an ideal tool for amplifying trinucleotide repeat expansions throughout the CGG repeat range in both males and females.

The triplet-primed PCR (TP-PCR) assay employs, in addition to two *FMR1* specific primers, annealing outside the CGG repeat, the use of a CGG primer, which randomly anneals within the CGG repeat element. PCR amplification gives arise to a series of amplicons that are then visualized as a smear on an agarose gel [43] or as a series of peaks on capillary electrophoresis (CE) [44] [**Figure 2**]. Several studies [44-47] have demonstrated that the TP-PCR provides results that are comparable to those obtained by the combined PCR-Southern blot approach, making it the method of choice for the diagnosis of FXS and Fragile X associated disorders, including FXTAS, in many Laboratories world-wide. The TP-PCR also allows the mapping of AGG interruptions, which knowledge enables to predict the risks of CGG expansion to a full mutation during mother-to-child transmission [5,48], which is important for genetic counseling of women premutation carriers as can further enhance the reproductive decision-making process.

2. Materials

2.1. DNA isolation from human blood, cultured cells and tissues

1. RNase A.

2. Isopropanol.

3. 70% ethanol (see Note 1).

4. RBC Lysis Solution: 0.16 M ammonium chloride in 0.01 M Tris-HCl buffer, pH 7.2 (see Note 2).

5. Cell Lysis Solution: 10mM Tris-HCl buffer, 1mM EDTA and 0.5% SDS (see Note 3).

6. DNA Hydration Solution: 1 mM EDTA, 10 mM Tris-HCl pH 7.5 (see Note 4).

7. Protein Precipitation Solution: 7.5M ammonium acetate (see Note 5).

2.2. Triplet-primed PCR (TP-PCR) in human

1. GC-Rich AMP Buffer: 7.5mM $MgCl_2$ and 7% w/w DMSO (see Note 6).

2. GC-Rich Polymerase Mix: 20mM Tris-HCL pH 8.0, 100mM KCL, 0.1mM EDTA, 1mM DTT, 0.5% Tween 20 (v/v), 0.5% Nonidet, P40 (v/v), 50% glycerol (v/v) (see Note 7).

3. *FMR1* Forward, Reverse FAM-Primer.

4. *FMR1* CGG repeat specific primer $(CGG)_5$.

5. Genomic DNA (Positive Control or Nuclease Free H_2O for negative control).

6. Nuclease Free H_2O.

7. ROX 1000 Size Ladder.

2.3. Isolation of DNA from mouse tails

1. Tail Buffer: 50 mM Tris pH=7.5, 10 mM EDTA, 150 mM NaCl, 1% SDS (see Note 8).

2. Proteinase K (10mg/ml) (see Note 9).

3. 6M NaCl (see Note 10).

4. Ethanol (100%, 70%).

5. Nuclease Free water.

2.4. CGG repeat sizing in mouse

1. 5x Expand HF plus buffer with Mg: 25 mM TAPS [tris(hydroxymethyl)methylamino] propanesulfonic acid -HCl (pH 9.3 @ 25°C), 50 mM KCl, 2 mM MgCl$_2$, 1 mM b-mercaptoethanol, 200 µM dNTPs including [^{3}H]-dTTP and 15 nM primed M13 DNA.

2. 5 M betaine (see Note 11).

3. DMSO. Store at room temperature in the dark.

4. dNTP solution: 25 mM (see Note 12).

5. Primers: (see Note 13)

   a. Forward (5'- CGGAGGCGCCGCTGCCAGG-3')

   b. Reverse (5'- TGCGGGCGCTCGAGGCCCAG-3')

6. Expand High Fidelity plus PCR system Enzyme.

7. Nuclease Free water.

2.5. Quantitative reverse transcriptase PCR (qRT-PCR) of *FMR1 mRNA*

1. 10x PCR Buffer: 500mM Tris.HCl pH 9.0, 15 mM MgCl$_2$, 220mM (NH$_4$)$_2$SO$_4$, 2% triton x-100 (see Note 14).

2. 25 mM MgCl$_2$ (see Note 15).

3. dNTP (25mM).

4. Hexamers (100 µM).

5. Rnase Inhibitor (40U/ µl).

6. Mulv RT (200U/ µl).

7. DEPC H2O.

8. *FMR1* specific primers (100μM).

9. Probe designed for a specific targeted region.

10. Taqman Master Mix.

11. 384 well plate.

12. 96 well plate.

13. Optical Adhesive seal

3. Methods

DNA isolation can be performed using standard reagents available from different companies like Qiagen Valencia.

3.1. DNA isolation from human blood

1. Add 900 μl, of RBC Lysis Solution into a 1.5 ml micro centrifuge tube and add 300 μl, whole blood mix by inverting 10 times.

2. Incubate for 1 min at room temperature (15–25°C) and invert at least once during the incubation.

3. Centrifuge for 20 s at 13,000–16,000 x *g* to pellet the white blood cells and remove the supernatant.

4. Vortex the tube vigorously to suspend the pellet in the residual liquid and then add 300 μl, Cell Lysis Solution, and pipet up and down to lyse the cells or vortex vigorously for 10 seconds.

5. To remove RNA, add 1.5 µl, RNase A Solution, and mix by inverting 25 times. Incubate for 15 min at 37°C. Then incubate for 1 min on ice to quickly cool the sample.

6. Add 100 µl, Protein Precipitation Solution, and vortex vigorously for 20 seconds at high speed. Centrifuge for 1 min at 13,000–16,000 x *g*.

7. Pipet 300 µl isopropanol into a clean 1.5 ml tube, and add the supernatant from the previous step by pouring carefully

8. Mix by inverting gently 50 times until the DNA is visible as threads or a clump.

9. Centrifuge for 1 min at 13,000–16,000 x *g* and the DNA may be visible as a small white pellet.

10. Carefully discard the supernatant and drain the tube by inverting on a clean piece of absorbent paper, taking care that the pellet remains in the tube.

11. Add 300 µl of 70% ethanol and invert several times to wash the DNA pellet.

12. Centrifuge for 1 min at 13,000–16,000 x *g* removes the ethanol and air dry the pellet for 5 min.

13. Carefully discard the supernatant. Drain the tube Add 100 µl DNA Hydration Solution and vortex for 5 s at medium speed to mix.

14. Incubate at 65°C for 5 min to dissolve the DNA then incubate at room temperature overnight with gentle shaking. Samples can then be centrifuged briefly and transferred to a storage tube.

3.2. DNA isolation from cultured cells

1. Harvest cells and determine the number of cells.

2. Take 1–2 x 10^6 cells in growth culture medium to a 1.5 ml micro centrifuge tube and centrifuge for 5 s at 13,000–16,000 x g to pellet cells.

3. Carefully discard the supernatant by pipetting or pouring, leaving approximately 20 μl residual liquid.

4. Now Vortex the tube vigorously to resuspend the cells in the residual supernatant and add 300 μl Cell Lysis Solution to the resuspended cells and pipet up and down or vortex on high speed for 10 s to lyse the cells.

5. To remove RNA, add 1.5 μl of RNase A Solution, and mix by inverting 25 times. Incubate for 5 min at 37°C. Incubate for 1 min on ice to quickly cool the sample.

6. Add 100 μl Protein Precipitation Solution, and vortex vigorously for 20 s at high speed.

7. Pipet 300 μl isopropanol into a clean 1.5 ml microcentrifuge tube add the supernatant from the previous step by pouring carefully.

8. Mix by inverting gently 50 times.

9. Centrifuge for 1 min at 13,000–16,000 x and carefully discard the supernatant.

10. Drain the tube by inverting on a clean piece of absorbent paper, taking care that the pellet remains in the tube.

11. Add 300 μl of 70% ethanol and invert several times to wash the DNA pellet. Centrifuge for 1 min at 13,000–16,000 x g.

12. Carefully discard the supernatant and drain the tube on a clean piece of absorbent paper. Allow to air dry for 5 min.

13. Add 100 μl of DNA Hydration Solution and vortex for 5 s at medium speed to mix.

14. Incubate at 65°C for 1 h to dissolve the DNA. Samples can then be centrifuged briefly and transferred to a storage tube.

3.3. DNA isolation from tissue

1. Dissect tissue sample quickly and freeze in liquid nitrogen. Grind 5–10 mg or frozen or fresh tissue in liquid nitrogen with a mortar and pestle

2. Add 300 µl Cell Lysis Solution into a 1.5 ml grinder tube on ice, and add the ground tissue from the previous step.

3. Add 1.5 µl Proteinase K, mix by inverting 25 times, and incubate at 55°C for 3 h or until tissue has completely lysed.

4. Add 1.5 µl RNase A Solution and mix the sample by inverting 25 times. Incubate at 37°C for 15–60 min and then cool down on ice quickly.

5. Add 100 µl Protein Precipitation Solution, and vortex vigorously for 20 s at high speed.

6. Centrifuge for 3 min at 13,000–16,000 x g.

7. Pipet 300 µl isopropanol into a clean 1.5 ml microcentrifuge tube and add the supernatant from the previous step by pouring carefully

8. Mix by inverting gently 50 times and centrifuge for 1 min at 13,000–16,000 x g.

9. Carefully discard the supernatant and drain the tube by inverting on a clean piece of absorbent paper.

10. Add 300 of 70% ethanol and invert several times to wash the DNA pellet. Centrifuge for 1 min at 13,000–16,000 x g.

11. Carefully discard the supernatant. Drain the tube on a clean piece of absorbent paper, taking care that the pellet remains in the tube. Allow to air dry for 5 min.

12. Add 100 µl DNA Hydration Solution and vortex for 5 s at medium speed to mix.

13. Incubate at room temperature (15–25°C) overnight with gentle shaking. Ensure tube cap is tightly closed to avoid leakage. Samples can then be centrifuged briefly and transferred to a storage tube.

3.4. Triplet-primed PCR (TP-PCR) in Human

1. The following volumes of the PCR mix are for one PCR-reaction: 11.45 µl of GC-rich AMP buffer, 0.5 µl of each primer: *FMR1* forward and *FMR1* reverse, 0.5 µl of *FMR1* CGG primer, 0.5 µl of Nuclease Free H_2O, 0.05 µl of GC-rich polymerase mix, 2 µl of DNA sample. Total volume is 15 µl.

2. Initiate the PCR program and wait until the block has reached at least 103˚C before putting the tubes into the cycler machine. PCR conditions are as: 95˚C 5 min, 10 cycles (97˚C 35 sec, 62˚C 35 sec, 68˚C 4 min), 20 cycles (97˚C 35 sec, 62˚C 35 sec, 68˚C 4 min + 20s/ cycle), 72˚C 10 min, then hold at 4˚C or store at -20˚C.

3. The products can be analyzed on an agarose gel or by capillary electrophoresis using the Hi-Di/ROX-MW Ladder (Hi-Di/ROX solution).

3.5. Premutation animal models

Premutation mouse models, a CGG –Knock in (CGG-KI), were developed even before the discovery of the FXTAS as they were designed to study the CGG repeat instability. These mouse models which express a CGG repeats in premutation range (81

CGG and 97 CGG), showed to stably inherited through generations compared to humans *(49,50)*. However, later the same authors demonstrated CGG repeat instability upon both maternal and paternal transmission in the same KI mouse model [51]. Further, several transgenic mouse lines showed the length-dependent instability in the form of small expansions and contractions in both male and female transmissions over five generations [52].

Increased *FMR1* mRNA levels and intranuclear inclusions throughout the brain were observed in these mice [53]. A different knock-in mouse model harboring an allele of 118 CGG repeats show repeat instability and high expression levels of *FMR1 mRNA* and low level of FMRP. The large expansion into the full mutation in one single generation was observed in these mice [54]. However, no methylation of the promoter region has been detected thus far in any these mice [53-57]. CGG mice display heightened anxiety, deficits in motor coordination and impaired gait and represent the first FXTAS model that exhibits an ataxia phenotype as observed in patients [35, 56, 58-60].

A Drosophila model was generated by expressing 90 CGG repeats, which results in neuronal death of the peripheral and central nervous system [61]. Further, the overexpression of Pur α, an RNA-binding protein expressed in the neuronal cytoplasm found to be associated with (CGG)n RNA, also suppress the eye neurodegeneration phenotype. This protein is present in the inclusions in Drosophila [62], as well as in human FXTAS brain [63] supporting the sequestration model of FXTAS as one of the mechanisms leading to altered cellular function and ultimately neuronal cell death [62].

3.5.1. Isolation of DNA from mouse tails

1. Incubate tail in 300µl tail buffer and 20 µl of Protease K (10 mg/ml) at 55ºC for 24 hrs.

2. Add 100µl 6 M NaCl to the tail/buffer mixture and shake vigorously.

3. Spin at maximum rpm for 10 minutes, collect the supernatant and add 1ml of 100% Ethanol.

4. Mix it well and take out the DNA cloud forming with pipette and put into the tube containing 500 µl ethanol.

5. Spin at maximum rpm for 7 minutes, discard supernatant and dried the pellet.

6. Suspend the DNA pellet into nuclease free water and store at -20 ºC for further use.

3.5.2. CGG repeat sizing in mouse

1. The following volumes for the PCR master mix are for one PCR-reactions: 10.5 µl of commercial water, 1 µl of 100 µM forward primer, 1 µl of 100µM reverse primer, 0.5 µl of 25mM dNTP mix, 1 µl of DMSO, 25 µl of 5 M betaine, 1 µl of Expand High Fidelity plus PCR system Enzyme and 10 µl of 5x Expand HF plus buffer with Mg and 1 µl of DNA sample. Final volume is 50 µl.

2. Initiate the PCR program and wait until the block has reached at least 103˚C before putting the tubes into the cycler machine. PCR conditions are as follow: 95˚C 10 min, 35 cycles (95˚C 1 min, 65˚C 1 min, 75˚C 5 min), 75˚C 10 min, then hold at 10˚C or store at -20˚C until ready to analyze.

3. The products can be analyzed by 1.5 % agarose gel electrophoresis. An approximate repeat length is calculated based on making a (logarithmic) standard curve.

4. For more accurate size determinations, the samples can be analyzed on a 6% polyacrylamide gel. Alternatively, if one the primer is FAM labeled, CGG sizing can be obtained on a capillary electrophoresis.

3.6. Analysis of mRNA expression of premutation career by qRT-PCR

The premutation clinical involvements, including FXTAS are thought to be associated with increased level of CGG expanded *FMR1* mRNA. The level of increased mRNA can be quantified by quantitative reverse transcriptase PCR (qRT-PCR) [64].

3.6.1. Reverse Transcriptase: first strand cDNA synthesis

For making cDNA, PCR master mix should be made on ice to give sufficient volume for several RT-PCR reactions. The following volumes are for one PCR-reaction: 10 μl of 10x PCR buffer, 22 μl MgCl2 at 25mM, 4 μl of dNTP at 25mM, 5 μl of hexamers at 100μM, 1 μl of Rnase Inhibitor at (40U/ μl), 1.25 μl of Mulv RT at 200U/ μl and 51.75 μl of DEPC water.

1. No RT-PCR control reaction is as follows: 10 μl of 10x PCR buffer, 22 μl MgCl2 at 25mM, 4 μl of dNTP at 25mM, 5 μl of hexamers at 100μM, 1 μl of Rnase Inhibitor at (40U/ μl, No Mulv) and 53 μl of DEPC water.

2. 500ng of total RNA should be used for each RT reaction. To control for RT efficiency three total RNA concentrations should be used (i.e., 500ng, 250ng, 125ng).

3. Initiate the PCR program and wait until the block has reached at least 103°C before putting the tubes into the cycler machine. PCR conditions are as follow: 25°C 10 min, 48°C 40 min, 95°C 5 min, then hold at 4°C or store at-20°C until ready to use.

3.6.2. Quantitative PCR (qPCR) of *FMR1 mRNA*

1. To analyze gene expression levels relate to a reference gene using the comparative method *(64)* prepare a primer /probe mixture (P/P) as follow: 152 µl DEPC H2O, 8 µl probe (*FMR1* or reference gene) (100µM), 40 µl Forward primer (100µM) and 40 µl Reverse primer (100µM). The final volume is 240 µl.

2. Prepare 7 µl of master mix which contains: 6 µl of Taqman master mix plus 0.42 µl of H2O and 0.58 µl of P/P. Add 5 µl of cDNA to each tube. The final volume is 12 µl. If you are using 96 or 384 plates, seal with foil.

3. Spin tunes or plates for 1min at 2000rpm at 4 °C.

4. Run the reaction in a 7300/7500 real time PCR system.

5. Expression data can be analyzed as detailed in [64] or https://assets.thermofisher.com/TFS-Assets/LSG/manuals/cms_053412.pdf

4. Notes

1. For 100 ml of 70% ethanol dissolve the 70 ml of 100% ethanol in 30 ml of water. For the higher volume the amount can be adjusted accordingly.

2. For 500ml of RBC lysis buffer dissolve 4.15 g of ammonium chloride (53.491 g/mol) and 605 mg of Tris-HCL (121.14g/mol) in a 450 ml of distilled water. Adjust the pH to 7.2 with HCL and bring the volume to 500ml.

3. Dissolve 605 mg of Tris-HCL (121.14g/mol), 146.12 mg of EDTA (292.24g/mol) and 250 mg of SDS (288.372g/mol) into 450ml of water. After dissolving properly add up more distilled water and bring the volume to 500ml.

4. Dissolve 146.12 mg of EDTA (292.24g/mol) and 605 mg of Tris-HCL (121.14g/mol) into 450ml of water. Adjust the pH to 7.5 with HCL and bring the volume to 500ml.

5. Dissolve 289g of ammonium acetate (77.0825g/mol) into 450ml of water. After proper dissolving add the distilled water to bring the volume to 500ml.

6. Dissolve 0.578 mg of $MgCl_2$ (77.0825g/mol) and 70 mg of DMSO (78.13 g/mol) into 0.5ml of water. After proper dissolving add the distilled water to make up the volume up to 1ml.

7. Add 200 μl of 1M Tris HCL pH 8.0, 74 mg of 1M KCl, 100 μl of 10mM EDTA, 10 μl of 1mM DTT, 50 μl of Tween 20, 50 μl of Nonidet P40 and 500 μl of glycerol. Bring final volume to 1ml with distilled water.

8. Add 50 μl of 1M Tris-HCL pH 7.5, 10 μl of 1M EDTA, 876 mg NaCl, 50 μl of 20% SDS and make the volume to 1ml.

9. Dissolve 10 mg of proteinase K into 1ml of TE buffer (10mM Tris-HCl, 1mM EDTA).

10. Dissolve 35 g of NaCl (58.44 g/mol) into 80 ml of water and bring up the volume to 100ml.

11. Dissolve 3.38 g betaine monohydrate (135.163) into 5ml of distilled water. Filter through a 0.2 μm filter to sterilize and store at 4˚C.

12. *For 1ml of 25 mM dNTP mix add 250* μl *of each deoxynucleotides (dATP, dCTP, dGTP, dTTP),* at a concentration of 100 mM.

13. Make a 100μM stock solution of each primer by resuspension in the appropriate volume of the nuclease free water. Use the appropriate dilution based on the final volume reaction.

14. Add 250ml of Tris-HCL (121.14g/mol), pH 9.0, 714 mg of $MgCl_2$ (95.211g/mol), 14.5354g of $(NH_4)_2SO_4$ (132.14 g/mol) and 10ml of triton x-100 (647g/mol) and bring the final volume to 500ml.

15. Dissolve 2.38 mg of $MgCl_2$ (95.211g/mol) into 1ml of water.

5. References

1. Eichler, E.E., Richards, S., Gibbs, R.A. and Nelson, D.L. (1993). Fine structure of the human FMR1 gene. *Human molecular genetics*, *2*(8), pp.1147-1153.

2. Tseng, E., Tang, H.T., AlOlaby, R.R., Hickey, L. and Tassone, F. (2017). Altered expression of the FMR1 splicing variants landscape in premutation carriers. *Biochimica et Biophysica Acta (BBA)-Gene Regulatory Mechanisms*, *1860*(11), pp.1117-1126.

3. Maddalena, A., Richards, C.S., McGinniss, M.J., Brothman, A., Desnick, R.J., Grier, R.E., Hirsch, B., Jacky, P., McDowell, G.A., Popovich, B. and Watson, M. (2001). Technical standards and guidelines for fragile X: the first of a series of disease-specific supplements to the Standards and Guidelines for Clinical Genetics Laboratories of the American College of Medical Genetics. *Genetics in Medicine*, *3*(3), p.200.

4. Nolin, S.L., Sah, S., Glicksman, A., Sherman, S.L., Allen, E., Berry-Kravis, E., Tassone, F., Yrigollen, C., Cronister, A., Jodah, M. and Ersalesi, N. (2013). Fragile X AGG analysis provides new risk predictions for 45–69 repeat alleles. *American Journal of Medical Genetics Part A*, *161*(4), pp.771-778.

5. Yrigollen, C.M., Martorell, L., Durbin-Johnson, B., Naudo, M., Genoves, J., Murgia, A., Polli, R., Zhou, L., Barbouth, D., Rupchock, A. and Finucane, B. (2014). AGG interruptions and maternal age affect FMR1 CGG repeat allele stability during transmission. *Journal of neurodevelopmental disorders*, *6*(1), p.24.

6. Tassone, F., Iong, K.P., Tong, T.H., Lo, J., Gane, L.W., Berry-Kravis, E., Nguyen, D., Mu, L.Y., Laffin, J., Bailey, D.B. and Hagerman, R.J. (2013). FMR1 CGG allele size and prevalence ascertained through newborn screening in the United States. *Genome medicine*, *4*(12), p.100.

7. Saldarriaga, W., Forero-Forero, J.V., González-Teshima, L.Y., Fandiño-Losada, A., Isaza, C., Tovar-Cuevas, J.R., Silva, M., Choudhary, N.S., Tang, H.T., Aguilar-Gaxiola, S. and Hagerman, R.J. (2018). Genetic cluster of fragile X syndrome in a Colombian district. *Journal of human genetics*, *63*(4), p.509.

8. Zlotogora, J., Grotto, I., Kaliner, E. and Gamzu, R. (2015). The Israeli national population program of genetic carrier screening for reproductive purposes. *Genetics in Medicine*, *18*(2), p.203.

9. Hamlin, A.A., Sukharev, D., Campos, L., Mu, Y., Tassone, F., Hessl, D., Nguyen, D.V., Loesch, D. and Hagerman, R.J. (2012). Hypertension in FMR1 premutation males with and without fragile X-associated tremor/ataxia syndrome (FXTAS). *American Journal of Medical Genetics Part A*, *158*(6), pp.1304-1309.

10. Summers, S.M., Cogswell, J., Goodrich, J.E., Mu, Y., Nguyen, D.V., Brass, S.D. and Hagerman, R.J. (2014). Prevalence of restless legs syndrome and sleep quality in carriers of the fragile X premutation. *Clinical genetics*, *86*(2), pp.181-184.

11. Au, J., Akins, R.S., Berkowitz-Sutherland, L., Tang, H.T., Chen, Y., Boyd, A., Tassone, F., Nguyen, D.V. and Hagerman, R. (2013). Prevalence and risk of migraine headaches in adult fragile X premutation carriers. *Clinical genetics*, *84*(6), pp.546-551.

12. Hall, D., Todorova-Koteva, K., Pandya, S., Bernard, B., Ouyang, B., Walsh, M., Pounardjian, T., Deburghraeve, C., Zhou, L., Losh, M. and Leehey, M. (2016). Neurological and endocrine phenotypes of fragile X carrier women. *Clinical genetics*, *89*(1), pp.60-67.

13. Doherty, B.R. and Scerif, G. (2017). Genetic syndromes and developmental risk for autism spectrum and attention deficit hyperactivity disorders: insights from fragile X syndrome. *Child Development Perspectives*, *11*(3), pp.161-166.

14. Hunter, J.E., Epstein, M.P., Tinker, S.W., Abramowitz, A. and Sherman, S.L. (2012). The FMR1 premutation and attention-deficit hyperactivity disorder (ADHD): evidence for a complex inheritance. *Behavior genetics*, *42*(3), pp.415-422.

15. Lozano, R., Rosero, C.A. and Hagerman, R.J. (2014). Fragile X spectrum disorders. *Intractable & rare diseases research*, *3*(4), pp.134-146.

16. Seritan, A., Cogswell, J. and Grigsby, J. (2013). Cognitive dysfunction in FMR1 premutation carriers. *Current psychiatry reviews*, *9*(1), pp.78-84.

17. Bourgeois, J.A., Seritan, A.L., Casillas, E.M., Hessl, D., Schneider, A., Yang, Y., Kaur, I., Cogswell, J.B., Nguyen, D.V. and Hagerman, R.J. (2011). Lifetime prevalence of mood and anxiety disorders in fragile X premutation carriers. *The Journal of clinical psychiatry*, *72*(2), p.175.

18. Besterman, A.D., Wilke, S.A., Mulligan, T.E., Allison, S.C., Hagerman, R., Seritan, A.L. and Bourgeois, J.A. (2014). Towards an understanding of neuropsychiatric manifestations in fragile X premutation carriers. *Future neurology*, *9*(2), pp.227-239.

19. Roberts, J.E., Bailey, D.B., Mankowski, J., Ford, A., Sideris, J., Weisenfeld, L.A., Heath, T.M. and Golden, R.N. (2009). Mood and anxiety disorders in females with the FMR1 premutation. *American Journal of Medical Genetics Part B: Neuropsychiatric Genetics*, *150*(1), pp.130-139.

20. Jacquemont, S., Hagerman, R.J., Leehey, M.A., Hall, D.A., Levine, R.A., Brunberg, J.A., Zhang, L., Jardini, T., Gane, L.W., Harris, S.W. and Herman, K. (2004). Penetrance of the fragile X–associated tremor/ataxia syndrome in a premutation carrier population. *Jama*, *291*(4), pp.460-469.

21. Alvarez-Mora, M.I., Rodriguez-Revenga, L., Madrigal, I., Guitart-Mampel, M., Garrabou, G. and Milà, M. (2017). Impaired mitochondrial function and dynamics in the pathogenesis of FXTAS. *Molecular neurobiology*, *54*(9), pp.6896-6902.

22. Sullivan, S.D., Welt, C. and Sherman, S. (2011). FMR1 and the continuum of primary ovarian insufficiency. In *Seminars in reproductive medicine* (Vol. 29, No. 04, pp. 299-307). © Thieme Medical Publishers.

23. Cronister, A., Schreiner, R., Wittenberger, M., Amiri, K., Harris, K. and Hagerman, R.J. (1991). Heterozygous fragile X female: historical, physical, cognitive, and cytogenetic features. *American Journal of Medical Genetics Part A*, *38*(2-3), pp.269-274.

24. Hagerman, R.J. and Hagerman, P. (2016). Fragile X-associated tremor/ataxia syndrome—features, mechanisms, and management. *Nature Reviews Neurology*, *12*(7), p.403.

25. Adams, J.S., Adams, P.E., Nguyen, D., Brunberg, J.A., Tassone, F., Zhang, W., Koldewyn, K., Rivera, S.M., Grigsby, J., Zhang, L. and DeCarli, C. (2007). Volumetric brain changes in females with fragile X-associated tremor/ataxia syndrome (FXTAS). *Neurology*, *69*(9), pp.851-859.

26. Brunberg, J.A., Jacquemont, S., Hagerman, R.J., Berry-Kravis, E.M., Grigsby, J., Leehey, M.A., Tassone, F., Brown, W.T., Greco, C.M. and Hagerman, P.J. (2002). Fragile X premutation carriers: characteristic MR imaging findings of adult male patients with progressive cerebellar and cognitive dysfunction. *American Journal of Neuroradiology*, *23*(10), pp.1757-1766.

27. Grigsby, J., Brega, A.G., Bennett, R.E., Bourgeois, J.A., Seritan, A.L., Goodrich, G.K. and Hagerman, R.J. (2016). Clinically significant psychiatric symptoms among male

carriers of the fragile X premutation, with and without FXTAS, and the mediating influence of executive functioning. *The Clinical Neuropsychologist*, *30*(6), pp.944-959.

28. Lisik, M.Z. (2017). Health problems in female's carriers of premutation in the FMR1 gene. *Psychiatria polska*, *51*(5), pp.899-907.

29. Coffey, S.M., Cook, K., Tartaglia, N., Tassone, F., Nguyen, D.V., Pan, R., Bronsky, H.E., Yuhas, J., Borodyanskaya, M., Grigsby, J. and Doerflinger, M. (2008). Expanded clinical phenotype of women with the FMR1 premutation. *American Journal of Medical Genetics Part A*, *146*(8), pp.1009-1016.

30. Primerano, B., Tassone, F., Hagerman, R.J., Hagerman, P., Amaldi, F. and Bagni, C. (2002). Reduced FMR1 mRNA translation efficiency in fragile X patients with premutations. *Rna*, *8*(12), pp.1482-1488.

31. Feng, Y., Zhang, F., Lokey, L.K., Chastain, J.L., Lakkis, L., Eberhart, D. and Warren, S.T. (1995). Translational suppression by trinucleotide repeat expansion at FMR1. *Science*, *268*(5211), pp.731-734.

32. Mankodi, A., Urbinati, C.R., Yuan, Q.P., Moxley, R.T., Sansone, V., Krym, M., Henderson, D., Schalling, M., Swanson, M.S. and Thornton, C.A. (2001). Muscleblind localizes to nuclear foci of aberrant RNA in myotonic dystrophy types 1 and 2. *Human molecular genetics*, *10*(19), pp.2165-2170.

33. Sellier, C., Rau, F., Liu, Y., Tassone, F., Hukema, R.K., Gattoni, R., Schneider, A., Richard, S., Willemsen, R., Elliott, D.J. and Hagerman, P.J. (2010). Sam68 sequestration and partial loss of function are associated with splicing alterations in FXTAS patients. *The EMBO journal*, *29*(7), pp.1248-1261.

34. Sellier, C., Freyermuth, F., Tabet, R., Tran, T., He, F., Ruffenach, F., Alunni, V., Moine, H., Thibault, C., Page, A. and Tassone, F. (2013). Sequestration of DROSHA and DGCR8 by expanded CGG RNA repeats alters microRNA processing in fragile X-associated tremor/ataxia syndrome. *Cell reports*, *3*(3), pp.869-880.

35. Todd, P.K., Oh, S.Y., Krans, A., He, F. and Paulson, H.L. (2013). Cgg Repeat Associated Translation Drives Neurodegeneration in Fragile X Tremor Ataxia Syndrome. *Annals of Neurology*, *74*, p.S60.

36. Boivin, M., Willemsen, R., Hukema, R.K. and Sellier, C. (2017). Potential pathogenic mechanisms underlying Fragile X Tremor Ataxia Syndrome: RAN translation and/or RNA gain-of-function? *European journal of medical genetics*

37. Sellier, C., Buijsen, R.A., He, F., Natla, S., Jung, L., Tropel, P., Gaucherot, A., Jacobs, H., Meziane, H., Vincent, A. and Champy, M.F. (2017). Translation of expanded CGG repeats into FMRpolyG is pathogenic and may contribute to fragile X tremor ataxia syndrome. *Neuron*, *93*(2), pp.331-347.

38. Loomis, E.W., Sanz, L.A., Chédin, F. and Hagerman, P.J. (2014). Transcription-associated R-loop formation across the human FMR1 CGG-repeat region. *PLoS genetics*, *10*(4), p. e1004294.

39. Flora Tassone and Elizbeth M. berry cravis. (2017) Springer New York Dordrecht Heidelberg London.

40. Tassone, F and Hall, D.A. (2016). FXTAS, FXPOI and other Premutation disorders. Springer Nature

41. Hall, D., Tassone, F., Klepitskaya, O. and Leehey, M. (2012). Fragile X–associated tremor ataxia syndrome in FMR1 gray zone allele carriers. *Movement Disorders*, *27*(2), pp.297 301.

42. Liu, Y., Winarni, T.I., Zhang, L., Tassone, F. and Hagerman, R.J. (2013). Fragile X-associated tremor/ataxia syndrome (FXTAS) in grey zone carriers. *Clinical genetics*, *84*(1), pp.74-77.

43. Tassone, F., Pan, R., Amiri, K., Taylor, A.K. and Hagerman, P.J. (2008). A rapid polymerase chain reaction-based screening method for identification of all expanded alleles of the fragile X (FMR1) gene in newborn and high-risk populations. *The Journal of Molecular Diagnostics*, *10*(1), pp.43-49.

44. Chen, L., Hadd, A., Sah, S., Filipovic-Sadic, S., Krosting, J., Sekinger, E., Pan, R., Hagerman, P.J., Stenzel, T.T., Tassone, F. and Latham, G.J. (2010). An information rich CGG repeat primed PCR that detects the full range of fragile X expanded alleles and minimizes the need for southern blot analysis. *The Journal of Molecular Diagnostics*, *12*(5), pp.589-600.

45. Filipovic-Sadic, S., Sah, S., Chen, L., Krosting, J., Sekinger, E., Zhang, W., Hagerman, P.J., Stenzel, T.T., Hadd, A.G., Latham, G.J. and Tassone, F. (2010). A novel FMR1 PCR method for the routine detection of low abundance expanded alleles and full mutations in fragile X syndrome. *Clinical Chemistry*, *56*(3), pp.399-408.

46. Hantash, F.M., Goos, D.G., Tsao, D., Quan, F., Buller-Burckle, A., Peng, M., Jarvis, M., Sun, W. and Strom, C.M. (2010). Qualitative assessment of FMR1 (CGG) n triplet repeat status in normal, intermediate, premutation, full mutation, and mosaic carriers

in both sexes: implications for fragile X syndrome carrier and newborn screening. *Genetics in Medicine*, *12*(3), p.162.

47. Strom, C.M., Huang, D., Li, Y., Hantash, F.M., Rooke, J., Potts, S.J. and Sun, W. (2007). Development of a novel, accurate, automated, rapid, high-throughput technique suitable for population-based carrier screening for Fragile X syndrome. *Genetics in Medicine*, *9*(4), p.199.

48. Yrigollen, C.M., Durbin-Johnson, B., Gane, L., Nelson, D.L., Hagerman, R., Hagerman, P.J. and Tassone, F. (2012). AGG interruptions within the maternal FMR1 gene reduce the risk of offspring with fragile X syndrome. *Genetics in medicine*, *14*(8), p.729.

49. Bontekoe, C.J., Nieuwenhuizen, I.M., Willemsen, R. and Oostra, B.A. (1997). FMR1 premutation allele (CGG) 81 is stable in mice. *European Journal of Human Genetics*, *5*(5), pp.293-298.

50. Lavedan, C., Grabczyk, E., Usdin, K. and Nussbaum, R.L. (1998). Long uninterrupted CGG repeats within the first exon of the human FMR1 gene are not intrinsically unstable in transgenic mice. *Genomics*, *50*(2), pp.229-240.

51. Bontekoe, C.J.M., Bakker, C.E., Nieuwenhuizen, I.M., van Der Linde, H., Lans, H., De Lange, D., Hirst, M.C. and Oostra, B.A. (2001). Instability of a (CGG) 98 repeat in the Fmr1 promoter. *Human molecular genetics*, *10*(16), pp.1693-1699.

52. Peier, A.M. and Nelson, D.L. (2002). Instability of a premutation-sized CGG repeat in FMR1 YAC transgenic mice. *Genomics*, *80*(4), pp.423-432.

53. Willemsen, R., Hoogeveen-Westerveld, M., Reis, S., Holstege, J., Severijnen, L.A.W., Nieuwenhuizen, I.M., Schrier, M., van Unen, L., Tassone, F., Hoogeveen, A.T. and

Hagerman, P.J. (2003). The FMR1 CGG repeat mouse displays ubiquitin-positive intranuclear neuronal inclusions; implications for the cerebellar tremor/ataxia syndrome. *Human molecular genetics*, *12*(9), pp.949-959.

54. Entezam, A., Biacsi, R., Orrison, B., Saha, T., Hoffman, G.E., Grabczyk, E., Nussbaum, R.L. and Usdin, K. (2007). Regional FMRP deficits and large repeat expansions into the full mutation range in a new Fragile X premutation mouse model. *Gene*, *395*(1), pp.125-134.

55. Brouwer, J.R., Mientjes, E.J., Bakker, C.E., Nieuwenhuizen, I.M., Severijnen, L.A., Van der Linde, H.C., Nelson, D.L., Oostra, B.A. and Willemsen, R. (2007). Elevated Fmr1 mRNA levels and reduced protein expression in a mouse model with an unmethylated Fragile X full mutation. *Experimental cell research*, *313*(2), pp.244-253.

56. Berman, R.F. and Willemsen, R. (2009). Mouse models of fragile X-associated tremor ataxia. *Journal of Investigative Medicine*, *57*(8), pp.837-841.

57. Alam, M.P., Datta, S., Majumdar, S., Mehta, A.K., Baskaran, S., Gulati, N. and Brahmachari, V. (2010). Comparative analysis of DNA methylation in transgenic mice with unstable CGG repeats from FMR1 gene. *Epigenetics*, *5*(3), pp.241-248.

58. Van Dam, D., Errijgers, V., Kooy, R.F., Willemsen, R., Mientjes, E., Oostra, B.A. and De Deyn, P.P. (2005). Cognitive decline, neuromotor and behavioural disturbances in a mouse model for fragile-X-associated tremor/ataxia syndrome (FXTAS). *Behavioural brain research*, *162*(2), pp.233-239.

59. Foote, M., Arque, G., Berman, R.F. and Santos, M. (2016). Fragile X-associated tremor/ataxia syndrome (FXTAS) motor dysfunction modeled in mice. *The Cerebellum*, *15*(5), pp.611-622.

60. Castro, H., Kul, E., Buijsen, R.A., Severijnen, L.A.W., Willemsen, R., Hukema, R.K., Stork, O. and Santos, M. (2017). Selective rescue of heightened anxiety but not gait ataxia in a premutation 90CGG mouse model of Fragile X-associated tremor/ataxia syndrome. *Human molecular genetics*, *26*(11), pp.2133-2145.

61. Jin, P., Zarnescu, D.C., Zhang, F., Pearson, C.E., Lucchesi, J.C., Moses, K. and Warren, S.T. (2003). RNA-mediated neurodegeneration caused by the fragile X premutation rCGG repeats in Drosophila. *Neuron*, *39*(5), pp.739-747.

62. Jin, P., Duan, R., Qurashi, A., Qin, Y., Tian, D., Rosser, T.C., Liu, H., Feng, Y. and Warren, S.T. (2007). Pur α binds to rCGG repeats and modulates repeat-mediated neurodegeneration in a Drosophila model of fragile X tremor/ataxia syndrome. *Neuron*, *55*(4), pp.556-564.

63. Iwahashi, C.K., Yasui, D.H., An, H.J., Greco, C.M., Tassone, F., Nannen, K., Babineau, B., Lebrilla, C.B., Hagerman, R.J. and Hagerman, P.J. (2005). Protein composition of the intranuclear inclusions of FXTAS. *Brain*, *129*(1), pp.256-271.

64. Tassone, F., Hagerman, R.J., Taylor, A.K., Gane, L.W., Godfrey, T.E. and Hagerman, P.J. (2000). Elevated levels of FMR1 mRNA in carrier males: a new mechanism of involvement in the Fragile-X syndrome. *The American Journal of Human Genetics*, *66*(1), pp.6-15.

6. Tables

Table 1 Diagnostic criteria of FXTAS

| Diagnostic criteria		
Definite	**Probable**	**Possible**
One clinical major + [one radiological or pathological major].	Two clinical major or [one clinical minor + one radiological major].	One clinical major + one radiological minor.
Molecular		
Required	*FMR1* mutation including the premutation and the gray zone.	
Clinical		
Major	Intention tremor, Cerebellar gait ataxia.	
Minor	Parkinsonism, Neuropathy, Executive function deficit, >Moderate generalized brain atrophy.	
Neuropathology		
Major	Ubiquitin-positive intranuclear inclusions.	
Radiological		
Major	MRI white matter lesions in MCPs or brainstem.	
Minor	MRI cerebral white matter lesions, >Moderate generalized brain atrophy.	

7. Figures
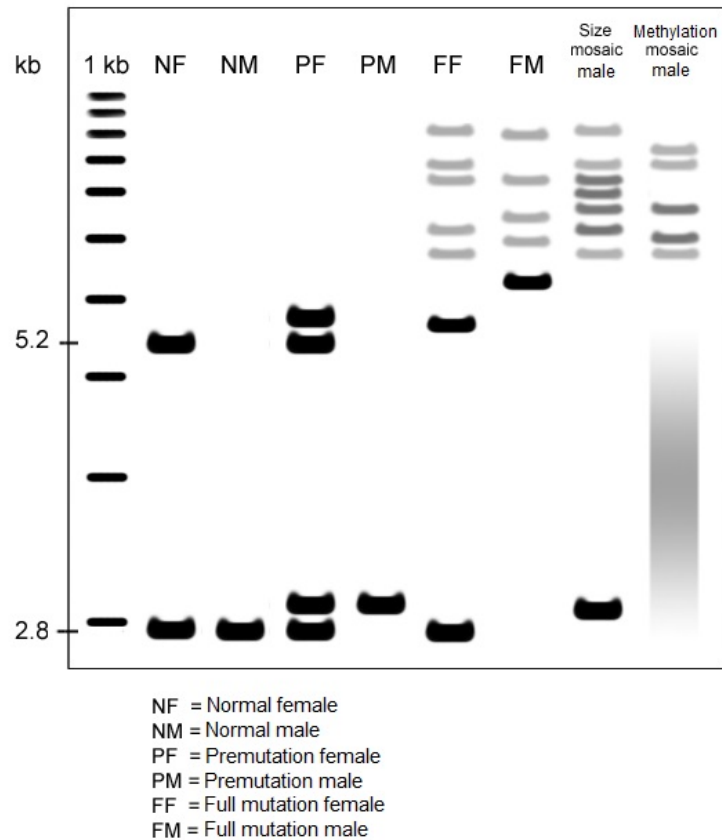
Figure 1: <u>Diagram of Southern blot analysis of genomic DNA</u> showing different CGG band patterns of alleles throughout the CGG range (normal to full mutation) in both males and females. The DNA marker, 1 kb ladder, is shown in Lane 1. Normal unmethylated band (2.8 kb) and normal methylated band (5.2 kb) in a normal female are shown in lane 2. Normal male, and premutation female and male are shown in lane 3, 4 and 5 respectively. Lanes 6 and 7 show a typical band pattern for full mutation female and full mutation male. In the last two lanes, 8 and 9, the mutation pattern of mosaic males, size, and methylation, are depicted.
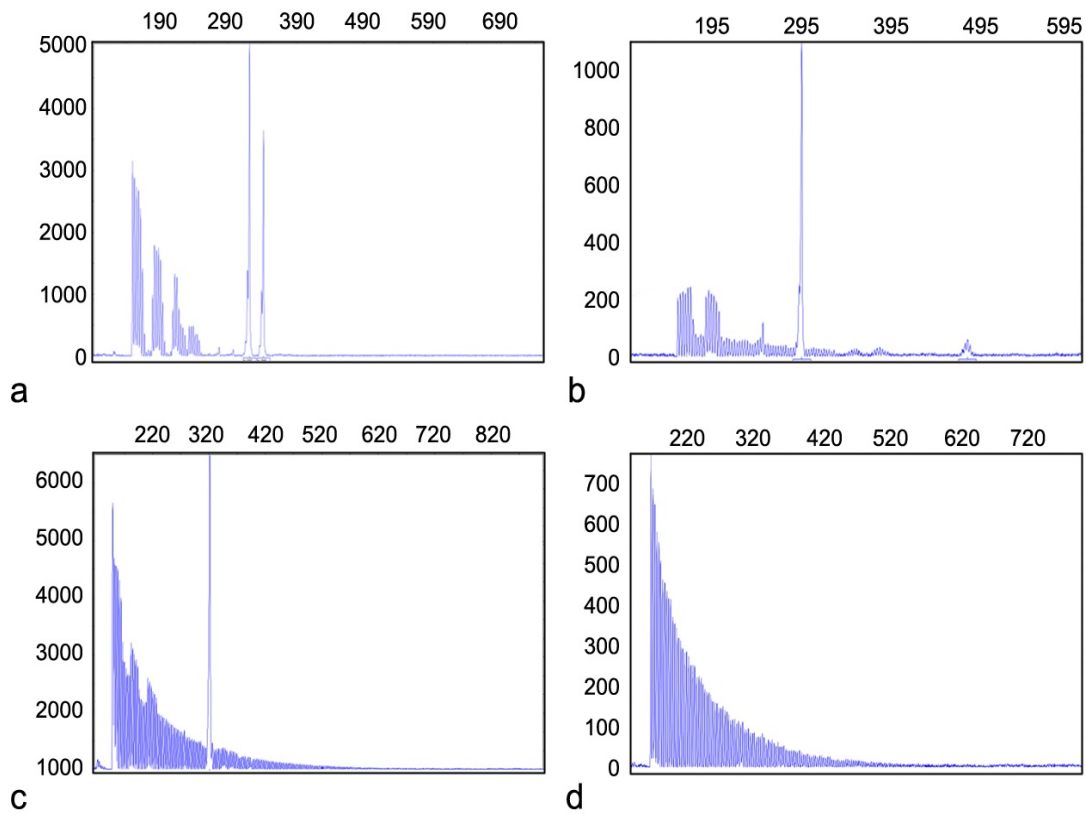
Figure 2: <u>Representative CE profiles of normal female</u> (a), premutation female (b), full-mutation female (c) and full mutation male (d) using the CGG repeat primed PCR which generates, in addition to the full-length specific *FMR1* allele also many CGG repeat primed products, which are resolved by CE as a series of peaks on each electropherogram.

Conclusion

Fragile X syndrome is the leading inherited form of intellectual disability and autism. The disorder is caused by expansion of a non-coding, trinucleotide CGG repeat tract in the fragile X (*FMR1*) gene to greater than 200 repeats (named "full mutation"). Full mutation CGG-repeat expansions are generally associated with methylation of the CGG-repeat and promoter regions, leading to silencing of the *FMR1* gene and the attendant loss of the FMR1 protein (FMRP); this protein is critically important for synaptic plasticity, memory, and brain development.

Individuals carriers of a premutation allele are at risk for *FMR1* associated disorders, including Fragile X-associated tremor/ataxia syndrome (FXTAS, which), a relatively newly recognized neurodegenerative disorder that was first reported in 2001 (Hagerman et al., 2001). FXTAS can occur in up to 75% of males with the premutation by the eighth decade of life (Jacquemont et al., 2004) and in approximately 16% of females (Hagerman and Hagerman, 2013; Rodriguez-Revenga et al., 2009). The clinical features of FXTAS include intention tremor, cerebellar ataxia, cognitive decline, neuropathy, and MRI changes. Patients with FXTAS have mitochondrial dysfunction and oxidative stress, likely caused by RNA toxicity due to the elevated *FMR1* mRNA levels observed in carriers. Currently it is unknown when an individual will develop FXTAS, as clinical assessment fails to identify carriers at risk before significant neurological symptoms are evident. Both the loss of FMRP and RNA toxicity affect multiple pathways and the need for molecular measures that accurately detect/predict and monitor disease progression and development, remains unmet.

To respond to this need; that is, to develop a reliable biomarker for an early diagnosis and progression of the premutation associated diseases, I have investigated the *FMR1* locus transcriptional landscape, the metabolic profile, and the association of observed isoforms and metabolites with the brain changes in the individuals who develop the FXTAs over time as compared to those who didn't and to healthy controls.

I observed altered expression of alternative spliced *FMR1/ASFMR1* mRNA isoforms (Zafarullah et al. 2020) and their strong association with the brain changes that suggests their role as potential biomarkers for early diagnosis of FXTAS. I also found a number of metabolites as biomarkers of early diagnosis, as they showed altered expression only in the individuals who developed the disorder over the time, even when they didn't show any clinical symptoms. In addition, I observed several metabolites being altered during the same time period as disease progression, and investigated the correlation of these isoforms and metabolites with measures of brain areas/volumes, including midbrain, MCP width, and the area of the pons. The altered expression observed was mainly related to phospholipids (Zafarullah et al. 2021)

Finally, I developed a non-invasive approach to establish epithelial cells lines from urine samples collected from patients with FXS and from healthy controls. These cell lines represent new resources for investigating the molecular mechanisms of FXS and related disorders. In conclusion, to date, there have been no identified molecular or metabolic biomarkers of FXTAS, which has delayed treatment, diagnosis, and prognosis of patients. So, these findings form these studies have translational potential, as the identified biomarkers could be used for the development of effective therapeutics Intervention.

References

1. Hagerman, R.J., Leehey, M., Heinrichs, W., Tassone, F., Wilson, R., Hills, J., Grigsby, J., Gage, B. and Hagerman, P.J., 2001. Intention tremor, parkinsonism, and generalized brain atrophy in male carriers of fragile X. *Neurology*, *57*(1), pp.127-130.

2. Jacquemont, S., Hagerman, R.J., Leehey, M.A., Hall, D.A., Levine, R.A., Brunberg, J.A., Zhang, L., Jardini, T., Gane, L.W., Harris, S.W. and Herman, K., 2004. Penetrance of the fragile X–associated tremor/ataxia syndrome in a premutation carrier population. *Jama*, *291*(4), pp.460-469.

3. Hagerman, R. and Hagerman, P., 2013. Advances in clinical and molecular understanding of the FMR1 premutation and fragile X-associated tremor/ataxia syndrome. *The Lancet Neurology*, *12*(8), pp.786-798.

4. Rodriguez-Revenga, L., Madrigal, I., Pagonabarraga, J., Xuncla, M., Badenas, C., Kulisevsky, J., Gomez, B. and Mila, M., 2009. Penetrance of FMR1 premutation associated pathologies in fragile X syndrome families. *European Journal of Human Genetics*, *17*(10), pp.1359-1362.

5. Zafarullah, M., Tang, H.T., Durbin-Johnson, B., Fourie, E., Hessl, D., Rivera, S.M. and Tassone, F., 2020. FMR1 locus isoforms: potential biomarker candidates in fragile X-associated tremor/ataxia syndrome (FXTAS). *Scientific reports*, *10*(1), pp.1-10.

6. Zafarullah, M., Palczewski, G., Rivera, S.M., Hessl, D.R. and Tassone, F., 2020. Metabolic profiling reveals dysregulated lipid metabolism and potential biomarkers

associated with the development and progression of Fragile X-Associated Tremor/Ataxia Syndrome (FXTAS). *The FASEB Journal*, *34*(12), pp.16676-16692.